UNIVERSITAT DE BARCELONA

Study and characterization of light pollution in Catalonia

Hector Linares Arroyo

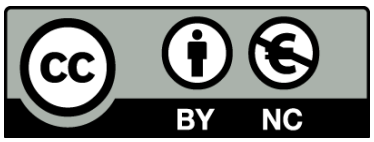

STUDY AND CHARACTERIZATION OF LIGHT POLLUTION IN CATALONIA

Hector Linares Arroyo

Directors:

Dr. Eduard Masana Fresno

Dr. Salvador J Ribas Rubio

UNIVERSITAT DE
BARCELONA

Study and characterization of light pollution in Catalonia

Memòria presentada per optar al grau de doctor per la Universitat de Barcelona

Programa de doctorat en física

Autor: Hector Linares Arroyo

Directors: Dr. Eduard Masana Fresno i Dr. Salvador J Ribas Rubio

Tutor: Dr. Alberto Manrique Oliva

UNIVERSITAT DE BARCELONA

Acknowledgements

To Eduard Masana and Salvador J Ribas for their dedication and deep involvement in the development of this thesis.

To Martin Aubé and Alexandre Simoneau for attentively guiding me into the Illumina light pollution model. Also to Martin for providing me access to the facilities that made most of the simulations possible.

To Manuel García-Gil for helping with result analysis and with deriving representative values of light sources.

To Francesca Figueras for introducing me to the light pollution scientific field, back in 2017, when I was finishing a master degree in astrophysics and cosmology.

To Ramon Canal for the technical support provided along the doctorate program. Specially, for recovering the hard drive where all the data from the thesis was saved after it starts malfunctioning.

To Salvador Bará for his masterclass about GIS software that allowed the creation of an important simulation product for this thesis. Also for his attentive support while working on the development of artificial radiance contribution maps.

To Fernando Jáuregui for providing information of light inventories of the towns from the Pyrenees area outside Catalonia. Also for providing images of the sky from Larra-Belagua.

To Alejandro Sánchez for providing and processing the ISS images that have been used in this thesis.

Abstract

The term light pollution refers to different harmful effects produced by artificial light sources. Concerns about it started to appear in the astronomy community decades ago, as it hinders the observation of the cosmos. Moreover, it also affects most of the flora and fauna (humans too) that is adapted to the natural light cycles. Additionally, it contributes to climate change by wasting energy that is mostly produced by fossil fuel consumption.

With this thesis, we aim to contribute to the understanding of the physics behind light pollution and to provide strategies to improve and ease its assessments. We established two different lines of action: measuring and modelling. The objectives of the measuring branch are to characterise the quality of the night sky in large areas within Catalonia and to study in detail the sky over key locations from the territory. The objectives of the modelling branch are to derive a tool to point out the principal sources of light pollution affecting a particular location, to find a methodology to reproduce measurements that can be used as a prediction tool and to define a process to assess very large areas.

For measuring the sky over large territories we used dynamic Sky Quality Meter (SQM) measurements of the zenith sky brightness. With this methodology we covered more than 3500 km in a total of 26 nights distributed in four annual campaigns. We created a processing software to deal with the resulting data and to ease and homogenize the process for obtaining reliable zenith sky brightness maps. The resulting zenith brightness maps provided reliable information about the quality of the sky in vast areas of Catalonia.

For measuring the sky over specific locations we used Digital Single Lens Reflex (DSLR) images processed with Sky Quality Camera (SQC) software. This methodology provides all-sky brightness images in the V band. The resulting all-sky maps are useful to point out the most polluted directions and as a consequence the most probable sources of light pollution. Eight different locations have been assessed using this methodology.

Light pollution models estimate the sky brightness by reproducing the interactions between the electromagnetic radiation and the molecules and aerosols that constitute the atmosphere. They have been validated as a helpful tool for assessing the night sky brightness and to understand light pollution at a physics level.

In particular we worked with the Illumina light pollution numerical model due

to its completeness. We used it with to create three different products, contribution maps, all-sky brightness maps and zenith sky brightness maps of large areas, each one of them related to one of the objectives of the modelling branch. The spectral range studied goes from 350 nm to 830 nm covering the Johnson-Cousins B, V and R bands.

Contribution maps show the percentage of the artificial radiance received that was emitted by each source. They were confirmed as a useful tool to sort the light pollution sources that are affecting the sky over a particular location. They have been found also useful for deciding which sources to include in all-sky brightness simulations.

All-sky brightness maps derived with Illumina have been found to be a reliable tool to reproduce all-sky brightness measurements. The difference between measurements and simulations are typically of the order of magnitude of 0.1-0.2 mag/arcsec^2. This kind of maps can be used for predicting the changes in the sky that would be produced by changes in the lighting systems.

We have used Illumina to create a zenith sky brightness map of Catalonia in B and V bands with a sampling grid of 5 km. It provides an accurate picture of the light pollution current situation of the country. As a relevant results, we found out that practically all the artificial light sources have an emission more dominant in the V band than in any other band. The maps reveals a complex pattern in agreement with the obtained in the measurements campaign, linked to the heterogeneity of the territory regarding population distribution and orography. The principal sources of light pollution are Barcelona and Tarragona metropolitan areas. The coastal line, in general, is very polluted. The darkest regions of the country are the Pyrenees, specially in the west, the Ports de Beseit natural park in the south west of the country, and the area around Montsec mountain range in the west.

Contents

List of Figures

List of Tables

Chapter 1

Introduction

1.1 Light pollution

Light pollution is the alteration of the natural brightness of the sky due to artificial light sources (Cinzano et al. 2000).

1.1.1 Historical context

Artificial light is linked to humankind from the dawn of civilisation. Control over fire constituted a key factor to improve the life conditions of hunter gatherer sapiens that once were an insignificant species in the ecosystem. It helped them conquer vast territories and fight back predators that could otherwise occupy the top spot in the animal hierarchy. However, the cycle of light due to day and night was almost unaffected. Humans, as most of the species, kept living under the natural light pace for millennia.

Beyond fire camps and torches, the first elaborated lighting devices were stone oil lamps. They have been found in prehistoric settlements dated to the 10th millennium BC. Candles made of tallow appeared many centuries later. Ancient Greece documents imply their use but the earliest surviving candles have been found in China and date to the 200 BC. These lighting systems were almost exclusively used to lit interior spaces. Thus, they did not affect the night sky.

It was not until the 15th century that lighting systems started to face outdoors. From there to the end of the 18th century public street lighting consisted in private oil lamps that were placed in windows facing to the street. However, they neither

altered the light cycle in a big scale due to its low efficiency. As a matter of fact, they served more as beacons than as brightening devices. So far, the night remained as dark as always.

During the 19th century permanent street lighting was installed in Europe and cities started to twinkle at night. First, gas combustion lamps were used, but they were replaced by arc lamps during the last decades of the century. In 1879, in parallel to the development of arc lamps, Thomas Edison created a carbon filament lamp that worked with electricity. At first it was not as efficient as the gas combustion and arc lamps available then, but this situation did not last long. Fast improvements as replacing the carbon filament for a metal filament, proposed by Carl Auer von Welsbach, made the new incandescent lamps a way better option. It was at the beginning of the 20th century when the infrastructure necessary for installing outdoor electrical lighting was deployed. During the 20th century gas discharge lamps replaced incandescent technology and dominate the market up to the present. But with the beginning of the new millennium their hegemony trembles with the increasing popularity of light emitting diodes (LED).

During the last hundred years outdoor lamps invaded the whole planet at an unprecedented pace. Cities, towns, rural areas and roads were lit all night long. An unforeseen problem derived from artificial lighting was becoming more and more evident: light pollution.

Nowadays, 60% of the total population worldwide live under light polluted skies. In Europe and USA the number increases up to more than 80%. Thus, light pollution has become a worldwide problem that affects specially highly populated areas and developed countries (see figure 1.1). Despite the increasing awareness and the efforts of the scientific community to mitigate the problem, light pollution is currently still increasing in a yearly basis trend of 2% (Kyba et al. 2017).

1.1.2 Light pollution effects and forms

Concerns about light pollution have been a common topic in astronomy for decades, as it hinders the observation of the cosmos. Artificial brightening of the sky affects astronomic studies to the extent that many observatories on Earth have become completely useless for scientific purposes due to its proximity to towns and cities. In this sense, light pollution was already studied and taken into account in the second half of the twentieth century when trying to find new locations for astronomical observatories (Riegel 1973; Walker 1970, 1973).

Nonetheless, light pollution should not be taken solely as a problem for

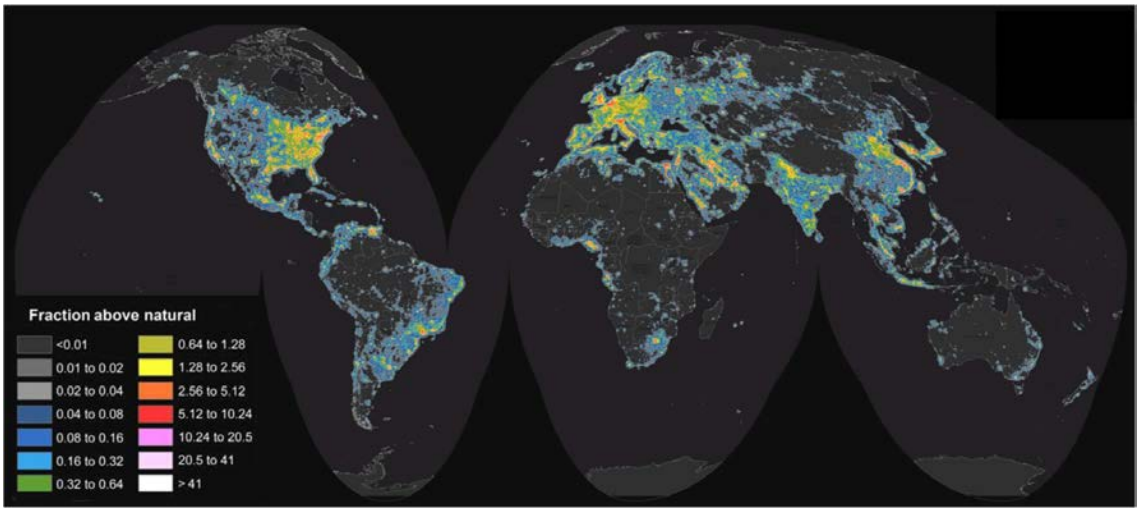

Figure 1.1: Light pollution world map represented as the artificial brightness ratio to the natural sky brightness in the year 2015. Source Falchi et al. (2016).

astronomers. It affects the vast majority of flora and fauna that lived for millennia according to the natural light cycles: day and night, variations of light exposure throughout the year and Moon phases (Sanders et al. 2020). Humans are no exception. Links between light pollution and some diseases have been shown recently (Garcia-Saenz et al. 2018). Moreover, it contributes indirectly to climate change through wasting energy that is mostly produced by fossil fuel combustion. Beyond that reasoning, as was stated in the Declaration in defense of the night sky and the right to starlight (2007): "An unpolluted night sky that allows the enjoyment and contemplation of the firmament should be considered an inalienable right of humankind equivalent to all other environmental, social, and cultural rights, due to its impact on the development of all peoples and on the conservation of biodiversity."

Light pollution presents itself in many forms. The main ones are light trespassing, glare, clutter and skyglow (see figure 1.2). Light trespassing is produced by brightening non desired areas, for example street lighting brightening the interior of buildings such as houses or offices. Glare is the direct emission towards the field of view of people. It can be harmful for the eyes and fatal to drivers. Clutter refers to using such different type of lamps and intensities that makes it difficult to see properly. Skyglow is the brightening of the sky produced by artificial sources and its study is the main topic of this thesis. It is the responsible for the increasing problems when observing the cosmos. It is easy to identify as the light dome above cities that can be seen (and then affects the sky) from tens and even hundreds of kilometers away (see figure 1.3 for a comparison between a sky barely affected by

skyglow and a heavily affected one).

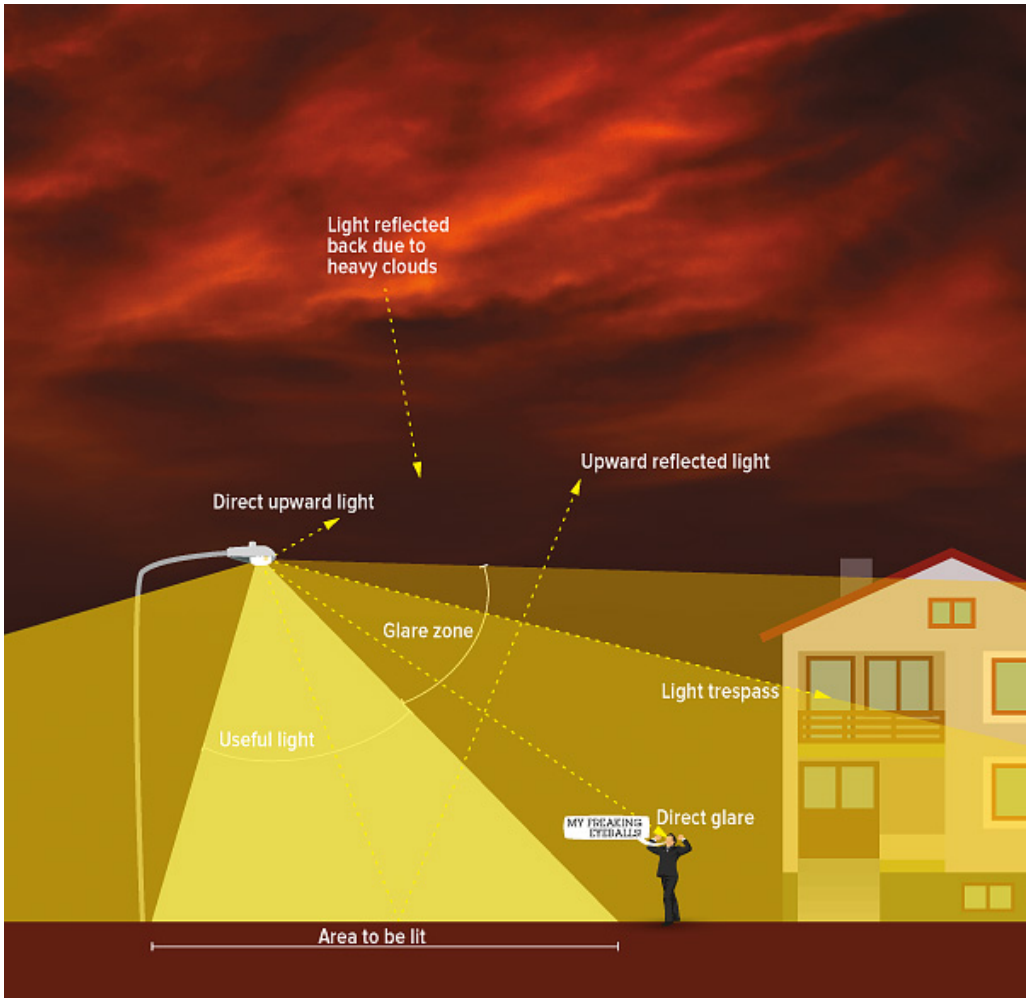

Figure 1.2: Light pollution manifestations scheme (Gocova 2013). Skyglow is produced by direct upward light and upward reflected light. It is worsened by light reflected on clouds. Glare is produced by light emitted within the field of view of the people around. Light trespassing corresponds to the brightening of non-desired areas. Clutter is not shown in this figure.

Sky brightness is normally measured with a dimensionless logarithmic scale called astronomic magnitudes (mag/arcsec^2). There is a detailed description of the scale in chapter 2. Here, just to point out that lower the value, brighter the sky; and that a difference of 1 in that scale represents a sky 2.51 times brighter. A night sky is typically considered almost non polluted if its sky brightness level is above 21.4 mag/arcsec^2. In such skies one can distinguish easily the Milky Way and observe directly with the naked eye more than 5000 stars. In urban areas or heavily polluted

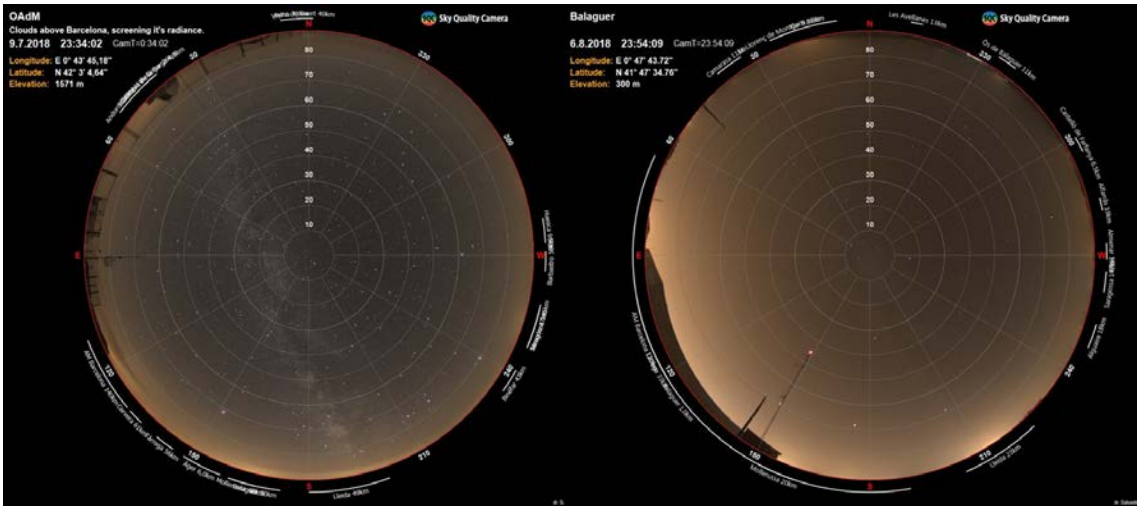

Figure 1.3: Photographs of the sky in Montsec Observatory, left, and Balaguer, right. The skyglow present in the right image prevents from seeing the Milky Way and most of the stars. Images courtesy of Parc Astronòmic Montsec (PAM) personnel.

sites the sky brightness level drops below 19.0 mag/arcsec^2. In such skies the Milky Way is hidden by light pollution and the number of stars observable is reduced by a factor 10 (Cinzano & Falchi 2020). In this sense, a visual representation of the correlation between the brightening of the sky, the visibility of the Milky Way and the number of visible stars can be found in figure 1.4.

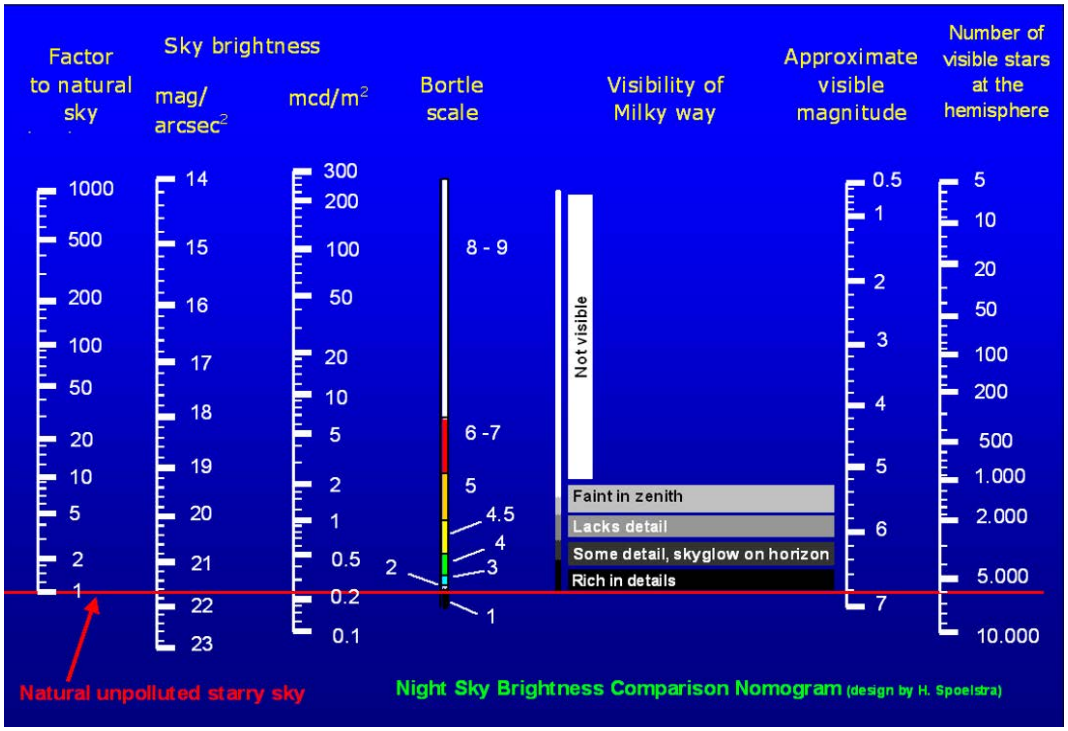

Figure 1.4: Sky brightness level nomogram designed by H. Spoelstra.

1.2 Light: beyond human vision

Visible light, also called visible spectrum or simply light, is defined as the wavelength range of the electromagnetic radiation that can be perceived by human vision.

Electromagnetic radiation can be understood as electromagnetic waves or photons that propagates through space. It is characterized by its frequency or wavelength. From the lowest wavelength to the highest, the electromagnetic spectrum is divided in Gamma rays, X-rays, ultraviolet, visible light, infrared, microwaves and radio waves (see figure 1.5).

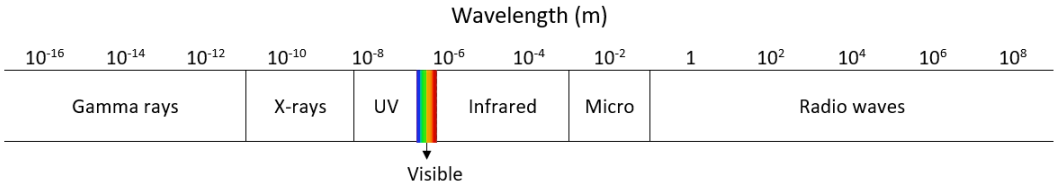

Figure 1.5: Electromagnetic radiation classification by wavelength.

Human's vision is sensible to electromagnetic radiation within the range between slightly below 400 nm and slightly over 700 nm. But its sensibility to electromagnetic radiation varies depending on the level of luminance. In this regard, there are two main vision systems: photopic and scotopic. Photopic vision dominates in high luminance situations. The receptor cells of this system allows color perception and its curve is centered approximately at 550 nm. On the other hand, scotopic vision dominates in low luminance levels. The receptor cells does not allow color perception (grey-scale system) and its curve is centered approximately at 500 nm. The sensitivity curves of both vision systems are bell shaped (see figure 1.6), meaning that the human vision responds more to some wavelength than to others.

There exists photometric magnitudes and units such as candelas, lumens or lux, that measure brightness according to the sensitivity curve of human vision (mostly photopic). However, when dealing with light pollution it is important to bear in mind that not all living beings have the same sensitivity to the electromagnetic radiation. For instance, some reptiles are sensible to the infrared radiation and some insects to the ultraviolet. Hence, it is crucial to reduce the emitted radiation in wavelengths outside the visible spectrum too.

For that reason, in this thesis light pollution measurements and simulations are not limited to the sensitivity of the human vision. We study a slightly broader range, from 350 nm to 830 nm, in order to include practically all the emission from the

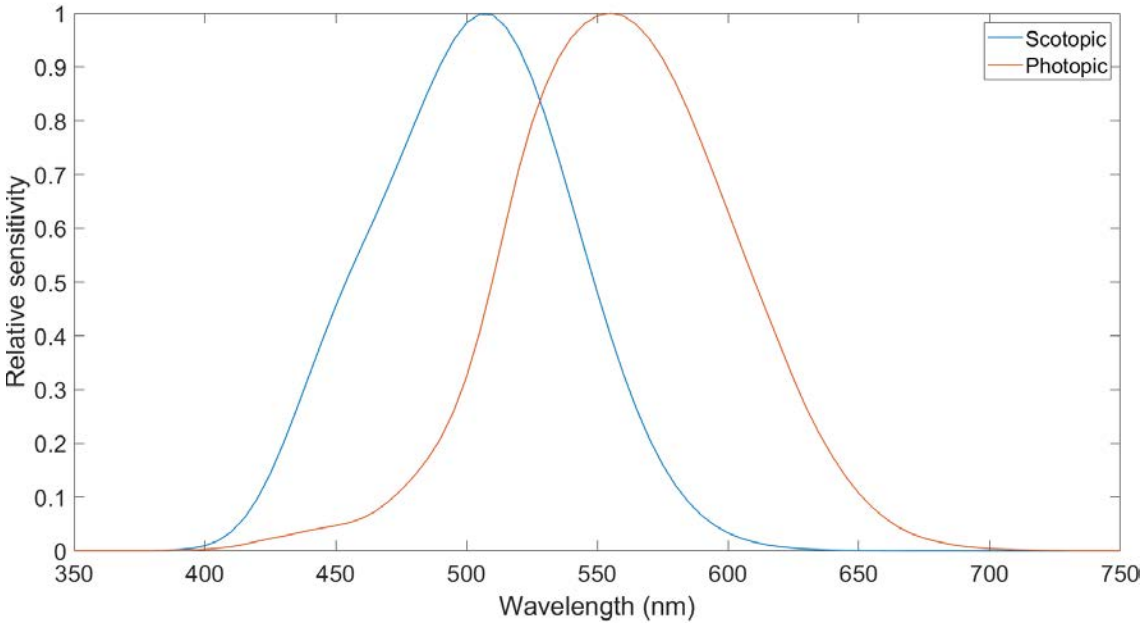

Figure 1.6: Human vision sensitivity. Blue: scotopic vision (CIE 1951). Red: photopic vision (CIE 1990).

most common artificial light sources. As the range exceeds the borders of the visible light, it makes no sense to work with magnitudes linked to human vision. We work with radiometric magnitudes instead, which by definition measure electromagnetic radiation in any spectrum range. The wavelength range studied is also chosen because it can be fully studied by the B, V and R bands of the Johnson-Cousins photometic system (Johnson & Morgan 1953, 1955). As seen in the previous section, astronomic magnitudes are a unitless measure of brightness based on a set of spectral functions or bands.

1.3 Sky brightness

Sky brightness depends on how electromagnetic radiation interacts with Earth's atmosphere. Electromagnetic radiation sources can be natural or artificial. During daytime artificial sources are practically negligible because the Sun completely outshines them. But during nighttime the situation changes drastically. Artificial sources can rapidly become the main stakeholder in densely populated areas and overlit locations.

The following subsections define first how light interacts with the atmosphere. Then, both the natural and artificial sources that are responsible for the night sky brightness are characterized.

1.3.1 Light interaction with the atmosphere

Earth atmosphere is formed mainly by molecules and aerosols. The molecular composition of the atmosphere remains almost unaltered whereas the atmosphere aerosol component varies with time and geographical location. Molecules in the atmosphere are normally in gaseous state and have a size of the order of magnitude of 10^{-10} m. Aerosols, on the other hand, are liquid or solid particles with a size of the order of magnitude of 10^{-6} m. Examples of aerosols are: water droplets of clouds, fog and mist, solid particles of dust, etc.

Photons that travel through the atmosphere interact with both components creating light extinction, that is the combination of two different and not mutually exclusive processes: absorption and scattering. Both processes depend on the size ratio between the wavelength of the electromagnetic radiation and the components of the atmosphere.

Absorption takes place when particles capture light and transform it to internal energy. Molecular absorption prevents gamma rays, x-rays, ultraviolet type B, far infrared, microwaves and long radio waves, from reaching to the surface of the planet. That is why it is necessary to rely on observations located outside the atmosphere (satellites) to study these ranges of the electromagnetic spectrum. On the other hand, a fraction of ultraviolet A, the whole visible range, some near infrared and radio waves go through the atmosphere and reach Earth's surface (see figure 1.7).

Scattering is the change of direction of the electromagnetic radiation when it encounters a particle. It is the responsible for the propagation of artificial light through the atmosphere that generates light pollution. Scattering strongly

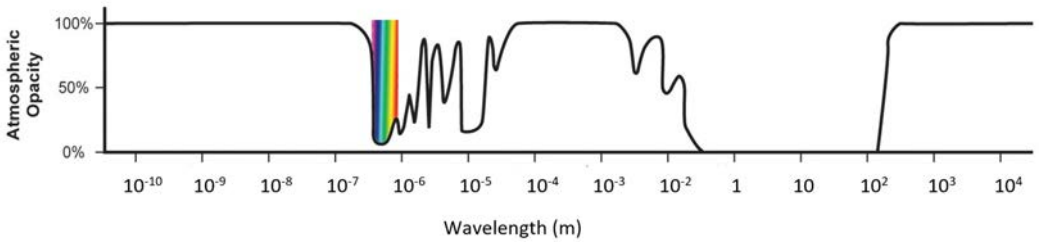

Figure 1.7: Atmospheric electromagnetic radiation opacity depending on the wavelength. Image credit: NASA.

depends on the ratio between the electromagnetic radiation wavelength and the size of the particle. If the scattering particle is much smaller than the wavelength of the electromagnetic radiation, as it happens with molecular scattering, it follows Rayleigh function. Rayleigh scattering defines an inversely proportional relation between scattering and the fourth power of the wavelength. Thus, shorter wavelengths scatters more than longer ones. This is the main reason of the blue color of the sky during daytime. If the scattering particle is of the order of magnitude of the wavelength of the electromagnetic radiation, as it happens with aerosols, it is approximated by Mie scattering. Mie scattering defines the scattering produced by a homogeneous sphere. It is almost independent of the wavelength (as long as it is similar to the particle size) and it is greater in the forward direction than in any other one.

Light extinction increases with the distance that photons have to go trough within Earth's atmosphere, as the air mass they encounter is larger. That process, added to the inverse square law relation, explains the strong decay of light pollution with distance. This is the reason why astronomical observatories are located far away from cities.

On the other hand, light extinction is a non-desired effect for astronomers when it happens when observing the target the natural source. In order to reduce this unwanted effect, astronomic observatories are typically found at high altitudes. Higher altitude means less air mass between astronomical objects and the telescopes. Thus, less information is lost by light extinction. Moreover, normally large cities and towns are at a lower altitude than observatories. Therefore, the most polluted directions appear close to the horizon where there are no celestial objects visible.

As stated, atmosphere composition depends on the presence of aerosols since molecular content is almost invariable. Aerosol presence has two opposite effects depending on the position of the observer. Aerosols increase light pollution in a

local level due to the increased scattering. We experienced the brightening effect of aerosols when taking measurements in places with abnormal humid conditions. On the contrary, the presence of aerosols around distant artificial light sources can result in a darker sky as more photons are absorbed close to the source.

1.3.2 Natural sources

Natural brightness sources can be divided in two subcategories: astrophysical sources, such as the Moon, zodiacal light, the nearby planets, visible stars or the starry figure of the Milky Way; and atmospheric sources, mainly airglow, that is caused by chemiluminescence (i.e. light emission due to the decay of excited states of the products of a chemical reaction) in the upper atmosphere triggered by the high-energy solar radiation.

Natural sky brightness can change notably depending on the cycles that some of those sources follow. The Moon stands out the most in this sense: between a full Moon night and a new Moon night the sky brightness level varies several orders of magnitude. In this thesis we work with moonless conditions only. The position of the Milky Way in the sky also follows a cycle that can change notably sky brightness levels, specially in very dark places. In pristine skies when the Milky Way passes close to the zenith, it increases the zenith sky brightness in almost 0.5 mag/arcsec^2. We took into account its position on the sky and its possible effects when interpreting measurements of the night sky brightness. In simulations, on the other hand, we did not model its presence since the focus is on the artificial brightness. These variable natural sources could be added in future projects.

1.3.3 Artificial sources

As stated before, artificial light sources are the responsible for light pollution. There are a vast number of different artificial sources and not all are equally harmful. Regarding light pollution, the most relevant characteristics of an artificial source are the spectrum of the emitted light, how it is spread (optics and physical characteristics), and the radiant flux emitted.

The light produced by different lamp technologies (LED lamps, discharge lamps as sodium or mecury lamps, etc.) have different emission spectrum (see appendix 7.1 for the spectrum of the most common technologies present in street lighting). In the lighting community, and by extent in the light pollution community, the Correlated Color Temperature (CCT) is used as a reference. It avoids having to check the

spectrum chart each time when dealing with a specific lamp technology. The idea is to assign a temperature to the source by approximating its spectrum to the spectrum of an ideal black-body radiator of a certain temperature. For instance, it is common to see this methodology when dealing with LED lamps. A LED 3000 K, means that the spectrum of that LED is associated with a black body radiation of 3000 K. CCT is far from being accurate, specially with technologies that have narrow emission bands such as mercury vapor lamps, metal halide lamps, low pressure sodium bands, etc. It is also a very confusing methodology for comparing lamps of different technology. However, it is useful for comparing lamps that share the same technology. Higher CCT means higher emission in the blue side of the spectrum (350-500 nm), known as cold light. Lower CCT means lower emission in the blue region of the spectrum, known as warm light. As an example, figure 1.8 shows the comparison between the spectrum of the light emitted by a LED with CCT 3000 K and 4000 K. A different system to characterize the spectral properties of lamps has been proposed by Galadí-Enríquez (2018). This system is an adaptation to lighting technology of the classical procedures of multi-band astronomical photometry with wide and intermediate-band filters.

It is an agreement in the community that cold light is the most harmful for humans and some other species (Aubé et al. 2013; Garcia-Saenz et al. 2018; Grubisic et al. 2018). Moreover, bluer light, as already seen, scatters in a greater extent due to Rayleigh scattering. Hence, outdoors lighting should be designed to reduce the blue content as much as possible.

Optics and physical characteristics do not depend on the technology of the light source (at least not in a great extent). The principal physical characteristic of the lamp is its height, specifically its relative height with respect to the possible obstacles present nearby. Optics characterization of a lamp, on the other hand, is not as simple. In professional lighting multi two-dimensional plane charts, that show how light is spread from the lamp from nadir to zenith angles in several azimuth angles are normally used (see figure 1.9). In order to simplify the characterization process, the Upper-hemisphere Light Output Ratio (ULOR) is used. As its name indicates is the ratio of light that is emitted directly above the horizon of the lamp. Although it seems a vague variable compared with the complexity of lamps optics, it is a good indicator of the light pollution a lamp can potentially produce. Figure 1.10 shows different optics design regarding its polluting effect. Figure 1.11 shows the relative emission of two light sources with ULOR 0 and ULOR 20 (in this case both light sources are symmetrical respect to the azimuth for simplicity).

Radiant flux is the electromagnetic energy emitted by unit of time. It is measured in watts in the International System of Units. As the radiant flux

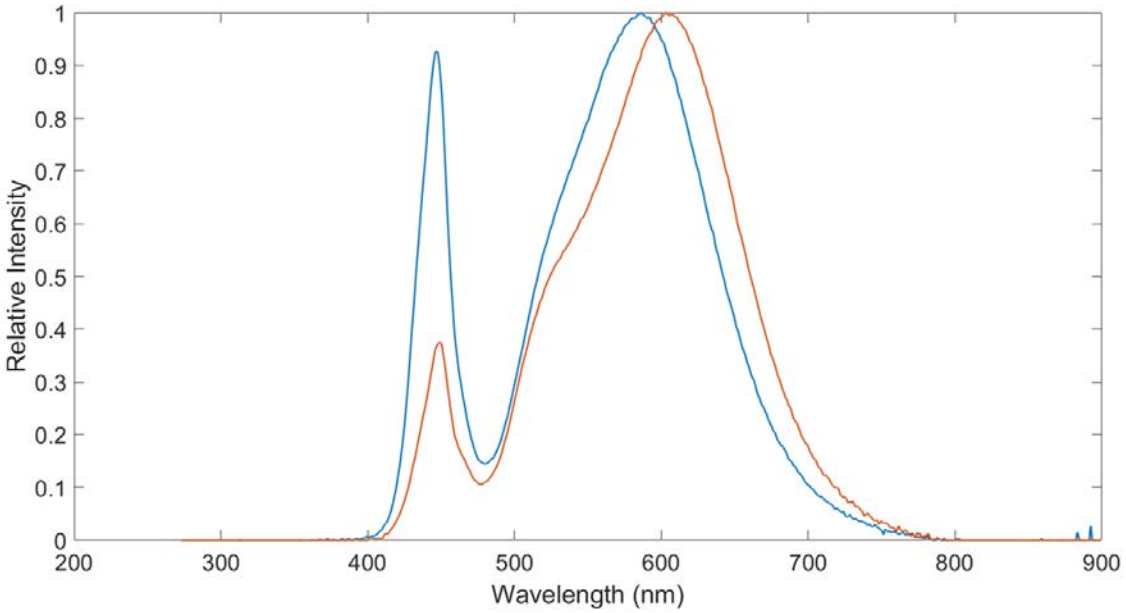

Figure 1.8: Spectrum of the light emitted by a LED with CCT 3000 K in red and CCT 4000 K in blue. As explained a lower CCT corresponds with less relative emission in the blue region of the spectrum.

increases, the brightness of the sky increases accordingly. It is important to design outdoor lighting to provide the minimum radiant flux necessary to carry out properly the purposes of the brightened area. Moreover, outdoor lighting should be used only when it is needed. However, switching on and off depending on the needs, for example using movement detectors, could be a problem. The operating life of some technologies are linked to the on/off cycles (LED) and other technologies (discharge) are not very responsive and they need some time to reach operational levels. As an alternative solution there are technologies, as LED lamps, that allow to reduce drastically the radiant flux emitted depending on the situation or by time slots. Others, such as high pressure sodium lamps, allows some reduction but are not as flexible as they have a threshold below which light is not produced. There are also very inflexible technologies, as mercury vapor lamps, that practically have a fixed radiant flux emission. Outdoor lighting design should take into account the changing needs along the night and choose technologies accordingly.

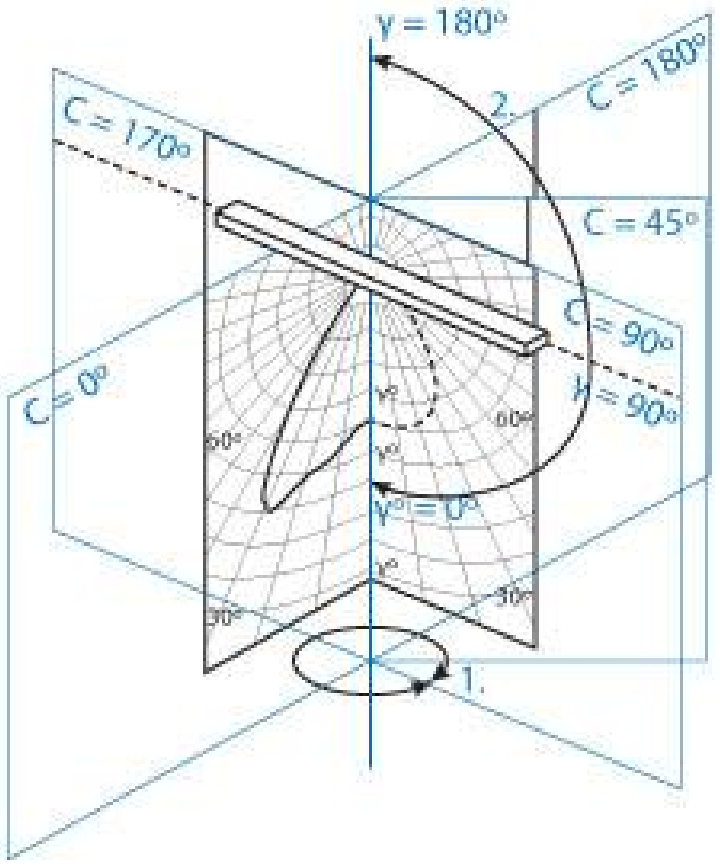

Figure 1.9: Example of a photometric chart of a ordinary lamp. Adaptation from Deco (2017)

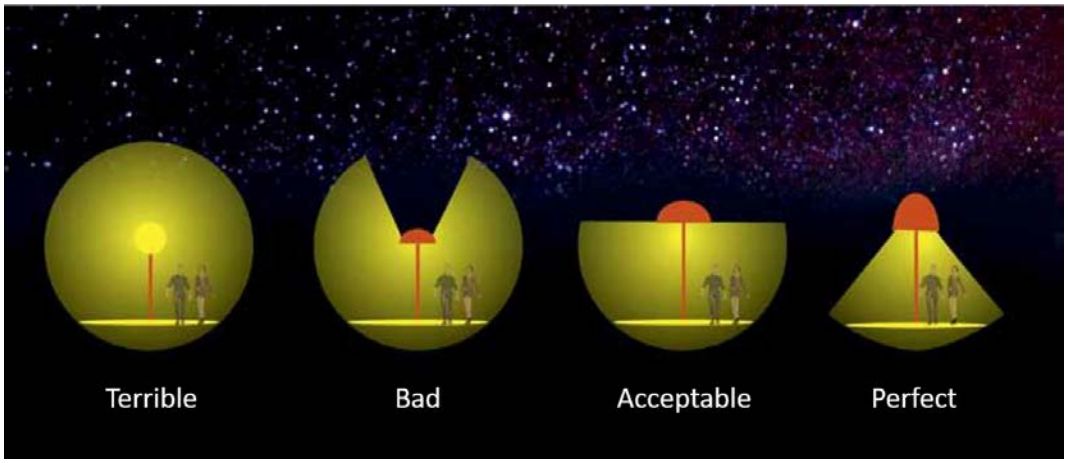

Figure 1.10: Simplified diagram showing different optics. Ordered from left to right, from the most polluting to the least. Adaptation from Ribas et al. (2013).

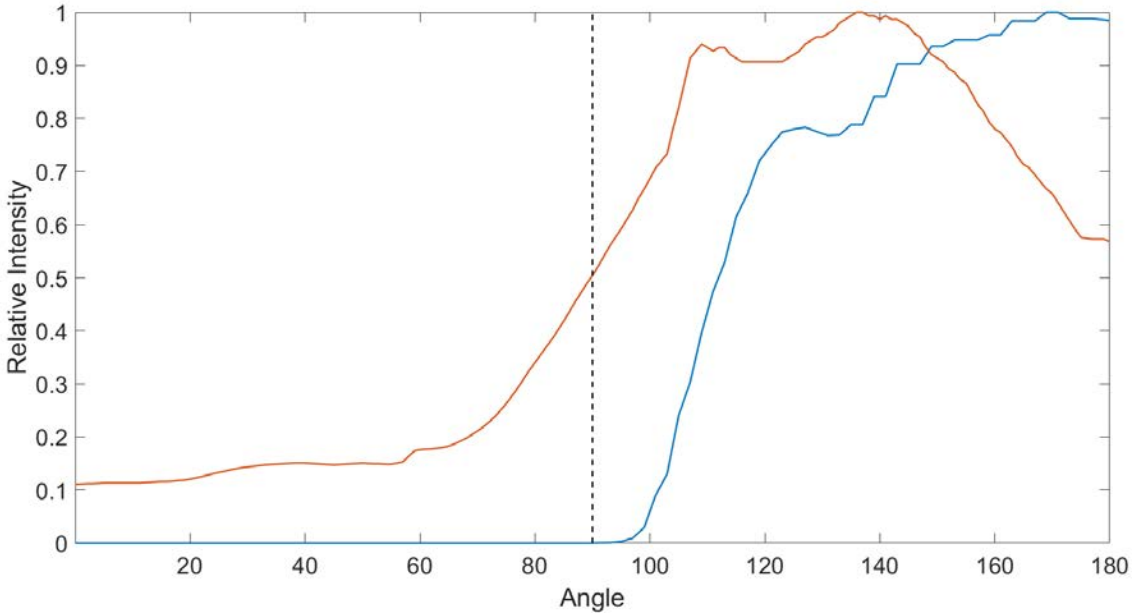

Figure 1.11: Relative intensity emitted with respect to the angle in the vertical plane. Being 0 the zenith and 180 the nadir. In red ULOR 20. In blue ULOR 0. Dashed black line represents the horizon of the lamp.

1.4 Light pollution studies in Catalonia

In this thesis light pollution is addressed as a global problem. The methodologies presented to measure and model it are applied mostly in Catalonia and the Pyrenees, but they are valid to address light pollution issues almost anywhere.

Light pollution is not a new topic in Catalonia, the fight for the protection of the darkness of the sky started to gain momentum in the decade of the 90's. During the early years of the decade light pollution was precisely measured for the first time in the country. The measurement took place in Montsec mountain range within the framework of the characterization of the area for hosting a professional astronomical observatory. Throughout the decade, the first artificial brightness local regulations started to appear. By the end of the decade, people from different backgrounds united their voice in the Cel Fosc association. Their purpose was to protect the darkness of the sky by participating in the regulation of the artificial lighting at the municipality level.

In 1998, the government of Catalonia acknowledged the need for a common regulation and started to prepare what would constitute in 2001 the first regional law against light pollution in Spain. Its aim was to create a regulation for indoor and outdoor lighting in order to minimize the harmful effects of light pollution. However, the regulation for the deployment of the law did not arrive until 2005. In the following years, it was updated to correct some contradictions and to add adjustments in the criteria for the street lighting design.

In 2007, the zoning of Catalonia regarding the level of protection against light pollution was established. The territory was divided in four protection levels (E1, E2, E3 and E4) according to several factors such as flora, fauna, scientific purposes, tourism, etc. E1 zones are formed, among other specific locations, by areas included in conservation plans, beaches, coastal lines, continental water shores and towns within protected areas. E2 zones are formed by non developable or slightly developed land outside E1 zones and areas chosen by each town council within their municipality. E3 zones are formed by developed or developable land outside E1, E2 and E4 zones, and night intensive use land due to high mobility or high commercial usage. E4 zones are formed by developed land of intensive night usage due to commercial or high human mobility. No land closer than 2 km from zones E1 can be classified as E4. The characteristics of each zone are defined in table 1.1. The types of lamps referenced in table 1.1 are defined in table 1.2. The resulting map is shown in figure 1.12.

The next milestone took place in 2013 with the declaration of Montsec mountain

Zone	Level of protection	Lamp spectrum evening	Lamp spectrum night	ULOR evening	ULOR night
E1	Maximum	Type I	Type I	1	1
E2	High	Type III	Type II	5	1
E3	Moderate	Type III	Type III	10	5
E4	Minor	Type III	Type III	15	10

Table 1.1: Zoning of Catalonia regarding the protection against light pollution. Night shift starts at 0h00 in winter and 01h00 during summer and ends at sunrise. In E1 and E2 zones the night shift starts one hour earlier.

Classification	Technology	Spectrum limitation
Type I	Discharge lamps	$< 2\%$ in wavelength < 440 nm
Type I	LED	$< 1\%$ in wavelength < 500 nm and predominant > 585 nm
Type II	Discharge lamps	$< 5\%$ in wavelength < 440 nm
Type II	LED	$< 15\%$ in wavelengths < 500 nm
Type III	Anyone	$< 15\%$ in wavelength < 440 nm

Table 1.2: Types of lamps referenced in table 1.1.

range as Reserve and Tourist Destination by the Starlight foundation, the first of this kind in Catalonia. In 2018, the National Park of Aigüestortes received the same certification.

The first extensive measurements campaigns were carried out within the framework of preparing the law against light pollution of 2001. They took place between 2000 and 2002 and were performed by the University of Barcelona (Torra et al. 2000). The methodology used was based on astronomic photometry. These campaigns were the predecessors of the annual campaigns that have been carried out from 2012 by the Parc Astronòmic Montsec and from 2014 also by the Institut d'Estudis Espacials de Catalunya, through the Institut de Ciències del Cosmos (ICCUB-IEEC). The methodology of the current campaigns has changed notably with respect of those started in 2000. They are based in measurements taken with a photometer (SQM, see chapter 3) installed in the roof of a vehicle. In this sense, Ribas (2016) developed a statistical method to create light pollution zenith maps of large areas. The campaigns are focused on dark regions as natural parks, but not

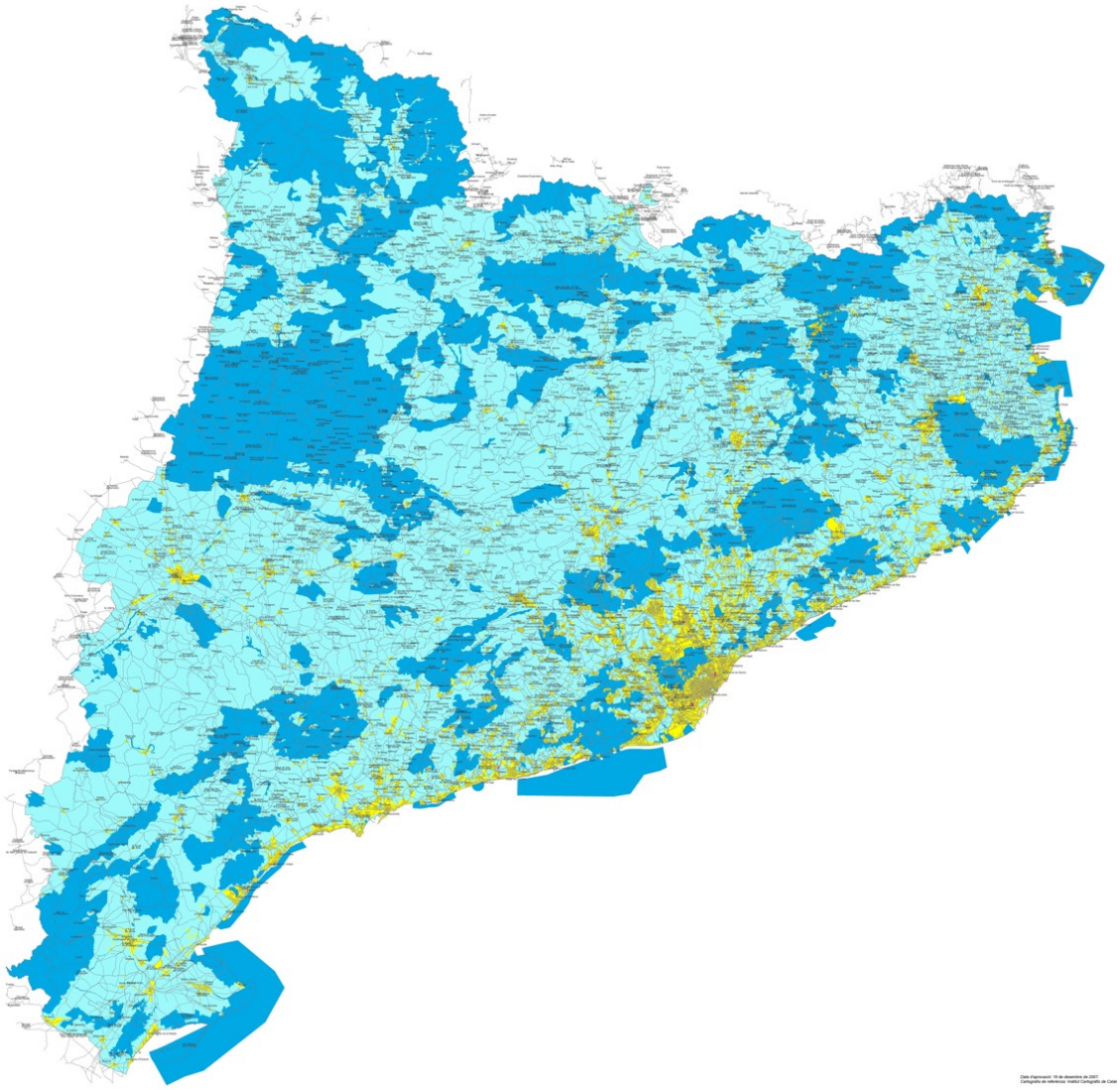

Figure 1.12: Division of Catalonia by zones regarding its level of protection against light pollution. Dark blue: E1 zones. Light blue: E2 zones. Yellow: E3 zones. Pink: E4 zones.

exclusively. As years went by, the number of areas studied increased, expanding this way the zenith light pollution map of Catalonia. The measurement branch of this thesis is partially linked to these annual campaigns (see chapter 4).

Besides these campaigns, there is a network of fixed photometers in Catalonia (Ribas 2016) that measures the sky brightness all year long. They are useful to study trends, weather affectation, changes in the lighting systems, etc.

1.5 Pyrenees La Nuit

Some of the work presented in this thesis is linked with the Interreg POCTEFA project Pyrenees la Nuit (PLN) that is financed by the European Union.

The project aims to protect and increase the darkness of the night to improve the quality of the ecosystems present in the Pyrenees. It also aims to create a reference for other regions that searches the same goal.

The outreach branch of the project is dedicated to rise awareness of the importance of protecting the darkness of the sky and how artificial brightness can affect it. Concrete actions are: creating The Night House placed in the Col du Tourmalet (France), that will be an educational center dedicated exclusively to the night of the Pyrenees; installing a digital planetarium in Pamplona (Spain) alongside the production of a documentary film to be played in this kind of facilities focused on the night of the Pyrenees; creating permanent and temporary expositions; and promoting a list of activities for different segments of the population, such as school visits to the planetarium, concerts under starry skies, night walks, etc.

The scientific branch of the project is divided in two subbranches: light pollution characterization and studying how it affects the Pyrenees ecosystem. The biology part consists in creating an inventory of species that are endangered by light pollution and studying which light sources affects the most each one of them. The subbranch that studies light pollution by itself consists in three actions: the creation of a static photometer network to measure the temporal patterns of light pollution in the area; taking all-sky measurements in each one of the key locations of the project (Parc Astronomic Montsec, Valle del Roncal and Pic du Midi); using and adapting a light pollution numerical model to simulate the night sky brightness of these locations and identifying the main sources of artificial brightness. This thesis includes results of the two last actions explained.

1.6 Objectives

From a general perspective, we aim to contribute to the understanding of light pollution and to provide strategies to ease its assessment. To face that challenge we divided the thesis in two lines of action: measuring and modelling.

The first objective of the measuring block is to increase the area covered by the Light Pollution map of Catalonia that was already mentioned in section 1.4. This project started in 2012 and has been carried on a yearly basis. Each year the map has been updated adding the areas studied. We dedicated 26 nights to cover more than 3500 km of paved and unpaved roads. To process the data we developed a new software to ease the task and to standardize the process.

The second goal of this block is to gather information of the whole sky over selected locations. The locations chosen are of particular interest because some of them are in close proximity to astronomic facilities and others are key points of protected areas as natural parks. Seven locations have been studied: Observatori Astronòmic Montsec, Centre Astròmic Prades, Pic du Midi de Bigorre, Valle del Roncal, Pic de l'Orri, Montgarri refuge and La Força d'Àreu (see figure 1.13).

Figure 1.13: Locations where sky brightness has been measured and/or simulated. A: Montsec Observatory, OAdM. B: Prades astronomy center. C: Montgarri. D: Montsant natural park. E: Estany Llong. F: Pic de l'Orri. G: Valle del Roncal. H: Pic du Midi. I: La Força D'Àreu.

The modelling block aims to assess the night sky brightness of two different targets: specific locations and vast areas.

Specific locations are assessed by simulated all-sky maps and contribution maps. All-sky maps provide brightness information for every direction of the sky. Contribution maps show which are the sources that are producing the artificial brightness that it is being received in the observation point. A reliable methodology to study specific locations is of great help to be able to produce simulated all-sky maps for inaccessible sites, as well as, to know how changes in the lighting systems or other variables can affect the sky. In this thesis eight specific locations have been studied: the locations mentioned above (except for la Força d'Áreu), Estany Llong (within Aigüestortes natural park) and Montsant natural park (see figure 1.13). For each location, simulated all-sky maps have been compared and validated against measurements.

The sky brightness of vast areas are difficult to assess using measurements. It takes many nights and the number of nights with the proper atmospheric conditions are normally scarce. Moreover, measuring is limited to the areas that can be accessed to. A reliable simulation tool might simplify, reduce the cost and speed up light pollution studies of vast areas. In this thesis, we used an existing light pollution numerical model for creating a simulated light pollution map of Catalonia that covers the whole country. The map shows the sky brightness value in the zenith direction with a spatial resolution of 5x5 km.

Chapter 2

Measuring light pollution

Measuring is the most basic strategy for assessing light pollution levels. With measurements we can quantify light pollution, compare the quality of the night of different locations, study seasonal or daily patterns, study the effects of light system changes, validate light pollution models, etc.

When measuring light pollution we can choose from several indicators depending on our purposes. They are characterized mainly by the area of the sky they focus on, the spectral range they cover and the physical magnitude they study.

With respect to the area of the sky they measure, light pollution indicators can be classified in three groups: those that measure one direction of the sky, those that measure a large region of the sky and those that measure the sky as a whole. The first group stands out for its simplicity. The zenith brightness lies within this group. It is one of the most spread indicators and it is often used as a standard value for assessing the quality of the night sky. It is also common to find in the bibliography the light pollution level at 45° in elevation. The second group is probably the least common, but this kind of indicators are very helpful when studying a particular region of the sky. For instance, normally astronomers observe the sky above 30°, thus it is interesting to assess the quality of the night in this region omitting the directions closer to the horizon. On the other hand, in biology, it could be interesting to use the complementary indicator, measuring below 30°, for studying how light pollution affects some species that have a field of view limited to that region. The third group corresponds to indicators that assess the whole sky with a single value. In this sense, the all-sky average light pollution ratio (ALR) introduced by Duriscoe (2016) is the most popular. It quantifies the ratio between the artificial brightness (averaged for all the sky) to the natural brightness.

Regarding the spectrum range, a part from the minimum and maximum wavelength, it is important to take into account the sensitivity curve. Normally, indicators are chosen in order that they have a great sensitivity in the target wavelengths of the study. For instance, in biology the focus normally is correlated with the spectral response of the species in study. In human epidemiology, a common topic is to study the suppression of melatonin secretion produced by exposure to blue light (around 400 nm). To specifically quantify it, Aubé et al. (2013) introduced the Melatonin Suppression Index (MSI).

The spectrum of the emitted light from artificial sources does not always lie completely within the visible range. As explained in section 1.2, in order to cover practically all the emission from the most common artificial light sources we study a spectrum range that covers the visible light, part of the near infrared and ultraviolet (from 350 nm to 830 nm). In section 2.1.1 there is a detailed explanation of the magnitudes and units we used in this thesis to characterized emitted and received light. The main characteristics of measurements and the instrumentation used in this thesis are also described in the following sections of this chapter.

2.1 Measurements

2.1.1 Radiometric magnitudes

Radiometry is the science that studies electromagnetic radiation. As there exists a vast amount of different magnitudes in radiometry, we have prepared a summary of the ones we are going to refer to in this work:

- **Radiant energy** is the energy of electromagnetic radiation. It has units of joules (J).
- **Radiant flux** is the radiant energy emitted or received per unit of time. It has units of watts (W).
- **Radiosity** is the radiant flux leaving a surface (emitted, reflected and transmitted) per unit surface (W/m^2).
- **Irradiance** is the radiant flux received per unit area (W/m^2).
- **Radiance** is the radiant flux emitted or received per unit of surface per unit of solid angle ($W/m^2/sr$). That is the radiant flux received in a surface coming from a projected area of solid angle.

All of the above magnitudes, except for radiant energy, are also expressed per unit of wavelength or frequency. For detailed information see table 2.1.

Magnitude	Symbol	Units	Description
Radiant energy	Q	J	Energy of the electromagnetic radiation
Radiant flux	Φ	W	Radiant energy per unit of time
Spectral flux	Φ_λ or Φ_ν	W/nm or W/Hz	Radiant flux per unit of wavelenght or frequency
Radiosity	J	W/m^2	Radiant flux emmited by a surface
Spectral radiosity	J_λ or J_ν	$W/m^2/nm$ or $W/m^2/Hz$	Radiosity per unit of wavelenght or frequency
Irradiance	E	W/m^2	Radiant flux received by a surface
Spectral irradiance	E_λ or E_ν	$W/m^2/nm$ or $W/m^2/Hz$	Irradiance per unit of wavelenght or frequency
Radiance	L	$W/m^2/sr$	Radiosity (emmited) or irradiance (received) per unit of solid angle
Spectral radiance	L_λ or L_ν	$W/m^2/sr/nm$ or $W/m^2/sr/Hz$	Radiance per unit of wavelenght or frequency

Table 2.1: Radiometric magnitudes.

In astronomy, brightness is normally expressed in astronomic magnitudes, that are a dimensionless logarithmic scale. This approach was originally designed for classifying stars by their brightness. Stars are point-like sources which have no projected radiation surface information. Astronomical magnitudes are defined as:

$$m = m_{ref} - 2.5log_{10}(\frac{E}{E_{ref}}) \tag{2.1}$$

where m_{ref} is the magnitude of a reference source with an irradiance E_{ref}, and E is the irradiance of the star. Astronomical magnitudes are a unit-less measure, however, they are commonly referred as "mag".

In light pollution, we study regions of the sky with defined solid angle, thus radiance is used instead of irradiance:

$$m_s = m_{s,ref} - 2.5log_{10}(\frac{L}{L_{ref}}) \tag{2.2}$$

where m_s is the surface brightness equivalent to a star of astronomical magnitude, m, spread over a surface equal to one square arcsec. Although unit-less too, it is referred as "mag/arcsec^2".

2.1.2 Spectral response

Measuring devices have variable sensitivity with wavelength, i.e. they respond differently to radiation depending on its wavelength. Normally the spectral response is represented by a curve or function of the sensitivity with respect to the wavelength. Spectral response functions can be normalized such as 1 being the maximum sensitivity of the instrument or 1 being the area below the spectral response curve. A sensitivity of 0 means that the device is completely blind to that wavelength.

Different spectral responses provide different measurements of the same object or region of the sky. Only measurements taken with instruments that share the same sensitivity function can be quantitatively compared. It is common to rely on a photometric system (not to be confused with photometric magnitudes, that are linked with the human vision response), that consists in a set of well-defined optical filters. One of the most used in astronomy is the Johnson-Cousins system (Johnson & Morgan 1953, 1955; Cousins 1976). In our case we are going to study artificially produced light, that normally goes from 350 nm to little further than 800 nm. The Johnson-Cousins filters that covers that range are called B, V and R, for blue, visual and red respectively (see figure 2.1).

2.1.3 Field of view

The field of view of an instrument refers to the region of the sky it is measuring. When all the information is gathered and assigned to a unique direction or line of sight the instrument is called one-dimensional. If the instruments maintains the spatial information within the field of view they are called bi-dimensional instruments.

The most common representation for measurements with spatial information are all-sky brightness maps. They are circular charts that show the brightness of the hemispherical dome that cover the sky. They go from 0 to 90° in elevation and

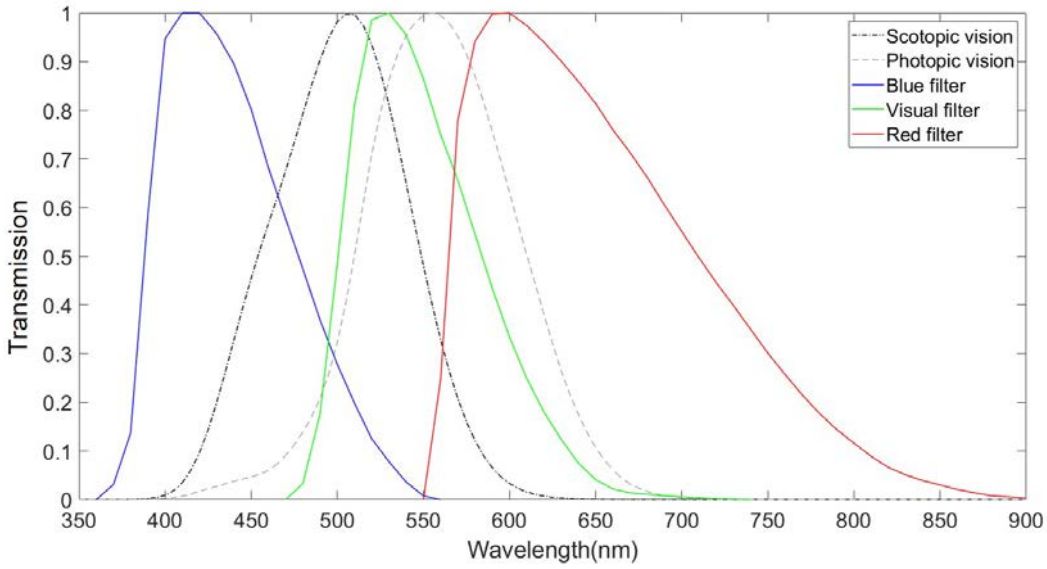

Figure 2.1: Transmission relative to wavelength. Blue: blue filter of the Johnson-Cousins system. Green: visual filter of the Johnson-Cousins system. Red: red filter of the Johnson-Cousins system. Dash-point black: scotopic vision. Dash grey: photopic vision.

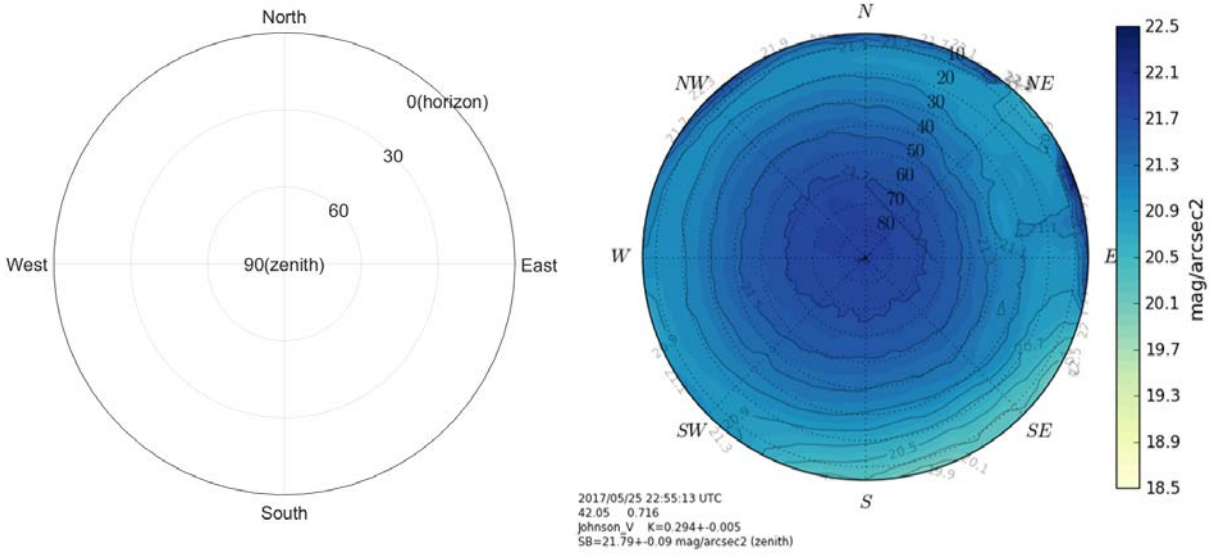

Figure 2.2: Left: scheme of an all-sky brightness map. Radius corresponds to elevation angle. Angle corresponds with azimuth. Right: all-sky brightness map produced using ASTMON instrumentation using PyASB code. See 2.2.3.

0 to 360° in azimuth. The centre of the circle corresponds to elevation 90° (zenith), as the radius increases elevation angles decreases reaching 0° (horizon) at the outer ring. Normally they are oriented such as the north (azimuth zero) is upwards and the south downwards. There is not a common rule to place east and west as right or left, so it is important to pay attention to this detail when observing all-sky maps. In figure 2.2 it is shown a template of a sky brightness map and a real measurement.

2.2 Instrumentation

In the following sections the instrumentation that has been used during the thesis is described. The Sky Quality Meter (SQM) and Digital Single Lens Reflex (DSLR) images calibrated with Sky Quality Camera (SQC) have been used directly for data acquisition. Available data obtained using the All-Sky Transmission MONitor (ASTMON) has been used as a validation tool for simulations.

Nevertheless, there exists a large list of different instruments to choose from when dealing with light pollution measurements. Hanel et al. (2018) described most of them in a paper that has become a reference guide for the topic. We dedicate the following lines to mention some of them.

One of the first approaches to assess the quality of the night sky was made in the area of astronomy. Telescopes combined with charge-coupled devices (CCD) were used to determine sky brightness based on classic astronomical photometry. The methodology consists in observing defined calibration stars and compare them to the sky background.

Nowadays there is a wide range of fields that need to measure light pollution. For instance in the area of law enforcement, administration normally uses lux meters to control brightness levels in the public space. They are mostly based on a solid state detector although there exists some based on CCD. For citizen science projects there also exists simpler and inexpensive instruments as the IYA-lightmeter that was developed for the international year of astronomy in 2009. It measures irradiance in a wide range (approximately from 300 nm to 700 nm).

In the light pollution community, a part from the instruments that are fully explained in the following sections, the Telescope Encoder and Sky Sensor (TESS) photometer is gaining momentum (Zamorano et al. 2016). It was developed in the framework of the European Union funded project Stars4all. It is a one-dimensional instrument with a field of view of close to 20° FWHM, with a spectral response covering from 400 nm to 750 nm. It is designed to monitor radiance levels

continuously during large periods. A feature that standout from other photometers is an IR detector that estimates the presence of clouds. This photometer is used in the Pyrenees la Nuit project to create a network of permanent devices (see section 1.5).

2.2.1 Sky quality meter (SQM)

Sky Quality Meter (SQM) is the most spread photometer in the light pollution community, mainly because of its low cost. They are used as permanent devices in fixed stations and as portable devices in dynamic measurements to cover large areas.

Figure 2.3: Two SQM. Right: inside its housing. Left: partially outside its housing. Image from Kyba et al. (2011).

The SQM is produced by Unihedron company (Grimsby, ON, Canada). It is equipped with a solid state detector (RAOS TSL237s) combined with a light-frequency converter and a filter (HOYA CM-500) that makes it sensible to the range between 320 nm and 720 nm (see figure 2.4). Although its sensitivity function

is far from similar to any of the most used astronomic photometric bands, it is normally compared qualitatively to the V band of the Johnson-Cousins system. The SQM's output is radiance expressed in astronomical magnitudes (mag/arcsec^2).

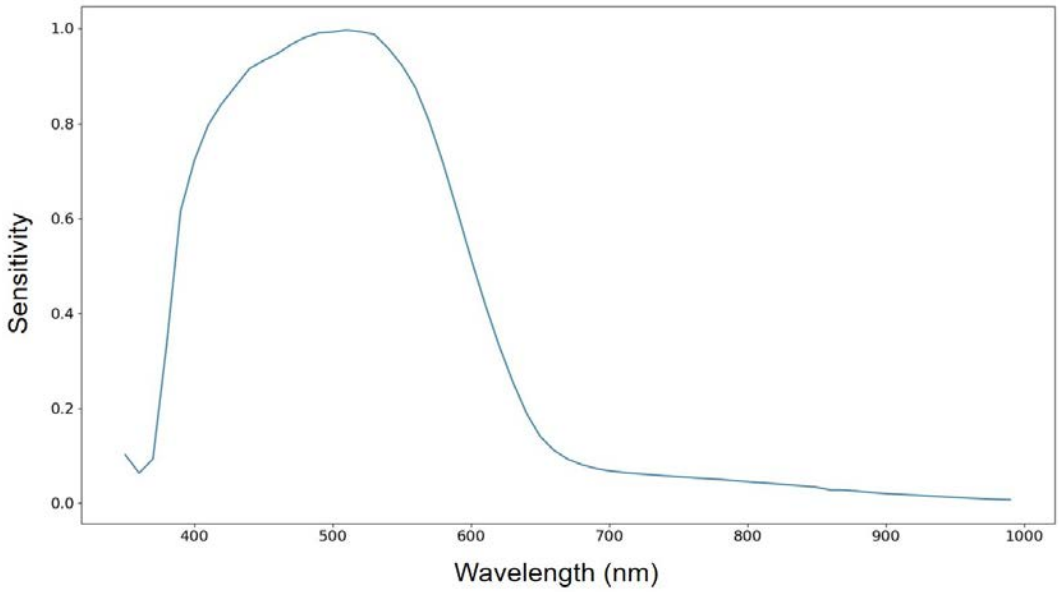

Figure 2.4: Averaged sensitivity of the SQM photometer with respect to the wavelength (Bará et al. 2019c).

It is a one-dimensional device, as it assigns the value measured to the central line of sight the instrument is pointing to. The first versions of the photometer had a wide field of view close to 90 degrees (FWHM), that made it hard to get information for specific directions. Following generations, branded SQM-L (SQM operator's manual, Unihedron), have a build-in lens which reduces the field of view to 20 degrees (FWHM). The reduced field of view make this generation of photometers better suited to measuring specific directions.

There have been some projects that aimed to use SQM as a bi-dimensional instrument, for instance the Nixnox project (Zamorano et al. 2014; Tilve et al. 2015). The strategy consists in using several SQM measurements pointing to different directions to create a sky brightness map (see figure 2.5). In this sense, there is a version under development of the instrument called SQM-LU-DL-V that incorporates position sensors to determine the lines of sight measured and a software to create the maps. The TESS group has recently developed the TAS (TESS Auto Scan) which measures automatically 145 different lines of sight to cover the sky dome. The process lasts several minutes, which can be a problem if during the process the atmospheric conditions change.

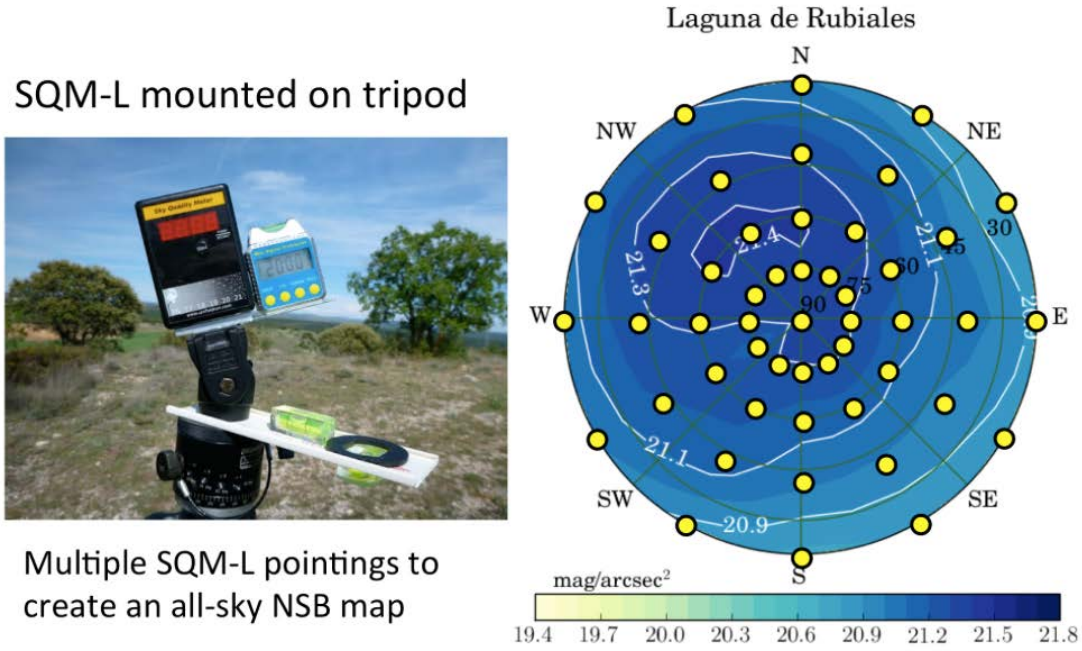

Figure 2.5: SQM-L mounted on a tripod to map the sky. Nixnox project. Image from Zamorano et al. (2014).

The SQM is factory calibrated by comparison to a reference calibrated light meter with a precision of 5%. The calibrated SQM has a operational radiance range between 0 and 24 mag/arcsec^2 (den Outer et al. 2011). The intrinsic error of the instrument is estimated to be around 10%, that is roughly equivalent of 0.10 mag/arcsec^2 (Kyba et al. 2011). Consistency between SQMs is not a negligible issue, specially when comparing different locations or when creating networks. It is possible to enhance it by intercalibration (den Outer et al. 2011, 2015; Ribas 2016; Bará et al. 2019c).

The long term behaviour of the photometer is an increasing concern. Particularly, it has been observed a darkening trend of the data in outdoors permanent placed devices. The exposure to sunlight during daytime is the main reason of this measurement darkening trend of the outdoor placed SQMs (Bará et al. 2020). One of the first studies in this matter was the one from Pun et al. (2014) centered in the Hong Kong permanent SQM network. More recent papers that show a darkening trend in permanent SQM networks are Bertolo et al. (2019) and Bará et al. (2019a), from the Veneto region in Italy and Galicia in Spain respectively. The SQM used in this thesis is stored in a dark place and it is only used during nigh-time, thus the exposure to sunlight is negligible.

Bará et al. (2019b) pointed out that changes in the lighting system could contribute to darker readings which may not necessary mean a reduction of the total radiance emitted. As the SQM's spectral sensitivity is lower in some regions than in others, the replacement of discharge lamps for technologies with emission peaks in low sensitivity wavelengths (see figure 2.4) produces a reduction of the radiance received by the instrument. The measurements carried out in this thesis using a SQM are almost unaffected by this problem. The inventory of lights of the regions we studied are mainly formed by high pressure sodium discharge lamps, LED of 3000 K and 4000 K CCT and metal halide lamps. Their emission spectrum coincides with high sensibility ranges of the SQM. Even the peak in the blue region of the LEDs, which is close to 450 nm, is not misread since the sensitivity of the SQM for this wavelength is over 80%.

The SQM-L is the instrumentation used for assessing the zenith sky brightness in large areas of Catalonia. The strategy is to place it on the roof of a vehicle and take measurements every few seconds while driving around the target region. As an example, figure 2.6 shows the zenith SQM sky brightness map from Montserrat area located north-west of Barcelona. See chapter 4 for further information of how this maps are obtained.

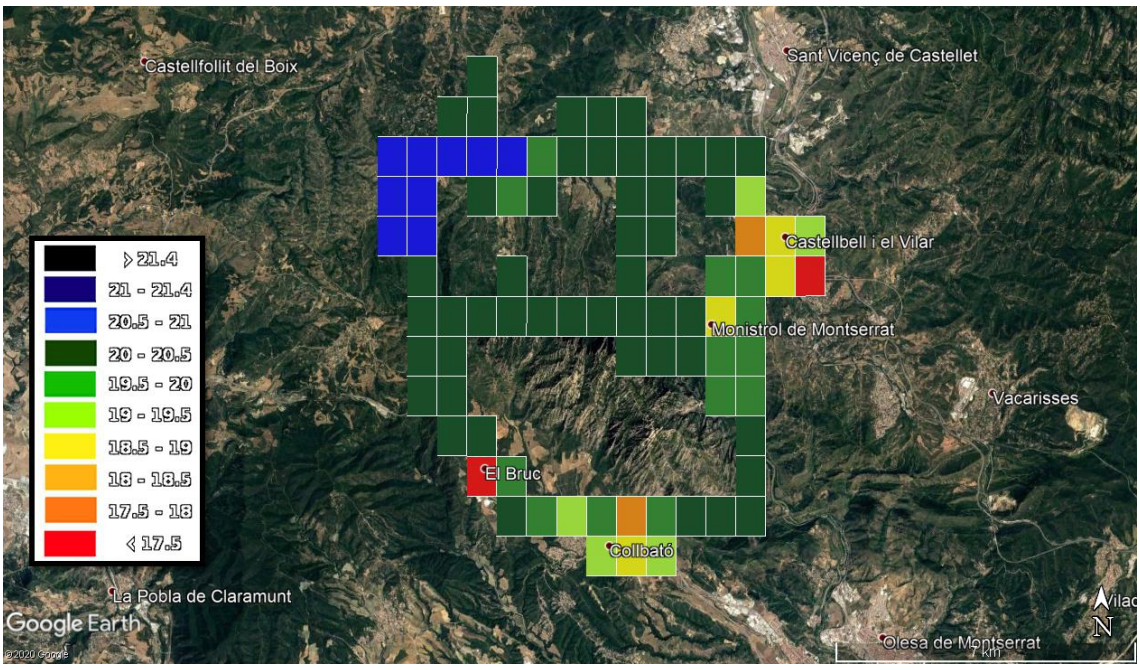

Figure 2.6: Zenith SQM brightness map made with dynamic measurements in the area of Montserrat near Barcelona.

2.2.2 Calibrated DSLR cameras

The combination of DSLR cameras with fish-eye lenses form a tool able to gather information from the whole sky dome in one measurement (image) (see figure 2.7). The reduced dimensions of a DSLR camera makes it easy to carry, a considerable advantage over other all-sky instrumentation like ASTMON (see section 2.2.3).

DSLR cameras are normally based on complementary metal oxide semiconductor (CMOS) sensors. State of the art cameras have normally a dynamic range of 1 to 4000 for a single exposure (Hanel et al. 2018). However, DSLR images cannot be used directly for measuring sky brightness. They should go through a reliable calibration process first, consisting in:

- Dark Frame Calibration. The DSLR cameras lack of cooling system produces an uneven accumulation of dark current in the pixels during an exposure. This effect can be removed by subtracting a dark frame that also deals with the bias of the camera.
- Vignetting. Fish-eye lens transmission can degenerate up to 50% in the image edges with respect to the center of the image. Typically the vignetting measure is taken in a lab with an integrating sphere that allows to correct the vignetting with an error below 2% (Hanel et al. 2018).
- Spectral response and color sensibility. Once the image is corrected by the two processes explained before, it is possible to extract brightness values. DSLR cameras use a Bayer matrix that consists in pixels sensible to red (R), green (G) and blue (B) colors. The combination of the different signals received by the pixels creates the full color images. The G sensitivity is similar to the Johnson-Cousins V band although it can vary slightly between camera models. Using a specific software the signal received in the three bands can be transformed to simulate the response of a Johnson-Cousins V band. The error in the color transformation is below 3% (Kolláth 2010).

There exists software programs that deal with DSLR calibration such as IRIS (Buil 2015), imageJ (ImageJ 2015), PyASB (Nievas & Zamorano 2013) (explained in section 2.2.3) and dclum (Kolláth 2010).

In this thesis, we used the Sky Quality Camera (SQC) system developed by Euromix. The system consists first in calibrating a commercial camera and then providing a image processing software that transforms the images taken with the calibrated camera to all-sky brightness maps for the V band expressed in mag/arcsec^2 (see figure 2.7).

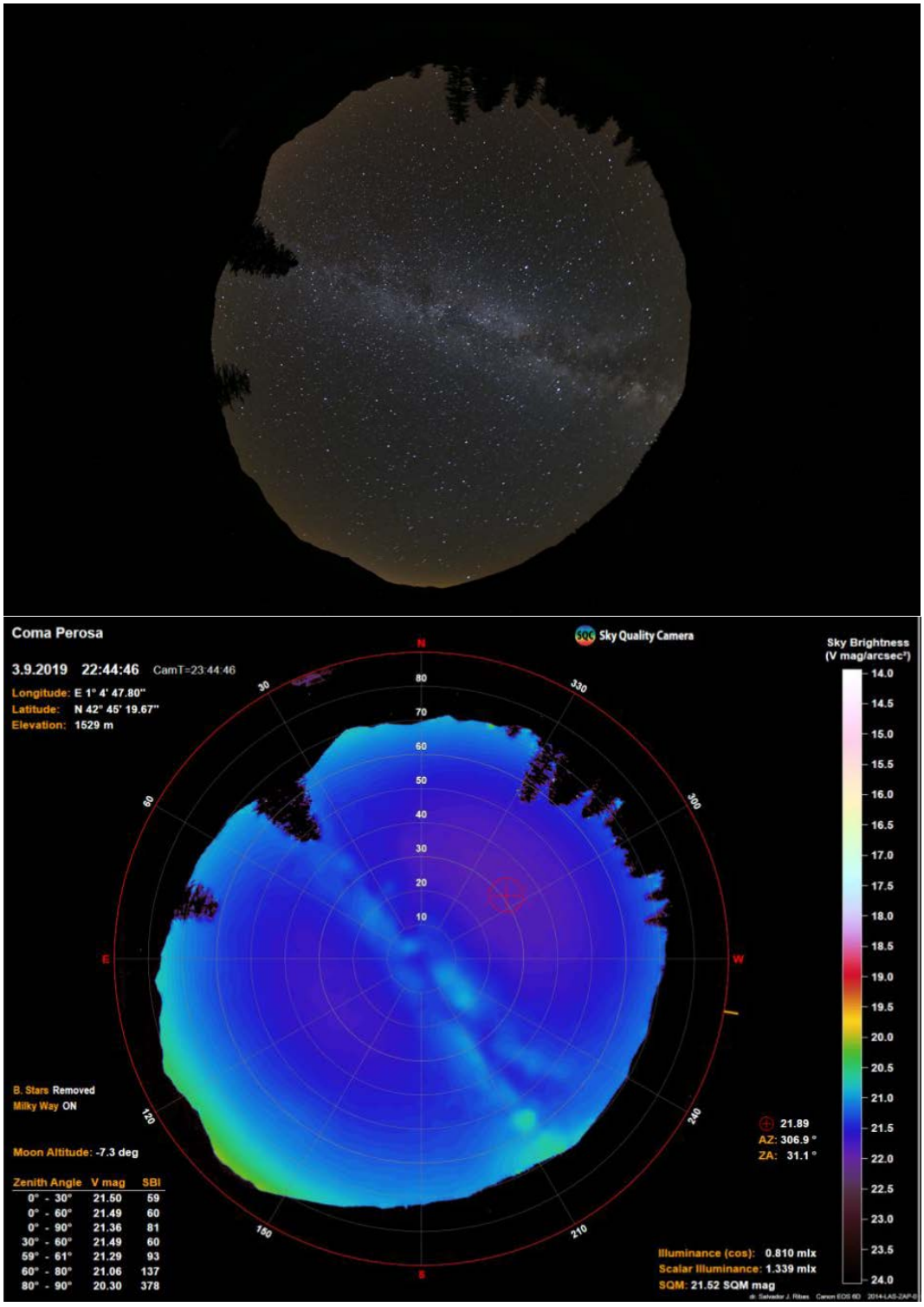

Figure 2.7: Top: fish-eye lens DSLR camera image taken by the author in the Pyrenees area close to Montgarri refuge in Vall d'Aran. Bottom: same image processed by SQC software showing sky brightness levels in mag/arcsec^2 in V band. The calibrated image is rotated in order to place the north in the upward direction.

Most of the target locations explained in the objectives of the thesis (section 1.6) have been measured using this methodology. Beyond the assessment the images provide, they have been used as a validation tool for simulation methodologies.

Processed DSLR camera images with SQC were already used in Catalonia for environmental projects. The projects aimed to study light pollution in different atmospheric conditions with different public inventories configurations (Jechow et al. 2018, 2017). The measurements taken in this thesis provide continuity to the measurements already available.

2.2.3 All-Sky Transmission Monitor (ASTMON)

The All-Sky Transmission Monitor (ASTMON) is a bi-dimensional instrument that maps the entire sky creating all-sky map (see Aceituno et al. (2011) and Hanel et al. (2018)). It measures sky radiance in mag/arcsec^2 allowing to use multiple spectral bands.

It is produced by ITEC Astronomica company. It is based on a f = 4.5 mm fisheye lens and an integrated astronomical CCD camera. The system is designed to perform a continuous monitoring of the surface brightness of the night sky background in a fully robotic mode. In addition to the sky radiance, ASTMON can provide atmospheric extinction and cloud coverage estimates for the entire sky surface at the same time. The CCD detector is usually a Kodak KAF-8300 sensor of 8.3 megapixels, with a pixel size of 5.4 μm. This configuration provides a scale of 3.8 arcmin per pixel. The filter wheel of the instrument can contain 1, 3 or 5 slots. The most common configuration is with B, V and R filters. Precision values of B, V and R can get close to 0.02 mag/arcsec^2.

The calibration process is based on astronomic photometry (Aceituno et al. 2011). It starts with an all-sky image acquisition in one of the available bands. This image have to fulfill the conditions of having a good signal to noise ratio and showing a fair quantity of stars. Cross-matching the image data with star catalogs allows to calibrate ASTMON images.

ASTMON has a software to process the images, but it is a closed system and does not allow to control quality parameters. This fact encouraged alternative programs. Nievas & Zamorano (2014) developed a Python code named PyASB to process ASTMON images and other all-sky devices that has been used in several light pollution studies (see figure 2.2). It has been used also with the ASTMON images used in this thesis. A comparison between the all-sky maps generated with the original software and PyASB for the same data is shown in figure 2.9.

Figure 2.8: ASTMON Lite instrumentation, this version is designed as a portable device.

There are ASTMON devices installed in several astronomic observatories and research centers in Spain. There are permament devices in the Calar Alto Observatory (Almeria), the Roque de los Muchachos Observatory (La Palma Island), the Teide Observatory (Tenerife Island) and the Universidad Complutense de Madrid; and portable devices in Doñana National Park and Montsec Protected Area.

Although the author did not use directly this device, measurements taken by Parc Astronomic Montsec have been used to validate results in the three Johnson-Cousins filters studied, B, V and R.

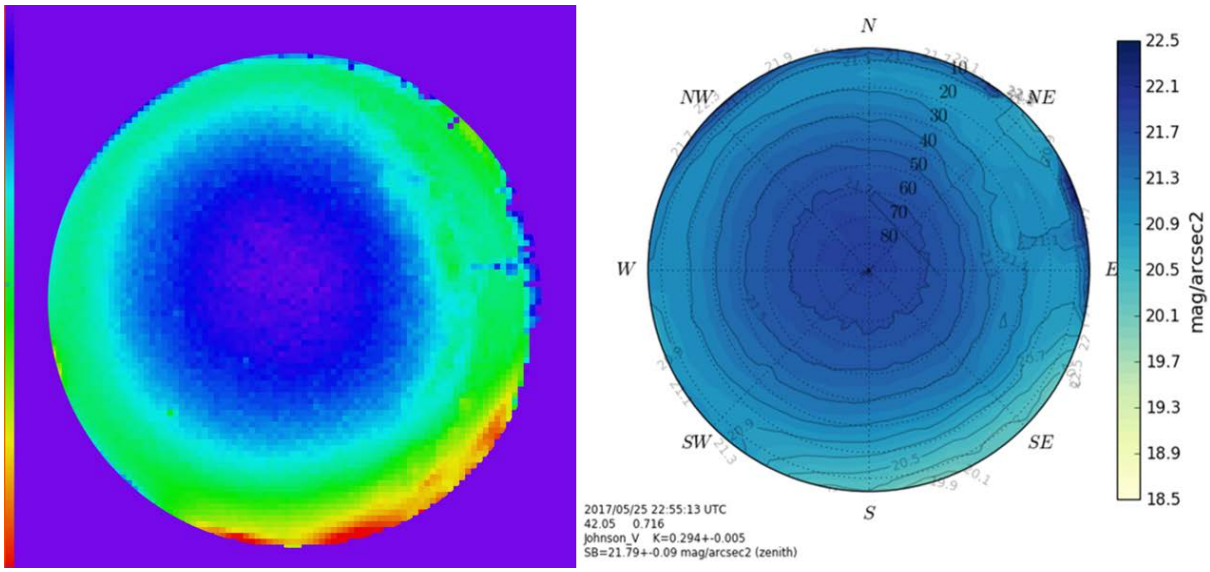

Figure 2.9: All-sky maps produced with data acquired by ASTMON instrumentation. Left: data processed with ASTMON original software. Right: data processed with PyASB.

Chapter 3

Measurement campaigns

In this chapter all the sky brightness measurements taken in the framework of the PhD program are gathered together. They are organized in annually campaigns, from 2017 to 2020.

The first goal of the measuring line of action is the characterisation of the night sky in large regions of Catalonia. Most of the areas covered fulfill the requirements of possessing a dark sky. Some of them are protected areas defined as natural parks (NP) within the framework of territories categorization defined by the Generalitat de Catalunya. However, measurements are not limited to them or their surrounding areas (see figure 3.1 to see the areas studied throughout the PhD program grouped by year).

The methodology used for covering such vast areas are SQM dynamic measurements. The setup consisted in linking the measurement taken with a SQM placed on the roof of a vehicle with its location, obtained with a GPS location tracker. Along the four campaigns more than 3500 km have been covered and measured assessing this way the night sky over a great percentage of the surface of the country. With the information gathered with this method, it is possible to create zenith brightness maps. In this sense, we developed the M2M processing tool, a software with the goal of easing and speeding up the data processing for creating zenith brightness maps from SQM measurements (see section 3.1).

The second goal of the measuring line of action is the detailed assessment of the sky over specific locations. We used DSLR images calibrated with SQC software to obtain all-sky brightness maps in the V band of the Johnson photometric system. Seven locations have been studied using this method: Observatori Astronòmic Montsec, Centre Astròmic Prades, Pic du midi de Bigorre, Valle del Roncal, Pic de

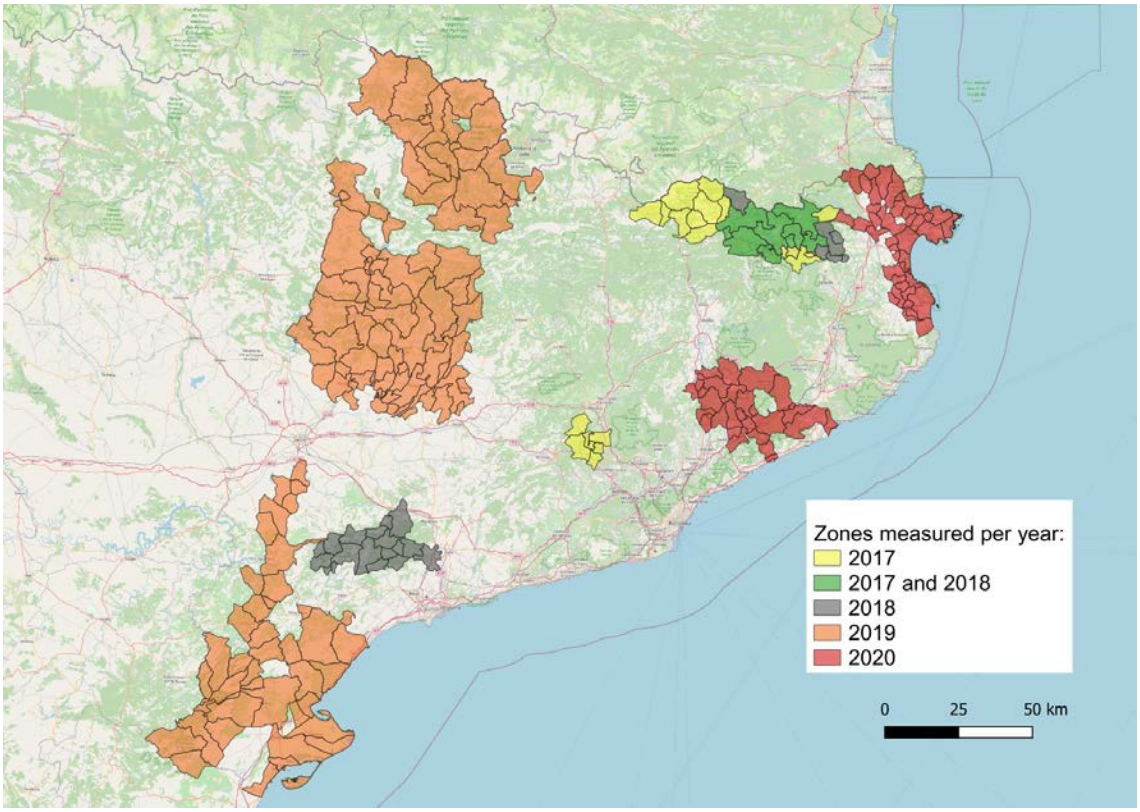

Figure 3.1: Areas covered during the zenith brightness assessment campaigns grouped by year.

l'Orri, Montgarri refuge and La Força d'Àreu (see figure 3.2). Most of the resulting all-sky maps were used too as a validation tool for simulations (see chapter 5).

The measurements presented in this chapter are part of at least one of the two following projects: the night quality assessment of natural zones in Catalonia defined by the Departament de Territori i Sostenibilitat de la Generalitat de Catalunya; and the Interreg POCTEFA project Pyrenees la Nuit (PLN) financed by the European Union.

The night quality assessment of natural zones in Catalonia project is carried away by two institutions, the Parc Astronòmic Montsec (PAM) from 2012 and the Institut d'Estudis Espacials de Catalunya (ICC-UB-IEEC) from 2014. We participated with both institutions. The dynamic SQM measurements are exclusively part of this project. The long term goal is the creation of a complete light pollution SQM map of the country. With our measurements we contributed greatly to achieve it. More information about the project in the web page of the Departament de Territori i Sostenibilitat, in the moment of the writing: http://mediambient.gencat.cat/.

Figure 3.2: Locations where sky brightness has been measured and/or simulated. A: Montsec Observatory, OAdM. B: Prades astronomy center. C: Montgarri. D: Montsant natural park. E: Estany Llong. F: Pic de l'Orri. G: Valle del Roncal. H: Pic du Midi. I: La Força D'Àreu.

The Pyrenees la Nuit project focused on the study of the night sky over specific locations. From the seven locations studied four are within the framework of the campaigns assigned by the Departament de Territori i Sostenibilitat, two within the framework of the Pyrenees la Nuit, and one shared by both projects.

The following sections are dedicated first to explain the data processing of the SQM measurements. Second, each campaign is described in detail: they include the results obtained using both methods (dynamic SQM measurements and DSLR images calibrated with SQC software) and a complete discussion of each area covered. Third, a summary of all the campaigns as well as an analysis of Catalonia using all the information obtained. Finally, a general discussion of the methodology, its limitations and the challenges to face in the near future.

3.1 Dynamic SQM data processing

As stated before, SQM dynamic measurements consist in gathering multiple SQM readings linked to their position and time. With this information it is possible to create zenith sky brightness maps of the regions covered. The goal is to obtain reliable sky brightness maps that are easy to interpret. In this sense, the best option found so far are cell maps. This kind of map consists in dividing the area studied in a set of surface cells that have a specific color linked to the mean brightness level of the area covered by the cell. The mean value of each cell is obtained by averaging all the measurements taken within the borders of the cell.

Before creating the maps, the data needs to be processed to remove outliers and invalid values such as those taken below street lamps, when crossing tunnels, when other vehicles brighten the sky, etc.

We have implemented the processing methodology presented by Ribas (2016) in a Python executable for Windows and Linux-based OS. The resulting software was baptized as M2M (Measurements to Map) and presented in the LPTMM conference of 2019 held in Szelic, Hungary. The goal is to make the software a standard in the community that uses SQM or similar devices for assessing the quality of the night sky. The software is free and available upon request.

M2M software is formed by three main blocks: data reading and display, filtering, and map creation. They are explained in detail in the following sections.

3.1.1 Data reading and display

M2M allows to work with the two main programs used to acquire SQM dynamic measurements:

- "Sistema de Medición de Contaminación Lumínica" best known by its former name "RoadRunner" (Rosa Infantes 2011). It works by linking the SQM with a GPS device through a laptop. Hence, every measurement is defined by its position and time. The output are two files: a *csv* and a *kml*. Both files show every measurement in its location, very useful for visual purposes as spotting strange values due to vegetation, tunnels, etc.

- Unihedron device manager. It is the software developed by Unihedron company, producer of the SQM device. It was presented some time after the RoadRunner software was already available. The idea is similar: to link SQM

values with their position and time. The output of this software is a generic data file.

Both data files (*csv* from RoadRunner and *dat* from Unihedron device manager) are organized in such a way that every row corresponds to a measure. Every row contains several columns with information as UTC time, local time, temperature, SQM brightness value, position, number of GPS satellites available, distance from the previous measurement, etc. M2M software computes and displays the most relevant information to the user once the data file is selected as it is shown in figure 3.3.

Besides the general information, M2M plots the data for visual purposes. The user can switch between seeing the data against the distance covered or the time when the measurements were taken. The plots are useful for identifying outliers and checking the filtering process.

3.1.2 Filtering

Normally, the data gathered needs filtering. The presence of vegetation, tunnels, light coming from crossing vehicles and other altering elements create wrong measurements that do not represent the quality of the sky we try to assess. In clear paths typically between 5 and 10% of the measurements have to be removed. In paths with dense vegetation the number can increase up to 60%.

Filtering by hand such a number of values is an arduous task. For that reason, Ribas (2016) proposed a statistical filtering methodology that has been slightly modified when creating the M2M software and complemented with an easy to use manual filtering option.

The statistical filtering consists in:

- Upper cut. The darkest value the user accepts as valid. It is useful for removing measurements under non-lit tunnels, clouds in dark sites and even wrong measurements of the SQM that occur sometimes when the brightness level changes abruptly. We used an upper cut of 22.0 mag/arcsec^2. The areas we covered are not expected to get close to this threshold. As a matter of fact the darkest valid measure we obtained was 21.78 mag/arcsec^2 close to the Parc Astronòmic Montsec.
- Lower cut. The brightest value the user accepts as valid. It normally gets rid of values affected by direct light from street lamps, lit tunnels and other

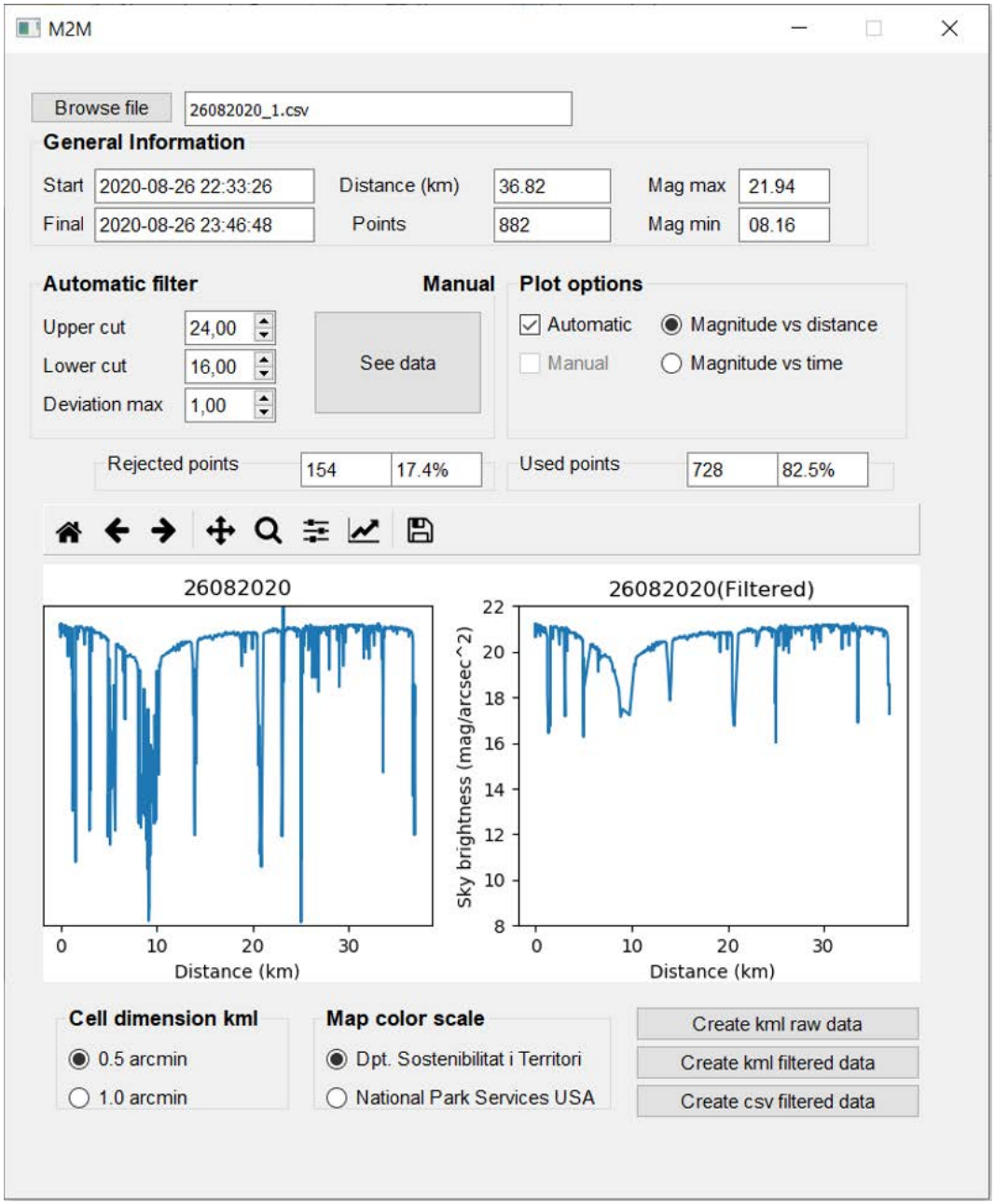

Figure 3.3: Visual appearance of M2M software. The top of the display corresponds to the general information of the file selected. Below it the filtering and plot options (the button "See data" leads to manual window panel). Below that, the graphic display of the data, in parallel raw and filtered data. At the bottom the features of the light pollution map and the menu for creating different files.

vehicles. We used a 16.0 mag/arcsec^2 threshold.

- Deviation from contiguous values. Each value is compared with its previous and posterior measurements. Originally, in the work of Ribas, if the measurement differed more than a certain threshold (darker and/or brighter) from both of the previous and posterior value, the measurement was discarded. After processing many nights, we found out that this method discarded valid data when measuring areas with dense vegetation. In this situation it happens that there are more wrong measurements than valid ones. For that reason M2M is designed to only discard values that are brighter than its companions but not darker ones. The default threshold is established in a deviation of 1.0 mag/arcsec^2, i.e. if a measure is 1.0 mag/arcsec^2 brighter that the previous and posterior ones, it is removed.

- Standard deviation. Before creating the final light pollution map, each cell is studied separately. The values that differ more than three times the standard deviation from the mean value of that particular cell are removed. The process is done again without taking into account the discarded values. This method aims to remove outliers that could have eluded the other filters. Unlike the other filters, this one can not be customized by the user.

The manual filtering option allows to discard values by hand. The knowledge of the casuistic of the routes covered is very helpful in this sense. For instance, manual filtering is necessary when dealing with dense vegetation that produces a brightening effect that has no relation with the quality of the sky. However, when the brightening effect is due to the proximity to towns the brightened values should not be removed.

Both filtering methods, statistic and manual, can be used separately or combined. In figure 3.4 we can see the comparison between raw data and filtered data with the different methods available.

The data display embedded in M2M shows the plot corresponding to unfiltered data and filtered one in an easy way to compare them and spot any mistakenly removed value (see figure 3.3).

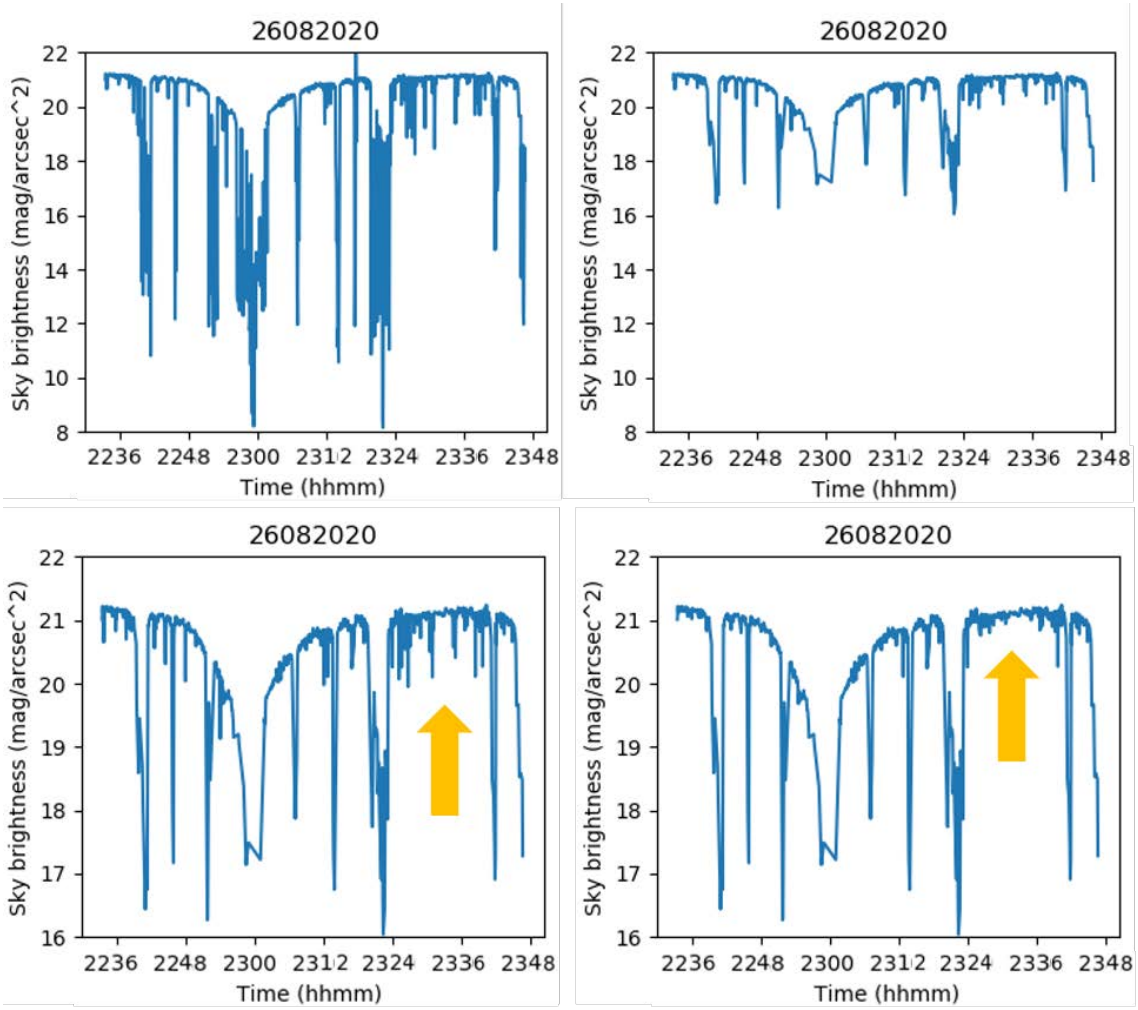

Figure 3.4: Top left: raw data. Top right: statistic filtering. Bottom left: statistic filtering zoomed plot. Bottom right: statistic and manual filtering. Orange arrows point out a particular set of data that shows significant changes after the manual filtering.

3.1.3 Map creation

As stated before, the map consists in surface cells that show the mean brightness level of the region they cover. The mean value is computed using every validated measurement taken within the range of the cell. M2M configuration allows to choose between cells of 1.0x1.0 or 0.5x0.5 arcmin (within Catalonia 1 arcmin is equal to approximately 1.4 km in longitude and 1.8 km in latitude). For our measurement campaigns we used 0.5x0.5 arcmin cells due to its higher resolution.

To make it visually user-friendly and quick to interpret, cells follow a color scale depending on its brightness levels. There is no consensus in the community in which color scale to use for representing sky brightness levels. As stated in the introduction of this chapter, the SQM measurements presented here are part of the project of creating a zenith sky brightness map of Catalonia. In that project a quite coarse color scale is used, we named it "Territory department scale". It is great for the outreach purposes of the project but it is not the best choice for scientific work. For that reason, in this thesis we use an adaptation of the more detailed color scale used by Parc Astronomic Montsec inspired in the scale from USA National Parks, we called it "National Park scale". Both scales are available in M2M software, they can be compared in figure 3.5.

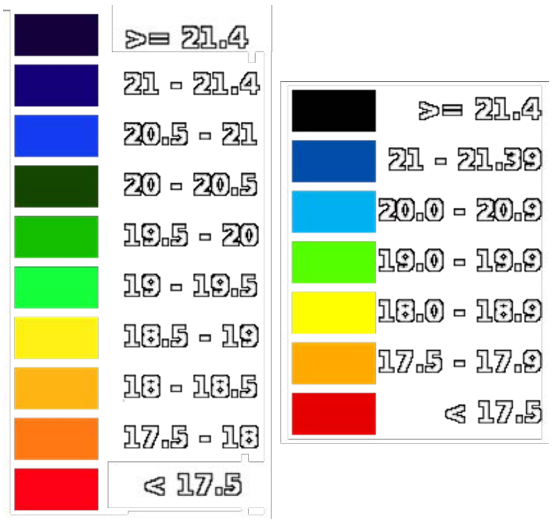

Figure 3.5: Color scales available in the software. Left: "National park scale" (used in this work). Right: "Territory department scale".

Another feature of the software is the displaying of the main characteristics of each cell (see figure 3.6). Map files are created in *kml* format compatible with Google Earth software and other geographic information systems (GIS) packages.

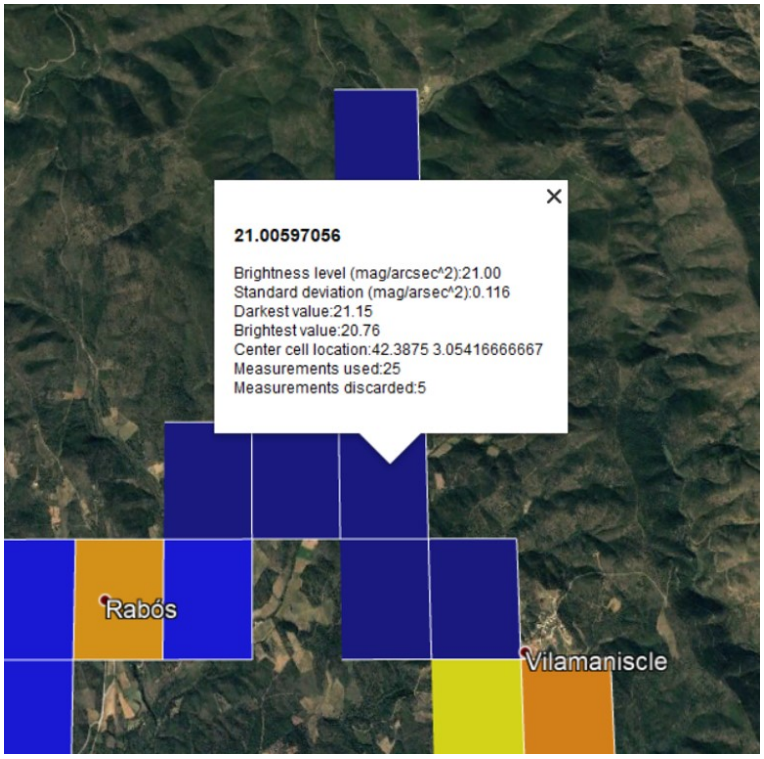

Figure 3.6: Information displayed when clicking in particular cell of the light pollution maps created with M2M software.

3.1.4 Expanding the map

When assessing the quality of the night sky of a region the best scenario would be gathering information that covers it all. However, dynamic measurements are taken following roads that cross or surround the target areas. Normally, the darkest regions are inaccessible sites far from towns and the roads that connect them.

In an attempt to assess these inaccessible regions we tried to develop a methodology that uses the available dynamic SQM measurements to assess nearby areas. The approach consisted in dividing the sky brightness in two components: a global component formed by the natural sky brightness and the artificial brightness coming from far away cities, and a local component produced by towns within the area measured. The sky brightness level is then computed by interpolating the global component and adding the local effect using a simple brightness-distance function. In figure 3.7 the results obtained using this method for Muntanyes de Prades and Montsant NP regions are shown.

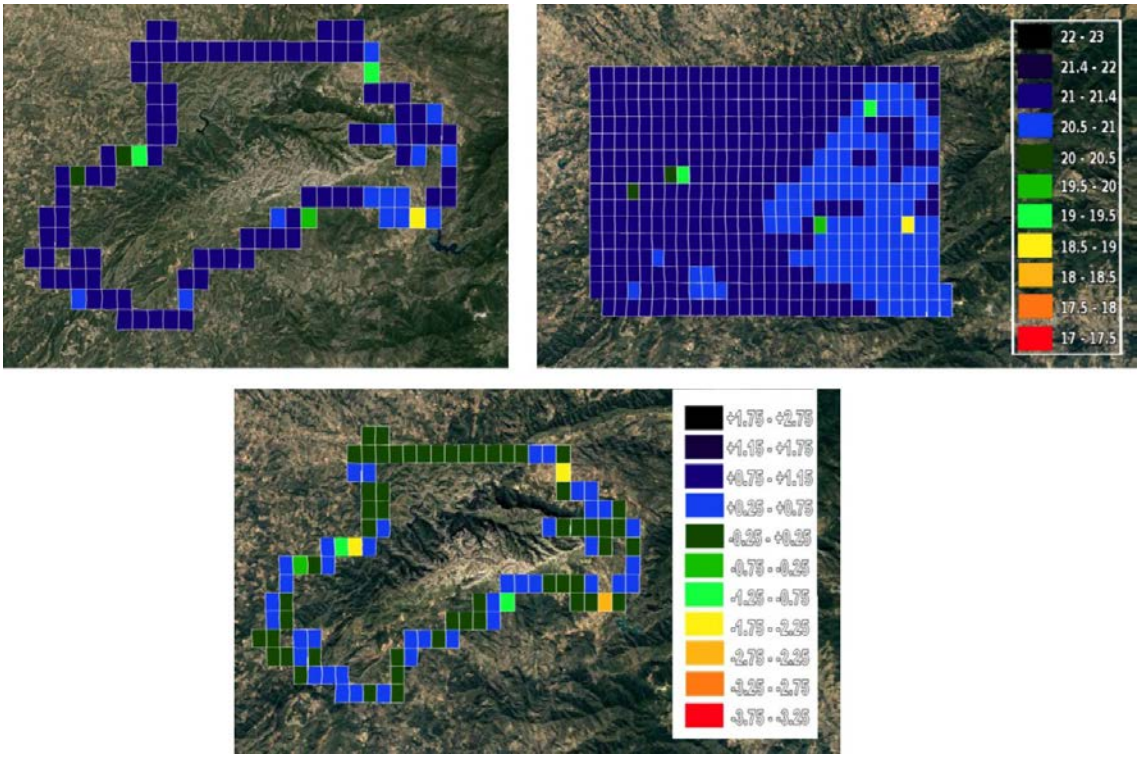

Figure 3.7: Top-left: light pollution cell map of the area of Montsant NP and Muntanyes de Prades created using real SQM measurements. Top-right: light pollution cell map of the same area using the proposed methodology. Bottom: map of the diferences between the the values of the cells measured using SQM measurements and the methodology explained.

The project was not developed further. We found out that this approach was strongly dependent to local variables and was not reliable to implement as a standard. On the other hand, using state of the art light pollution models fix the problem of assessing inaccessible sites. As we advanced in the study and comprehension of complex and accurate light pollution models we were able to obtain products as the zenith brightness map of Catalonia, see section 5.4, that covers the whole country in a grid of 5x5 km.

3.2 Measurement campaigns

The instrumentation used for the SQM dynamic measurements presented in the following sections were a photometer SQM-LU (serial number 1871), a GPS Garmin eTrex Hcx (16C145169) and a PC DELL Latitude E6320. The camera used for obtaining the calibrated all-sky images is a commercial DSLR camera, a Canon EOS 6D, which has a full-frame CMOS sensor with 20.2 Megapixel (5496 x 3670 pixels). The camera has a built-in GPS sensor, and allows ISO settings from 100 to 25600 and shutter speed ranges down to 30 s in automatic mode. We operated the camera with a circular fisheye lens (Sigma EX DG with 8 mm focal length) always at full aperture of 3.5. For further information about the instrumentation see section 2.2.

All measurements were taken during moonless clear nights. A maximum velocity of 80 km/h was established when taking dynamic SQM data. The limitation is imposed in order to avoid alterations due to air turbulence and to ensure that measurements are close enough to each other to provide continuity to the cell maps.

The annual campaigns that took place between 2017 and 2020 are described in detail in the following sections. For a quick summary see table 3.5 in section 3.3.

3.2.1 2017 campaign

During this campaign three regions were studied: Capçalera del Ter and Alta Garrotxa in the east Pyrenees (covered by P. Massana, G. Martí and the author), and Montserrat NP in central Catalonia (assessed by E. Masana and the author) (see figure 3.1). The areas were covered in five nights: four nights for the two first areas and one night for Montserrat.

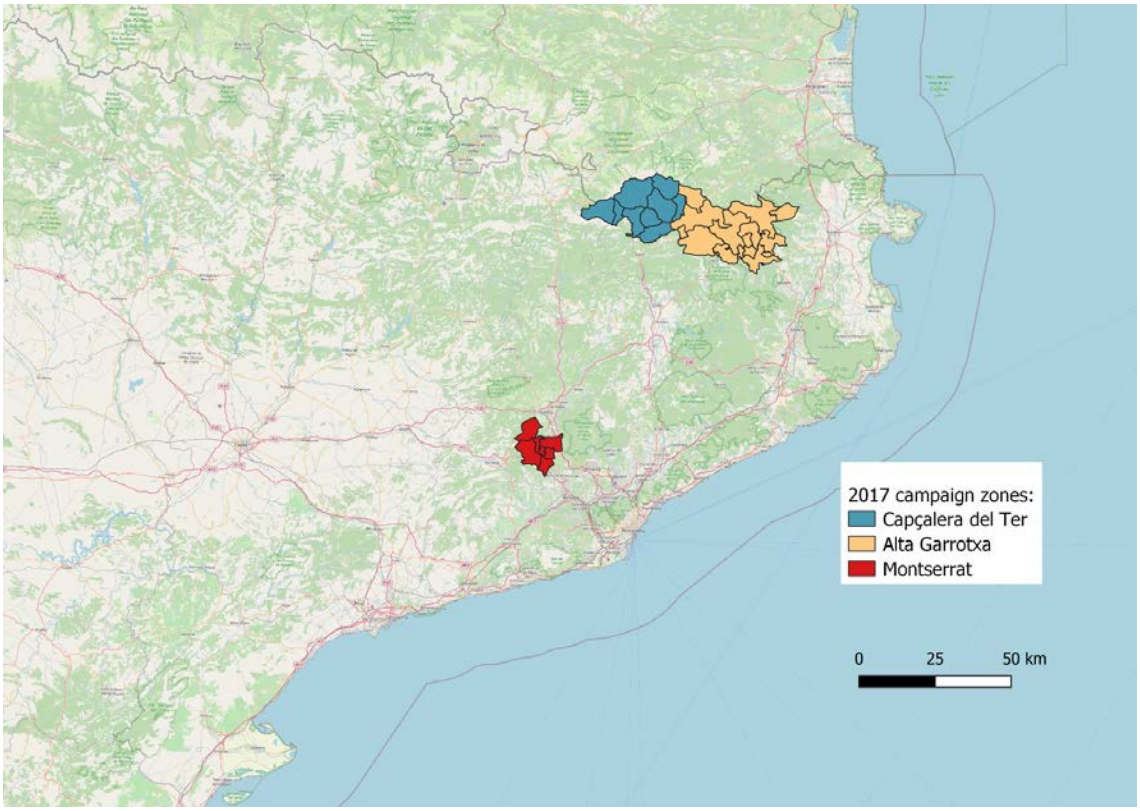

Figure 3.8: Areas covered during the 2017 campaign.

Region	Dates	Distance covered (km)
Capçalera del Ter	24-08-17, 13-09-17, 21-09-17	225
Alta Garrotxa	13-09-17, 21-09-17, 13-11-17	150
Montserrat	23-10-17	80

Table 3.1: Area covered in the 2017 light pollution assessment campaign.

Eastern Pyrenees

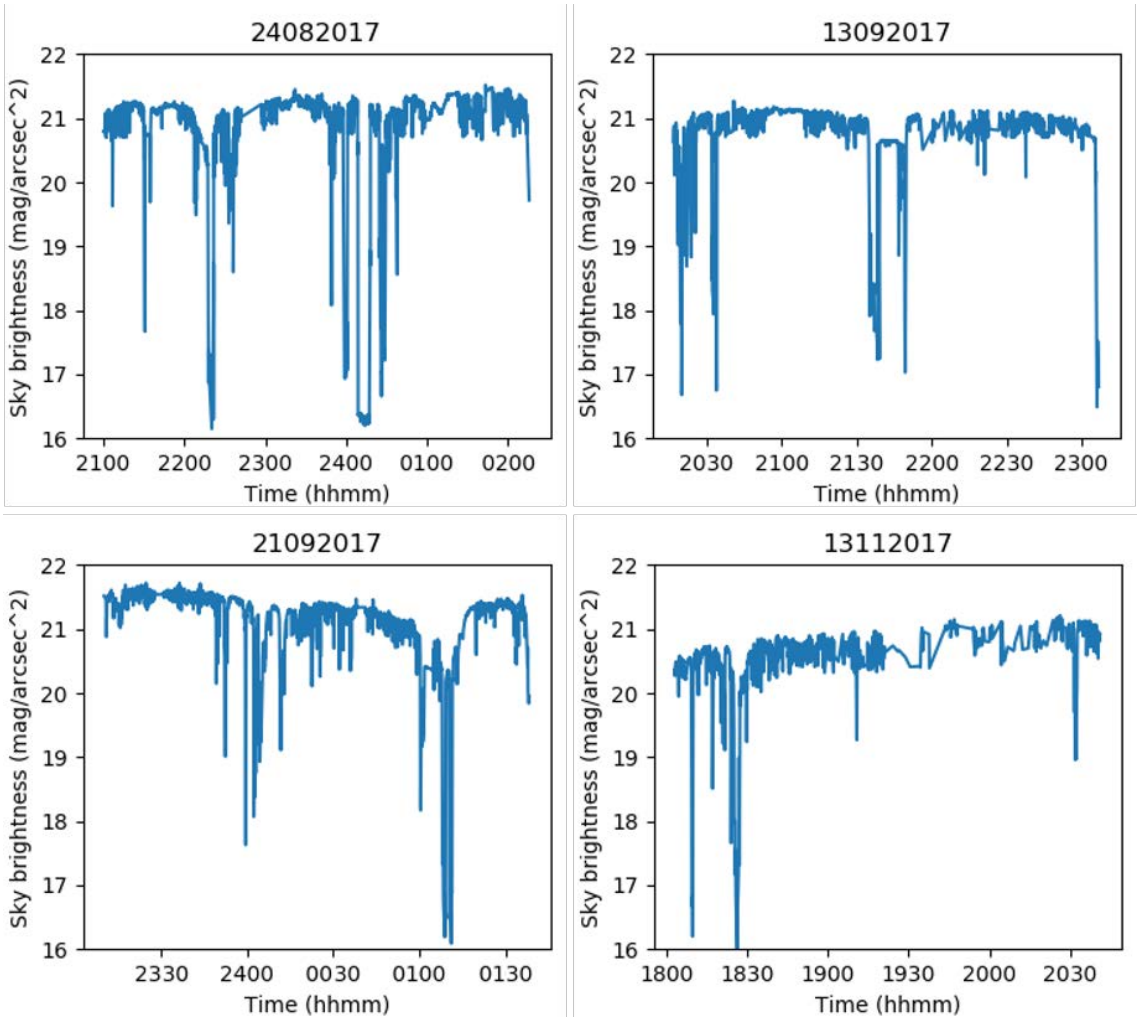

Figure 3.9: SQM values along the nights when the eastern Pyrenees region was studied in the 2017 campaign. Time code: hhmm.

The eastern Pyrenees is a quiet dark region. Most of the cells that are not close to towns are above 21.0 mag/arcsec^2 or very close to that value. The most northern region studied possesses an excellent quality of the night sky with values over 21.4 mag/arcsec^2, even with some close to 21.6 mag/arcsec^2. The eastern region appears slightly brighter probably due to its proximity to cities as Figueres, Girona and the coastal line.

The towns present in the area studied have small areas of influence. The three biggest areas are the ones produced by Camprodon, Ribes de Freser and the conglomerate between Olot and Besalú in the south path.

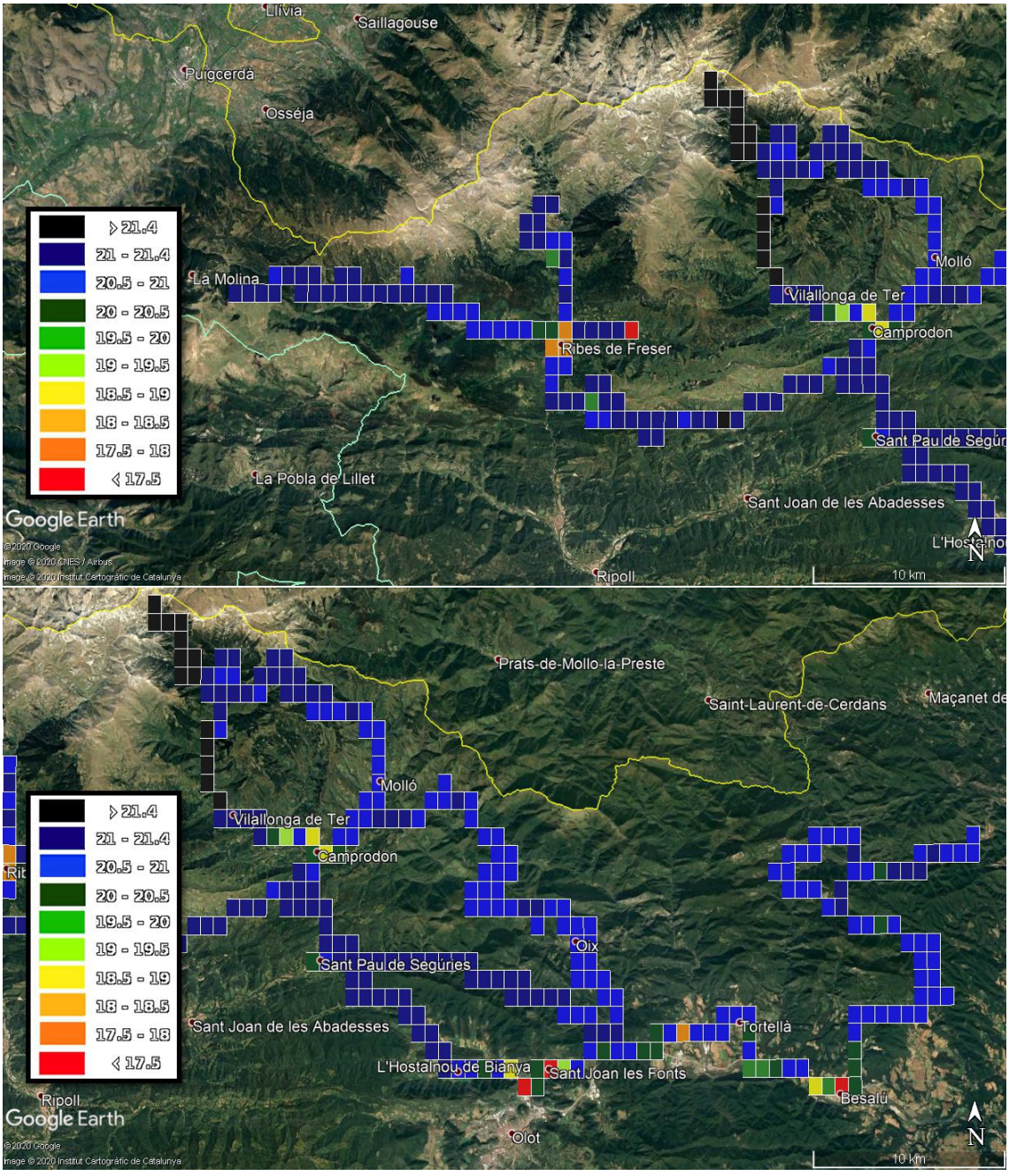

Figure 3.10: Light pollution map of the eastern Pyrenees, formed by Capçalera del Ter (mostly top image) and Alta Garrotxa (mostly bottom image) sub-regions.

The whole region presents dense vegetation that complicated the processing of the data. In the most eastern part, the branch located to the north of Besalú, an average of 60% of the measurements had to be filtered. The initial route for this branch was a loop that finished at Tortellà, but due to a heavy storm the road was inaccessible. The following year the loop was finished.

Another anomaly was the unexpected bright values in the valley that crosses Oix. We think that an unusual high humidity level brightened the measurements. The following year we repeated this route with darker results.

Montserrat

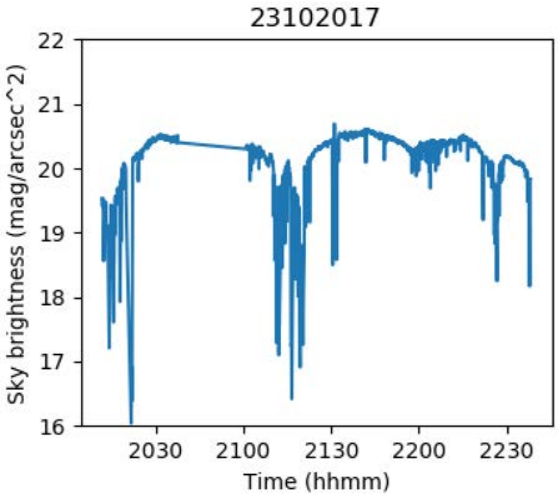

Figure 3.11: SQM values along the night when the Montserrat region was studied in the 2017 campaign. Time code: hhmm.

Montserrat mountain range is located around 40 km north-west from Barcelona. We can see the influence of the metropolitan area as a gradient of darkness towards the furthest side. It should not be considered as a dark sky region. Most of the cells that are unaffected from local towns show values between 20.0 and 20.5 mag/arcsec^2. The darkest cells, placed in the north-west surpass slightly the threshold of 20.5 mag/arcsec^2.

The light pollution coming from Barcelona disguises the effects of the local towns in this region. The light coming from the metropolitan area smooths the contrast between cells that are placed around towns and those that are far away. In spite of that, there are middle-size towns in the east (Castellbí and Monistrol de Montserrat) and south (Collbató) that show a quite big area of influence.

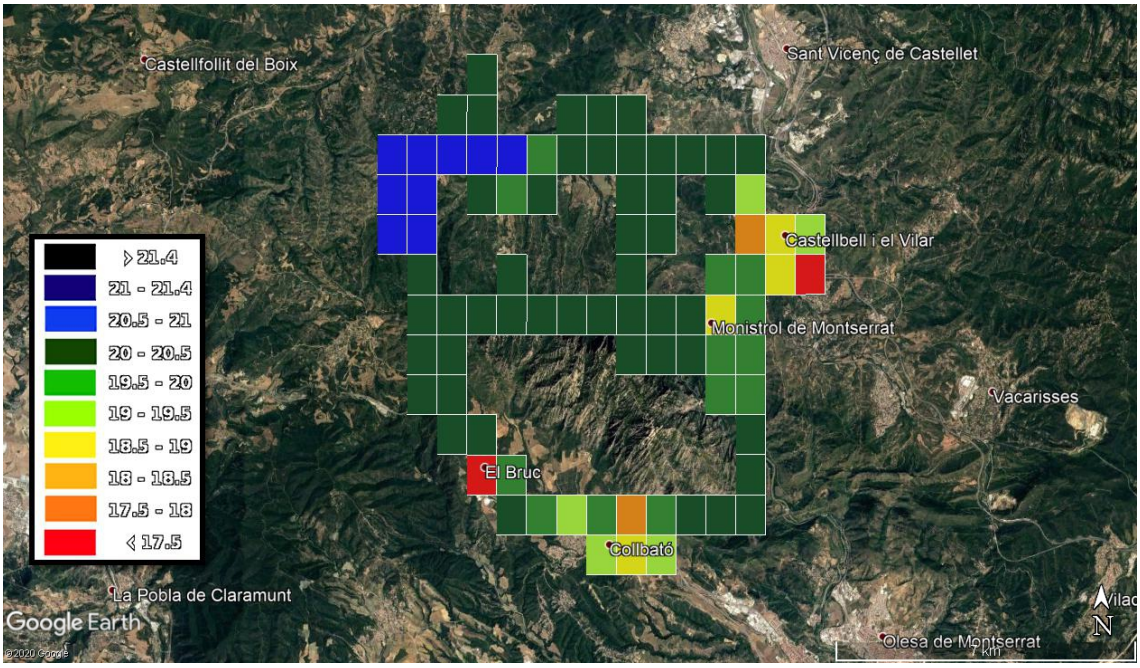

Figure 3.12: Light pollution map of Montserrat region.

The path followed is completely clear from vegetation. The statistic filtering explained in section 3.1 was enough. Only one value was removed manually and curiously was an abnormal dark value.

3.2.2 2018 campaign

During this campaign the area of east Pyrenees (Alta Garrotxa) was partly repeated and partially expanded from the 2017 campaign. The area comprising Prades and Montsant mountains in the province of Tarragona was also covered. The measures were taken by the undergraduate physics student P. Cova and the author. The areas were covered in five nights: three nights for the Montsant NP and Muntanyes de Prades areas and two nights for the north-east Pyrenees. In fact, there was a sixth night of measurements that had to be discarded due to the presence of clouds.

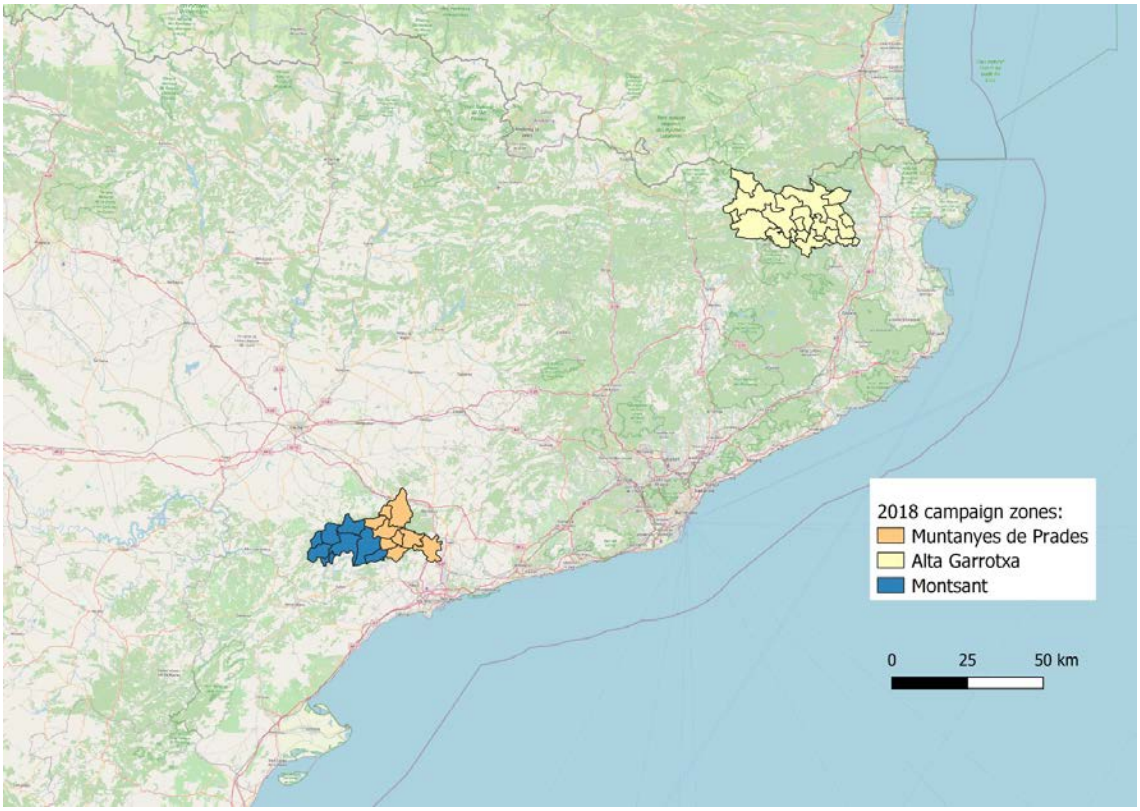

Figure 3.13: Areas covered during the 2018 campaign.

Region	Dates	Distance covered (km)
Alta Garrotxa	12-07-18, 03-10-18	167
Muntanyes de Prades	13-06-18	160
Montsant NP	13-07-18, 13-09-18	152

Table 3.2: Area covered in the 2018 light pollution assessment campaign.

Eastern Pyrenees

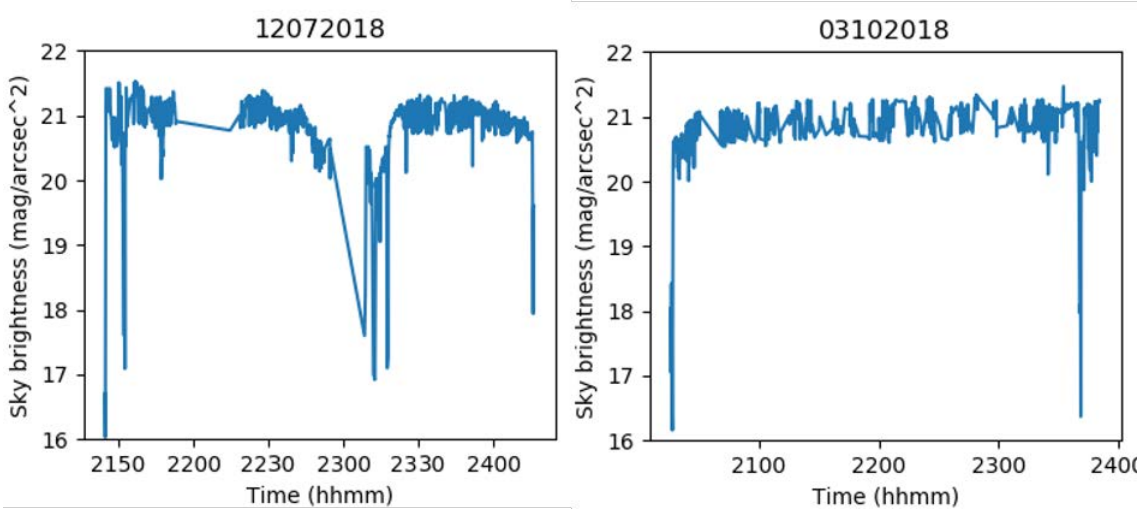

Figure 3.14: SQM values along the nights when the eastern Pyrenees region was studied in the 2018 campaign. Time code: hhmm.

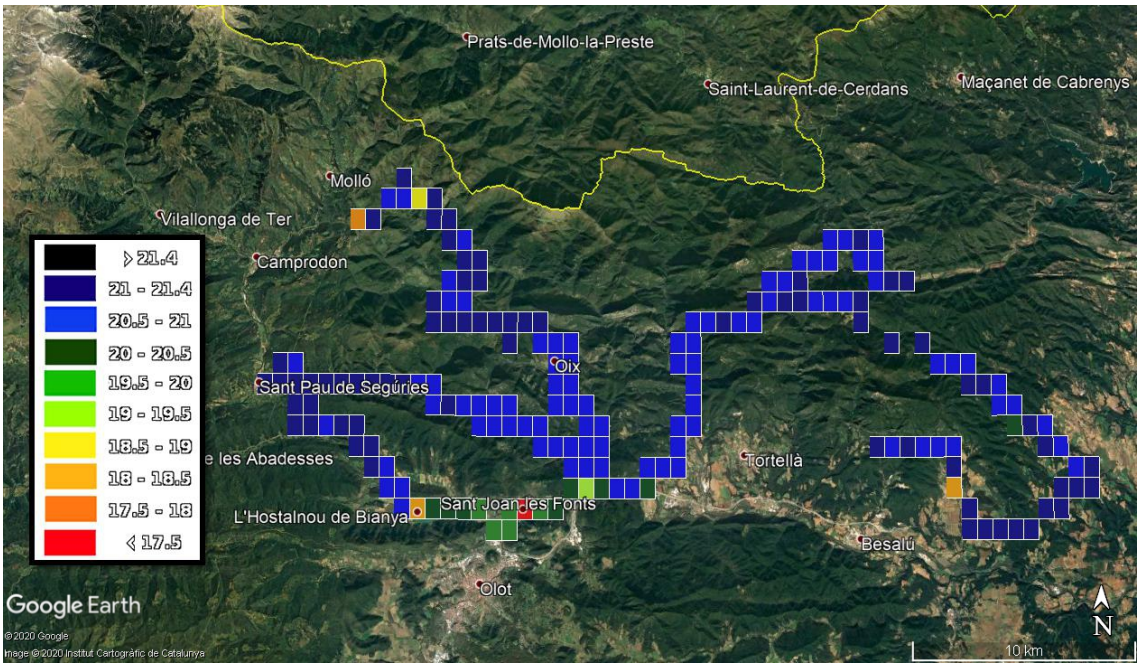

Figure 3.15: Light pollution map of the eastern Pyrenees (Alta Garrotxa subregion).

Alta Garrotxa, as seen in the previous campaign, is a quite dark place. All the cells have values above 20.5 mag/arcsec^2 and many of them go beyond 21.0 mag/arcsec^2. However, zenith brightness does not reach 21.4 mag/arcsec^2 considered the threshold for an excellent dark sky.

The western half of the route was already done in the previous campaign. The loop at the south have similar values but the valley that goes through Oix is notably darker than the year before. This result confirms our hypothesis that during the 2017 campaign that region was measured under unusual humid conditions that brightened the measurements.

The goal on the eastern half was to cover the branch that closes the loop started in 2017. It was inaccessible then due to road damage created by heavy storms. The northern part passes by Albanyà educational astronomy center. With a zenith brightness slightly over 21.0 mag/arcsec^2, it is a good location for an outreach oriented facility but far from ideal for scientific purposes.

Vegetation was dense in the west half and even worse in the east part. In figure 3.14 the filtered data is shown with close than 40% of values removed for the night of the 12th of July (western part) and close to 60% for the night of the 3rd of October (eastern part). Even with that exhaustive filtering, there exists an abrupt profile of measurements, characteristic from areas with dense vegetation.

Muntanyes de Prades and Montsant NP

The weather in Montsant NP and Muntanyes de Prades was far from ideal for our purposes. We achieved to cover all the tracks despite the scarce number of clear nights during moonless periods. Only three nights in a time span of four months met the conditions to measure the night sky brightness. There was a fourth night when the weather prevision seemed to indicate proper conditions, but when we were already there we had to cancel out and head back due to the unexpected formation of extensive clouds.

Montsant NP and Muntanyes de Prades regions are located closer than 40 km north-west from Tarragona, Reus and their metropolitan area. That explains the visible gradient with brighter values in the south-east and darker in the north and west cells. All the cells outside town limits show brightness levels above 20.5 mag/arcsec^2. Many of them surpass 21.0 mag/arcsec^2, although very few go darker. The darkest cells get close to 21.2 mag/arcsec^2.

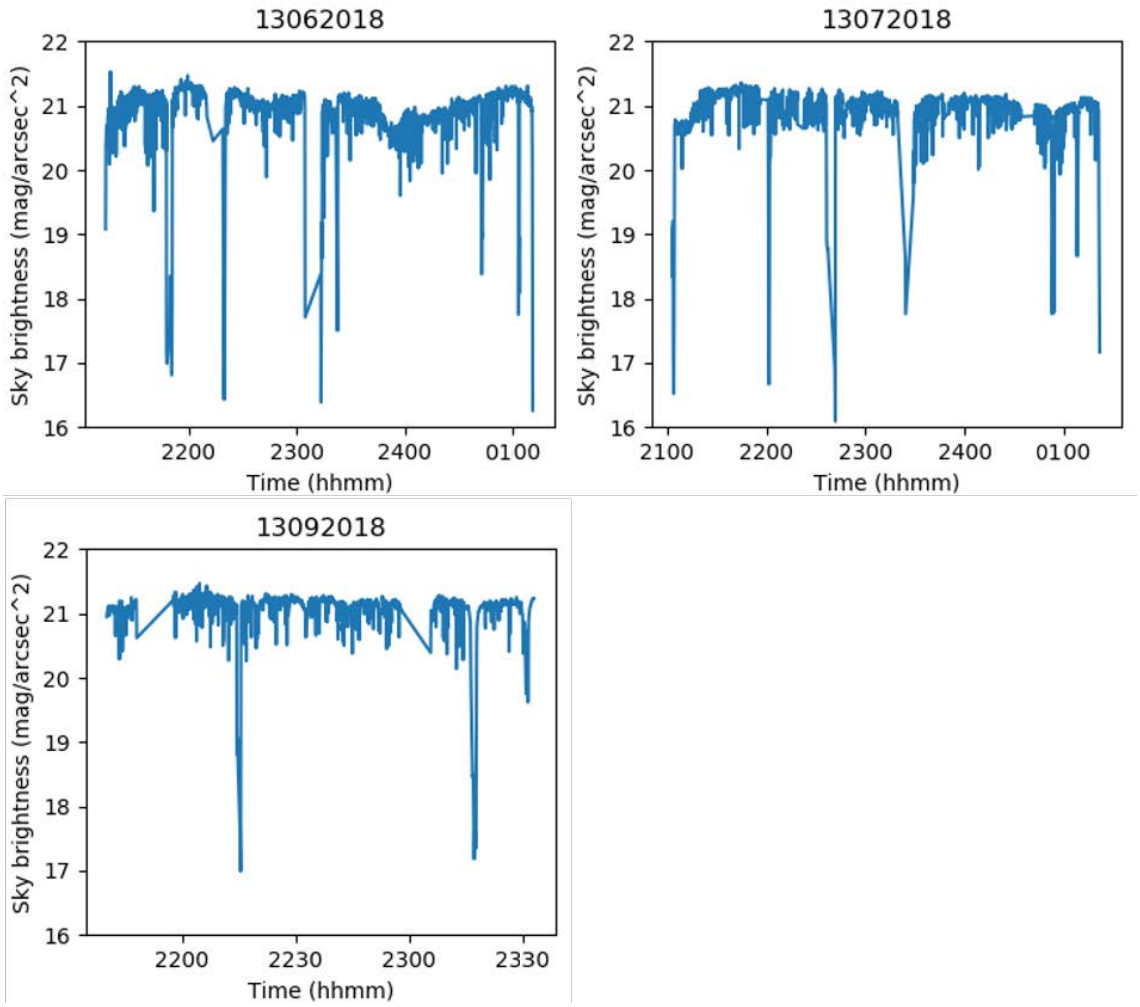

Figure 3.16: SQM values along the night when the Montsant NP and Muntanyes de Prades regions were studied in the 2018 campaign. Time code: hhmm.

The few towns present in the itinerary are small. Consequently, their radius of influence are expected to be small too. However, they are smaller than in similar cases in other regions, meaning that these towns have a proper lighting system. Close to Prades there is the educational astronomy center Centre Astrònomic Muntanyes de Prades. Similarly to the situation in Albanyà in the Pyrenees, it is a well chosen location for astronomy outreach purposes but it is not dark enough for professional astronomy projects.

The vegetation in the area was scarce in most of the branches. Some forest trails, as the ones present in the south-west that are inside the outer ring, presented some vegetation easy to filter.

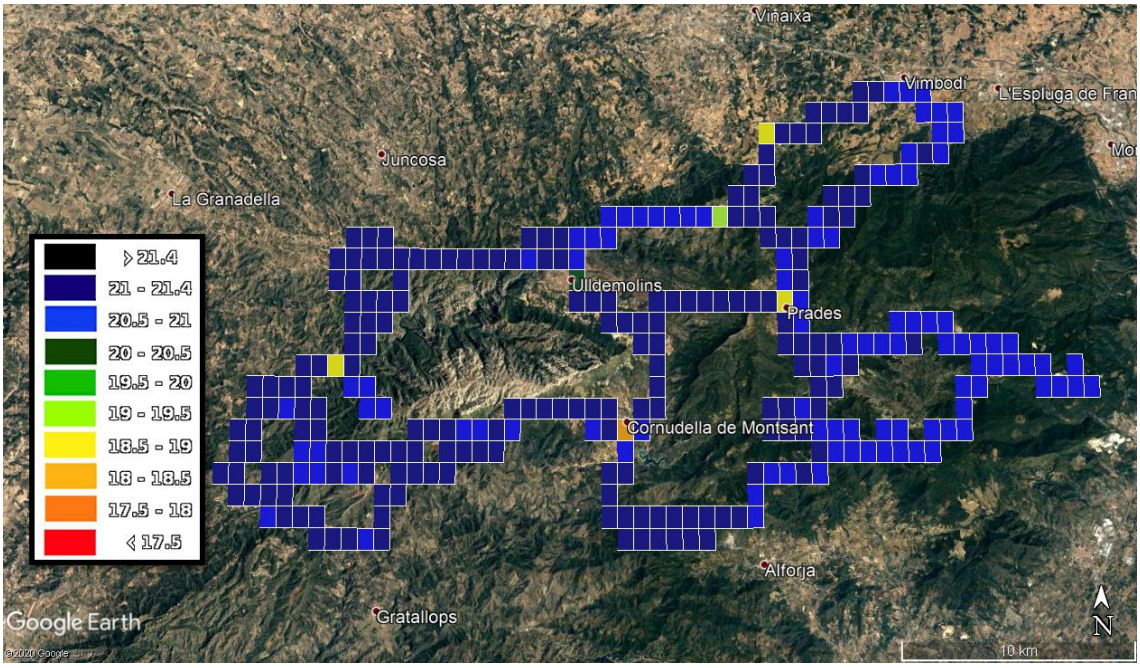

Figure 3.17: Light pollution map of Montsant NP and Muntanyes de Prades regions.

In the 2019 campaign a set of DSLR images was taken near Prades (figure 3.18). It is presented here because it adds information to the 2018 SQM campaign of the same region. The images were processed with SQC software. The estimated SQM value from the SQC image is of 20.70 mag/arcsec^2 slightly brighter than what was measured (between 21.0 and 21.1 mag/arcsec^2). This discrepancy is mainly explained due to the presence of the Milky Way close to the zenith in the DSLR image. The Milky Way was far from zenith when the area was measured with SQM. The darkest direction is shifted to the west from the zenith and has a value of 20.96 mag/arcsec^2. There is a huge source of light pollution from south to north-east that dominates the brightness pattern, due to Tarragona metropolitan area.

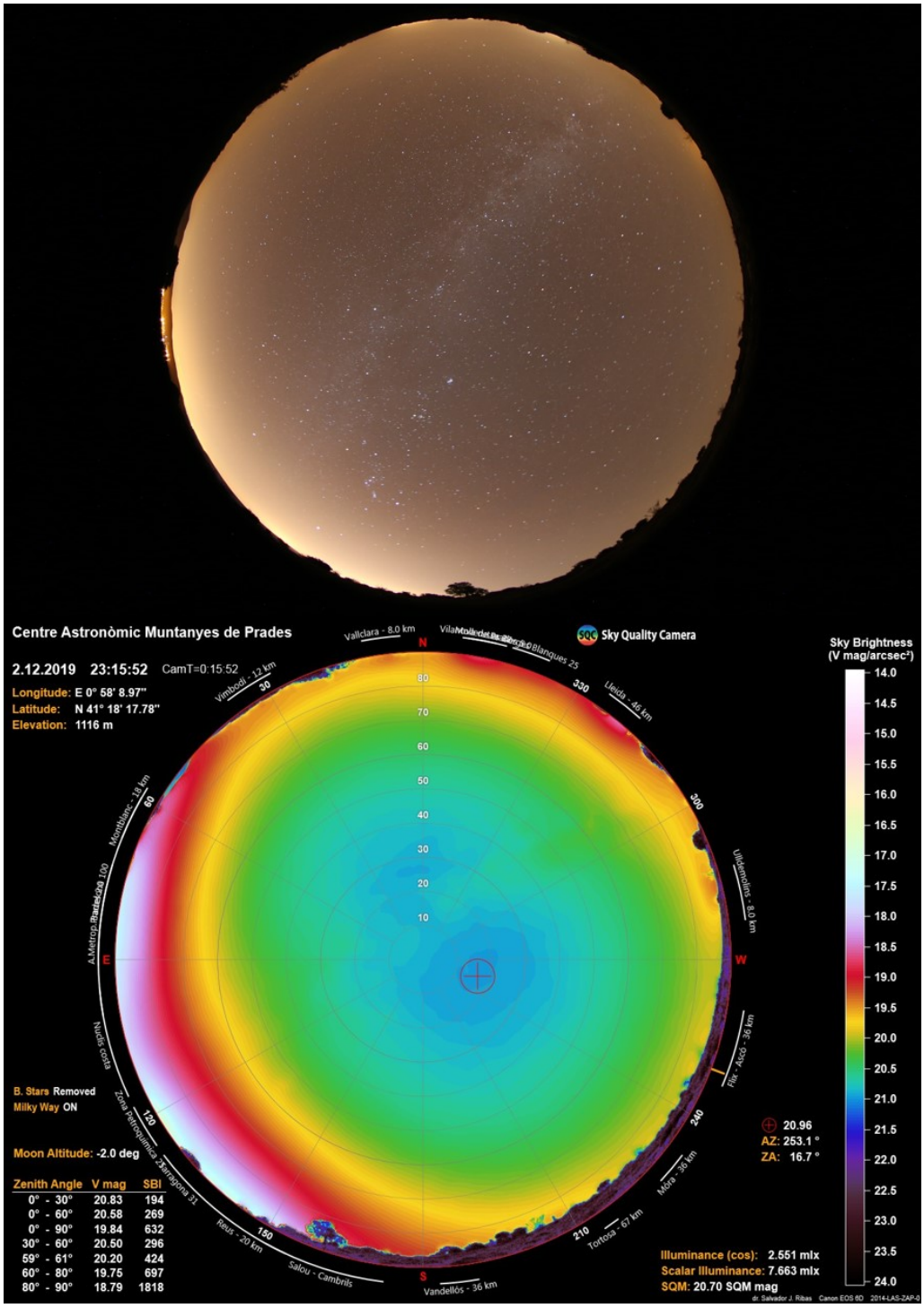

Figure 3.18: All-sky image near Prades astronomic center on the night of the 2nd of December of 2019. Top: raw data. Bottom: processed with SQC.

3.2.3 2019 campaign

The 2019 campaign was the largest in terms of distance and areas covered. It is also the campaign that includes most of the DSLR measurements. It can be divided in three different sub-campaigns. First, the Delta de l'Ebre NP and Ports de Beseit NP, located in the province of Tarragona and partly in the south part of Lleida province. This campaign was performed by M. Monguió and the author. Second, catalan western Pyrenees. Approximately half of this area was covered by the author alone and the other half accompanied by M. Garriga, director of the Alt Pirineu NP, which allowed covering restricted areas with very difficult access. In this area three locations were measured with DSLR images. The third sub-campaign covered most of the central part of the province of Lleida, including the area surrounding Montsec mountains where the Parc Astronòmic Montsec (PAM) is located. This region was covered by the author alone. In this area one location was studied with DSLR images. A part from these three areas a set of DSLR images were taken in Prades, the resulting images have already been presented in the previous campaign when Prades was studied with SQM for simplification. All the DSLR images were processed with SQC software, the processed images are presented here alongside the corresponding raw image. In chapter 5 some of them are used as a validation tool by comparing them to simulations.

It took a total of 12 nights to cover all the areas: two nights for the Delta de l'Ebre NP and Ports de Beseit NP, five nights for the catalan west Pyrenees and five more nights for covering the rest of the Lleida province.

Region	Dates	Distance (km)
Ebre's delta and Ports de Beseit NP	30-05-19, 31-05-19	579
Alt Pirineu NP	02-08, 03-08, 03-09, 26-09, 19-11-19	564
Montsec influence area	28-08, 30-08, 01-10, 03-10, 25-10	907

Table 3.3: Area covered in the 2019 light pollution assessment campaign.

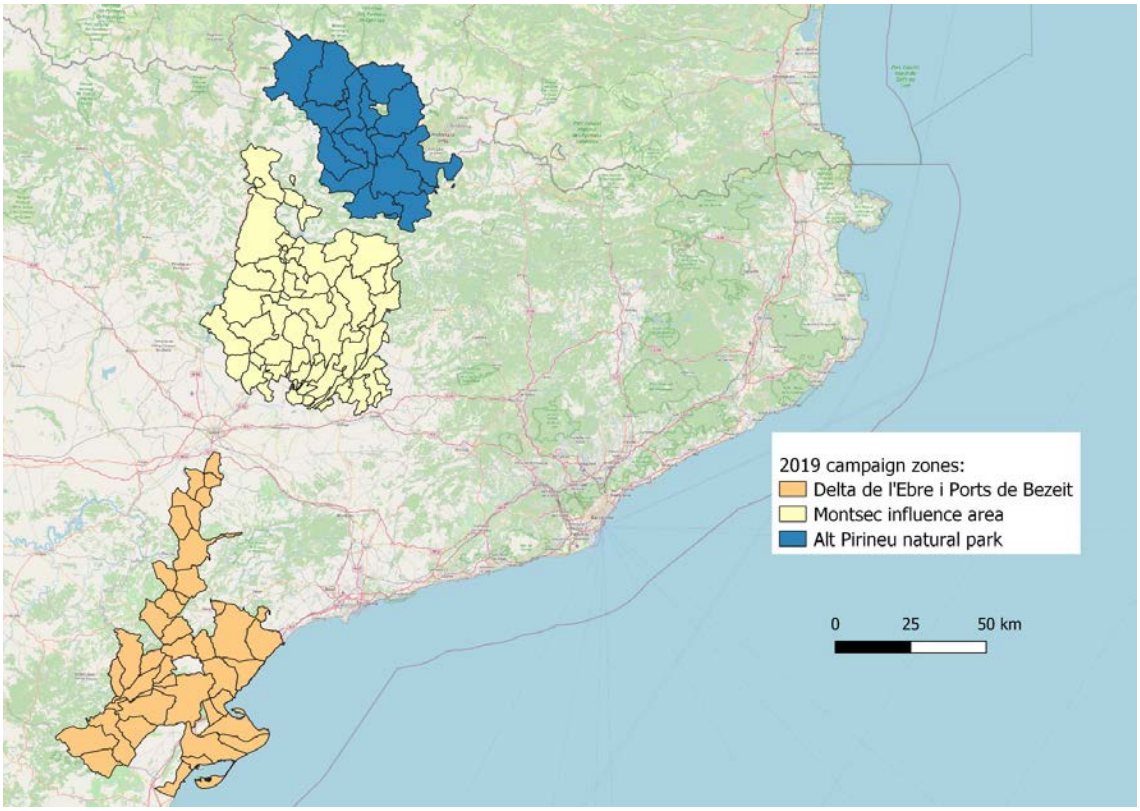

Figure 3.19: Areas covered during the 2019 campaign.

Ebre's delta and Ports de Beseit NP

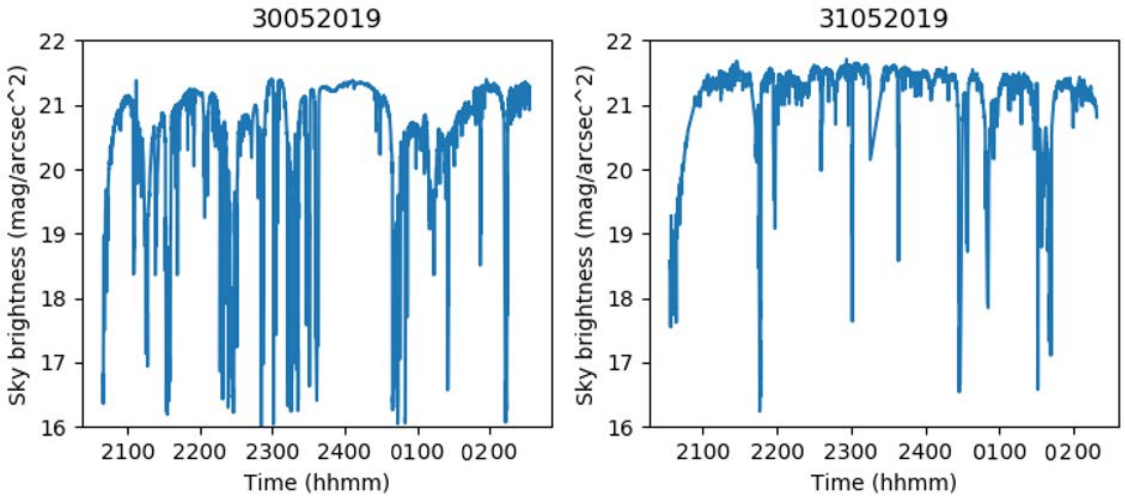

Figure 3.20: SQM values along the nights when the Delta de l'Ebre NP and Ports de Beseit NP were studied in the 2019 campaign. Time code: hhmm.

The path followed to cover the Delta de l'Ebre and Ports de Beseit NP cover many areas of different characteristics. Let's describe them as we go down the itinerary starting at Móra d'Ebre, that is the orange cell at the top of the eastern branch (see figure 3.21).

As we move to the coast the sky gets darker rapidly obtaining value slightly above 21.0 mag/arcsec^2. Cells close to the coast are quite bright due to coastal towns and cities. The nuclear plant of Vandellós that is located within the three bright green color cells in the coastal line is clearly affecting the sky nearby. Once outside the influence of the nuclear plant, zenith brightness reach values close to 21.0 mag/arcsec^2 and surpass that threshold when moving away from the coast. Entering the delta from the north we find sky brightness values very close to 21.0 mag/arcsec^2. In the central and south part of the delta it gets darker with most of the cells over 21.2 mag/arcsec^2 and many of them over 21.3 mag/arcsec^2. In the most southern part the sky is again affected by coastal towns as Sant Carles de la Rápita. Vegetation barely affected measurements so far and, although we encountered other vehicles, the statistic filtering was enough to process the data. As a matter of fact not one value was removed manually.

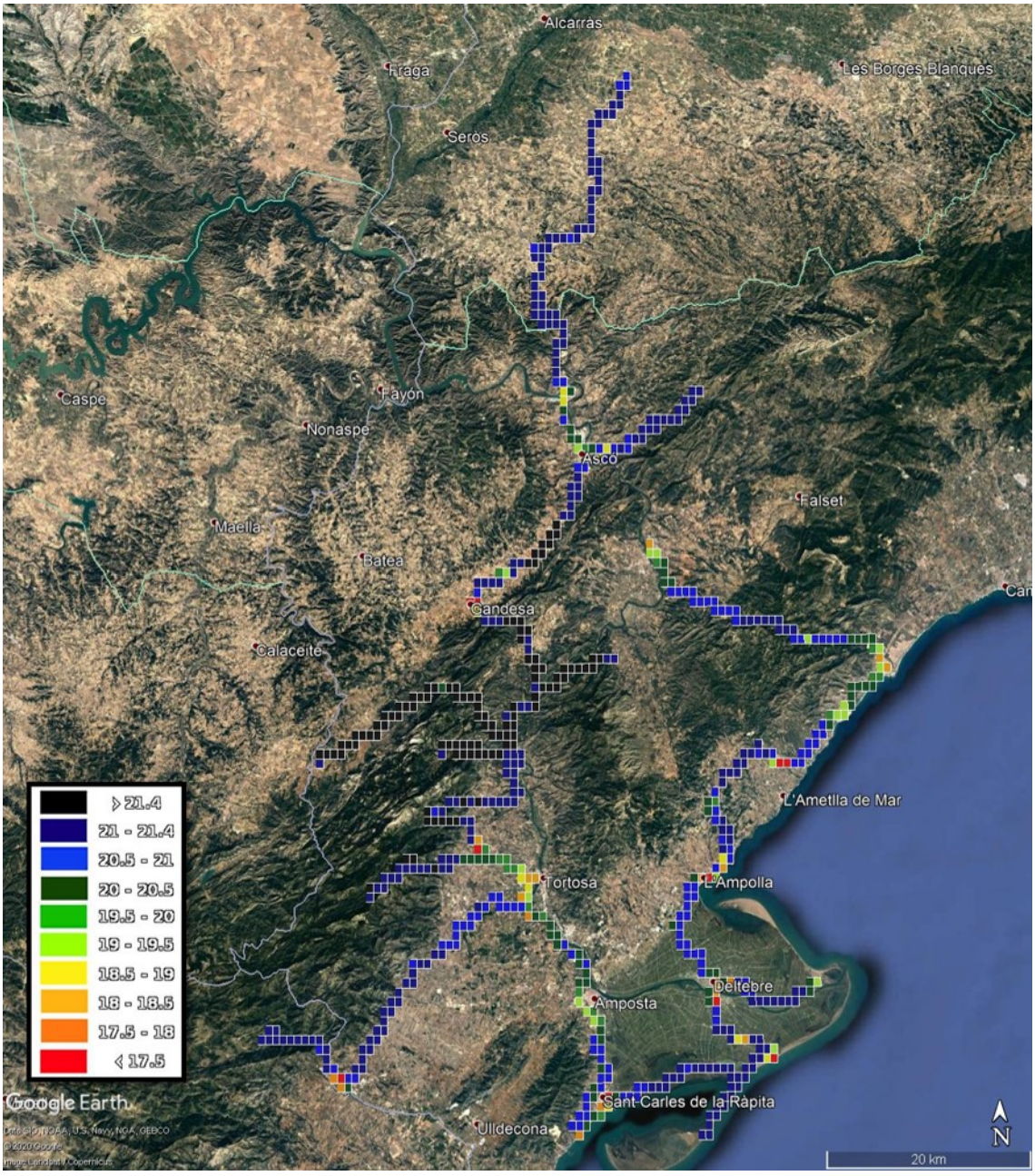

Figure 3.21: Light pollution maps of the regions of Ebre's delta and Ports de Beseit NP. The map is presented a double figure for resolution issues.

The delta area was already assessed with SQM dynamic measurements in 2014 and 2015. We found middle-sized cities that have reduced their area of influence but the remaining affected area presents brighter values. The most probable explanation is that the street lighting in the cities was changed from gas discharge lamps with some emission in the upper hemisphere to LED lamps with more radiant flux emitted but with almost no emission to the upper hemisphere. Hence, the adjacent regions are more affected due to the increase in the total radiant flux emitted, but the affectation decays faster due to the reduction of the emission in the upper hemisphere.

The western branch starts with the two biggest cities of the zone studied: Amposta and Tortosa. We can estimate their dimension through its relatively big areas of influence. The trail that goes south-west from Tortosa rapidly increases its darkness arriving at average levels well above 21.0 mag/arcsec^2. Going north, zenith sky brightness levels are extraordinarily dark. It is an area almost unaffected by light pollution with several cells above 21.5 mag/arcsec^2 and individual measurements that go as dark as 21.68 mag/arcsec^2. The vegetation in this area, especially in the branches that goes to the west from the central trail, is moderate. Manual filtering was necessary to represent the real sky darkness of this area.

Continuing to the north, the sky continues to be dark but not so pristine. Most of the values are around 21.2 mag/arcsec^2. It is remarkable the brightening effect of Ascó and its nuclear plant. In the northern cells the influence of the city of Lleida starts to be noticed, as we go north the average values decreases steadily. This area is almost free from vegetation.

Alt Pirineu NP

The catalan west Pyrenees area is very dark. As shown in seen in figure 3.23, the cells with values below 21.0 mag/arcsec^2 are scarce. There are many cells above 21.4 mag/arcsec^2 and some of them around 21.6 mag/arcsec^2. We found many individual measurements above 21.7 mag/arcsec^2 in different trails. With the exception of some principal roads, the whole region has dense vegetation that made necessary to perform an exhaustively manual filtering. The big gaps present in some plots of the figure 3.22 corresponds to the time needed to obtain the all-sky images that were processed afterwards with SQC software. It is important to point out that in the night of the 19th of November there was abundant snow in the area. Sky brightness is expected to be increased due to the higher albedo of the snow. During that night the track of the north-east was covered.

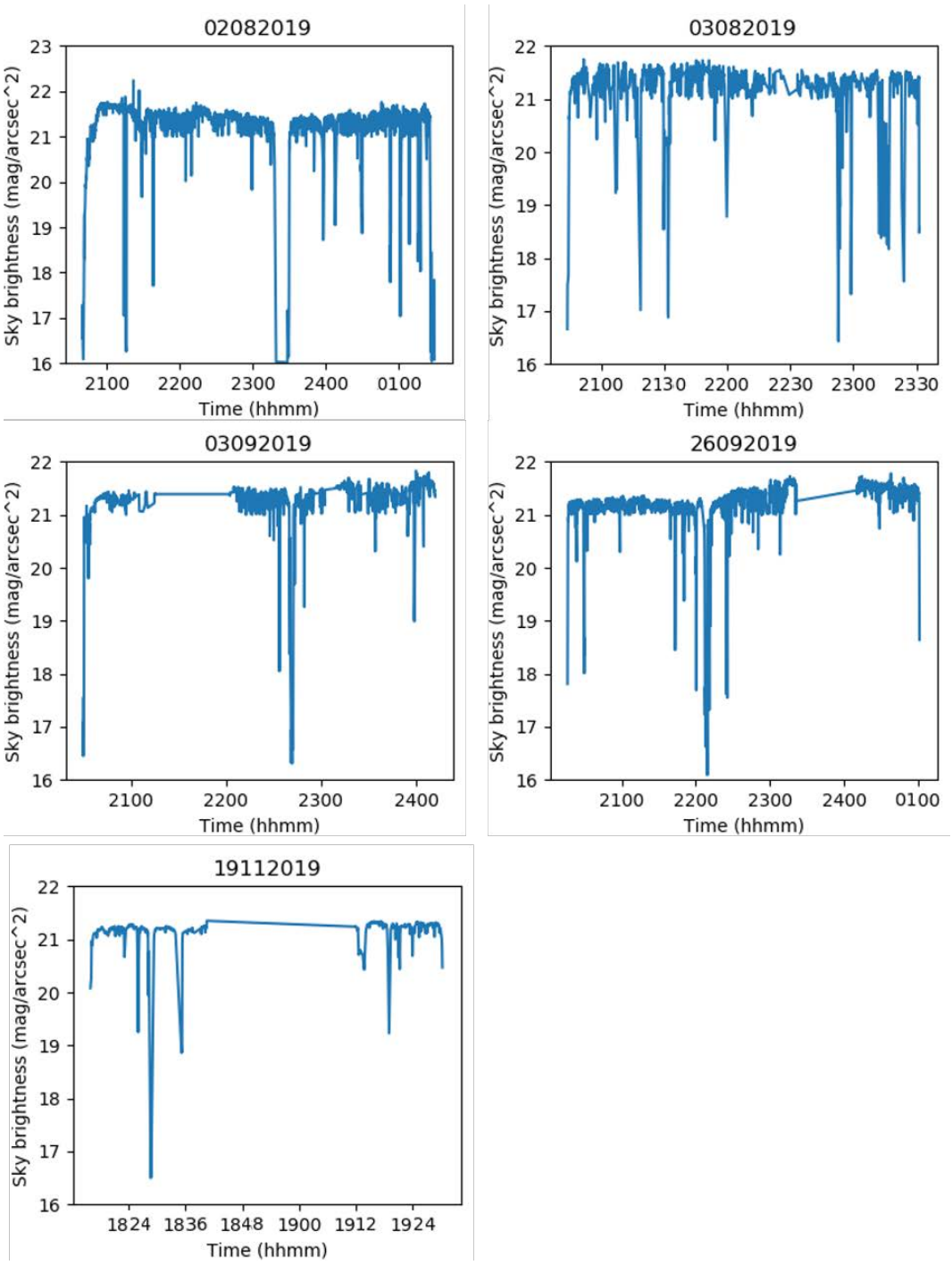

Figure 3.22: SQM values along the nights when the catalan western Pyrenees were studied in the 2019 campaign. Time code: hhmm.

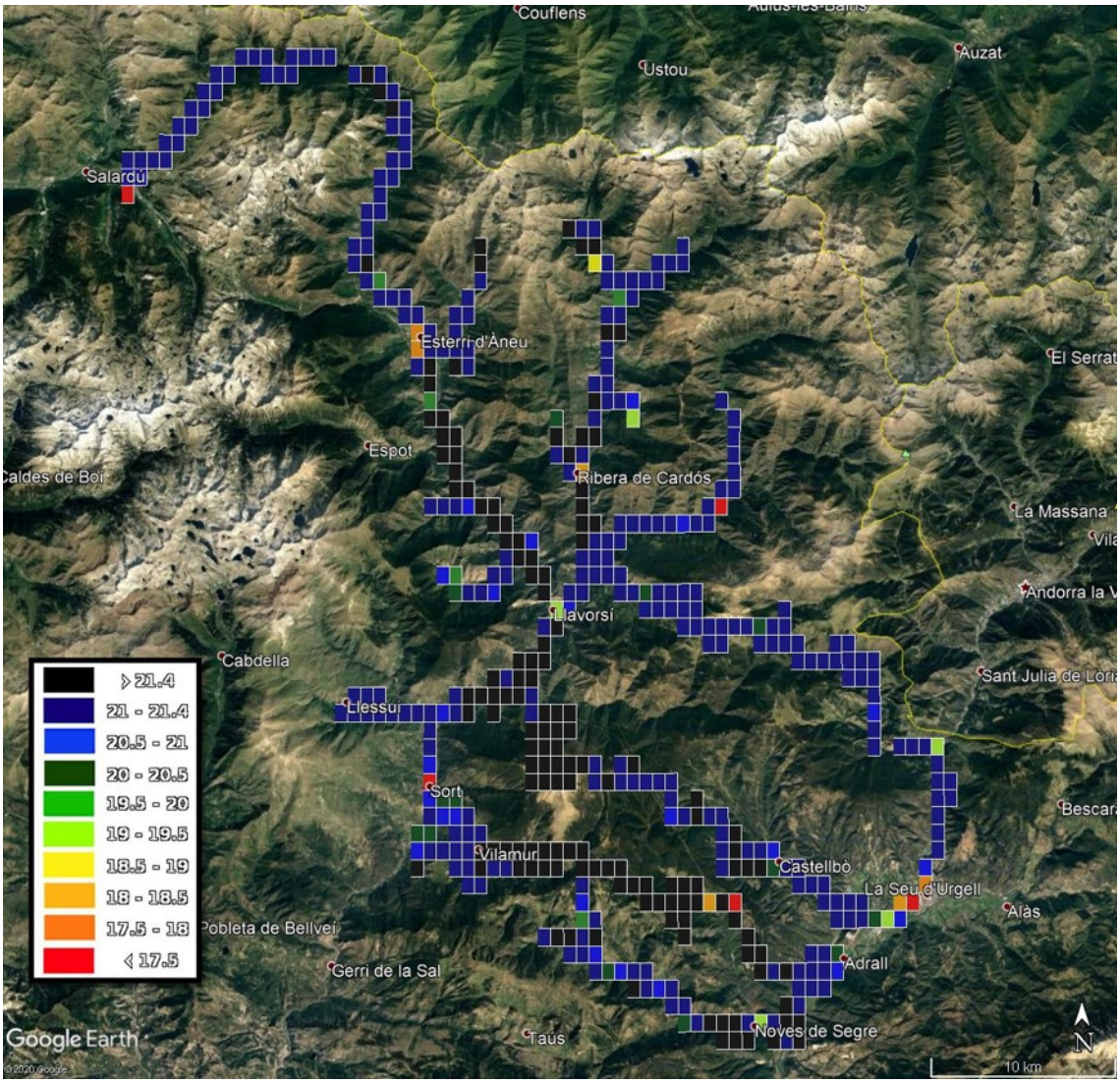

Figure 3.23: Light pollution maps of the catalan western Pyrenees.

The two trails that are closer to Andorra present brighter values than parallel and similar trails further away. Althought, the north-east track is affected by the presence of snow that can explain to some extent the brightening, it is a reasonable hypothesis to assume that Andorra is affecting their zenith sky brightness. Satellite images and all-sky maps add arguments in this direction. The northern track starts at Baqueira. The sky is affected by the skiing resort and probably by the towns from La Vall d'Aran to the west. Sky brightness does not surpass 21.4 mag/arcsec^2 until the track goes around the skiing resort and is hidden from the towns in the opposite side of the peak.

There are mainly two areas affected by towns. In the south-west around Sort and Rialp, and in the south-east around La Seu d'Urgell. The sporadic bright cells are the result of crossing small towns, but their area of influence spread no further than the cell they are located in.

As stated, during the Pyrenees campaign all-sky images from three locations were also taken. To locate properly the location of the images we suggest turning to figure 1.13.

The first location studied was close to Montgarri refuge in the northern trail (see figure 3.24). The set of images were taken without complications on the night of the 3rd of September. The processed data shows an estimated SQM value of 21.52 mag/arcsec^2. The darkest measured value is 21.89 mag/arcsec^2 in a direction far from the zenith (approx at 60^o in elevation to the NW in azimuth) because of the presence of the Milky Way, that is easily distinguished crossing the sky from NNE to SSW and passing through the zenith. The most polluted directions are close to the horizon in azimuth between ESE and SSE pointing towards Andorra and La Seu d'Urgell, there is a smaller light pollution dome in the SSW direction that probably is caused by Vielha.

The second location studied was in Orri peak (see figure 3.25). The images were taken on the night of the 26th of September. The communication center placed at the top of the peak was illuminated although we were told the lighting system would be shut down. Images from opposite sites were taken in an attempt to process half image in each case and unify the results but in the end it was not possible. No quantifiable information could be extracted from the set of images taken. However, the following year Canal-Domingo was able to get a set of images from the same spot when the lights of the communication center were shut down. The set of images were taken the 16th September 2020 (see figure 3.26). The processed data shows an estimated SQM value of 21.61 mag/arcsec^2 that is the same value obtained with SQM. The darkest measured values is 21.87 mag/arcsec^2 south from the zenith

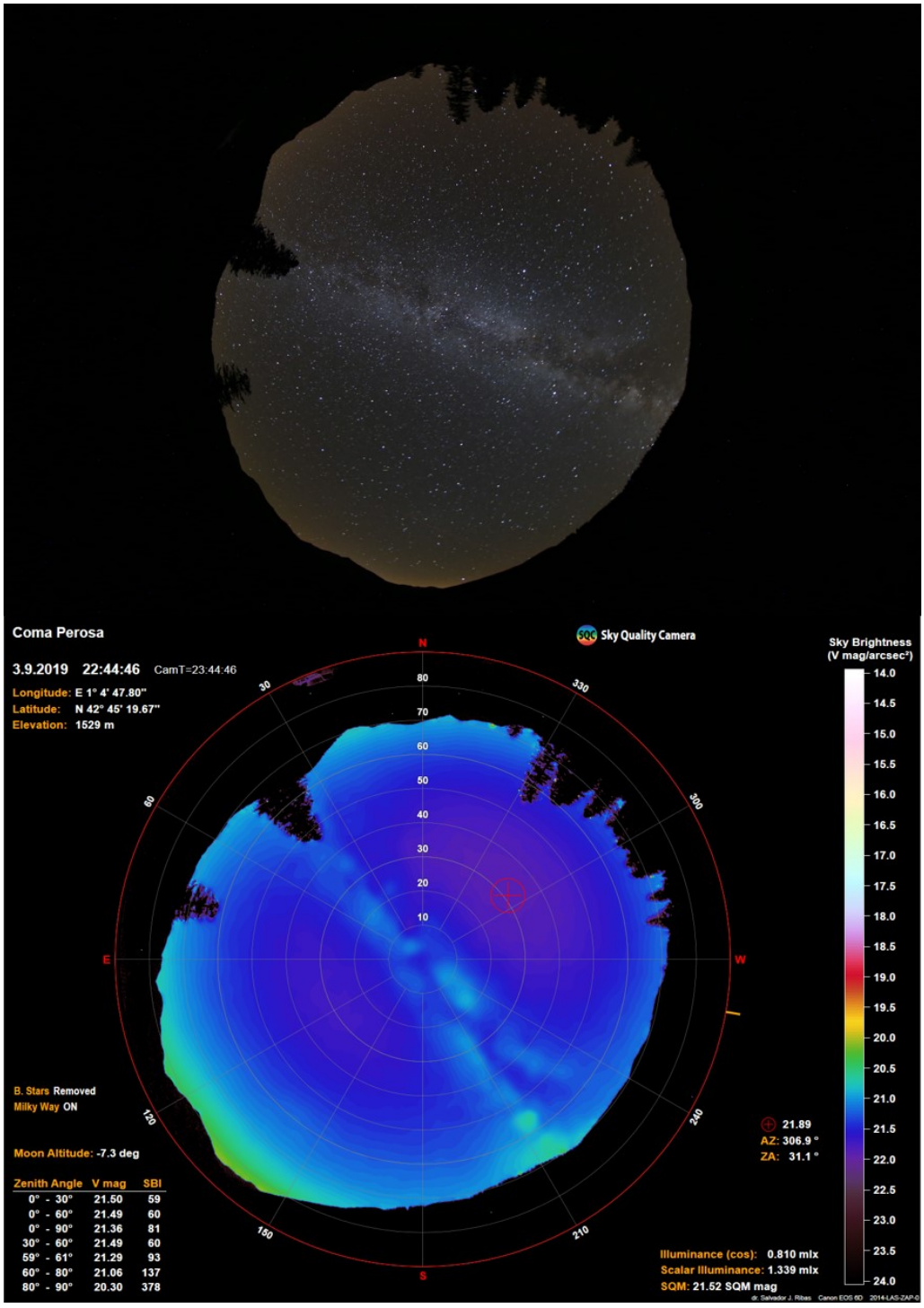

Figure 3.24: All-sky image near Montgarri refuge on the night of the 3rd of September. Top: raw data. Bottom: processed with SQC.

(approx at 75º in elevation) because of the presence of the Milky Way, that is easily distinguished crossing the sky from WSW to ENE and passing slightly north from the zenith. Close to the horizon, from NE to SE, the presence of clouds can be observed. Clouds increases the brightness observed over cities and towns. In this particular case clouds produce a double dome brightness pattern in the NE towards Andorra and a widening of the brightness dome in the SE towards Barcelona.

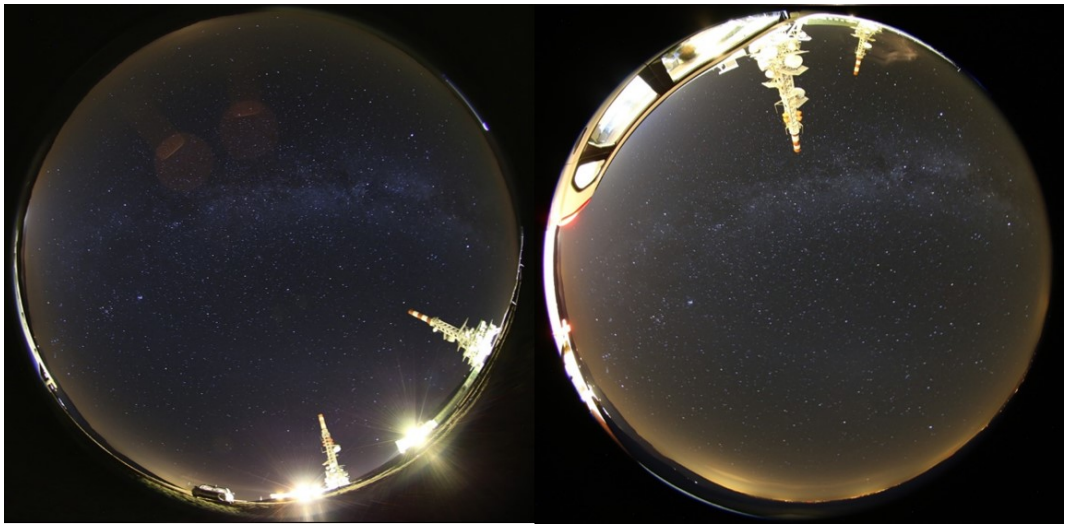

Figure 3.25: All-sky image of the sky in Orri peak on the night of the 26th of September. Top: camera located south of the communication center. Bottom: camera located north of the communication center.

The third location was close to the small town called La Força d'Àreu, in the northern point of the north-east track where it was quite difficult to find an open space to take the images. The images were taken on the night of the 19th of November. The SQM estimated value of the SQC image is 21.10 mag/arcsec^2 that matches well the averaged values of the SQM cells around the measurement. The darkest direction has a brightness value of 21.36 mag/arcsec^2, it is located at 60º in elevation and to the north in azimuth. The Milky Way crosses the sky from the ENE to the WSW passing north of the zenith. The major source of artificial brightness comes from the SW pointing to Andorra and La Seu d'Urgell.

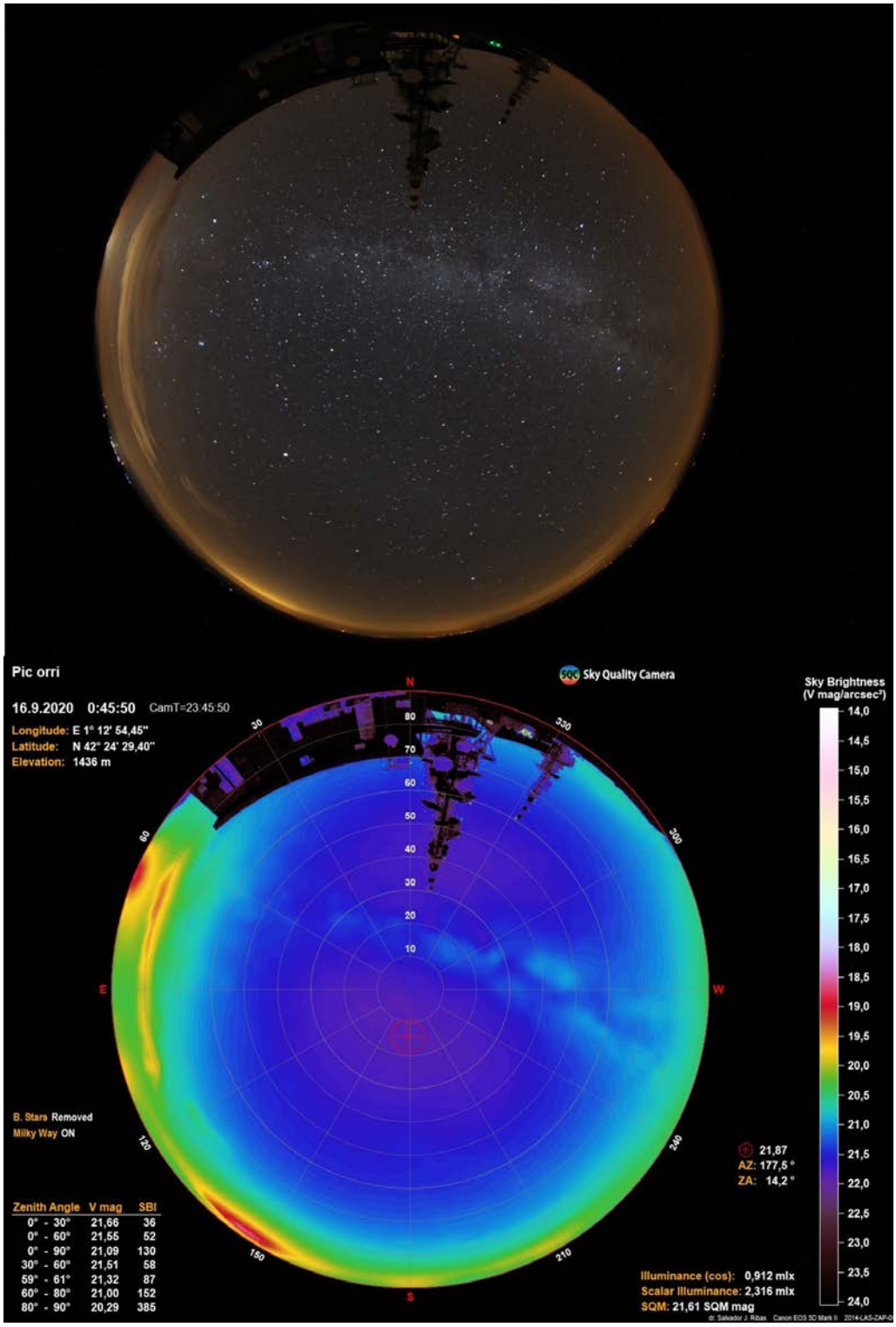

Figure 3.26: All-sky image of the sky in Orri peak on the night of the 16th of September 2020. Image taken by Canal-Domingo and processed by the author. Top: raw data. Bottom: processed with SQC.

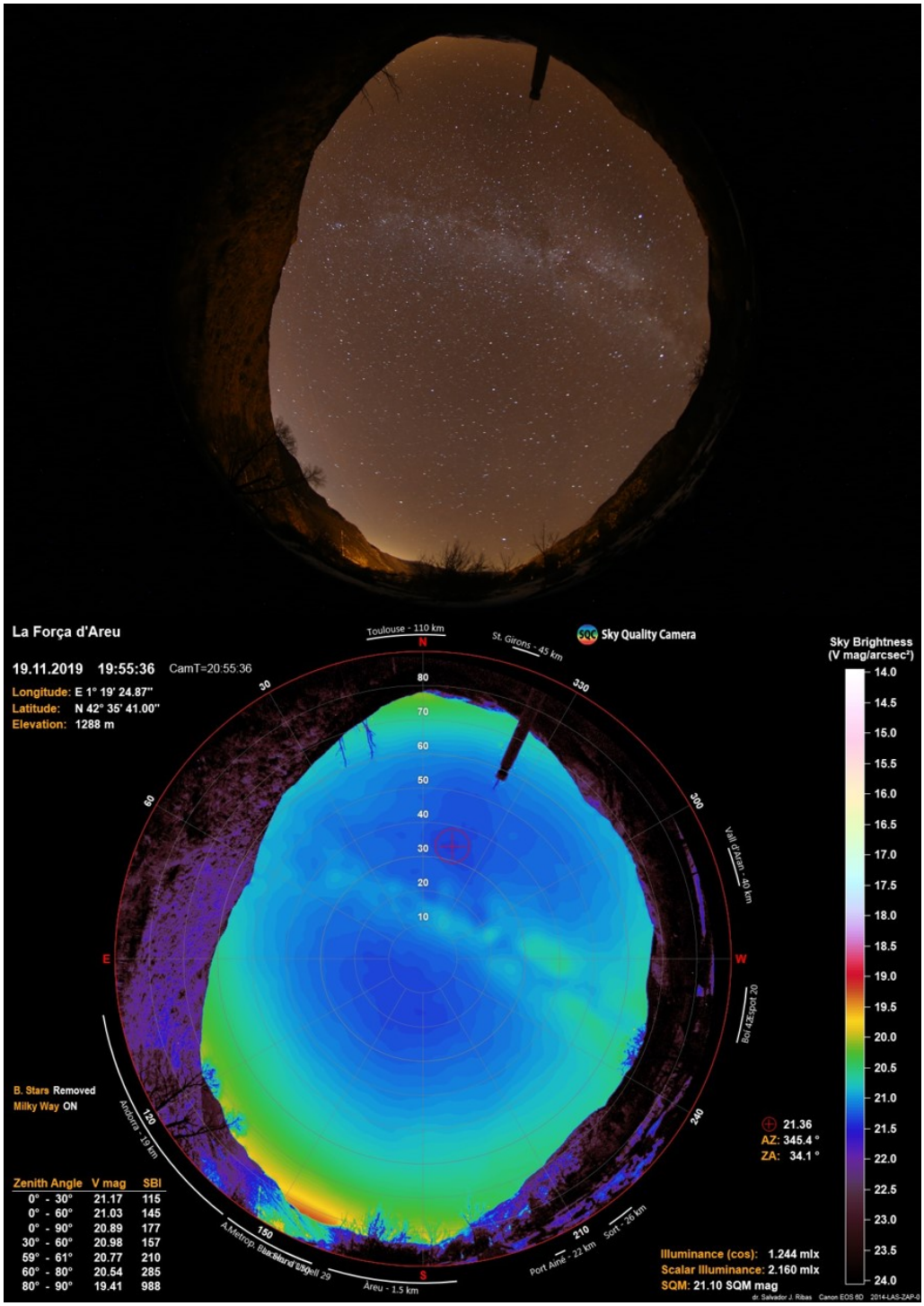

Figure 3.27: All-sky image near Áreu on the night of the 19th of November. Top: raw data. Bottom: processed with SQC.

Montsec's influence area

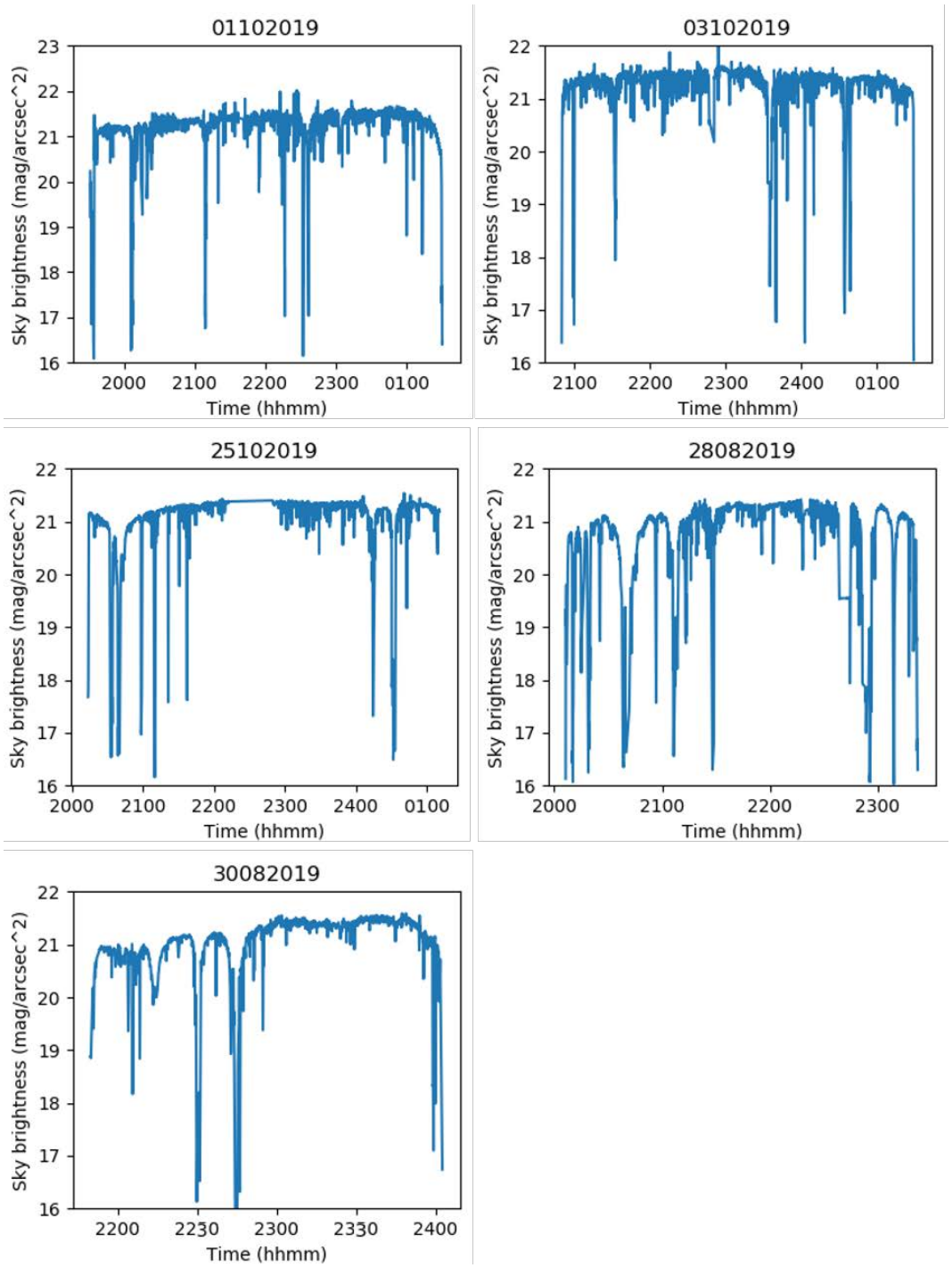

Figure 3.28: SQM values along the nights when Montsec influence area was studied in the 2019 campaign. Time code: hhmm.

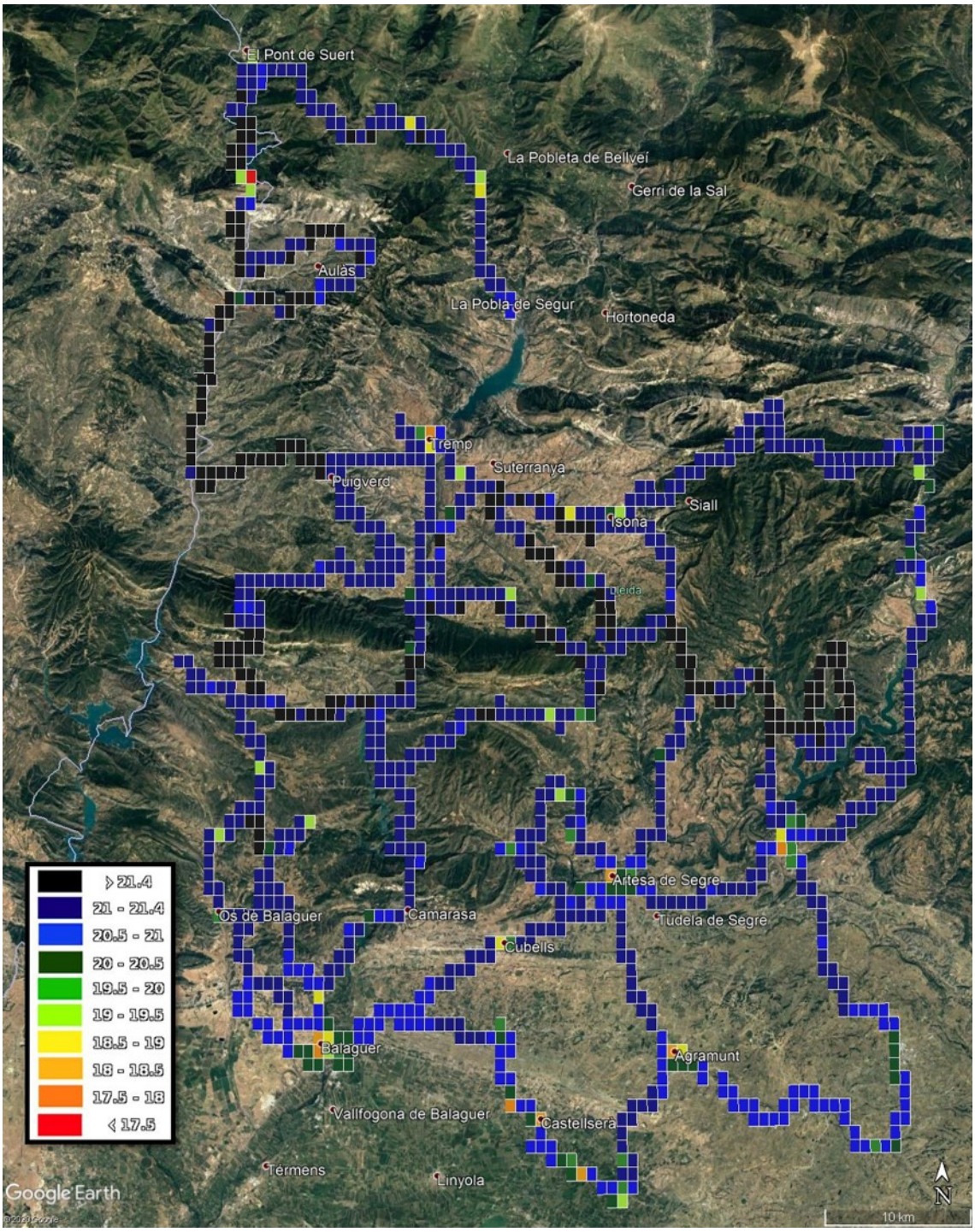

Figure 3.29: Light pollution map of the Lleida province.

Montsec's influence area covers most of the central part of Lleida's province. Although it is formed by several regions with different characteristics that need an individual discussion, we can see that in general is a dark area, with most of the cells outside towns with values above 21.0 mag/arcsec^2. There are few regions of exceptional dark sky brightness with individual values that reach 21.7 mag/arcsec^2. It is also worth mentioning that almost all the towns have almost no influence beyond city limits. The exception is Balaguer located south-west in figure 3.29.

In the south-east region, we find average values below 21.0 mag/arcsec^2. This area is less than 5 km away from the highway that connects Barcelona and Lleida that goes near middle-sized cities as Tàrrega, Cervera and Mollerussa. In the south-west Balaguer dominates the area. There is a clear pattern of brightening as measurements get closer to the city. The areas commented so far are free from vegetation that made manual filtering unnecessary.

As we move north, cells with values above 21.0 mag/arcsec^2 become the norm. There are even a few cells above 21.4 mag/arcsec^2 in the western trail. There are two towns that stand out: Ponts to the east and Artesa de Segre in the centre[1]. Both cities have a small but noticeable influence on the zenith brightness around them. Vegetation is scarce with very few values affected by it.

Keep moving to the north, we find many values above 21.4 mag/arcsec^2 in all the tracks. It is worth commenting that the west branch passes by the PAM (the educational facility at the bottom of Montsec mountain range) and the OAdM (the scientific facility at the top of the mountain range). Values around them are close to 21.7 mag/arcsec^2, confirming the almost pristine conditions of the night in this area. The vegetation in most of the trails started to appear in a regular basis.

Following north there is a strip that crosses the map from east to west at Tremp's latitude. The city has barely no influence in the cells adjacent to it. In the eastern region values go over 21.0 mag/arcsec^2 but does not cross the threshold of 21.4 mag/arcsec^2. The east track was brighter than expected especially when comparing it to other trails of this region. An unusual humid night could have brightened slightly the measurements. On the other hand, in the west part zenith values surpass 21.5 mag/arcsec^2. Vegetation was dense, particularly in the east part.

The remaining subarea of the Lleida's province is the north-west trail. The west

[1]As an anecdote, when covering the loop to the north-west of Artesa de Segre, I took the wrong trail. It is a common thing when going down non asphalted forest trails, but this time resulted in fatal car damages that barely allowed me to cover the planned path for that night. The day after, my beloved car was moved directly to the scrapyard.

branch that follows the border between Catalonia and Aragon is very low populated. That explains its dark sky. Most of the cells show values above 21.5 mag/arcsec^2 and individual values reach 21.7 mag/arcsec^2. The north and east branches however were not so dark, with sporadic individual measurements above 21.4 mag/arcsec^2 most of the cells have values around 21.2 mag/arcsec^2. In this trail vegetation was not as dense as in the previous area.

On the night of the 25th of October a DSLR set of images was taken at the OAdM (see figure 3.30). It is worth mentioning that the SQM measurements around the OAdM during that night were quite brighter (around 21.35 mag/arcsec^2) than the ones of the night of the 1st of October when the SQM values surpassed several times 21.60 mag/arcsec^2. The difference is explained by two factors: presence of the Milky Way close to the zenith and abnormal atmospheric conditions such as higher presence of aerosols and higher humidity. The values of the darker night match with most of the measurements taken in the OAdM in previous campaigns. The processed image has a darkest value of 21.47 mag/arcsec^2 and an estimated SQM value of 21.23 mag/arcsec^2. The Milky Way crosses the sky from East to West slightly north of the zenith. The principal polluted directions can be seen clearly due to the high altitude of the observatory that ensures an horizon free from obstacles. Towards ESE there is a big light pollution dome. In this direction we find, from closest to farthest, Artesa de Segre, Agramunt, Cervera, Igualada, Manresa and Barcelona metropolitan area. From SSE to S there is also a big light pollution dome. It is probably caused by the close town of Àger and the city of Balaguer. The third biggest dome is found at SSW towards the city of Lleida. Other minor domes are at WSW towards Monzón and NE towards Tremp.

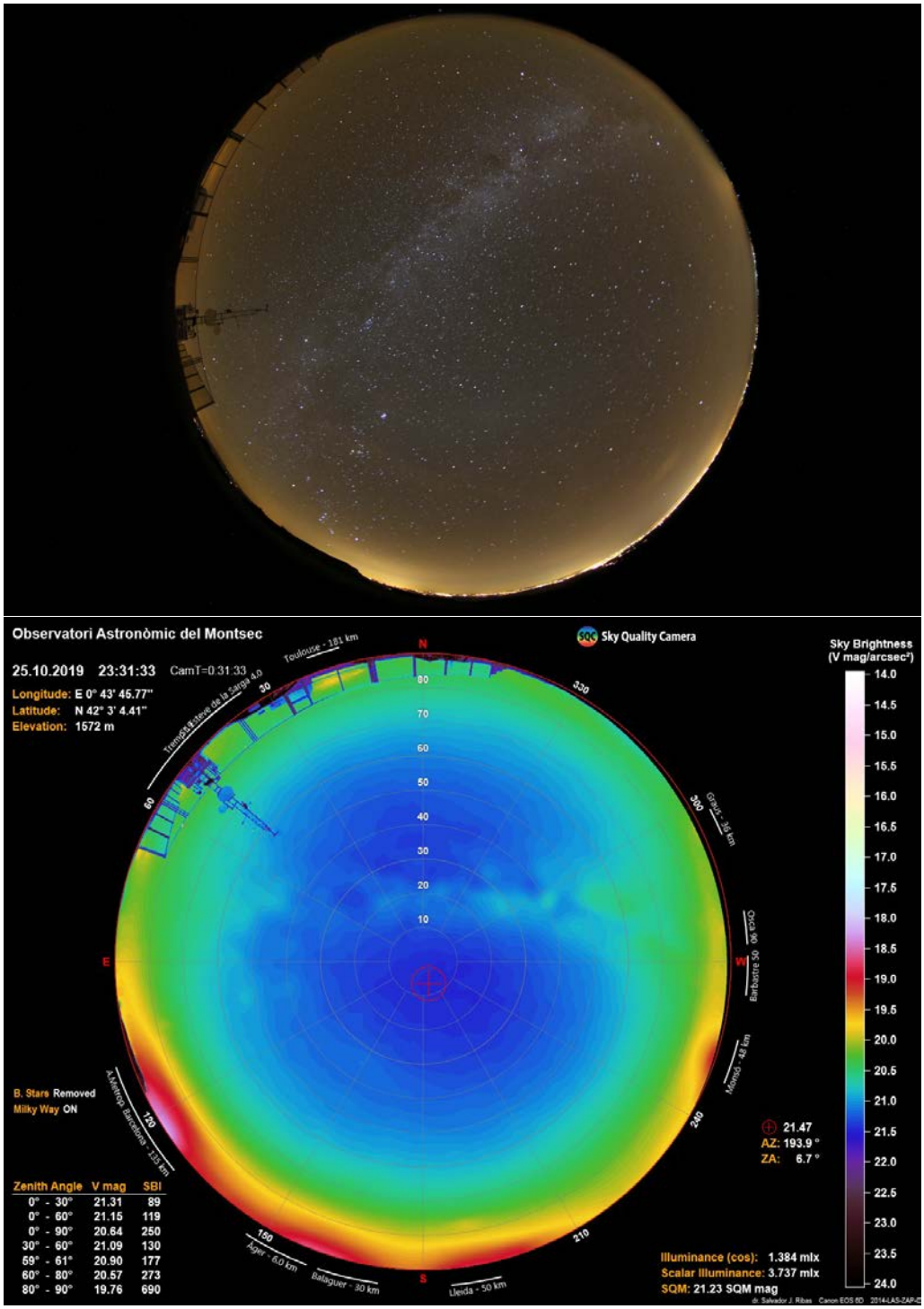

Figure 3.30: All-sky image at the OAdM on the night of the 25th of October. Top: raw data. Bottom: processed with SQC.

3.2.4 2020 campaign

During 2020 two areas were studied with SQM dynamic measurements. The north-east area of Catalonia in the province of Girona, that includes the Creus Cape, eastern Pyrenees and the Empordà wetlands. The second area is Montseny NP and some of the coastal regions adjacent to it. It took three nights to cover the first area mentioned and only a long one to cover the natural park. Moreover, two locations were studied with DSLR images: the astronomic observatory of the Pic du Midi de Bigorre and the north region of Valle del Roncal.

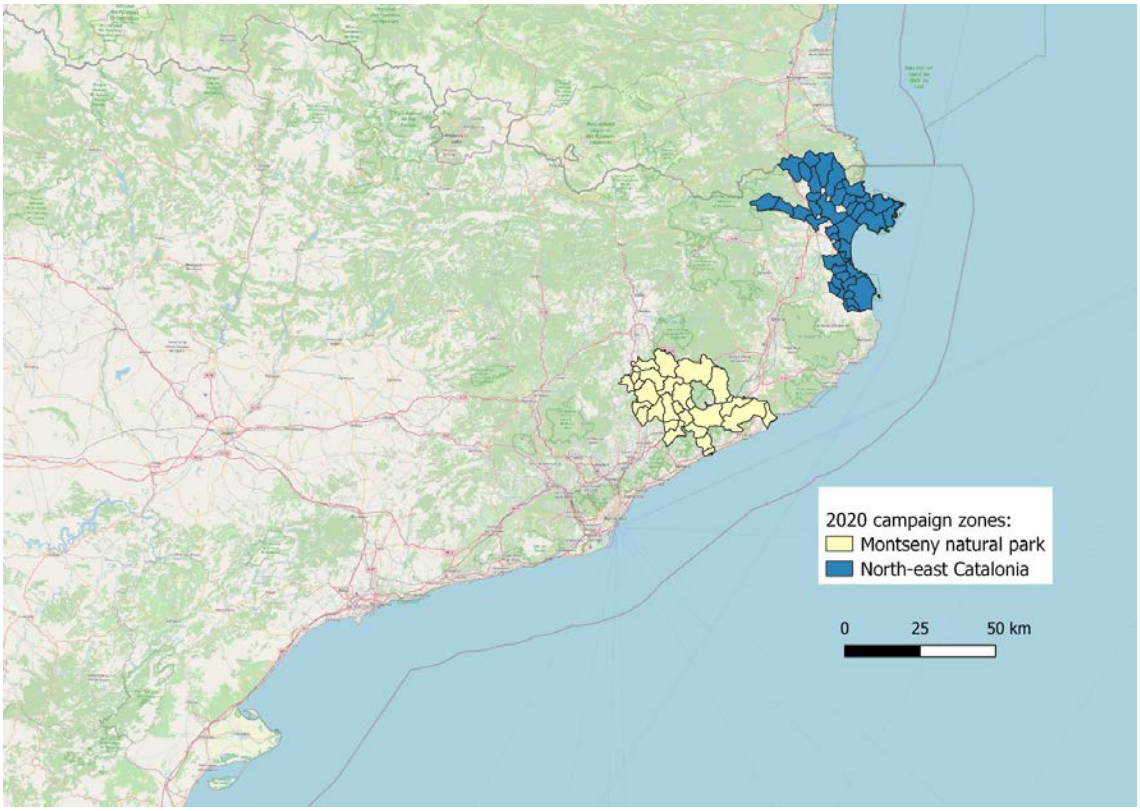

Figure 3.31: Areas covered during the 2020 campaign.

Region	Dates	Distance covered (km)
North-east Catalonia	25-05-20, 18-07-20, 26-08-20	350
Montseny NP	19-08-20	248

Table 3.4: Area covered in the 2020 light pollution assessment campaign.

North-east Catalonia

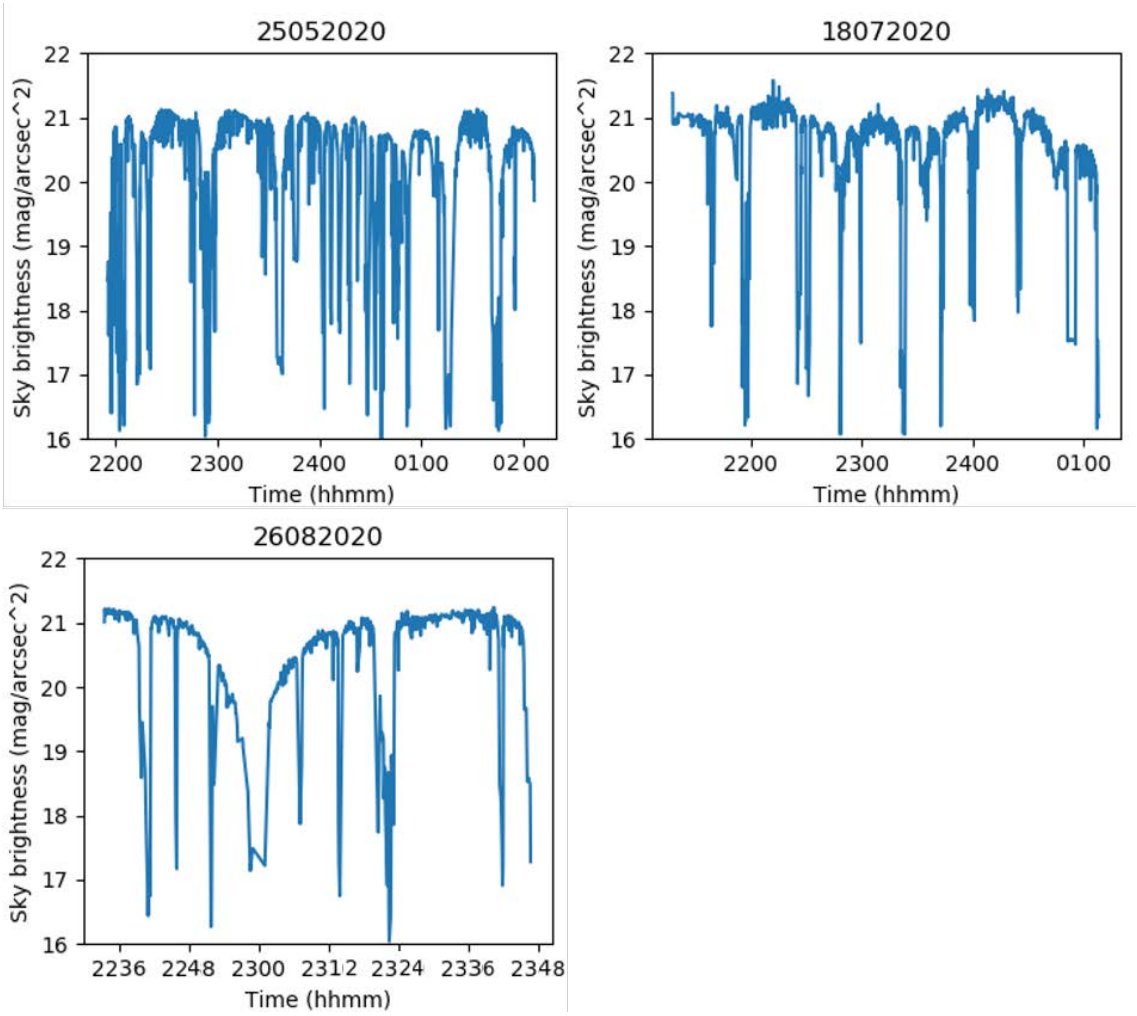

Figure 3.32: SQM values along the nights when the north-east region of Catalonia was studied during the 2020 campaign. Time code: hhmm.

The north-east region of Catalonia measurement track was designed to connect with the maps of the eastern Pyrenees obtained during the 2017 and 2018 campaigns. The linking point is located around Albanyà (western part of the map in figure 3.33). Sky brightness values are not specially dark in any sub-region of this area. There are cities and coastal towns that have a wide spread influence. Far from the influence of the local towns most of the cells present values between 20.5 mag/arcsec^2 and 21.0 mag/arcsec^2, with only the most remote sites over 21.0 mag/arcsec^2.

The darkest zenith brightness values are found in the eastern cells, close to the lighthouse of the Creus Cape, with values around 21.2 mag/arcsec^2. The other areas

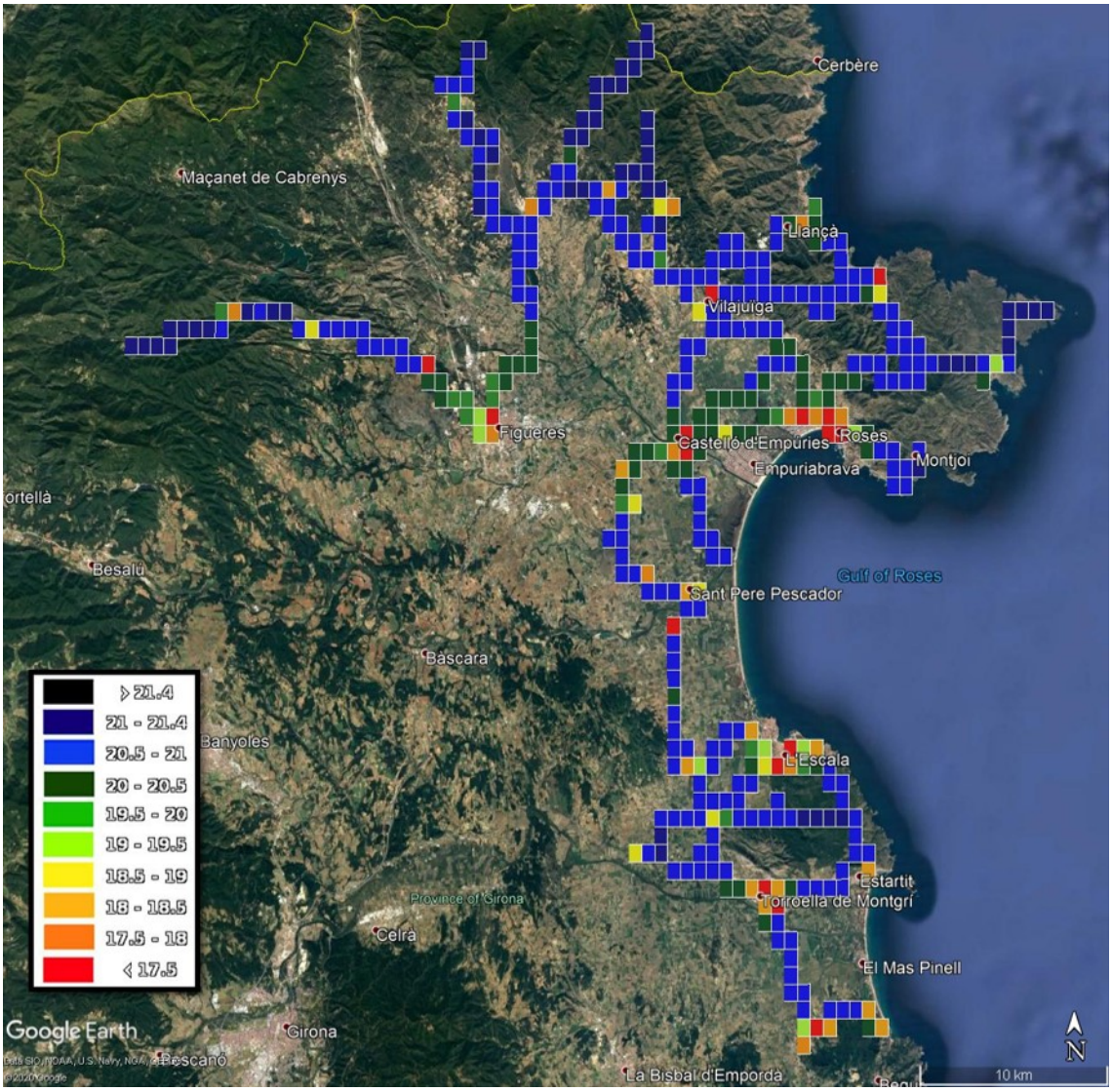

Figure 3.33: Light pollution map of the north-east region of Catalonia.

above 21.0 mag/arcsec^2 are: in the north close to the France border, to the east close to Albanyà and to the south in a track that crosses a forest between l'Escala and Torroella de Montgrí. The values obtained in Albanyà are in agreement with those of the 2017 and 2018 campaigns, a dark sky but not pristine.

As commented above, there are several cities that brightens their surroundings. In the coastal line from south to north: Pals, Torroella de Mongrí, l'Escala, Castelló d'Empúries and Roses south of the Creus Cape. The city with the biggest influence area is Figueres, located in the west branch. Its influence is clearly showed in figure 3.32. We can see the brightening trend of measurements as we get close or move

away to the city, that was crossed around 23h 00m. It is worth mentioning too the small town of Cantallops, located in the green cell of the west branch of the two that goes north to the French border. It could be a good candidate as one of the worst illuminated towns we have encountered during all the campaigns. Lamps with free emission to the upper hemisphere were visible from far away in what could have been a quite dark place. The adjacent cells to the north decay rapidly from values over 21.0 mag/arcsec^2 to well below that threshold due to the artificial light from that town.

Vegetation in the trails of the Pyrennes and the forest between l'Escala and Torroella de Montgrí was dense and therefore manual filtering was needed. Outside these areas vegetation was scarce.

Montseny NP

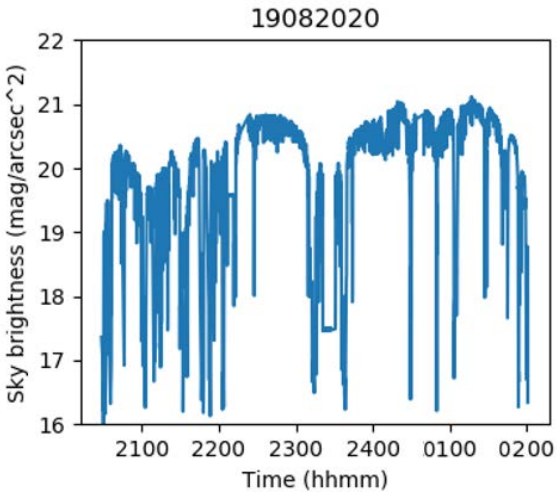

Figure 3.34: SQM values along the nights when the Montseny NP was studied during the 2020 campaign. Time code: hhmm.

The natural park of Montseny and its surroundings are quite polluted. However, the most inner part of the park have reasonably dark sky with values between 20.5 and 21.0 mag/arcsec^2. In this region there are two gradients that dominate the sky brightness. First, light pollution coming from the coastal line. The concatenation of cities from Mataró to Blanes, such as Arenys, Calella and Malgrat de Mar have a big influence on zenith values kilometers away from the coast. Second, light pollution coming from Barcelona metropolitan area located closer than 40 km in the south-west. In the same direction but closer middle-size cities, as Granollers,

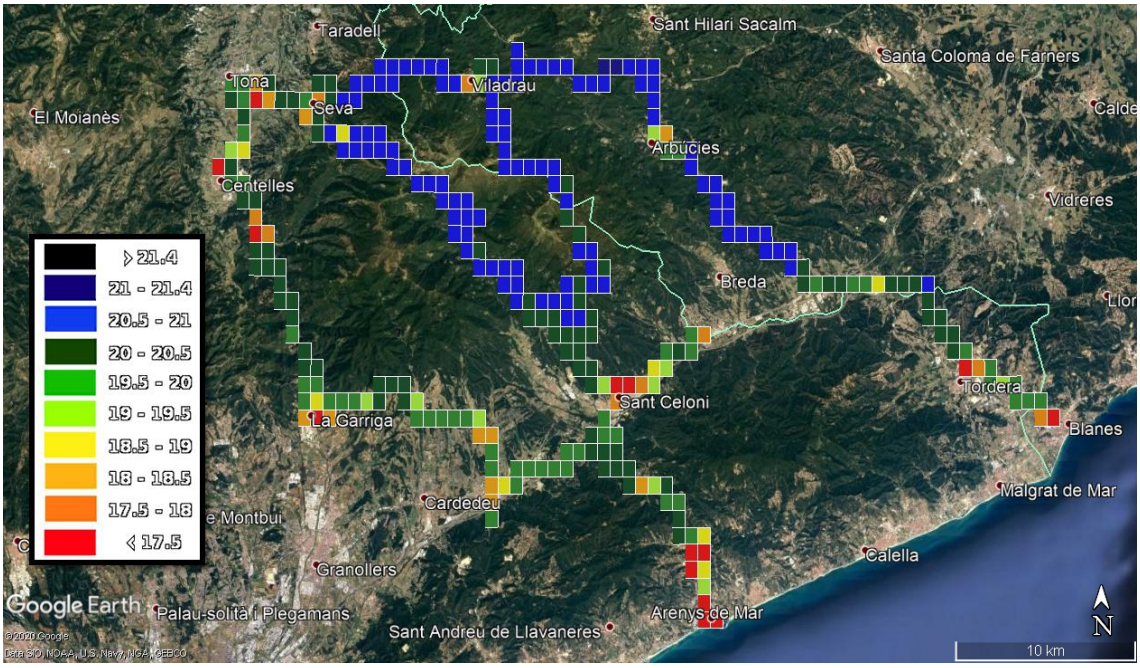

Figure 3.35: Light pollution map of Montseny NP.

worsen the problem. As a result, tracks closer to the coast and to the west present values below 20.5 mag/arcsec^2 and even many below 20.0 mag/arcsec^2. Following this reasoning we should find the darkest values in the north-east corner of the area covered, and that is the case. The only two cells above 21.0 mag/arcsec^2 are located there.

Vegetation inside the natural park was dense, as well as in the trail that goes from Arenys de Mar to Sant Celoni. The rest of the tracks presented scarce vegetation. We faced with many vehicles in most of the area studied, their light affected the measurements and had to be filtered.

Pic du Midi de Bigorre

Pic du Midi de Bigorre is a mountain of the Pyrenees placed in the french region of the Haute-Pyrénées. It is one of the three key regions of the Pyrenees La Nuit project.

On the night of the 18th of October a set of DSLR images were taken at the astronomic observatory of the Pic du Midi de Bigorre. The facility is placed at the top of the mountain at almost 2900 m. The observatory and its surroundings were completely covered by snow which is very uncommon at that time of the year. As

stated previously, snow increases the night sky brightness by increasing the albedo of the ground.

The astronomic observatory is composed by several buildings and facilities such as domes for the telescopes. That fact added to the abundant presence of snow that prevented from reaching remote spots made it impossible to take pictures with a complete vision of the sky dome. To gather information from all the directions we took pictures from three different points within the facility (see figure 3.36).

Figure 3.36: Locations from where the all-sky images were taken in the Pic du Midi. The first location aimed to cover the north area, the second location from west to south and the third from south to east.

The data from the three set of images are coherent with each other (see figures 3.37, 3.38 and 3.39). The sky over Pic du Midi is almost unpolluted above 25° in elevation. In the images the Milky Way crosses the sky from east to west passing north from the zenith. That's the reason the darkest value, 21.63 mag/arcsec^2, is shifted towards south from the zenith.

Close to the horizon there are some easily distinguishable artificial light sources. To the NE there is Toulouse that affects the sky up to 15° in elevation. The shape of the light dome indicates that there were high clouds over the city that increased

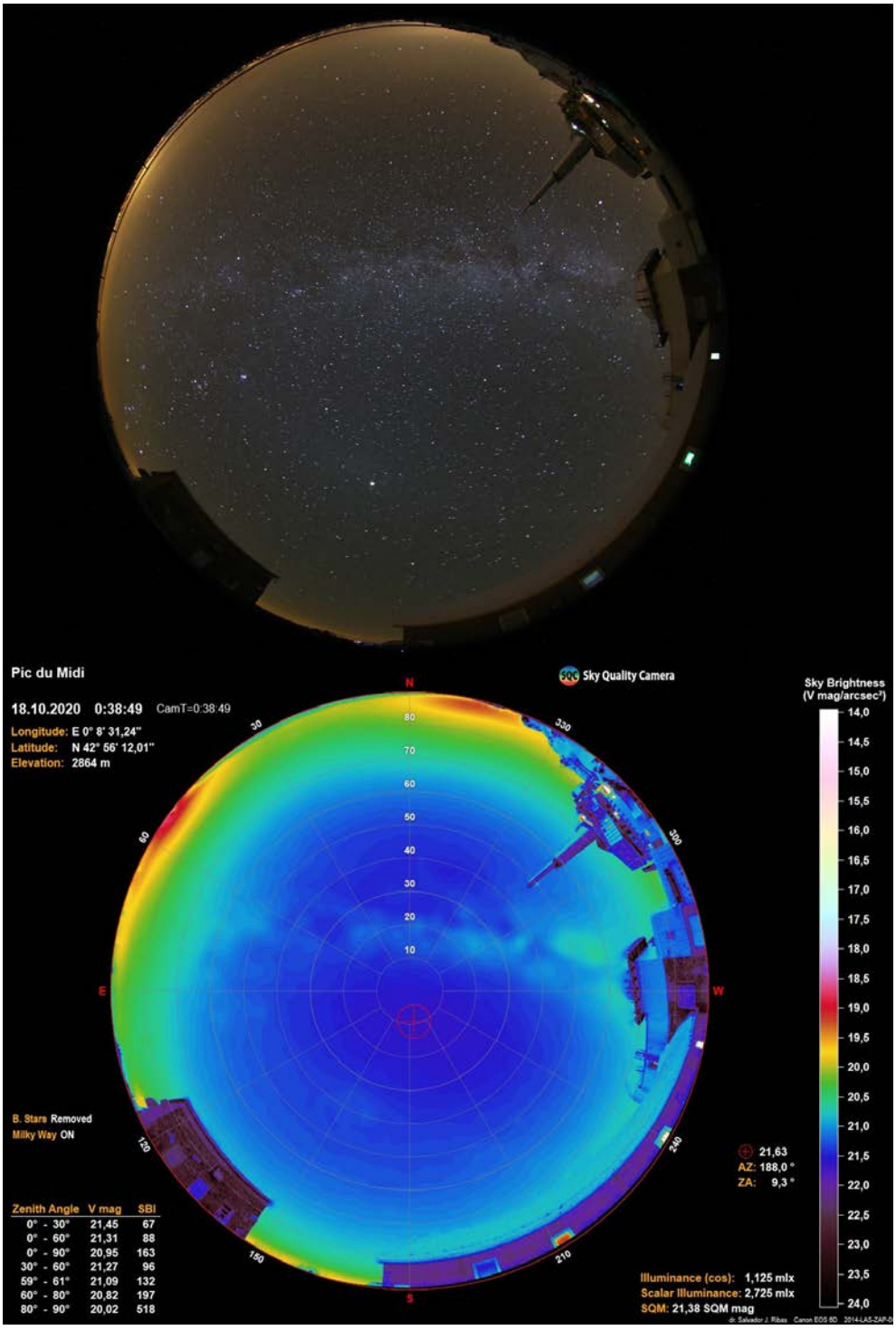

Figure 3.37: All-sky image at the Pic du midi on the night of the 18th of October. Top: raw data. Bottom: processed with SQC. Location one.

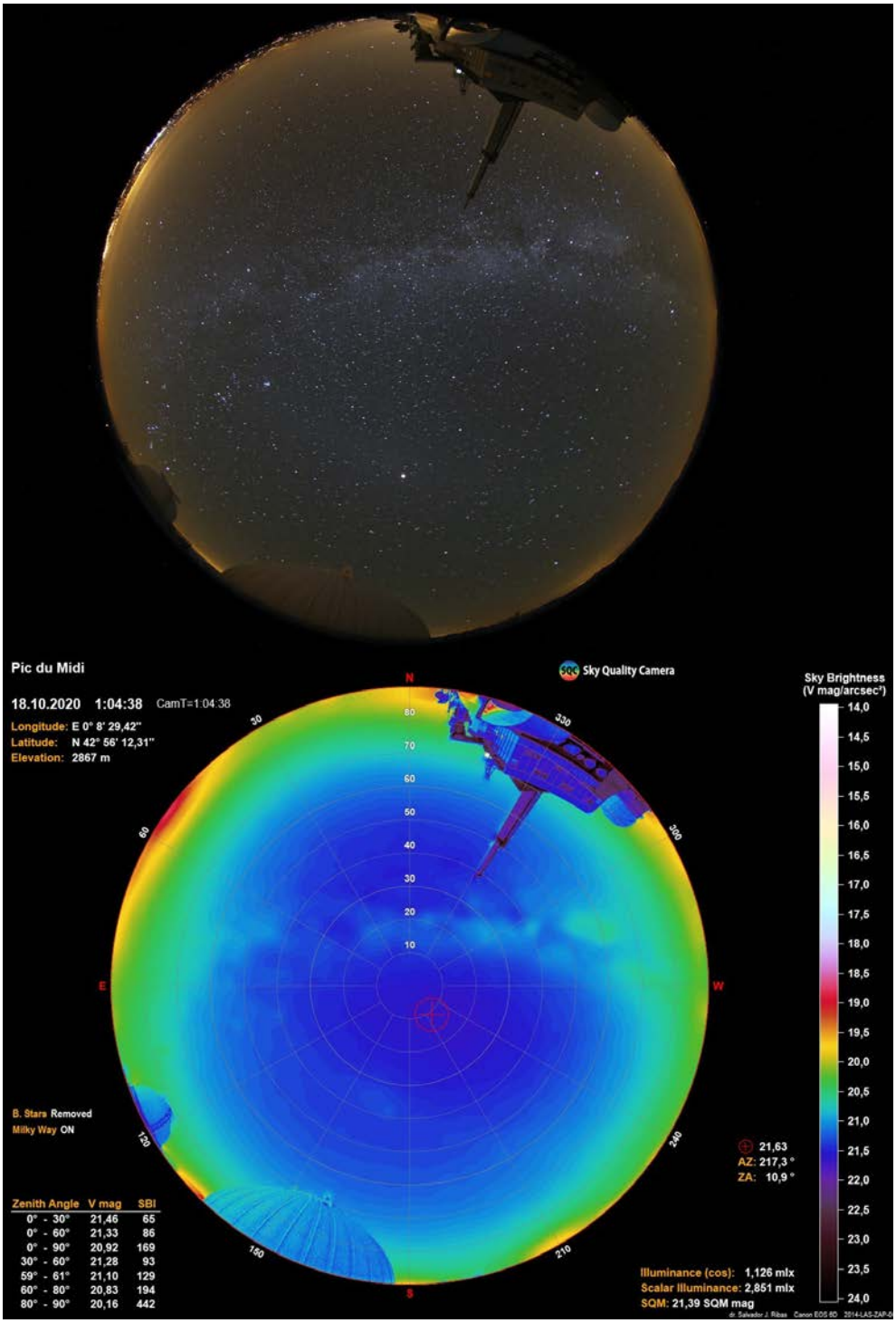

Figure 3.38: All-sky image at the Pic du midi on the night of the 18th of October. Top: raw data. Bottom: processed with SQC. Location two.

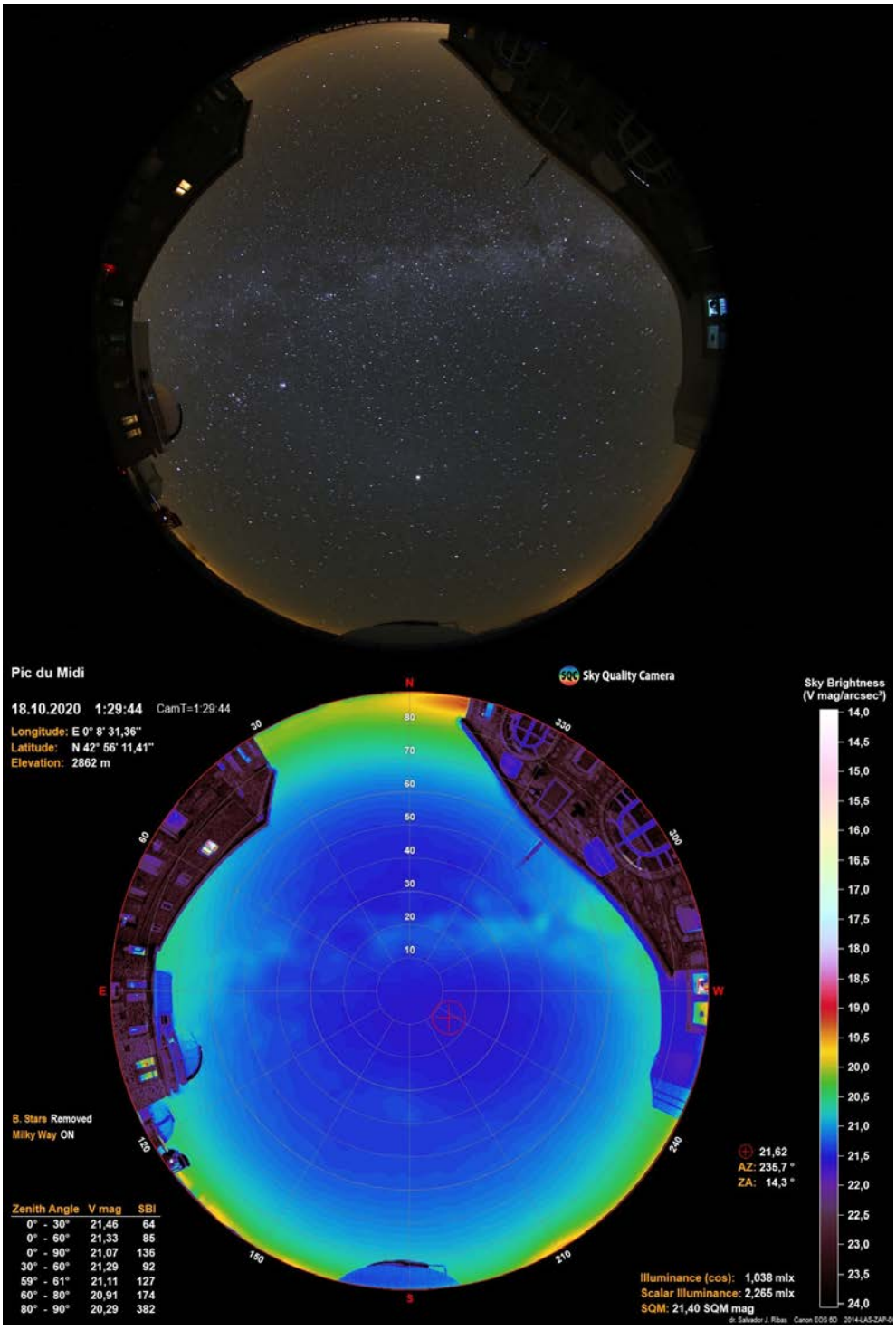

Figure 3.39: All-sky image at the Pic du midi on the night of the 18th of October. Top: raw data. Bottom: processed with SQC. Location three.

its polluting effect. To the NNW there is the light dome produced by Tarbes, a city with more than 50k inhabitants placed at 20 km. To the SW and to the SE there are tiny light pollution domes probably produced by close and small sources. The NE direction is blocked by buildings in the three set of images. One can sense a light dome in that direction similar in size to the one of Tarbes. In that direction there is the city of Lourdes at 12 km from the observatory that has a population of 14k inhabitants, and the city of Pau further away, at 35 km, with a population of 80k inhabitants.

Valle del Roncal

Valle del Roncal is within the Pyrenees of Navarra region. The mountain range that surrounds the valley is known as Larra-Belagua. This area is one of the three key regions of the Pyrenees La Nuit project.

On the night of the 7th of April of 2021 a set of DSLR images were taken at the top of Larra-Belagua mountain range at more than 1700 m, just over the border between Spain and France. There was uneven snow coverage exclusively at the top of the mountain. It took more than eight months to have a chance to take the measurements due to bad weather and SARS-COVID2 mobility restrictions.

The SQM estimated value of the images is 21.64 mag/arcsec^2 and the darkest value is 21.97 mag/arcsec^2 at 70° in elevation to the NE. The Milky Way crosses the sky from S to N in a constant elevation of approx 30°.

There are four distinguishable polluted directions close to the horizon: NE towards Pau, Olorons Saint Marie and the skiing resort of Pierre Saint Martin; ENE towards Tarbes and Toulouse; NW probably due to Bayonne, Donosti and Irun; and SW towards Pamplona.

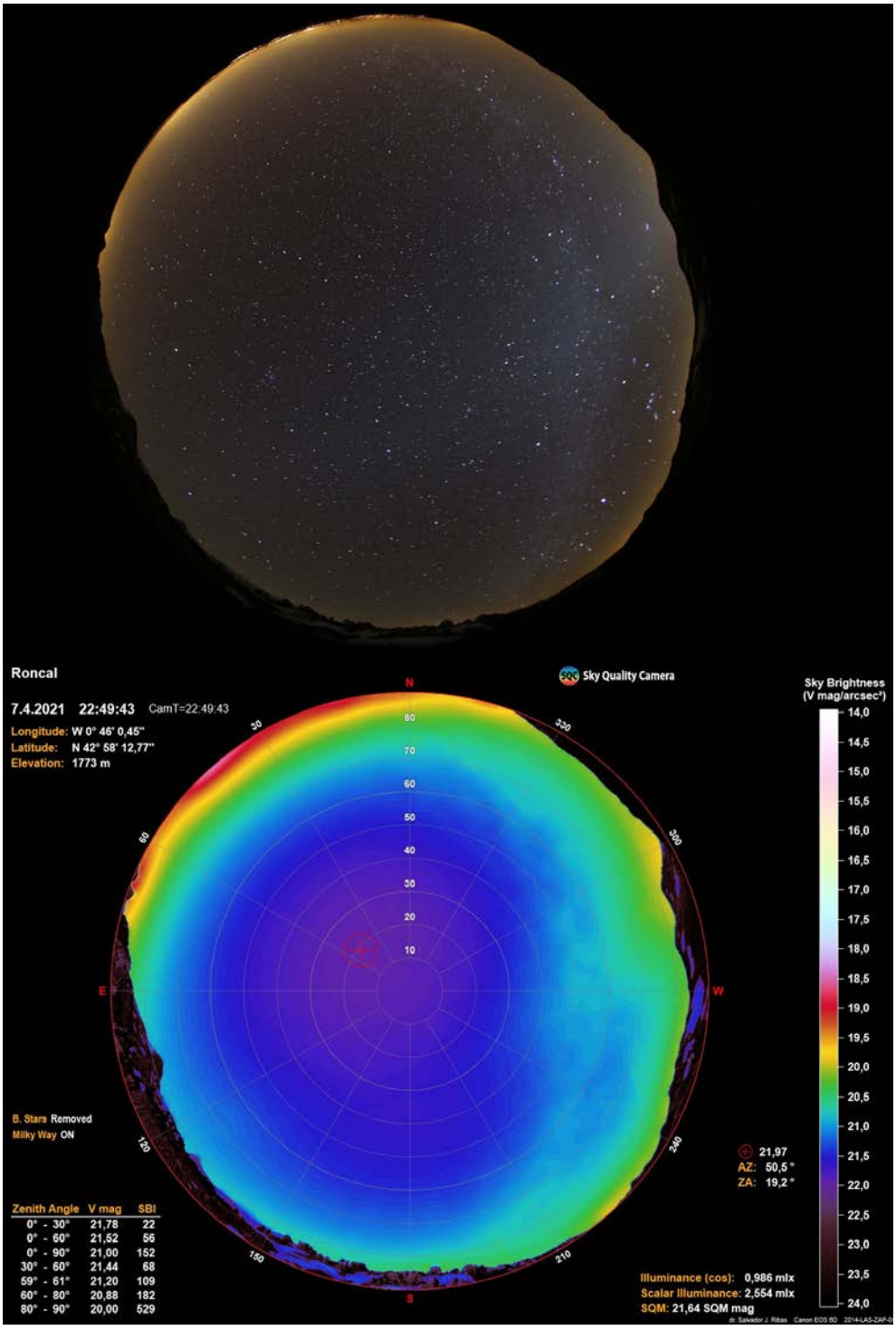

Figure 3.40: All-sky image at Valle del Roncal on the night of the 7th of April 2021. Top: raw data. Bottom: processed with SQC.

3.3 Measurements summary

Each campaign is discussed in detail in their respective sections. We present here a summary in table 3.5 and a global analysis of the night sky scenario of the country.

The measurements described in the previous sections cover a significant part of Catalonia. They evidence the heterogeneity of the country and the impossibility to analyse it as a whole: there is a large and densely populated coastal line, mountain ranges that reach 3000 m, scarcely populated interior regions with continental climates and two big metropolitan areas.

As a general description of Catalonia scenario we found:

- Barcelona and Tarragona metropolitan areas are by far the greatest and second greatest artificial light sources of Catalonia. Sky brightness in a radius of tens of kilometers are heavily influenced by them.
- In a lesser extent, the rest of the coastal line is also a source of light pollution. There is a general pattern of darkening as we move away from the coast. The exception is the Ebre's delta that is barely populated.
- The Pyrenees is a dark region, although not the darkest measured, due to its remoteness and low population. In the east, Girona, Figueres and the coastal line brighten the sky, really dark values are only found in a few valleys close to the border with France. In the center, Andorra dominates the sky brightness. And in the west, although it is the darkest region of the Pyrenees, skiing resorts also pollute the sky. In general, we found really dark values but not as pristine as expected.
- The two darkest regions we studied are Montsec mountain range and its surroundings, and Ports de Beseit NP. Both areas present multiple values above 21.5 mag/arcsec^2. Moreover, both regions were already covered in previous campaigns with similar results. Ports de Beseit was covered in 2013 and Montsec mountain range is studied every year due to its importance as a protected area against light pollution.

Region	Year	Description
Eastern Pyrenees	2017, 2018	Dark sky. Several cells above 21.0. Few cells in the north over 21.4. Brightest levels to the east due to the presence of Girona, Figueres and the coastal line. Dense vegetation. In some areas up to 60% of the values were discarded.
Montserrat NP	2017	Polluted sky. Most of the cells between 20.0 and 20.5 due to the proximity to Barcelona metropolitan area. Clear routes.
Muntanyes de Prades and Montsant NP	2018	Slitghtly polluted sky. Most of the cells are above 20.5, there are no values beyond 21.2. The proximity to Tarragona metropolitan area creates a gradient of brightness towards the city. Moderate vegetation easy to filter. Clear nights were scarce.
Ebre's delta and Ports de Beseit NP	2019	Pristine sky in the NP with multiple values above 21.5. Dark in Ebre's delta, most of the cells over 21.2. The biggest pollutants are the coastal line, Amposta, Tortosa, and Vandellós and Ascó nuclear plants. Scarce to moderate vegetation and numerous crossing vehicles.
Alt Pirineu NP	2019	Very dark. Almost every cell not adjacent to a town is over 21.0, many over 21.4 and even a few close to 21.6. Andorra in the east and skiing station and towns in the west are the main pollutants. Dense vegetation. Exhaustive filtering needed.
Montsec influence area	2019	Pristine around PAM and in north in the west border of Catalonia. Very Dark in general with several values above 21.4. There is a brightening trend around Balaguer and in the south close to middle-size cities. Almost no vegetation in the south, dense in the center and moderate in the north.
North-east Catalonia	2020	Slightly polluted sky far from towns. Most of the cells with values between 20.5 and 21.0. Darkest values in the Creus cape reaching 21.2. There are cities with big areas of influence as Figueres, Castelló d'Empúries and Roses. Dense vegetation in the north. Close to undisturbed anywhere else.
Montseny NP	2020	Polluted sky. Many cells below 20.5, some below 20.0. In the deepest region of the NP cells over 20.5. The polluting sources are Barcelona in the south-west and the coastal line in the south-east. Dense vegetation inside the NP. Numerous vehicles in the west side.

Table 3.5: Summary of the areas covered during the PhD program.

3.4 Dynamic SQM measurements methodology discussion

In this section we discuss the most important aspects about the SQM dynamic measurements methodology. Spectral and optical features of the instrumentation are not addressed though. See chapter 2 for detailed information about those issues.

The methodology presented allows to cover vast areas in relatively short time. In long and stable nights we achieved to cover around 300 km. It has also an easy setup and requires small training to be able to gather data properly. Contrarily, processing properly the data is not trivial. We tried to ease and homogenize the process by creating the M2M software. However, the hand of an expert is still required when the routes covered have dense vegetation or other altering elements. As a matter of fact, the data from the campaign of 2017, 2018 and even slightly data from 2019 had to be reprocessed with the expertise gained through the years. Changes in the maps were significant.

The resulting light pollution cell maps have demonstrated to be an easy to read tool for both experts and non-experts in light pollution. The use of cells smooths the inherent variability of individual measurements. On the other hand, the dimension of the cells should be small enough to recognize the paths that have been followed and to reveal the differences present within each region.

The color scale that represents the sky brightness level is other topic open for discussion. As we explained in section 3.1.3, there is no standard color scale for representing sky brightness levels. Big steps help to palliate the variability problem (variability due to intrinsic errors and filtering is of the order of magnitude of 0.2 mag/arsec^2) and are useful for its simplicity, but this kind of color scales are sometimes misleading. Skies with significant different brightness levels could share the same color in the map if the steps were too wide. Big steps also mask the gradient of light pollution around small and middle size towns. We used a color scale that lies at a midpoint between wide and narrow regarding step size. With a step of 0.5 mag/arcsec^2 we ensure stability of the map, keep its simplicity, have enough steps to distinguish quite well sky brightness levels and reveal the gradient of sky brightness produced by cities and big and middle towns. However, it is not perfect. With this scale the gradient produced by small towns are normally undetected. Moreover, a difference of 0.1 mag/arsec^2 can produce a change of color and a difference of 0.4 mag/arsec^2 could not. When reading the maps it is important taking into account those limitations. For a detailed analysis, raw data should be used instead.

Regarding towns, it is more important to see their area of influence than the value of the cells where they reside. Measurements inside the city are not reliable because sky brightness levels are affected by direct light coming from street lamps. As a result, there are abrupt changes within meters. The area affected by light coming from cities and towns depends on their population and how the street lighting is designed. Hence, the radius of affectation around towns, once the population is taken into account, could be a reliable source of information to assess the design of their street lighting. As a rule of thumb, small and middle sized towns that are properly lit do not influence their surroundings. Equally sized towns but wrongly lit can have an area of influence of several kilometers. Big cities always have an impact on their surroundings, but an efficient street lighting can reduce notably the radius of the area brightened.

One of the major concerns is the temporary nature of the maps. As we explained in the campaigns discussion, some trails were probably studied with abnormal conditions of humidity that brightened the results. Some tracks that have been covered more than once in different nights, or even in the same night with several hours of difference, presented zenith values that differ 0.2 mag/arcsec^2 (in extreme cases the difference reached 0.3 mag/arcsec^2). One could think that measuring the same area twice or even more times could mitigate the problem. However, clear sky moonless nights are not common and this approach would reduce significantly the capacity to cover vast areas. Although aerosol content at night is quite difficult to get[2], hygrometers could be included to measure humidity levels along the routes covered. A quantitative relation between humidity and sky brightness is very complex to derive, but as a future project it would be interesting if there is a clear pattern. They could also be used to define a maximum threshold of relative humidity beyond which measurements would not be reliable.

It is also crucial to take into account the position of the Milky Way when taking SQM measurements. Neglecting it could lead to wrong conclusions. In this sense, taking DSLR images along SQM dynamic campaigns has been of great help. In addition, DSLR images processed with SQC software estimates the zenith SQM value of the sky. Differences between the actual SQM values and the estimated by the SQC from images taken the same night reach 0.2 mag/arcsec^2. As there is no information available about how SQC software estimates the SQM value we rely on the actual SQM value and use the estimated value for qualitatively comparisons.

[2]Aerosol content is typically estimated using a worldwide network called Aerosol Robotic Network (AERONET) that tracks is optical depth during daytime. At night there are some systems that uses the Moon as a reference for estimating aerosol content. In our case, moonless nights, there is no reference for estimating aerosol content.

As a conclusion, the SQM dynamic measurements are a valid methodology for assessing vast areas as long as they are processed by experienced teams. Information about the Milky Way, humidity levels and other phenomena is very important when assessing the quality of the sky. Different color scales should be used depending on the goals of the assessment: coarse scales for outreach and simple studies and detailed ones when focusing in sky brightness gradients. It is important too to recall that the SQM device must not be used as a permanent device and must be stored in a dark place between campaigns. Otherwise, deterioration due to sunlight exposure would make that different campaigns could not be compared (see section 2.2.1).

Chapter 4

Modelling light pollution

Light pollution modelling aims to reproduce and predict how artificial light affects the sky. In this thesis we focus on models that estimate the sky brightness by reproducing the interactions between the electromagnetic radiation and the molecules and aerosols that constitute the atmosphere. It is an arduous task as sky brightness depends on multiple variables such as air mass, atmospheric content, altitude, direction, light spectrum, cities architecture, ground surface, etc. Such models are useful for multiple purposes. They help us to:

- Understand light pollution in a physics level, i.e. the role that the variables play in the phenomena. That knowledge is helpful to be more efficient when trying to reduce the harmful effects of light pollution.

- Asses light pollution levels. Measurements are not always possible due to bad weather, inaccessible sites, lack of funds to perform measurement campaigns, etc.

- Provide predictions. We can study the consequences of changing light systems before it actually happens.

This chapter contains a brief historical review of the main models developed during the last 50 years and a detailed description of the model that is the base of our simulations.

How we used light pollution models and the results obtained are presented in the next chapter (see chapter 5)

4.1 Historical review

4.1.1 First attempts

The first light pollution model was defined by Treanor (1973). He derived a semi-empirical propagation law that estimated the zenith brightness produced by towns (considered as point like sources) in the B band of the Johnson-Cousins photometric system. The model took into account first and second order aerosol scattering (i.e. light paths with one and two changes of directions respectively between the source and the observer). However, the first change of direction of the second order scattering path was limited to a small angle in the direction of the incident beam (see figure 4.1). The model was based on three variables: distance, population and atmospheric attenuation. The effect of the first order scattering was modeled by an inverse square distance law and the effect of the second order scattering by an inverse linear dependence on distance. City emission was estimated using its population and adapted to different kind of towns by an urban development factor.

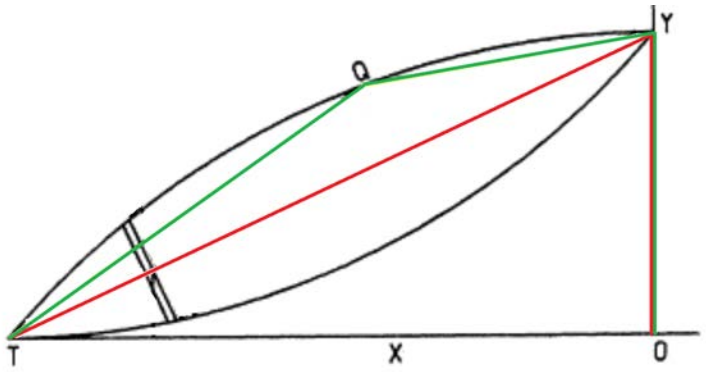

Figure 4.1: Treanor model scheme. Modified from Treanor (1973). T for town, O for observer position, X distance between town and observer, Y position where the last scattering take place, Q first scattering of the second order scattering. In red the path that follows a photon coming from first order scattering, in green the path that follows a photon coming from second order scattering. Second order scattering is limited to the volume inside the black arcs going from T to Y due to the limitation of scattering angles imposed.

The zenith sky brightness, SB_z, in units of the natural sky brightness, is expressed by:

$$SB_z = aP(\frac{A}{X} + \frac{B}{X^2})exp(-kX) \tag{4.1}$$

being P population in 10^5 inhabitants, X distance in km, a dimensionless urban development factor, k empirical attenuation factor and A and B empirical constants.

The empirical constants were estimated as $A = 1.8$, $B = 13.6$ and $k = 0.026$, using three towns as sources: Rome (2.6M inhabitants and $a = 1$), L'Aquila (61k inhabitants and $a = 0.77$) and Teramo (48k inhabitants and $a = 0.77$). The resulting law was used by Bertiau et al. (1973) to create a map showing the expected artificial sky brightness for the whole Italian country. The model was well accepted by the light pollution community.

Some authors tried to adjust Treanor's model to fit their own measurements. Berry (1976) attempted to do so with his measurements in B and V bands in the region of Ontario, Canada. In the process he modified the zenith brightness-population relation by proposing that the brightness produced by a city was proportional to the square root of the population. That new relation agreed quite accurately with the observations from Normandin (1974) in the province of Quebec, Canada.

Walker (1977) was the first to attempt to model light pollution in a direction different than zenith. He measured sky brightness at 45° in elevation and azimuth directly pointing towards towns. For the measurements, he used as a reference towns with different characteristics within California. He came back to the proportional relation between city light emission and population. He also defined a brightness exponential decay of factor 2.5 with distance:

$$SB_{45} \propto D^{-2.5} \tag{4.2}$$

4.1.2 The first elaborate physical model: Garstang

A major step towards a more complete model was proposed by Garstang (1986). The aim was to create a model that could take into account the main features of the real scenario.

The atmosphere was defined as a combination of molecules and aerosols, being aerosol content an adjustable parameter. Their vertical profiles followed exponential decrease functions with altitude. First and second order aerosol and molecular scattering were taken into account. The scattering phase function, that is the angular distribution of light intensity scattered by a particle at a given wavelength, was assumed as Rayleigh scattering for molecules; for the aerosol, the scattering constant coefficient used in previous models was replaced by an ad-hoc phase function. Absorption was modelled in relation to the scattering, particularly as a

constant percentage of the scattering value.

City light emission continued to be linked to population, but cities were modeled as circular surfaces of homogeneous radiosity instead of point like sources. Upwards light emission was the combination of light emitted directly above the horizon angle and light emitted downwards and reflected off the ground. Direct upwards emission was defined as a fixed percentage of the total emission, and its distribution followed an arbitrary function with zenith angle. The amount of light reflected off the ground was fixed as a percentage of the light emitted downwards and was scattered following a Lambert distribution (see figure 4.2). Lambert distribution is defined by:

$$L_\theta = L\ cos(\theta) \tag{4.3}$$

being L the radiance along the normal and θ the angle with respect to the normal.

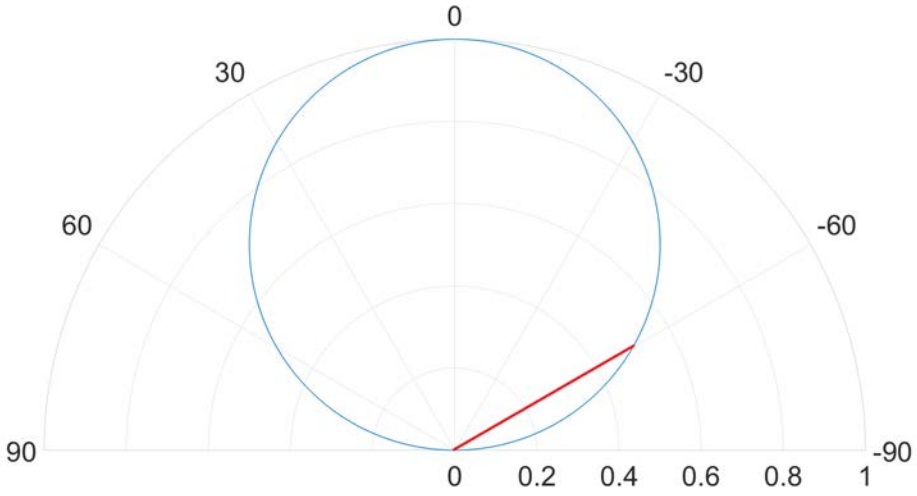

Figure 4.2: Projection of Lambert's cosine law, being 0° the normal to the surface, and θ the angle respect to the normal. The blue circumference corresponds to the radiance emitted in any direction relative to the normal. In red the relative radiance of -60° as an example.

Garstang's model was designed for B and V Johnson bands and it was not limited to zenith: any line of sight could be computed. It went through some refinements over the years (Garstang 1988 and 1991). This model was widely spread and used to calculate sky brightness in locations in the US, Chile, France, Australia and Mexico. Based on Garstang's model, Cinzano et al. (2001) developed a method to create zenith sky brightness maps in V band for large territories. Falchi et al. (2016) expanded the study by creating a zenith brightness world atlas map. For further information see 5.4.

4.1.3 State of the art

Nowadays, there are two light pollution models that standout in the light pollution community: **MSNsR** (Kocifaj 2007) and **Illumina** (Aubé et al. 2005, 2018, 2020). Each of them is embedded in a software that makes the simulation process more user friendly. In this section both models are introduced and compared. It is also explained why Illumina was chosen to perform our simulations. Section 4.2 is dedicated to describe the Illumina model in detail.

Both models, MSNsR and Illumina, share a feature never accounted before: spectral heterogeneity of light sources. Previous models used a constant value of radiant flux for each filter studied, normally B and V. These two models compute spectral flux based on the actual mix of lamp technologies present in each city.

MSNsR is based on a physical model that only takes into account first order scattering. That makes it very fast but the accuracy of its results is uncertain when studying distant sources specially with thick atmospheres. In this sense, Kocifaj (2018) concluded that higher orders than first order scattering are not negligible for distances superior to 30 km for blue light and 60 km for red light. The atmosphere is modelled as vertically stratified and composed by molecules and aerosols. Molecular scattering is simulated in accordance with Rayleigh theory, and aerosol scattering is approximated by the Henyey–Greenstein (HG) function (Braak et al. 2001). Molecular absorption is neglected and aerosol absorption is a variable parameter depending of the kind of aerosol defined in each case (Kocifaj 2017).

Although this model does not take into account topographic information, it allows to mask certain lines of sight in order to simulate the effect of mountains around the observation point. The mask model is empirical and based on observational data collected in Stará Lesná, Slovakia.

Sources such as cities and towns are modelled as flat surfaces of homogeneous emission. Radiant flux emitted by a town depends on the population, although, if known, the user can introduce the radiant flux of the city in watts or the luminous power in lumens. The spectrum of the emitted light is homogeneous for the city and defined by the user. The model allows to choose for each city or town between three different city emission functions:

- Garstang's city emission definition. Explained in the previous section. The ratio of light emitted towards the upper hemisphere (ULOR) is defined by the user for each city.
- Lambertian, (see figure 4.2), meaning that the luminous intensity obeys

Lambert's cosine law.

- Customized simple function with respect of the elevation angle.

The operational wavelength range of MSNsR goes from 350 nm to 800 nm, and the user can choose which range to study within these margins. The output of the model is the diffusive irradiance (W/m2) on horizontal surface and the radiance (W/m2/sr) received in a set of directions covering the whole sky dome.

Illumina, on the other hand, uses a complete new approach. The model scheme is similar to ray-tracing software: a statistically selected set of photons is thrown from luminaries to the atmosphere and interactions with the ground, molecules and aerosols are computed along the light paths towards a simulated observer (Aubé & Kocifaj 2012). It accounts for first and second order scattering without limitation in direction or distance. Aubé (2007) showed that the second order relative contribution rises with distance from city limits and may contribute up to 66% of the total zenith radiance for remote sites. Therefore, experiments with observer's location far from cities should take into account second order scattering.

Another major novelty of this model is that it uses satellite data to compute the radiance emitted by light sources, making population-brightness function no longer necessary. Satellite data also allows to take into account heterogeneity in radiance emitted between different regions within a city. Topographic information is gathered using satellite data too. The model includes obstacles, as buildings and trees, to define each city emission function. Optical and spectral information are estimated by the combination of luminaries and lamps within the city. This numerical approach is very time consuming due mostly to second order scattering computation. The model allows to run cases only accounting for single scattering contribution as well. Illumina model is explained in detail in the next section.

The two models explained (in their early stage versions) were compared in a study in the Canary Islands (Aubé & Kocifaj 2012). It was shown that under low-turbidity conditions and for elevation angles over 30° the two models agreed well. In that particular case, when comparing to observations, low elevation angles agreed well with both models, although MSNsR was slightly darker. However, close to zenith the discrepancy between observations and simulations in both models increased, probably due to bad weather conditions during observations (Aubé & Kocifaj 2012).

As stated before, our light pollution simulations are mainly based on Illumina. We made that decision for multiple reasons:

- Taking into account second order scattering widens the range of city distances and atmospheric conditions we can study.
- It includes topographic information, a key factor when studying light pollution in mountain ranges as the Pyrenees.
- The way how Illumina uses satellite data simplifies the characterisation of similar sources allowing to group multiple towns into large source areas. For comparison, in MSNsR towns and cities are bound to their surfaces thus they have to be defined one by one, making the task very time consuming.
- Its structure allowed us to derive ad hoc functions to apply in contribution maps (section 5.1). It also eased the process of creating zenith sky maps (section 5.4), that would have been much complex with other models.

4.2 Illumina

4.2.1 Overview

In the moment of the writing there coexists two versions of Illumina. The newest one, Illumina v2 was released in 2020. In this section we are going to describe Illumina v1 and how it evolved from its early stages to its final version. The novelties of Illumina v2 are described in an independent section. Both versions share the same structure and many features.

Illumina was developed initially as a tool for measuring aerosol content in the atmosphere. The strategy was to first measure the radiance received with a spectrometer and then adjust the aerosol optical depth in a light pollution model in order to obtain the same radiance values (Aubé et al. 2005) (see figure 4.3). The aim of the model was redefined later on to focus on assessing and studying light pollution itself.

As existing models were not accurate enough for the initial purpose, the authors decided to create a new light pollution model from scratch that accounted for the heterogeneity of the environment. The main features of the model are:

1. First order and second order molecular and aerosol scattering. It depends on: the transmittance of the atmosphere in every path, defined as the fraction of incident electromagnetic radiation that is transmitted by the atmosphere; the scattering probability; and the scattering phase function (see 4.2.2).

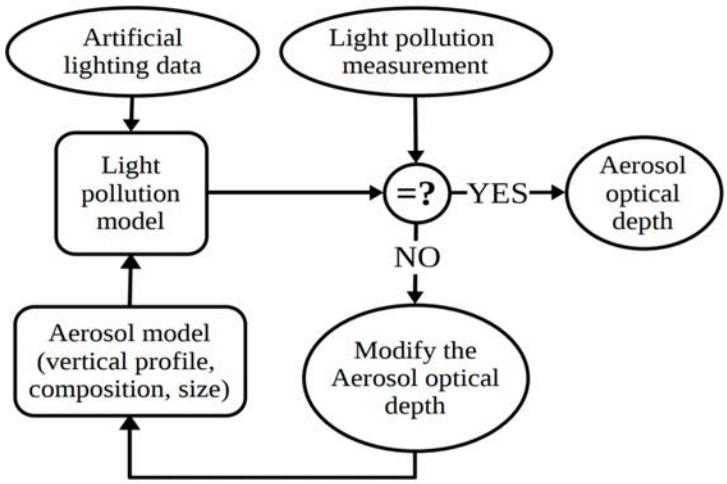

Figure 4.3: Scheme of the initial strategy to measure aerosol content using Illumina model. Aubé et al. (2005).

2. Vertical variations in atmospheric optical properties (see 4.2.2).

3. Satellite data for source definition. Non uniform ground reflectance values and non-uniform distribution of light fixture luminosity (see 4.2.3).

4. Heterogeneous characterisation of lamps. It allows to combine different spectra and angular patterns within the same town, and define differently light sources within an experiment (see 4.2.3).

5. Topographic information to determine differences in altitude between observer and light sources and also for determining the orographic blocking effects (see 4.2.4).

Illumina produces three outputs:

1. The artificial radiance received in each location, direction and wavelength chosen.

2. Radiance contribution maps. For each combination of spectral window and direction studied, Illumina provides a map showing the relative contribution of each surface source to the total radiance received.

3. The sensitivity to light pollution for every direction and wavelength window. That is how each source contributed per unit of luminous flux installed.

4.2.2 Atmospheric characterization

To compute the artificial radiance received in a given direction, Illumina divides the atmosphere in voxels (three dimensional cells or pixels) and adds up the contribution coming from the voxels along the corresponding line of sight (n in figure 4.4). The model assumes that the total radiance received is mainly explained by the combination of first order (I_1 and I_{r1} in figure 4.4) and second order molecular and aerosol scattering (I_2 and I_{r2} in figure 4.4), either scattered directly from the source or after light is reflected off the ground.

First order scattering paths (I_1 and I_{r1}) are also used to generate the set of sources to compute the second order scattering (I_2 and I_{r2}). Since they are very numerous, the computation of second order contribution becomes rapidly a crucial problem in term of computation time. To restrict it, the voxels that can produce second order scattering are limited by a radius around the path between the source (or the ground in case of reflection) and the voxel where the last scattering takes place. The radius is adjustable by the user. Aubé (2007) computed an optimal value for this radius defined as the minimum value with a maximum loss of total radiance of 1%. They showed that it is achieved when the radius includes all city lights (i.e. the distance from city centre plus the city radius).

For every path, aerosol absorption is taken into account and molecular absorption is assumed to be negligible. Early versions of the model studied the visible and part of the near infrared spectral regions with a single broad band. Since molecular absorption is not negligible in the infrared, the error induced by not taking it into account was very difficult to assess. For simplicity the model was restricted to spectral bands that were not affected by molecular absorption (mainly the visible range, see figure 4.5). In following versions of Illumina, the model changed to support hyperspectral modelling (Aubé et al. 2018), that allowed to study possible affected wavelengths separately. Anyway, the accuracy of the results is only assured when studying the visible range (330nm-730nm), where molecular absorption is very low (Gueymard 2001) (see figure 4.5).

Aerosol and molecular extinction (that is the combination of scattering and absorption) are computed assuming that their vertical concentration profiles follow exponentially decreasing functions. The atmosphere is modeled with constant scale height, H_a=2 km for aerosols and H_{mol}=8 km for molecules. The voxel vertical scale is logarithmic. Thinner voxels close to the surface ensure better accuracy in low-altitude phenomena, where atmospheric concentration and light intensity are higher. The vertical profile extends from the lowest altitude of the region of study to 30 km above it. It is also assumed that aerosol and molecular concentration profiles

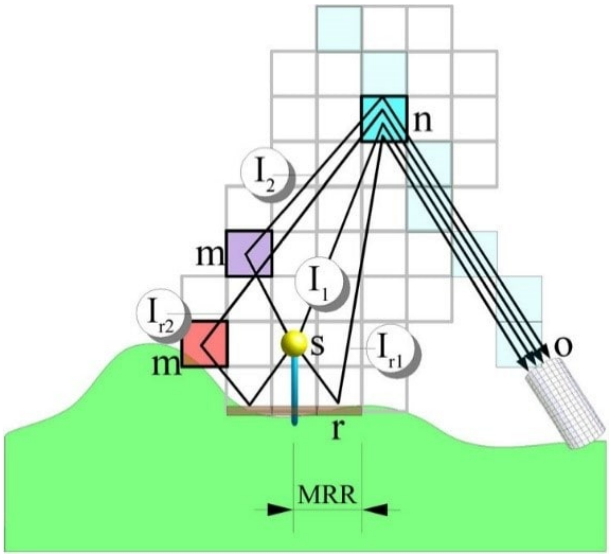

Figure 4.4: Scheme of the model used by ILLUMINA to compute the flux received in each direction. S, source of light; O, observer's location; n, any voxel in the line of sight of the observer; m, cells that scatter light to n; I_1, first order scattering path; I_2, second order scattering path; I_{r1}, reflection and first order scattering path; I_{r2}, reflection and second order scattering path; r, reflection on the ground; MRR, maximum radius taken into account for the reflection. Image from Aubé et al. (2005).

with respect to the altitude are the same over the modeling domain.

The scattering phase function is precomputed using the Mie or Rayleigh theory, depending if we are to consider aerosol or molecular contributions respectively (Aubé et al. 2005).

To determine the atmospheric transmittance, T, defined as the fraction of incident light that is transmitted by the atmosphere, it is assumed that:

$$T = T_a T_{mol} \tag{4.4}$$

Both aerosol transmittance, T_a, and molecular transmittance, T_{mol}, are defined for every path in relation to the total atmospheric transmittance, T_∞. As long as we assume an exponential vertical profile for aerosol and molecular atmospheric content, it can be shown that T_a and T_{mol} for an air slice starting at altitude z_1 to altitude z_2 is given by:

$$T_a = T_{a\infty}^{exp(-z_1/H_a)-exp(-z_2/H_a)} \tag{4.5}$$

$$T_{mol} = T_{mol\infty}^{exp(-z_1/H_{mol})-exp(-z_2/H_{mol})} \tag{4.6}$$

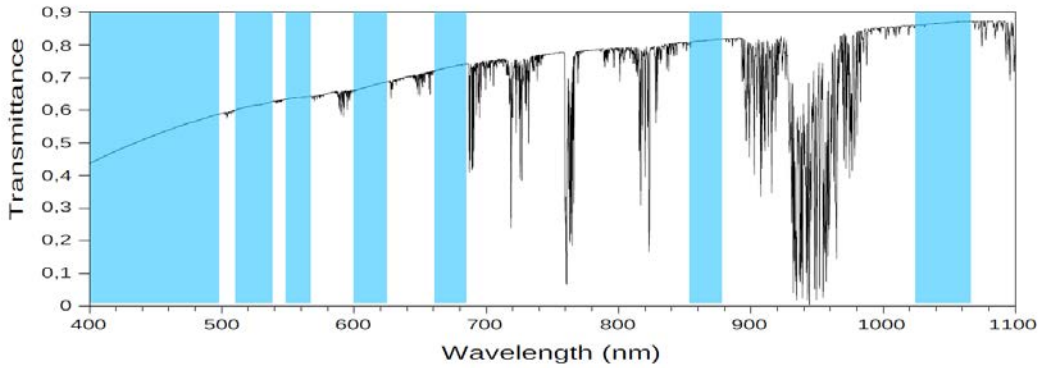

Figure 4.5: MODTRAN (Kneizys et al. 1996) simulation of the atmospheric extinction for mid latitudes. The positive trend of transmittance with wavelength is due to molecular scattering, effect accounted in the model. Abrupt changes in the pattern are due to molecular absorption, mainly by water vapour and carbon dioxide molecules. Blue regions were the range allowed in the first versions of Illumina. Image from Aubé et al. (2005).

where $T_{a\infty}$ is estimated with the total aerosol optical depth, τ_a, corrected for the air mass M_∞ (Bird 1984):

$$T_{a\infty} = exp(-M_\infty \tau_a) \tag{4.7}$$

τ_a depends on the wavelength of the incident light. The relation is described by the power law:

$$\tau_a = \tau_0 (\frac{\lambda}{\lambda_0})^\alpha \tag{4.8}$$

being α the Angstrom coefficient.

$T_{mol\infty}$ is defined according to Kneizys et al. (1980):

$$T_{mol\infty} = exp(-M_\infty \tau_{mol}) \tag{4.9}$$

being τ_{mol}:

$$\tau_{mol} = \frac{1}{\lambda^4 (115.6406 - \frac{1.335}{\lambda^2})} \tag{4.10}$$

The model assumes plane parallel atmosphere:

$$M_\infty \propto \frac{1}{cos(\theta)} \tag{4.11}$$

Extinction is the combination of scattering and absorption. As Illumina does not take into account molecular absorption, molecular extinction is exclusively molecular scattering. Thus, the probability of molecular scattering, P_{molS}, is directly:

$$P_{molS} = 1 - T_{mol} \tag{4.12}$$

For aerosols, transmittance is a combination of scattering and absorption, therefore the probability of aerosol scattering is proportional to the ratio between scattering and extinction cross sections, σ_S and σ_E respectively:

$$P_{aS} = \frac{\sigma_S}{\sigma_E} P_a = \frac{\sigma_S}{\sigma_E}(1 - T_a) \tag{4.13}$$

4.2.3 Sources characterization

Light sources as cities and towns are defined by circular areas. Radiance emitted by sources is computed using satellite that allows accounting for the heterogeneity of the radiance emitted between different regions within the same source. Older versions of Illumina used DMSP-OLS data which was replaced for VIIRS-DNB sensor data because of its better radiometric accuracy, spatial resolution (742x742 m) and geometric quality (see figure 4.6). However, spectral sensitivity of the VIIRS DNB sensor is very low in the blue region (see figure 4.7). The hyperspectral capabilities of Illumina included during 2016 (Aubé et al. 2018) make it possible to correct it. Knowing the spectrum of each source, Illumina computes the ratio of the total radiance that the VIIRS can measure and corrects accordingly the underestimation. This is crucial, particularly with sources with blue-rich emission as most of LEDs or mercury vapor discharge lamps. For instance, the VIIRS DNB sensor only detects the 79% of the radiance emitted by high pressure sodium lamps, 66% from LED of 4000K CCT and 59% of mercury vapor lamps.

The area where light coming from a source can be reflected off the ground is limited (MRR in figure 4.4), and determined by the presence of obstacles, such as trees, buildings or orography. The reflectance of the ground is estimated using satellite spectral albedo information from the Moderate Resolution Imaging Spectroradiometer (MODIS) that has a resolution of 500x500 m. Its angular function

Figure 4.6: VIIRS-DNB sensor image of the Iberian peninsula, south of France and North Africa.

is assumed to be Lambertian (see figure 4.2), meaning the surface's luminance is isotropic, and the luminous intensity obeys Lambert's cosine law (see equation 4.3).

A part from radiance and ground reflectivity, the remaining characteristics of light sources inside each circular area are defined homogeneously: lamp spectra, light output angular distribution with respect to the vertical axis, lamp height respective to the ground, obstacle's size and distance, and the probability for a photon of hitting an obstacle. Normally these properties are the mean or typical values of the points of light within each area. Illumina allows to mix different kind of lamps weighted by its emission. It is of great help having access to the detailed inventory of the lighting systems of cities and towns. Big cities can be defined in an independent and unique circular area or be split in several areas if the characteristics of the lamps differ between regions inside the city. On the other hand, smaller and similar towns can be grouped together.

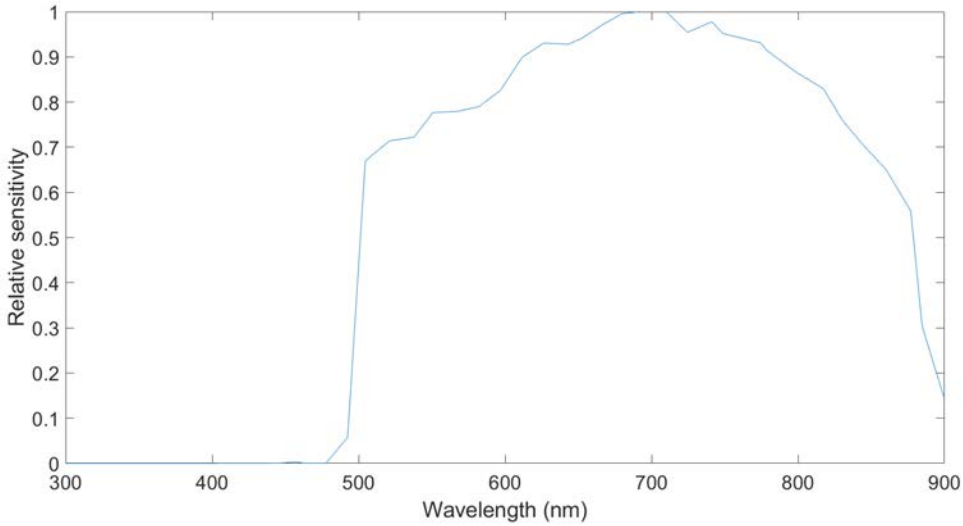

Figure 4.7: Sensitivity of the VIIRS-DNB sensor with respect to the wavelength (Liao et al. 2013).

4.2.4 Scenario characterization

When running an experiment with Illumina the user has to specify the geographic domain. First, the location where the artificial brightness received is to be estimated. Second, the working map projection since the model works with coordinates in distance units instead of geographic coordinates. Third, the limits of the geographic domain, i.e. the extreme SW and NE points. Finally, the pixel size in meters of the grid that defines the spatial resolution of the domain. That information, as commented before, is combined with: VIIRS-DNB data for obtaining radiance information; MODIS data for the reflectivity of the ground; and the digital elevation model of the Shuttle Radar Topography Mission (SRTM) to get topographic information (see figure 4.8). The topographic information is used to determine the altitude of the observer and the sources, and to determine the blocking effect of the orography.

Beyond defining sources (see previous section) the user has to select other relevant parameters:

1. The location (multiple location possible) of the observation point.
2. The directions to study, defined by elevation and azimuth angles.
3. The wavelength range. Illumina allows to study the range between 330 nm

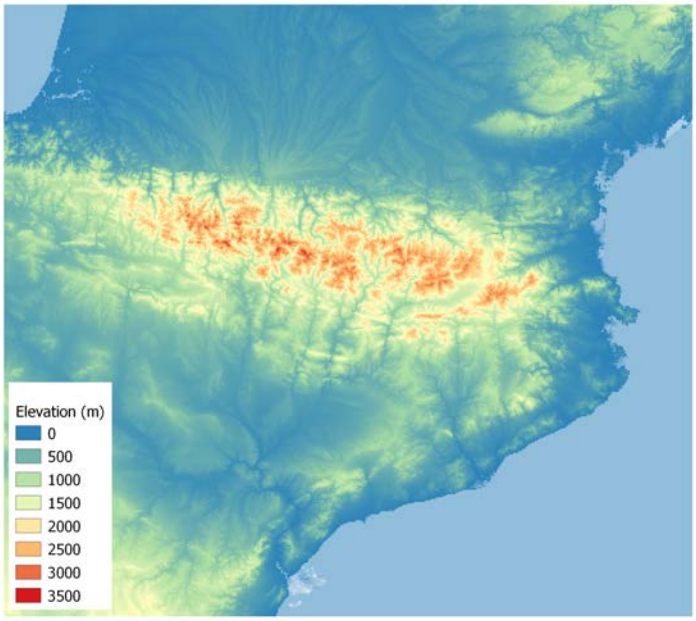

Figure 4.8: Digital elevation model made from SRTM data for the area of Catalonia. Color scale added by the author for visual purposes.

and 850 nm. The user can choose any range within these limits. However, the accuracy of the results between 730 and 850 nm is not ensured since above 730 nm the molecular absorption is not negligible.

4. The number of spectral windows in which the wavelength range will be divided. The range selected can be studies in windows from 1 nm to a unique window that encompasses the whole range selected.

5. Atmospheric conditions: humidity, aerosol optical depth, Angstrom coefficient, sea level pressure and the kind of aerosol dominant (rural, maritime, urban, etc.)

Although it is not used in our work, Illumina offers the possibility of adding clouds in the experiments. They are characterized by the cloud base height, which becomes the effective maximum height of the atmosphere. The reflectance of the surface of the clouds is different for each kind of cloud and based on the work of Saphiro (1982).

4.2.5 Our contribution to Illumina

Illumina has been used in the last decade for assessing light pollution levels in many sites: Mont-Megantic in Quebec, Oukaimeden in Morocco, Canary Islands in Spain, Asiago in Italy... However, it has been rarely used from outside the developing team.

We have been using Illumina intensively for the last three years (Linares et al. 2018, 2020). We started by simulating the artificial brightness received in the Parc Astronomic Montsec coming from the city of Lleida. Then we expanded the map adding more sources. First, the cities of Balaguer and Tremp. Afterwards, all the light sources in a radius of 50 km. Lastly, we simulated the sky brightness in several other locations and at the same time we were developing other products (see chapter 5).

During this time we have contributed to enhance the model by reporting errors and clarifying misunderstandings with the developers. Every update in the program was tested and compared with previous results. The difference in the results lead to spotting errors in the new versions of the code. We present a list with some of the most relevant contributions:

1. When studying how Lleida was affecting the sky over Montsec, that is located 50 km away, we realized that the radiance received in azimuths not pointing to Lleida were higher than the ones pointing directly to it. As Lleida was the only source in the simulation, that could not be realistic. We spotted that the model was using a geometric system to select which voxels where within the line of sight in a given direction that was too restrictive. In some cases it excluded highly contributing ones. The problem was solved by changing the parameters to include all the voxels that lied in the line of sight of the direction studied.

2. We performed a simulation of the sky over Montsec with only three sources, Lleida, Balaguer and Tremp, in order to measure its impact. Then we simulated a more complete experiment adding more and smaller sources. The second simulation showed that the radiance received in the direction of Lleida was lower than in the previous case. It happened because the model was not taking into account the voxels close to Lleida. Illumina is programmed to start computing the contribution of the closest voxel in the line of sight and move to further voxels, it stops when the contribution of the voxel is below a percentage of the total contribution. We spotted that when the line of sight went over two consecutive towns separated by a few kilometers the program stopped after going over the first town never taking into account the cells close

to the second one. The problem was the voxels between the two towns had little contribution and the program stopped. In our case, a small town was making to ignore significant contribution from Lleida, the biggest city around, just a few kilometers further away. The threshold was redefined to avoid this problem.

3. We used Illumina as it was never used before when deriving a point spread function to estimate the radiance received at distance d from any source (see section 5.1). We used a simplified scenario with no obstacles and flat orography that made possible very low angle path contributions. The case revealed that a normally negligible contribution to first order scattering was not computed because the horizon line was blocked 0.5 degree above real horizon. The blocking angle was then reduced.

4.2.6 Illumina v2

In 2020 the group that created Illumina released a major update of the model (Aubé et al. 2020). It included core changes, such as an update in the extinction modelling and a new atmospheric definition, therefore they decided to call it Illumina v2 and re-brand the former version to Illumina v1. We collaborated in the process by using the new version in simplified cases.

The philosophy of the model remains the same: computing aerosol (scattering and absorption) and molecular (scattering) extinction taking into account first and second order scattering; modelling reflection on the ground as a lambertian function; accounting for spectral and optical heterogeneity of the sources; including topographic information; and defining the obstacle characterization of elements as buildings and trees.

The most fundamental changes that affects our cases (clear sky and scattered sky radiance) are listed below:

1. Calculation of the scattering probability and extinction (see equations 4.4 to 4.13 to compare with Illumina v1). The probability of scattering is defined by:

$$P = 1 - exp(\frac{ln(T_\infty)exp(-z/H)dl}{H}) \tag{4.14}$$

Maintaining the same terminology than in previous equations, T_∞ is the atmospheric vertical column transmittance, z is the altitude above ground, H is the scale height for molecules or aerosols, and dl the length of the scattering voxel.

The transmittance along a light path is defined by equation 4.15 for horizontal directions and 4.16 for oblique directions:

$$T_{hor} = exp(\frac{ln(T_\infty)exp(-z/H)d}{H}) \tag{4.15}$$

$$T_{obl} = exp(\frac{ln(T_\infty)}{cos(\theta_z)}[exp(-z_a/H) - exp(-z_b/H)]) \tag{4.16}$$

Where d is the horizontal distance of the light path, z_a and z_b are the bottom and top heights and θ_z is the zenith angle. T_∞ for molecules and aerosols are defined as in the previous version of the model (see equations 4.7 and 4.8).

2. Modelling grid. In Illumina v1, the spatial resolution was fixed for the whole domain. In Illumina v2 the surface grid is made up with overlapping layers of different resolution. In Illumina v1 the vertical grid was exponential and fixed. In Illumina v2 there is no vertical grid for the line of sight but a fixed resolution grid for the calculation of the 2nd order of scattering. The modification of the modelling grid is a major improvement. On one hand, it allows to speed up computations by using fewer cells for computing the contribution of distant sources where high resolution is not necessary. And, on the other hand, a higher resolution around the observation point improve the accuracy of the estimation of the radiance coming from scattering that takes place near the observer.

3. Ground reflectance. In Illumina v1 it was linked to the location according to the data from MODIS satellite. However, the resolution was low (500x500m), averaging different types of surfaces. In order to simplify the setup and speed up the computation, in Illumina v2 reflectance values are fixed all over the domain by the user by combining some typical surface reflectance spectra. With the new method accuracy is practically the same as the with the old one, but it is easier and faster to compute.

4. Point source inventory. The new version allows to define an inventory of lights one by one. This feature is useful when in possession of detailed information of public inventories that include coordinates. The new version of the model also works with inventories defined as in the previous one. The two methods can be combined.

There are other changes in the new version of Illumina that are not relevant in our work. For instance the definition of clouds. It also includes some new outputs as direct radiance (no scattering), irradiance, and radiance coming from clouds.

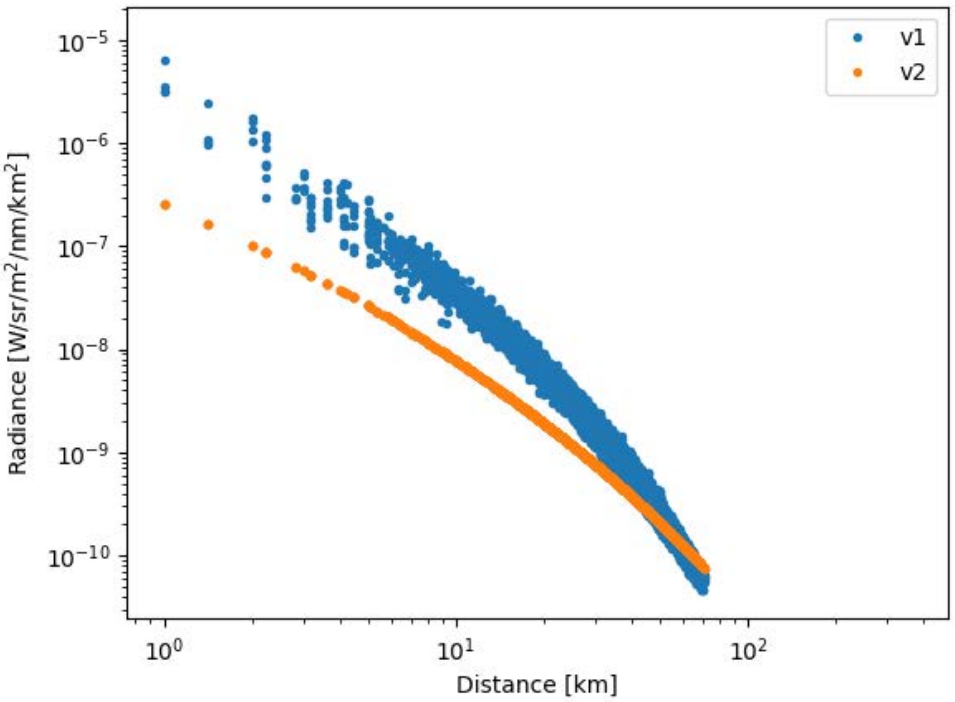

Figure 4.9: Comparison of the computed received radiance originated by the same source by Illumina v1 in blue and Illumina v2 in orange as a function of the distance. Source: image provided by Aubé.

Aubé published in the user guide of the model how both versions compare. Figure 4.9 shows how Illumina v1 supposedly overestimated the radiance received by close artificial source. The difference starts from one order of magnitude for distances below 2 m and it decreases as the distance increases up to 25 km approx where both models coincide.

In chapter 5 we studied the sky brightness using the two versions. We started using Illumina v1, as the second version was not already available. Most of the case studied with Illumina v1 do not have big light pollution sources nearby, thus the results obtained are still valid. As a matter of fact, they show great similarities with measurements (see section 5.3). There was one exception (see section 5.3.6) that did have with big sources nearby. We used it to compare both versions against measurements.

After using both versions, results indicate that the new one is more accurate in cases with important light sources close to the observation point. It is also faster

when the overlapping layers of the surface grid are properly defined. As mentioned, the results obtained with Illumina v1 for the cases with no big light sources nearby are valid and reliable. The latest version of the model was used for simulating the remaining cases and in the project of creating a zenith brightness map of Catalonia (see section 5.4). In this latter project, the features of the new version of Illumina were essential to ensure proper results, since we studied thousands of locations, many of them with huge light sources nearby.

Chapter 5

Assessing the night sky using light pollution models

This chapter is focused on studying sky brightness through light pollution models. In particular, we aimed at two different targets: specific locations and vast areas.

Specific locations have been assessed using contribution maps and all-sky brightness maps. Contribution maps are a fast tool to know where the artificial radiance received in a location is coming from. All-sky brightness maps show brightness levels in every direction of the sky over a particular location, similarly to the products obtained with ASTMON instrumentation and DSLR cameras.

Vast areas have been studied using zenith sky brightness maps. They assign a single value (zenith sky brightness) to each point as an indicator of night sky quality, similarly as in the SQM maps presented in chapter 3. As a matter of fact, other indicators can be used for these maps such as the integrated radiance for the all sky. We chose the zenith brightness for its simplicity, faster computation and because it provides a reliable evaluation of the quality of the sky.

We worked with the Illumina light pollution numerical model for creating these simulation products. As explained in chapter 4, we have chosen this model due to its completeness. Both versions of the model have been validated in published studies: Illumina v1 in Aubé & Roby (2014); Aubé & Kocifaj (2012); Aubé et al. (2018); Linares et al. (2020) and Illumina v2 in Aubé et al. (2020).

We used the first version of the model for creating contribution maps and some all-sky brightness maps, since the second version of the model did not exist yet. Right after Illumina v2 was released in 2020, we used one of the locations already studied with Illumina v1 to perform a comparison between the two versions of the

model (section 5.3.6). Once the improvements of the new version were validated, we used Illumina v2 for creating all-sky brightness maps of the remaining locations and a zenith sky brightness map of Catalonia.

As explained in section 1.2, the spectral range studied goes from 350 nm to 830 nm. We divided this range in 16 rectangular windows of 30 nm that allow to estimate the values obtained in the B, V and R filter of the Johnson-Cousins system (see figure 5.1). The R filter is not completely covered because over 830 nm there is no known emission lines of the most used lighting technologies. Adding two more bands over 830 nm will not modify the radiance received in R filter and will increase the CPU time needed to run the computations.

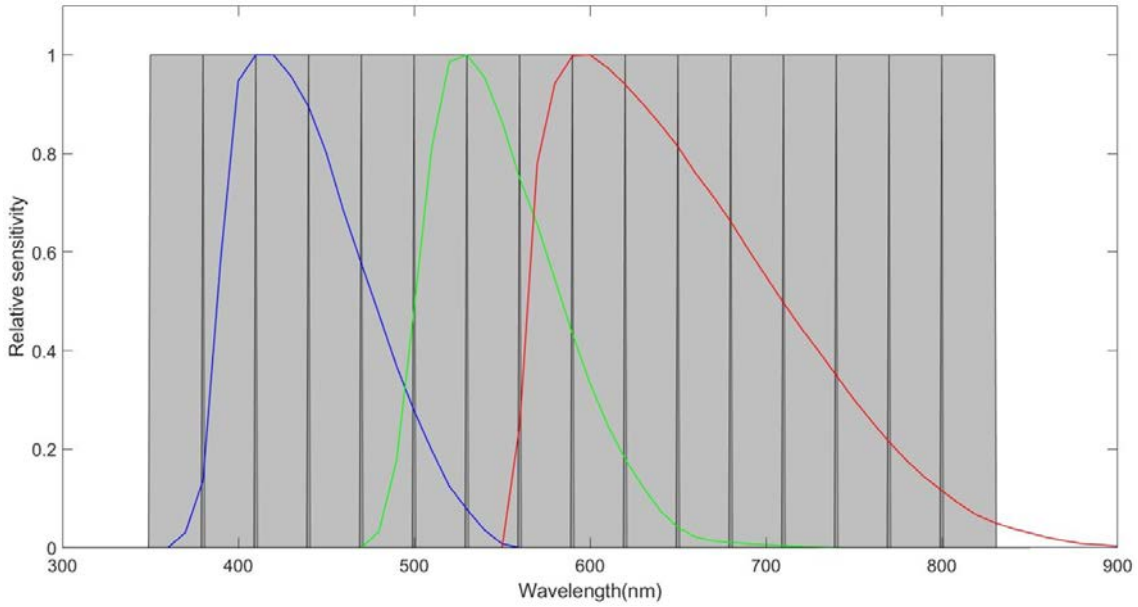

Figure 5.1: Spectral range studied (350-830 nm) divided in 16 windows of 30 nm (grey areas). In blue, green and red the B, V and R bands of Johnson-Cousins system respectively.

The chapter is structured as follows. First, it is explained the characteristics and the process for obtaining contribution and all-sky brightness maps. Then, we compute both kind of maps for eight locations (six within Catalonia and two in the Pyrenees mountain range outside Catalonia) and compare the results to the available measurements. The methodology and the study of one location (the OAdM) was already published in Linares et al. (2020). The last block of the chapter is the zenith brightness simulated map of Catalonia. It covers the country in a grid of 5x5 km resulting in more than 1300 locations. The resulting maps are compared to the current reference light pollution atlas (Falchi et al. 2016).

5.1 Contribution maps

Contribution maps show which sources, and to what extent, are contributing to the total artificial radiance received in a specific location (see figure 5.2). We divided the potential artificial sky brightness sources by municipalities. Thus, the resulting maps show the percent contribution coming from each one of them.

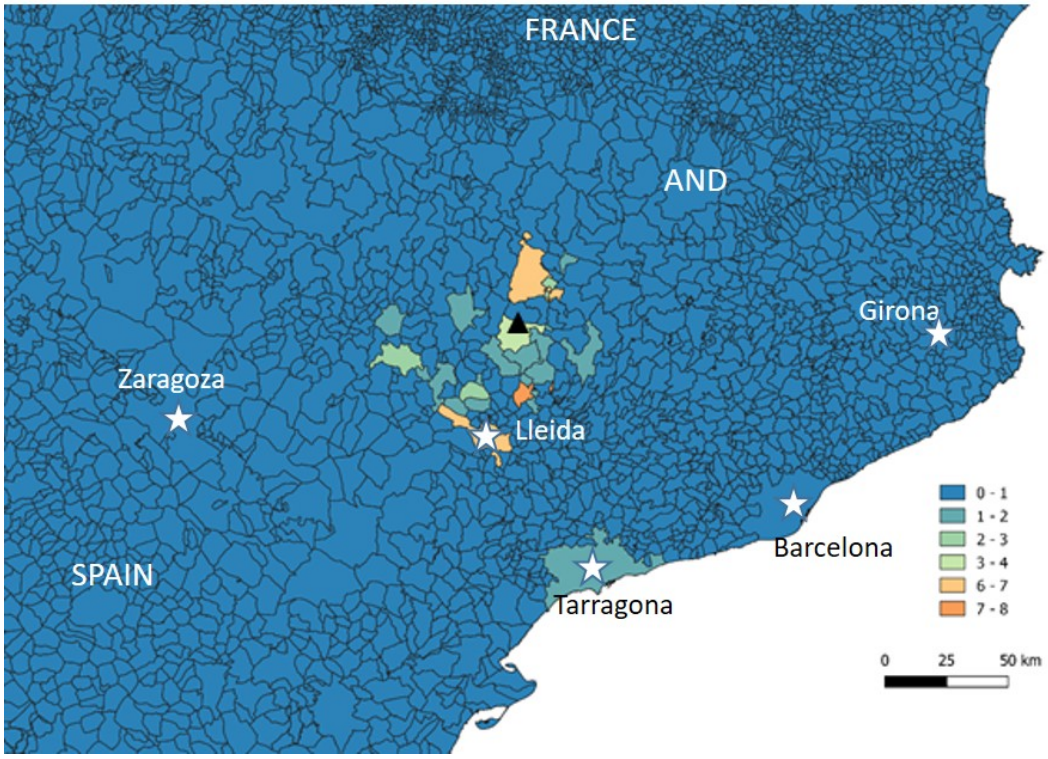

Figure 5.2: Contribution map showing the contribution, in %, to the artificial radiance received in the OAdM per municipality in the V band. Municipalities that form Barcelona and Tarragona metropolitan areas are grouped together. The black triangle is the location studied.

Knowing where the artificial radiance received is coming from allows to create better strategies to reduce light pollution. It also allows to estimate the changes that those strategies would produce in the sky. Moreover, they are also very useful for deciding which municipalities (or the division the user decides) should be included in an all-sky brightness simulation. They ensure that all major contributors are accounted for and also they help avoiding including sources with negligible contribution, speeding up this way the simulation calculus.

In the particular case of Illumina, minor contributors are already partially

neglected by the model. The software adds the artificial radiance coming from voxels within a line of sight, starting from the closest one until the contribution of the voxel is below a certain ratio to the total amount received from the voxels already studied. Nevertheless, minor contributors do increase the CPU time in voxels that surpass the threshold. For those voxels, Illumina computes the contribution coming from every source regardless how small they are. Therefore, CPU time is wasted computing negligible contributions to the total radiance. Knowing beforehand the sources that really have an impact on the sky allows to maintain the accuracy of the results using the minimum computing time possible.

The methodology used in this thesis for creating contribution maps is based on the work of Bará & Lima (2018), who showed how to use a point spread function (PSF) to create them. In this case, the PSF describes the behaviour of the light emitted by a point like source through the atmosphere and estimates the radiance received from it in any location at distance d. There exists different PSFs of this king in the bibliography, but almost all of them empiric. Hence, they are defined by the conditions of the place and date where the measurements took place and the set of lights used as a source. Moreover, the region of the sky studied is fixed. In order to avoid those restrictions, we proceeded to use Illumina for the first time as a tool for deriving a PSF. Using Illumina enhances accuracy because atmospheric conditions and lighting systems are defined ad-hoc to reproduce the values of the region where the PSF is going to be applied on. It also allows to define different PSF regarding the target region of the sky.

As stated in section 4.2, one of the outputs of Illumina is already a contribution map. Alongside the radiance received in a location, Illumina shows the main contributors for each combination of line of sight and wavelength window. For each line of sight, maps in different bands (for instance R, V and B of the Johnson-Cousins system) can be created combining the appropriate wavelength windows. In particular, Aubé et al. (2020) studied the zenith brightness contribution in the V band in the Canary Island using this approach. However, using a PSF has three main benefits over using the contribution maps provided by Illumina. First, the sky region assessed: each contribution map from Illumina assess a particular line of sight, with the PSF it is possible to assess wide regions of the sky, even creating a map of the contribution to the integrated sky dome. Second, computing time: once obtained the PSF it takes no more than 5 minutes to complete the map, whereas a full experiment in Illumina can take hundreds of hours (CPU time). Third, accounting for sources: the contribution map provided by Illumina is limited to the sources included in the experiment, with the methodology presented here we study all the light sources detected with the VIIRS-DNB satellite in a radius of hundreds

of kilometers around the location, making sure no relevant contributor is omitted.

The process we followed to obtain a PSF consists in computing the radiance received at several distances from a point-like source and deriving a mathematical function with the distance that fit the data. For each distance any set of directions can be computed. In our case, we used multiple lines of sight to cover the whole sky. However, PSFs focused in different regions of the sky can be created too. For instance, the ring between 0 and 30^{o} in elevation could be interesting for biology studies, or the dome over 30^{o} for observation studies in astronomy (Duriscoe 2016). With our method it is possible to use the best suited indicator for each case.

In the following section it is explained in detail the process we followed to obtain the PSF that studies the integrated brightness value for the whole sky. Other PSFs can be derived using the same process changing the lines of sight used, in this sense we also present in section 5.1.2 some contribution maps created with PSFs that focus on other regions of the sky.

5.1.1 Obtaining the PSF

In this section it is explained the process followed for obtaining a PSF able to describe how the artificial light affects the sky as a whole as a function of distance.

With the purpose to be able to work with non-monochromatic light sources, the spectrum is divided in 16 windows of 30 nm covering the range from 350 nm to 830 nm. As a result we obtain 16 quasi-monochromatic PSF, that can be combined to estimate the PSF corresponding to the spectrum of any real set of lights.

The main characteristics of the scenario used to derive the PSF are:

- Unique point-like light source
- Flat orography
- Homogeneous light reflection on the ground
- Typical atmospheric conditions of the area
- Clear sky (i.e. absence of clouds)

Point light source characterisation

The source of light is defined to have the minimum surface area to simulate a point light source. The minimum size of a light source allowed by Illumina was the corresponding of one pixel of the satellite images from the VIIRS-DNB sensor, close to 1x1 km.

The point-like source is defined by a spectrum with a monochromatic emission line every 30 nm (16 in total) that coincides with the center of the spectral windows we used to divide the spectral range studied (see figure 5.1). This way the 16 PSF can be combined to fit any light source spectrum.

Other parameters needed to define the source when working with Illumina are:

1. The angular distribution, the pattern that describes how the light escapes from the lamp.

2. The obstacle characterization, distance to blocking elements, their heights and the probability of the light to be blocked.

Therefore, oppositely of what happens with the spectrum of light sources that will be needed only in the last step of the process, the resulting PSF is linked from the beginning to these two features. In the case of study, the typical values for the towns and cities around the locations we wanted to study have been used (see table 5.1). These values have been derived from several available public inventories, after checking personally multiple towns (most of them during the measurements campaigns) and validated by the Departament de Territori i Sostenibilitat from the Generalitat de Catalunya.

Scenario characterisation

As previously stated, Illumina takes into account orography and ground reflection. Since the goal of the methodology is to create contribution maps in a fast and easy way, we derived a generic PSF using flat terrain with a reflection value approximated to the mean value found in most towns. Otherwise, a specific PSF should be derived for each location and direction.

Regarding atmosphere characterization, it has been assumed a rural environment with a relative humidity of 70%, atmospheric standard pressure (101,3 kPa at sea level) and clear sky (no clouds). Typical aerosol optical depth (AOD) and

Angstrom coefficients (α) are representative of the AERONET data (AErosol RObotic NETwork, Holben et al. (1998)) (see table 5.1).

ULOR	10%
Lamps height	6 m
Obstacles height	6 m
Horizontal distance to obstacles	5 m
Probability of photons to hit an obstacle	0.5
Atmospheric pressure at sea level	101.3 hPa
Relative humidity	70%
Aerosol optical depth at 500 nm	0.09
Angstrom exponent	1.0

Table 5.1: Main characteristics of the source and atmosphere used in the experiment to derive the PSF.

The distance range goes as far as 200 km from the light source. Beyond this distance is very unusual that light sources pollute significantly the sky. Huge cities could often be seen farther away but only from elevated observation points and only close to the horizon (even below it) in the direction pointing to the source.

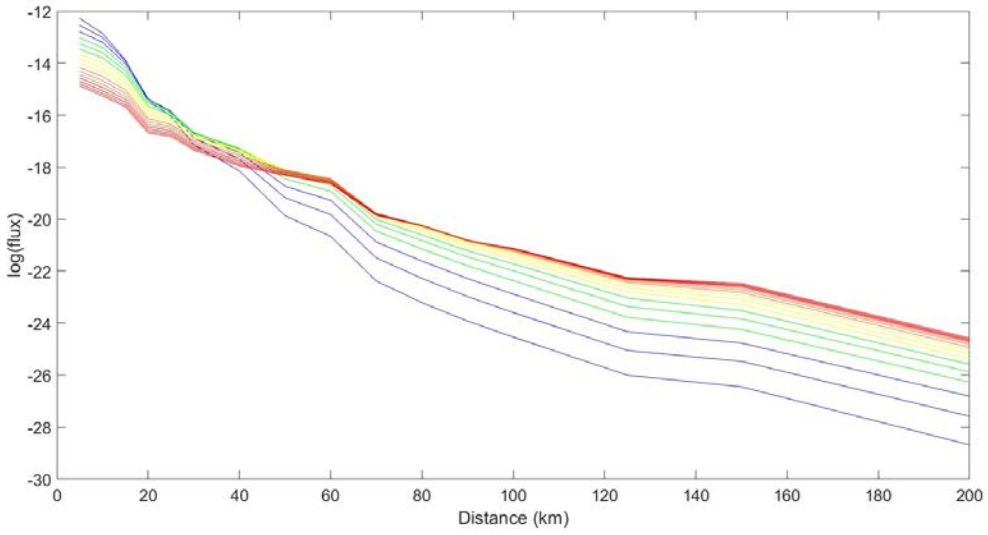

Figure 5.3: Radiance ($Wsr^{-1}m^{-2}$) received from the point-like source in each one of the 16 spectral windows with respect to the distance.

The integrated radiance for the entire sky of the 16 different emission lines

behave differently with distance (see figure 5.3). As we have imposed a small AOD, the radiance received is mainly produced by molecular Rayleigh scattering. Rayleigh scattering, as explained in section 1.3.1, is inversely proportional to the fourth power of wavelength. As a consequence, most of the radiance received at a shorter distance comes from bluer sources. However, as the distance increases most of the blue light is dissipated by scattering to other directions rarely reaching the receiver. In those cases, redder light, that is the least scattered, is the main contributor to the total radiance received.

Fitting the data to a curve

The next step for obtaining the PSF is fitting the data shown in figure 5.3 to a mathematical function. The purposes are having the same kind of expression for each one of the 16 spectral window and that it is reliable for the entire distance range. After observing the data, an exponential curve for each spectral window is the best match. Being d the distance and F the function that describes how radiance propagates, the curves take the form:

$$logF(d) = ad^2 + bd + c \tag{5.1}$$

For obtaining the coefficients for each wavelength window (see table 5.2) we used the least-squares fitting method. The resulting curve for every wavelength has a determination coefficient (R^2) over 0.97. For visual purposes the comparison between the data and the curve for the window centered in 545 nm is shown in figure 5.4, the rest of the spectral windows have a similar behaviour.

Adding the light source inventory

The 16 resulting curves represent the behavior of radiance emitted in the different spectral windows defined. We can work with any set of lights by adjusting the curves to the spectrum of the inventory of lights we want to simulate. The spectral information of the inventory of lights is introduced as a scale factor in each of the 16 curves.

We used this approach instead of defining the source directly (with the actual spectrum of lights) because it allows to deal with modifications by just adjusting the scale factors.

A simplified representation of the typical inventories of the towns around the

Center wavelength	a	b	c	R^2
365	-5.0958	-7.7321e-02	2.0988e-04	0.9838
395	-5.2148	-6.8715e-02	1.8016e-04	0.9803
425	-5.3438	-6.1841e-02	1.5633e-04	0.9789
455	-5.4710	-5.6384e-02	1.3751e-04	0.9787
485	-5.5909	-5.2069e-02	1.2288e-04	0.9790
515	-5.7026	-4.8617e-02	1.1144e-04	0.9791
545	-5.8079	-4.5850e-02	1.0254e-04	0.9795
575	-5.8995	-4.3625e-02	9.5512e-05	0.9792
605	-5.9828	-4.1882e-02	9.0599e-05	0.9791
635	-6.0625	-4.0353e-02	8.6015e-05	0.9788
665	-6.1336	-3.9139e-02	8.2864e-05	0.9785
695	-6.1997	-3.8026e-02	7.9649e-05	0.9781
725	-6.2583	-3.7128e-02	7.7250e-05	0.9774
755	-6.3163	-3.6303e-02	7.5009e-05	0.9768
785	-6.3660	-3.5582e-02	7.3107e-05	0.9759
815	-6.4086	-3.4976e-02	7.1683e-05	0.9750

Table 5.2: Coefficients of the 16 curves that model the integrated radiance in the whole sky as a function of the distance.

locations we wanted study have been used in this thesis. Mostly high sodium pressure lamps, 85%, with a fraction of light emitting diodes of 4000 K of CCT, 15%. The resulting combined spectrum is shown in figure 5.5.

The simplifications used in the process allow to determine accurately enough for our purposes the major contributors to the light pollution in a location in a quick way. For a detailed and very accurate result we recommend to rely on Illumina all-sky brightness maps.

5.1.2 Using a PSF to create a contribution map

Once obtained the formula that describes how the light emitted from our point-like light source (with a fixed spectrum) propagates in function of the distance, we are ready to create the contribution maps.

We worked with the monthly averaged VIIRS-DNB images that provide the radiance emitted in any location of the map. These images are geo-referenced, which allows to compute the distance between two locations using a Geographic

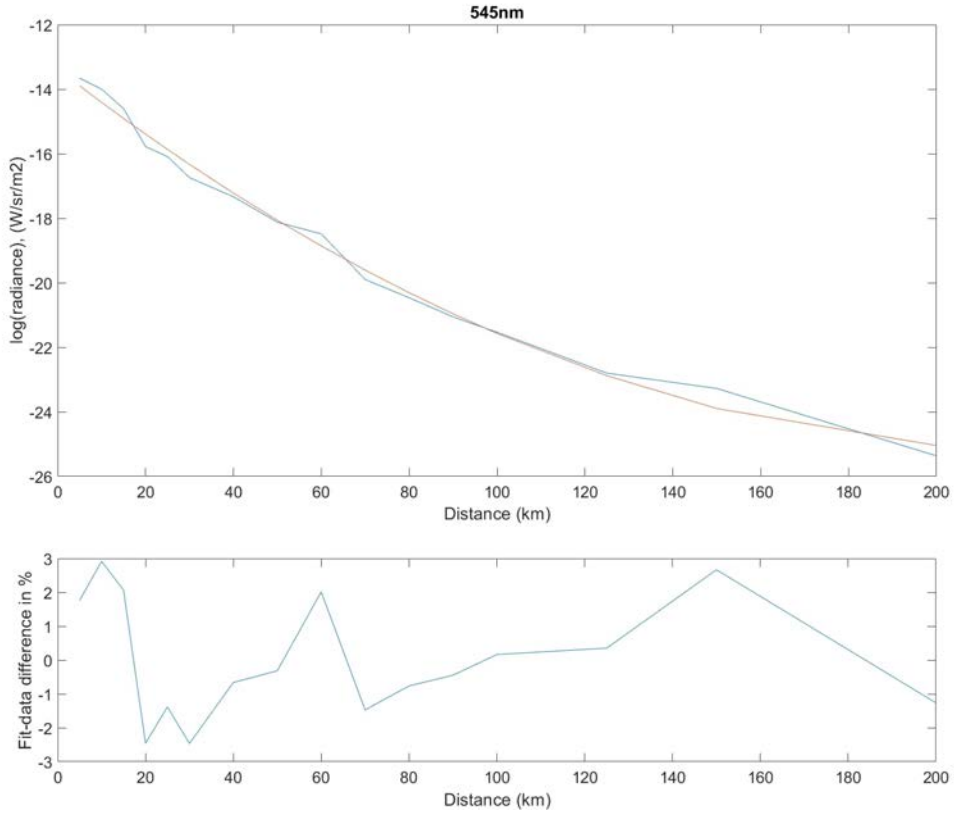

Figure 5.4: Comparison between the data and the fitting function for the wavelength window centered at 545 nm. Top: data in blue and fitting function in red. Bottom: difference between them in % following the expression 100*(log(function)-log(data))/log(data).

Information System (GIS) software. The total radiance received in the target location (filtered by the spectral band chosen) is computed taking into account the radiance of each pixel and its distance to the target location. Finally, the radiance received coming from each municipality is divided by the total artificial radiance received, obtaining this way the percentage of artificial radiance coming from each municipality.

Some examples of different contribution maps for the OAdM (Observatori Astronòmic del Montsec) location are shown in figure 5.6 and figure 5.7. In the first figure there are maps that show the percentage of the received artificial light that comes from each municipality for the B, V and R bands of the Johnson-Cousins system; in the second one there are maps that show, for the V band, how municipalities contribute to artificial brightness received in different regions of the

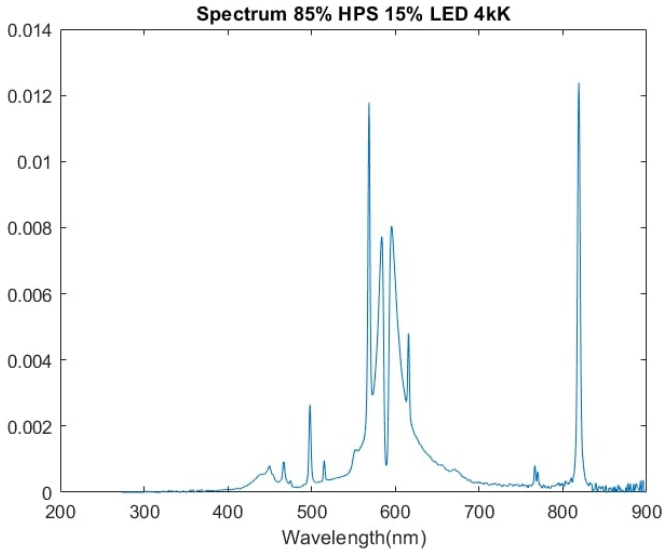

Figure 5.5: Spectrum of the combination of high pressure sodium lamps and light emitting diode in a relation of luminous flux of 85% to 15%.

Source	Contr. filter B (%)	Contr. filter V (%)	Contr. filter R (%)
Tarragona MA	0.35	1.02	1.20
Barcelona MA	0.24	0.80	0.98
Andorra	0.23	0.53	0.60

Table 5.3: Percentage artificial radiance contribution received in the OAdM from Tarragona metropolitan area, Barcelona metropolitan area and Andorra in the B, V and R filters of the Johnson-Cousins system.

sky. As stated, to make each map we assumed flat orography and a inventory of lights of 85% high pressure sodium and 15% LED of 4000 K CCT lamps.

The results shown in figure 5.6 are in agreement with the behavior of the PSF at different wavelengths. For the B filter, closer sources have a greater contribution than in V and R bands. We can see this effect for instance in the contribution of the small town of Àger that is more than double in B than in the other two filters. On the other hand, in R filter distant (and big) sources have a greater contribution than in the other two bands. Examples of this effect are the metropolitan areas of Barcelona and Tarragona, and Andorra (see table 5.3). As expected, results for the filter V fall in between the ones obtained with the other two filters.

For the sake of simplification, in section 5.3 we present only the results for V

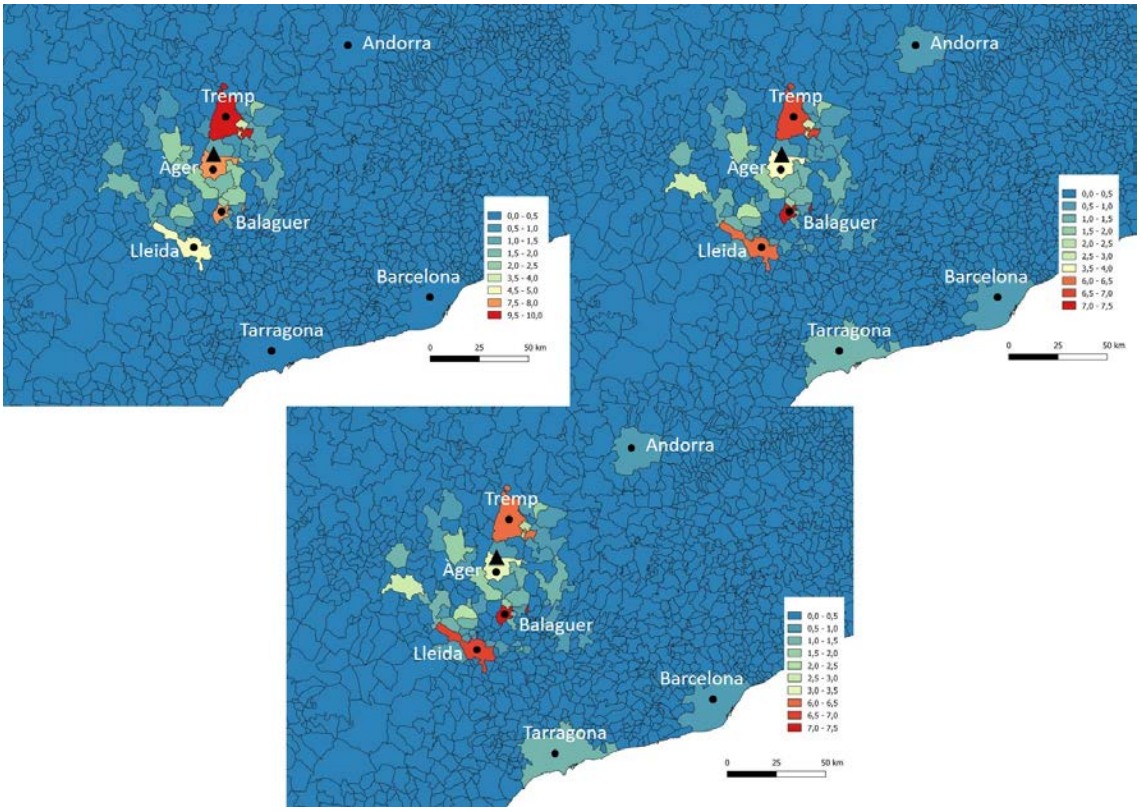

Figure 5.6: Contribution map showing the contribution, in %, to the integrated artificial radiance for the whole sky received in the OAdM per municipality. Top-left: B filter. Top-right: V filter. Bottom-left: R filter. The municipalities that form Barcelona and Tarragona metropolitan areas are grouped together.

filter. Most of the spectrum of the artificial lights falls within the V filter. However, for each location studied maps in the three bands have been created and used as a reference for deciding the sources that should be included in the simulations.

The contribution from each municipality to the radiance received in the different regions of the sky is shown in figure 5.7. We studied different elevation angles but in azimuth we always covered all the circumference. It is possible to study only certain azimuths, for instance to determine the source of a specific light dome. In this case we should determine a PSF for each relative angle between source and observer and apply them depending on the distance and direction of the source with respect to the location studied. Although interesting, it is beyond of the scope of this thesis.

It is remarkable the little differences between the maps shown in figure 5.7. Nevertheless, there is a weak relation between lower elevation and a higher contribution from distant sources, for instance Barcelona and Tarragona metropolitan

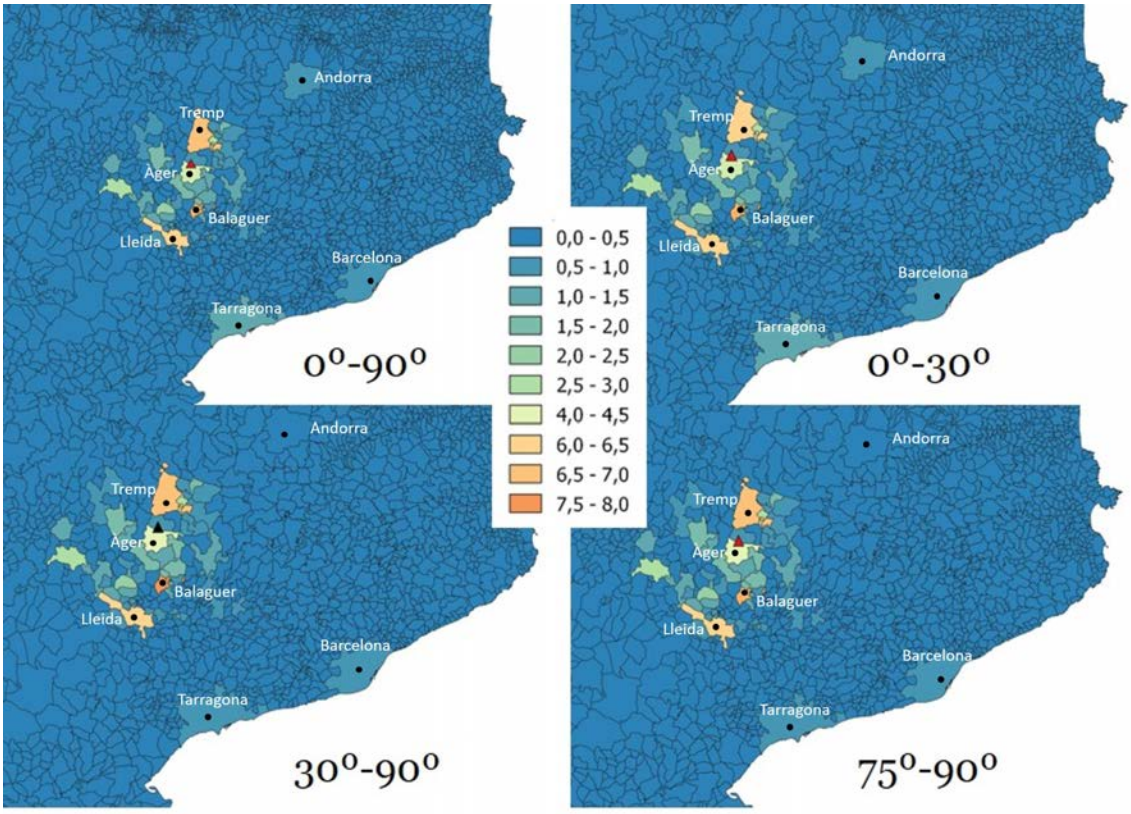

Figure 5.7: Contribution map showing the contribution, in %, to the artificial radiance received in the V filter in different regions of the sky. Top-left: integrated value for the whole sky. Top-right: integrated value for all the azimuths within 0 and 30 degrees in elevation. Bottom-left: integrated value for all the azimuths within 30 and 90 degrees in elevation. Bottom-right: integrated value for every direction with elevation within 75 and 90 degrees. The municipalities that form Barcelona and Tarragona metropolitan area are grouped together.

area when comparing 0-30 degrees (1.15% and 0.94% respectively) and 75-90 degrees maps (0.81% and 0.55% respectively). We used the integrated sky (0-90 degrees) when studying specific locations, since they provide enough information for characterizing the radiance sources and for helping in choosing the sources to include when creating the all-sky maps.

5.2 All-sky brightness maps

As we have seen in chapter 2, all-sky maps are a good tool to show light pollution levels in every direction of the sky when studying a particular location. It allows to point out the most polluted directions and the patterns that brightness describes with elevation.

The maps presented in this work show brightness in units of mag/arcsec^2, making it easier this way to compare with ASTMON and SQC measurements. Vega star has been used as a reference source for the conversion between radiance in $\mathrm{Wm^{-2}sr^{-1}}$ to mag/arsec^2 (see table 5.4).

Measurements show total brightness that includes artificial and natural sources. Illumina provides only artificial radiance so we added the natural brightness using a reference value (Walker 1987) of 22.7 mag/arcsec^2 in B, 21.8 mag/arcsec^2 in V and 20.9 mag/arcsec^2 in R filters. Bear in mind that in the absence of artificial brightness those would be the values present in the map. Therefore the final expression for each filter is:

$$m = m_{Vega} - 2.5log_{10}(\frac{L_{Illumina} + L_{Natural}}{L_{Vega}}) \tag{5.2}$$

being $L_{Natural}$ for each filter:

$$L_{Natural} = L_{Vega}10^{-0.4(m_{Natural} - m_{Vega})} \tag{5.3}$$

Johnson Filter	Vega (mag)	Vega (W/m^2)	Natural Sky (mag/arcsec^2)	Natural sky (Wm^{-2}arsec^{-2})
B	0.03	1.2687e-09	22.7	1.0331e-18
V	0.03	9.4053e-10	21.8	1.7546e-18
R	0.03	1.3039e-09	20.9	5.5723e-18

Table 5.4: Reference values of Vega and natural sky brightness at zenith.

The high CPU time consumption of Illumina made us optimize the number of simulated directions. Narrow angular steps reduces the capacity of studying multiple scenarios or different locations due to the CPU time available. On the other hand, using steps too wide implies losing relevant information: in azimuth, it could make to overlook the artificial radiance coming from small or distant towns that normally brighten a small region of the sky; in elevation, using wide steps degenerates the pattern of artificial radiance, particularly close to the horizon.

We used the OAdM case to find the optimal value for the angular steps in azimuth and elevation, and to find also the best interpolation method to derive the values in between the simulated lines of sight. The OAdM case is well suited for this purpose because its major contributor are middle distant cities (20-50 km) that affect narrower sky regions than closer light sources (see figures 5.6 and 5.7).

For the azimuth step, we simulated the whole circumference at elevation equal to five degrees in steps of five degrees in azimuth. We used that elevation because smaller the elevation bigger the difference in radiance received between azimuths. Then, we compared the values obtained by linearly interpolating the radiance using steps of 10, 15 and 20 degrees to the simulated ones (see figure 5.8). We automatically discarded the 20 degree step because it showed differences over 10%. The 10 and 15 degree step showed similar maximum differences, over 4%, but the standard deviation of the 10 degree step was much smaller. Between 5 and 10 degree step we chose the latter due to the CPU time required is cut by half and the differences with the interpolated values are typically below 2%, only surpassing 3% in very special cases.

For the elevation step, we followed a similar procedure: we simulated lines of sight every 5 degrees in elevation for the azimuth 180 degrees and then compared the results obtained by using steps of 10, 15 and 20 degrees. We chose that azimuth because it is one of the most polluted ones (in the case of the OAdM), and the differences in radiance as a function of the elevation angle are greater than in non polluted azimuths.

Contrarily to azimuth, the elevation step was not so straightforward to decide, since radiance is not a linear function of the elevation angle (see figure 5.9). Therefore, the errors induced by interpolating radiance are huge even for a 10° step. Interpolation after converting radiance to astronomical magnitudes shows much better results. The process consists in converting radiance to mag/arcsec^2 in the simulated lines of sight, and then interpolate linearly. The differences between different angular steps reduces substantially as seen in figure 5.10. However, it is not good enough for all the directions. We concluded that in lower elevations there is a need for finer resolution than in higher elevation directions. This is so because the artificial light gradient with elevation is larger as we move close to the horizon. The final set of simulated elevation angles are: 5, 10, 15, 20, 30, 45, 60, 75 and 90 (see figure 5.11), and the directions in between are estimated by interpolating after converting radiance to astronomical magnitudes.

A total of 289 lines of sights have been used for creating each all-sky map presented. A scheme of the set of directions can be seen in figure 5.11.

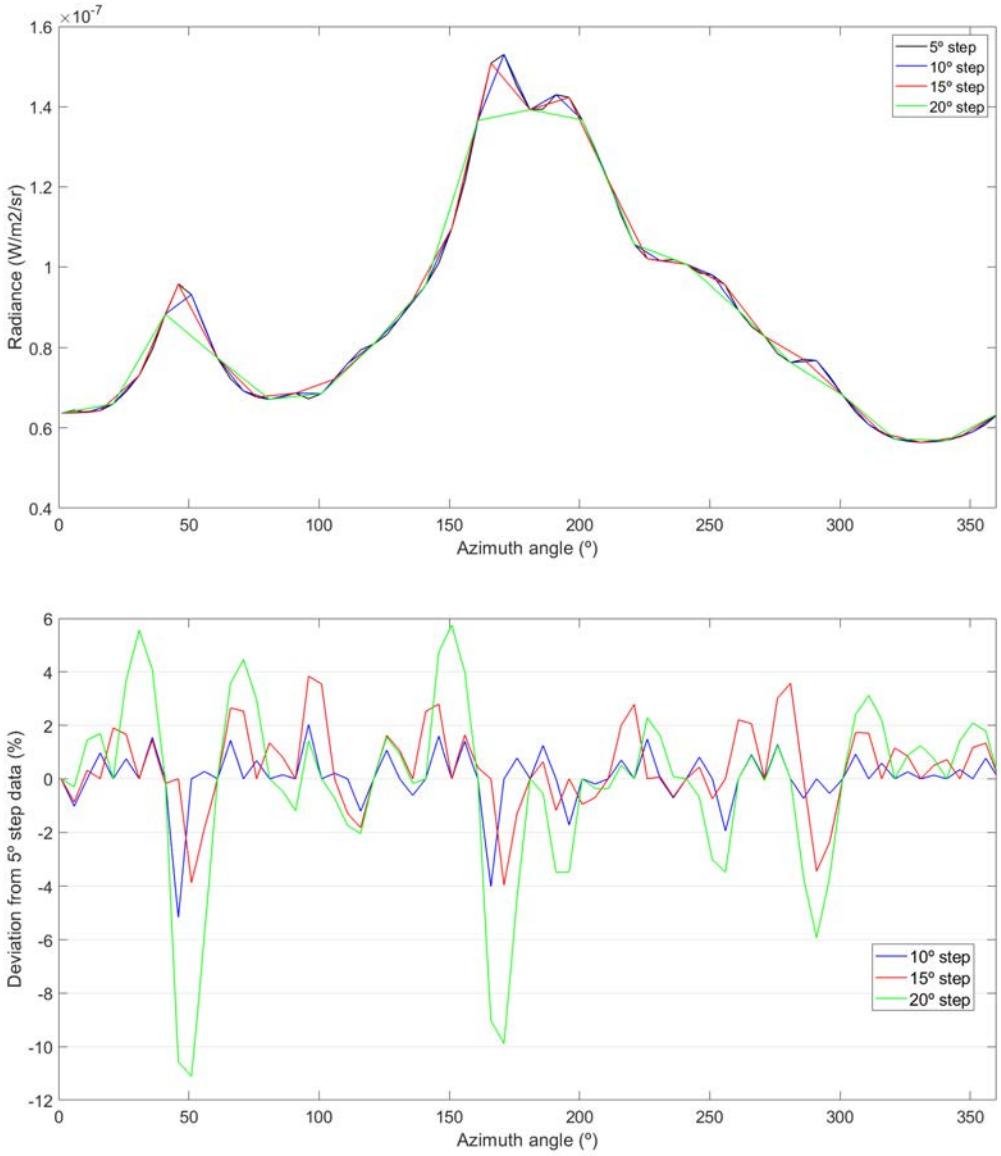

Figure 5.8: Top: simulated radiance with respect to azimuth in the OAdM at 5^o elevation for different azimuth steps. Black 5^o (reference value), blue 10^o, red 15^o and green 20^o. Bottom: relative deviation to the simulated radiance using 5^o step in %. Blue 10^o, red 15^o and green 20^o.

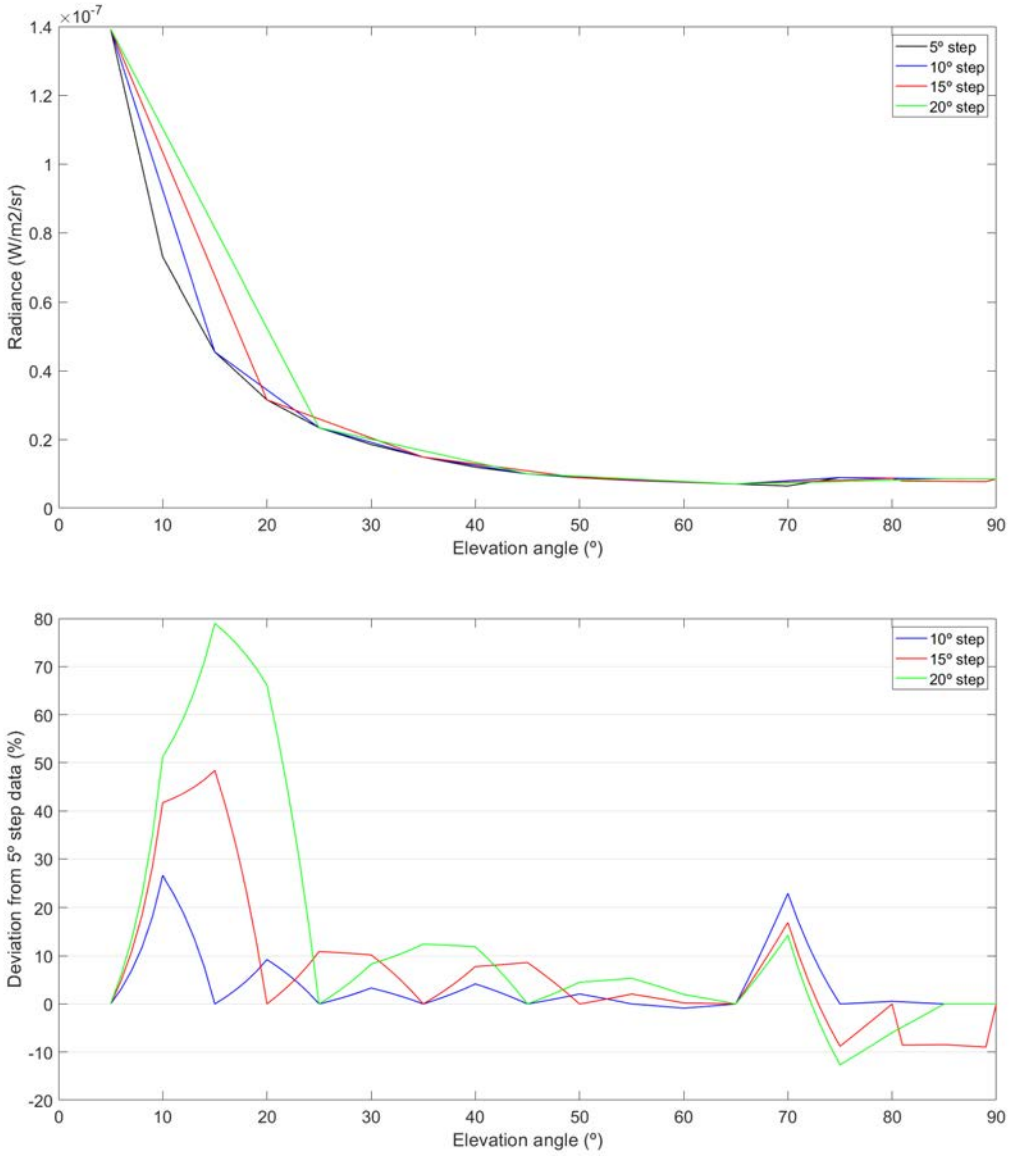

Figure 5.9: Top: simulated radiance with respect to elevation in the OAdM at 180^o azimuth for different elevation steps. Black 5^o (reference value), blue 10^o, red 15^o and green 20^o. Bottom: relative deviation to the simulated radiance using 5^o step in %. Blue 10^o, red 15^o and green 20^o.

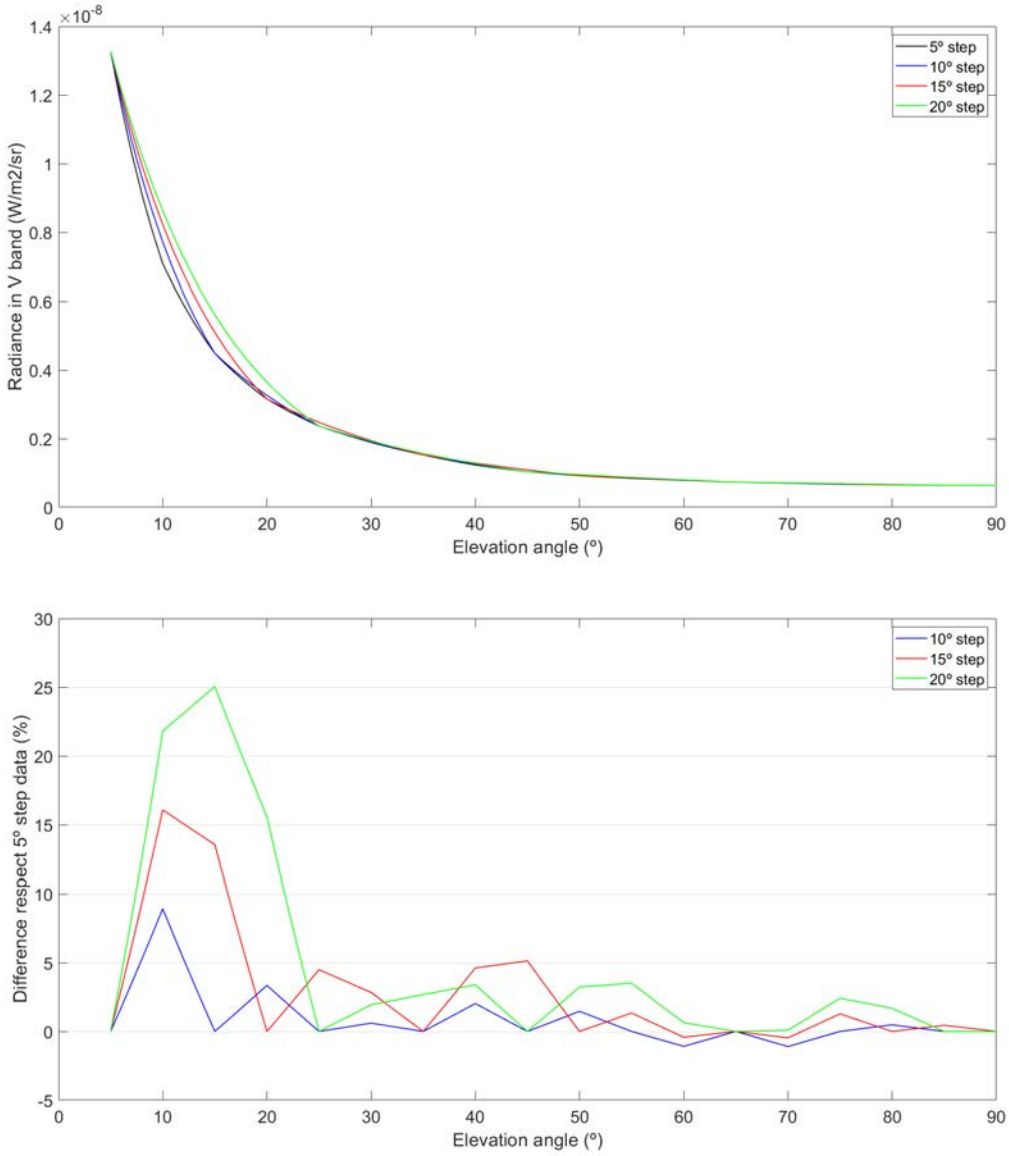

Figure 5.10: Top: simulated V band radiance with respect to elevation in the OAdM at 180^o azimuth for different elevation steps. Interpolation between simulated LoS is linear using mag/arcsec^2 in the V band. Black 5^o (reference value), blue 10^o, red 15^o and green 20^o. Bottom: relative deviation to the simulated radiance using 5^o step in %. Blue 10^o, red 15^o and green 20^o.

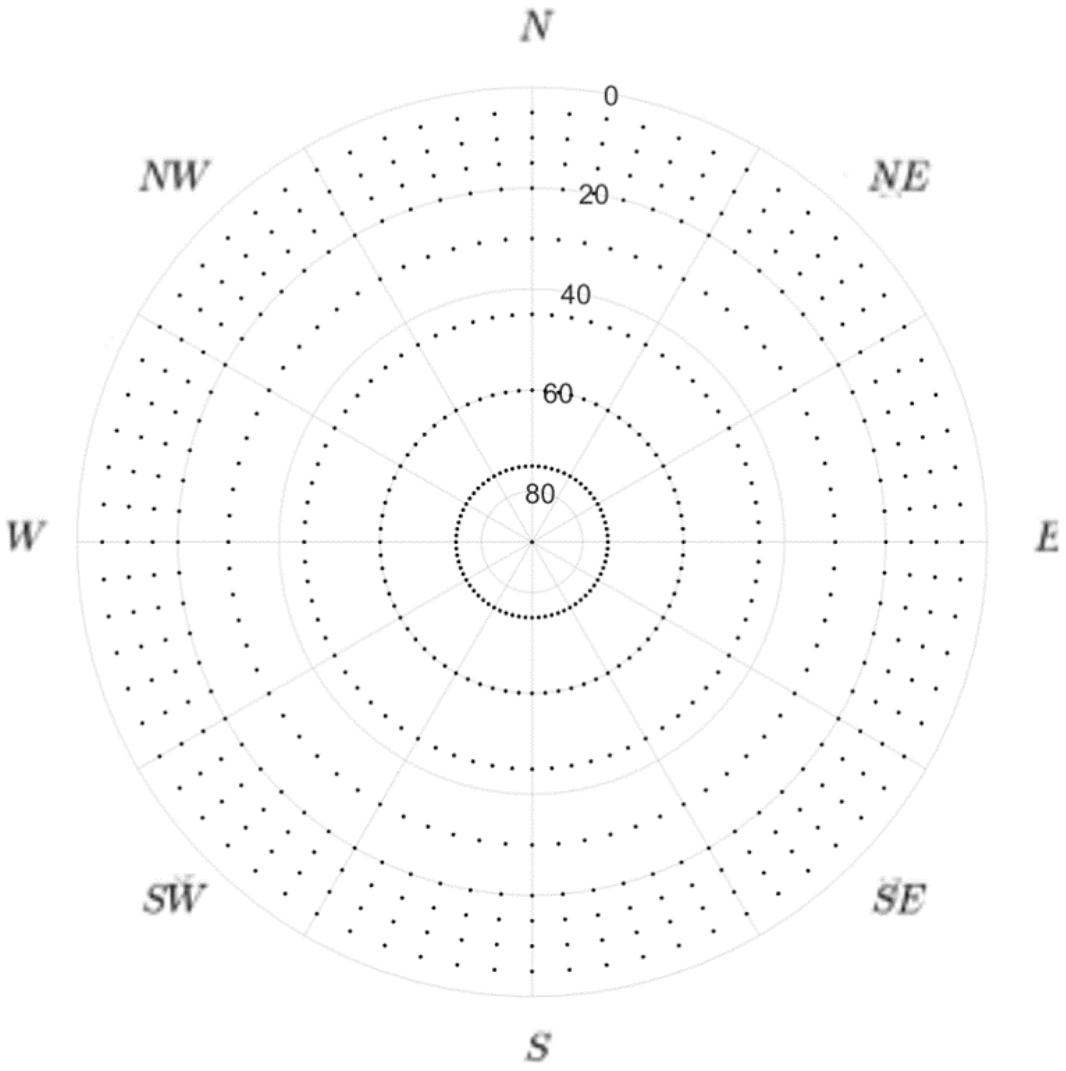

Figure 5.11: Distribution of LoS simulated to create the all-sky brightness maps.

5.3 Night sky brightness study by location

In this section the night sky brightness of eight different locations are studied using contribution maps and all-sky brightness maps (see figure 5.12). The locations were chosen for several reasons: they possess a dark night-sky, there were all-sky measurements of the site (or we planned on taking measurements), and they are close to astronomic facilities and/or are reference points for protected areas such as natural parks.

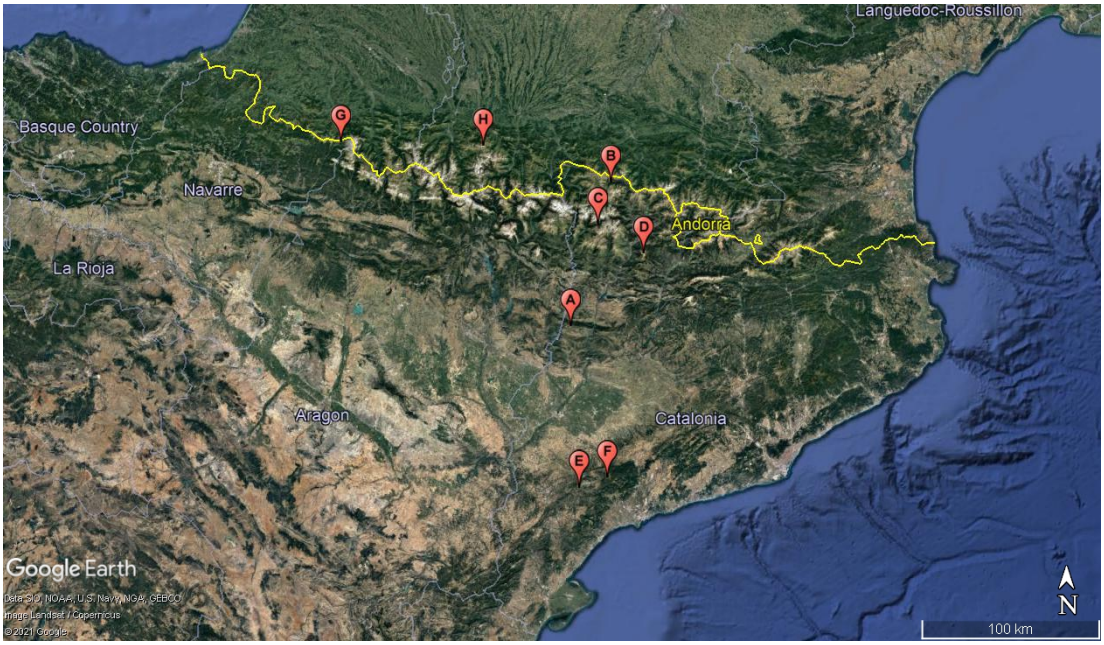

Figure 5.12: Map centered in the Pyrenees region with the locations studied. A: Observatori Astronomic del Montsec (OAdM). B: Montgarri refuge. C: Aigüestortes NP (Estany Llong). D: Alt Pirineu NP (Pic de l'Orri). E: Montsant NP. F: Prades Astronomic Center. G: Valle del Roncal (Larra-Belagua). H: Pic du Midi de Bigorre.

As explained, contribution maps establish which sources and to what extent are polluting the night sky. They are also used as a guideline to decide which sources should be included in the all-sky map simulation and if it is worth to invest time in deriving very detailed inventories for each source. The all-sky brightness maps presented for each location have been created by including every light source in a 50 km radius from the location (referred as general area in the following sections) and all the towns beyond that distance that have a value over a 2% in the contribution map for the whole sky. This norm ensures that no relevant contributor is neglected and that most of the artificial sky brightness is taken into account.

The inventory of lights used when obtaining the PSF has been adopted for sources with contribution below 2% and closer to 50 km. It was derived from averaging several public inventories, checking personally some lighting systems and validated by the lighting experts from the Departament de Territori i Sostenibilitat. Sources that contributes more than 2% (regardless of the distance) have been defined independently as long as there was information available. In this sense, we worked only with the public street-lighting inventory for creating the spectrum of the artificial light emitted. Private light sources normally are rich in blue light, thus we are probably using a spectrum more dominant in the V filter than it is in reality. In R filters the differences are very small due to both private and public light emit approximately the same amount in this filter. It is important to recall that the Illumina model does not take into account molecular absorption, that is no negligible in the R band. Therefore, simulated values could be slightly brighter than measured ones.

The resulting all-sky maps are compared to the measurements available for each location. In some locations we have ASTMON data, that allow us to compare and validate the estimated values in the three filters (B, V and R). In other locations, measurements were taken with DSLR cameras processed with SQC software. Thus, the comparison is only possible in the V filter. In this section we applied two modifications to the SQC processed images in order to match with the characteristics of ASTMON data and simulated maps. First, the W-E axis of the SQC processed images presented in this section is flipped: the west is in the left and the east in the right part of the image. Second, the information from 0^o to 5^o in elevation is removed as it is not available in the other two kind of maps.

Oppositely to measured maps, simulated maps do not include the presence of the Milky Way and other natural phenomena that could affect brightness levels in some directions. As a matter of fact, in some measured maps the Milky Way is easily distinguishable. Other difference between measured and simulated maps are obstacles that block the direct site of the sky, normally close to the horizon. Measured maps show no information in the blocked directions but simulated maps show brightness values in those directions taking into account the darkening effect of the potential obstacles.

Simulated maps are computed with the same atmospheric conditions used for deriving the PSF (see table 5.1). We tried to ensure similar conditions for the measurements, mostly cloudless and relative humidity under 80% but is possible that the atmospheric conditions are slightly different (thin high clouds, aerosol abnormal composition, etc.).

5.3.1 Observatori Astronòmic del Montsec (OAdM)

The Observatori Astronòmic del Montsec (OAdM) is a professional scientific observatory located in the province of Lleida, in the western part of Catalonia, in a low density population area.

The OAdM meets the conditions to be a perfect location for an astronomic observatory for three main reasons. First, it is far from big cities. Second, it is located at the top of Montsec hills, close to 1500 m above sea level. The altitude enhances observations. Higher the altitude thinner the atmospheric layer between the target objects and the observatory, thinner the atmospheric layer less light absorption. Third, the climate conditions of Montsec area ensure a great number of clear sky nights.

The area surrounding the observatory is labeled as a Reserve and Tourist Destination by the Starlight foundation since 2013. The sky brightness over this region is assessed annually. Moreover, it is one of the three key locations of the Pyrenees la Nuit project.

Contribution map

The main sources of the artificial radiance received in the OAdM are within 50 km. Being the three biggest ones: Balaguer with 7.3% (17k inhabitants at 30 km), Tremp with 6.6% (6k inhabitants at 18 km), and Lleida 6.4% (140k inhabitants at 50 km).

One of the closest towns is Àger, 6 km south-east, with a population of less than 600 inhabitants. Although its low population, the close proximity makes the town the 4th biggest contributor to light pollution, 3.7%, in the OAdM. Big cities are quite far: Tarragona metropolitan area and Andorra at roughly 100 km and Barcelona beyond 150 km. Although they have a slightly greater contribution than the rest of distant sources they do not surpass 1.5% in any case.

All-sky brightness map

The three main artificial radiance sources were defined in detail thanks to the information provided by Parc Astronomic Montsec (PAM), as well as some town councils (see table 5.5).

Simulated values agree with measurements in showing an extraordinarily dark sky (see figures 5.14, 5.15 and 5.16). In every filter, brightness values above 35º are

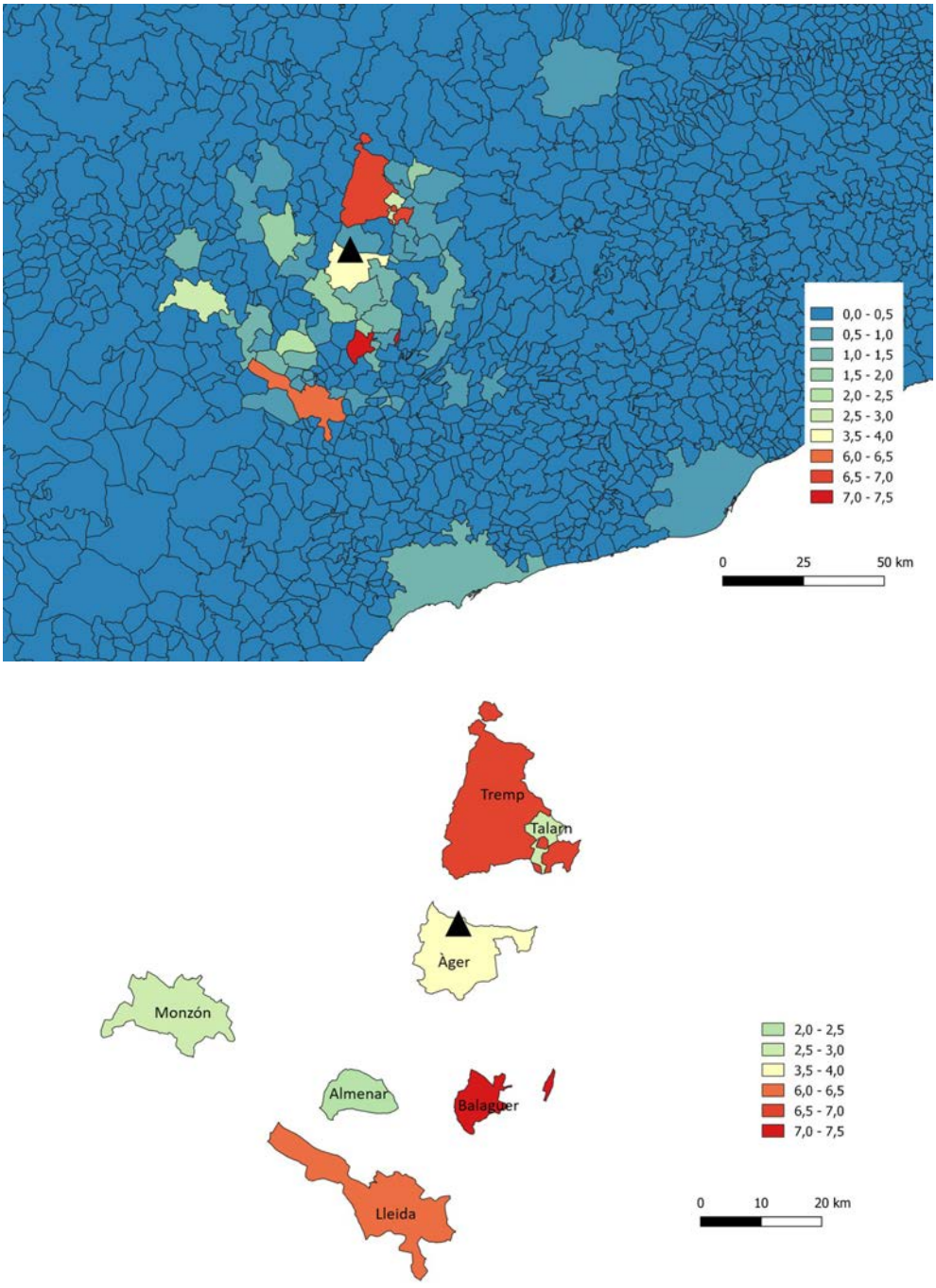

Figure 5.13: Percentage of artificial light emission by municipality received in the V band in the OAdM. Top: all the municipalities. Bottom: municipalities that contribute more than a 2%.

Source	Inventory (%radiance emitted-Techonology-ULOR)
Balaguer	49-HPS-0, 21-HPS-5, 11-MH-0, 9-HPS-20, 8-HPS-15, 2-4LED-0
Lleida	67-HPS-0, 14-4LED-0, 12-MH-0, 7-HPS-10
Tremp	31-HPS-1, 28-HPS-15, 19-HPS-20, 11-HPS-0, 11-HPS-5
General zone	43-HPS-10, 42-HPS-5, 15-4LED-1

Table 5.5: Characteristics of the light pollution sources included in the all-sky simulation over the OAdM. HPS: high pressure sodium. MH: metal halide. 4LED: LED 4000K CCT.

less than 0.3 mag/arcsec^2 brighter than the theoretical natural background, so it is practically non-polluted.

The darkest direction coincides with the zenith in every filter, both in ASTMON data and simulations. Their values are 22.8 and 22.6 mag/arcsec^2 for the B filter, 21.8 and 21.6 mag/arcsec^2 for V filter, and 20.9 and 20.5 mag/arcsec^2 for R filter (ASTMON and simulation respectively).

The zenith direction in the R filter shows the largest difference between simulated and measured values. As stated, it is a expected pattern due to molecular absorption in this band.

All the maps show polluting sources close to the horizon pointing to the south and south-east, that corresponds to the directions towards Lleida, Balaguer and Àger, and north-east towards Tremp and Talarn.

The brightest direction is the same for every map: close to the horizon in SSE azimuth towards Áger and Balaguer. Lleida is located at azimuth S and also contributes to the brightening in the SSE direction. The values are 22.1 and 22.2 mag/arcsec^2 for the B filter, 19.9 and 20.1 mag/arcsec^2 for V filter, and 19.1 and 19.4 mag/arcsec^2 for R filter (ASTMON and simulation respectively).

Measurements and simulated values show a very similar brightness pattern. Quantitatively, the differences are typically less than 0.2 mag/arcsec^2, compatible with the associated uncertainties.

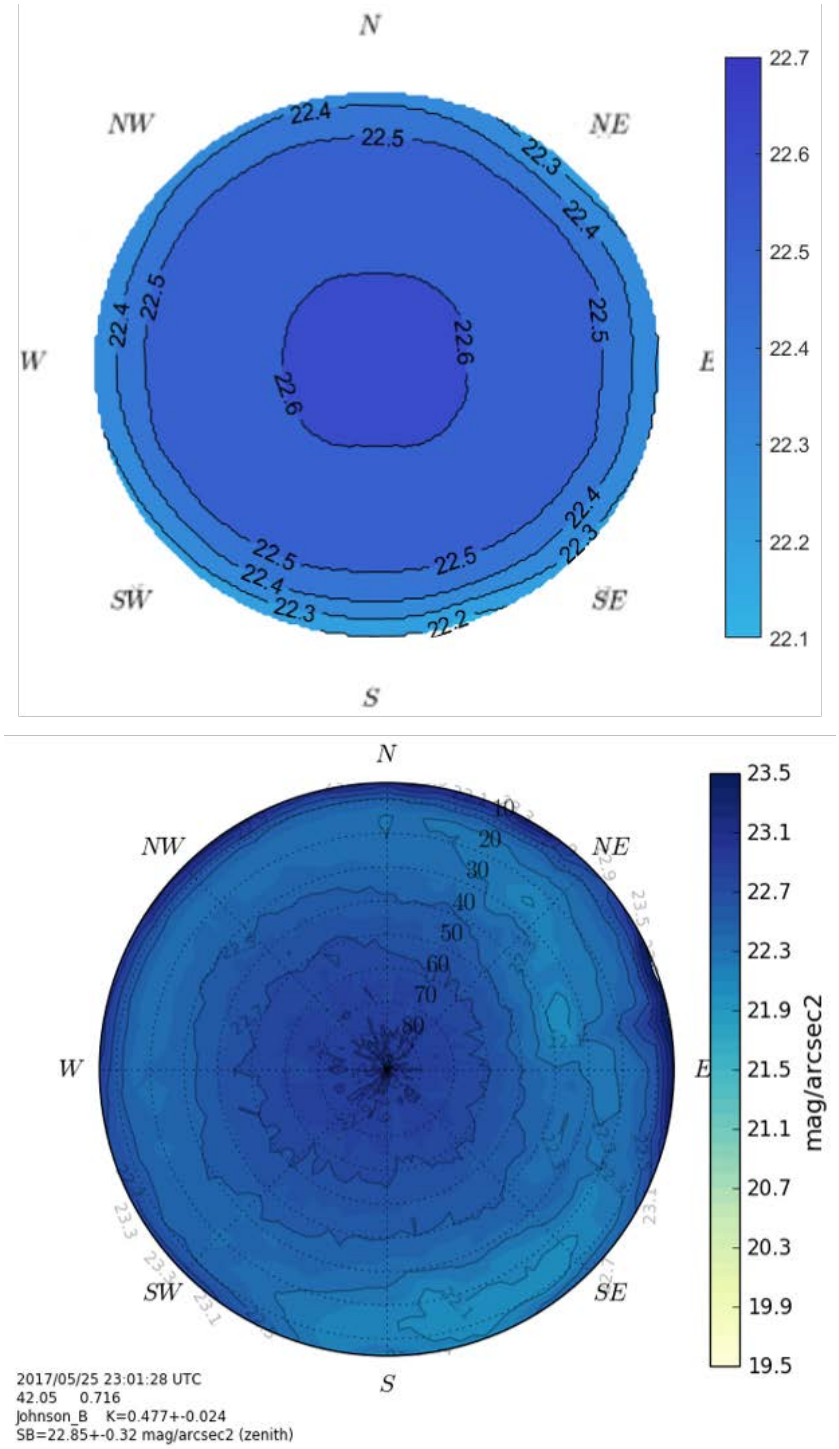

Figure 5.14: OAdM all-sky brightness maps in the B band. Top: simulation. Bottom: ASTMON data.

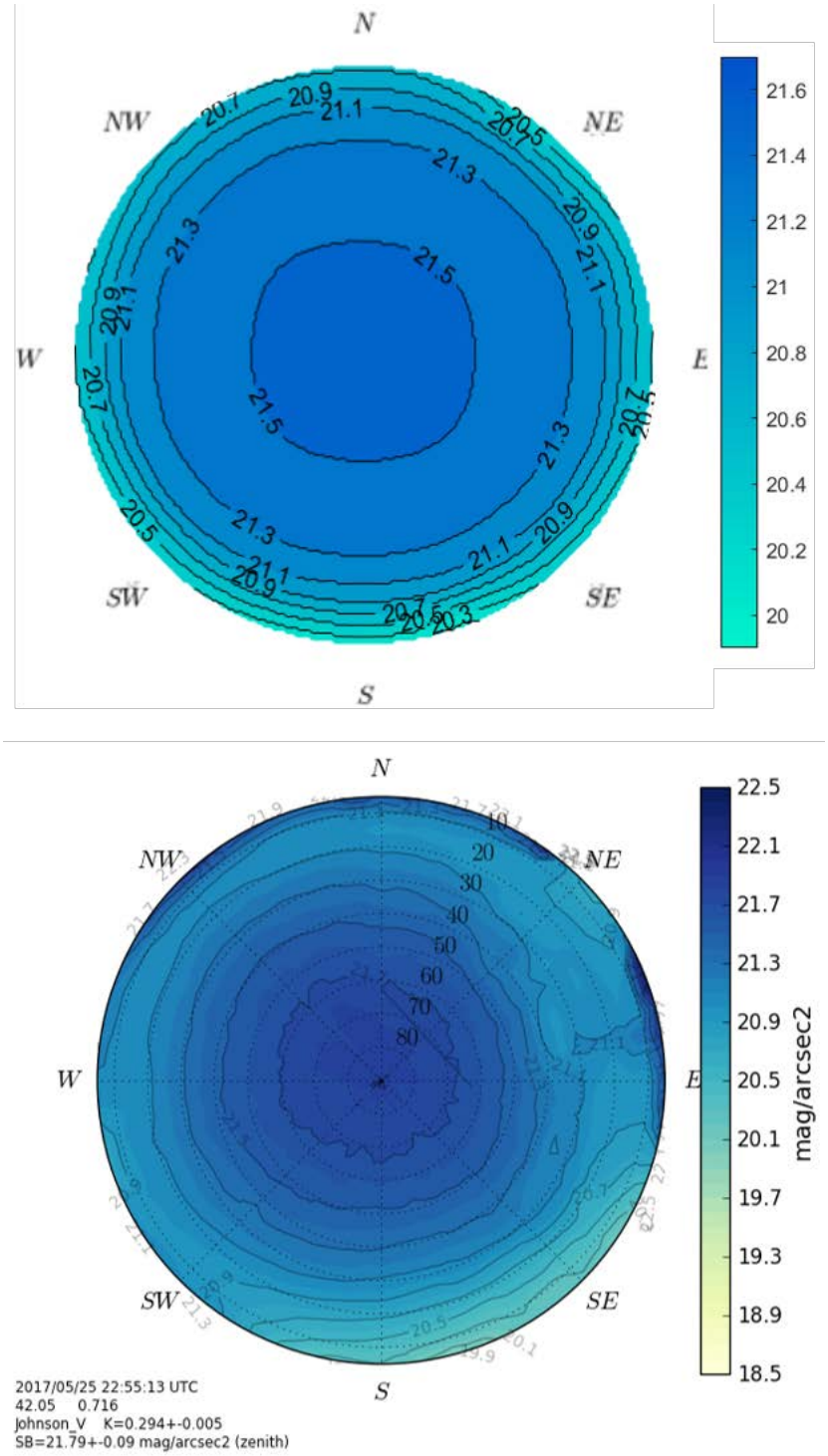

Figure 5.15: OAdM all-sky brightness maps in the V band. Top: simulation. Bottom: ASTMON data.

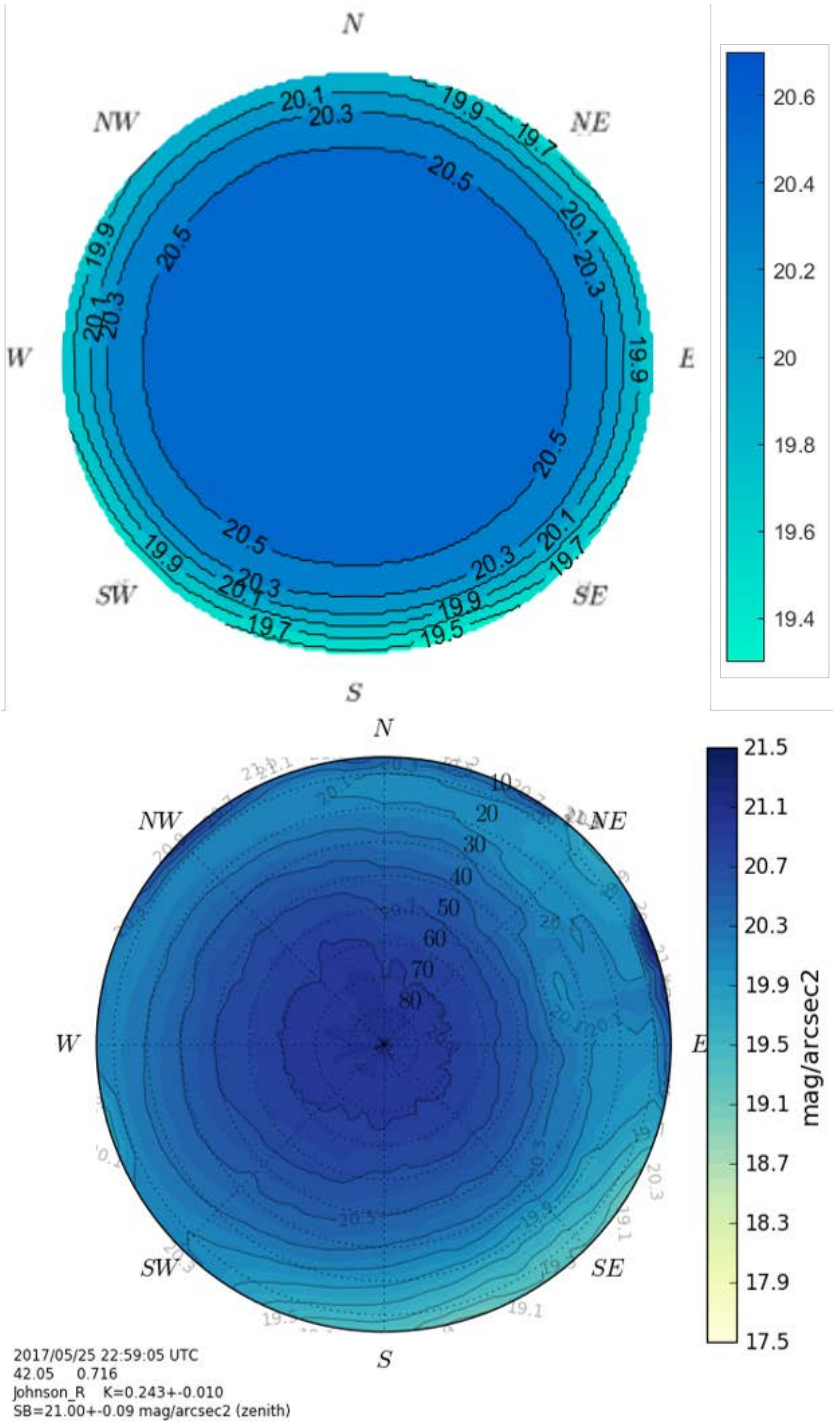

Figure 5.16: OAdM all-sky brightness maps in the R band. Top: simulation. Bottom: ASTMON data.

5.3.2 Montgarri

This location is placed close to Montgarri's refuge in the catalan west Pyrenees, in the northern part of the Alt Pirineu Natural Park. Although it is a high mountain region with scarce towns and low population density, the location is close to the skiing resort of Baqueira-Beret. With an altitude slightly over 1600 m above sea level, it is one of the highest location studied in the thesis.

Contribution map

There are only five regions that surpass the 2% contribution threshold: Vielha e Mijaran with 11.1%, Naut Aran with 10.7%, Andorra with 9.8%, Saint Girons with 4.2% and Alt Áneu with 2.3%.

The three most contributing ones are responsible for more than 30% of the total radiance received. The biggest source is Vielha e Mijaran. The city of Vielha (5k inhabitants) is located at 17 km south-west. The second greatest source is the municipality of Naut Aran (2k inhabitants), where the observation point resides. Probably the ski resort that is also located in the same municipality at less than 10 km SSW is the main responsible. The third most contributing source is Andorra (75k inhabitants). Its capital, Andorra la Vella, is located at 50 km SE. The city altogether with its closer towns adds up to 30k inhabitants.

In the french side, St. Girons stands out from the rest of municipalities. It has a population of 6k inhabitants and is located at 25 km NNE. It is remarkable the low contribution of the french regions near the location despite the close distance. Toulouse far north has a contribution of around 1% to the total brightness.

All-sky brightness map

We did not have specific information of the inventory of lights of the most polluting sources, so we did not differentiate them from the general area. Our fieldwork confirms that the inventory used fits quite well the real situation. The exception is Andorra, that has a completely different set of lights, mostly LED of high CCT. Aided by satellite images (see section 5.4) and lighting experts from the Departament de Territori i Sostenibilitat and the Alt Pirineu Natural Park we defined Andorra independently as it is shown in table 5.6.

There are not ASTMON measurements for this location. The all-sky measurement data used is the DSLR image processed with SQC that was taken by

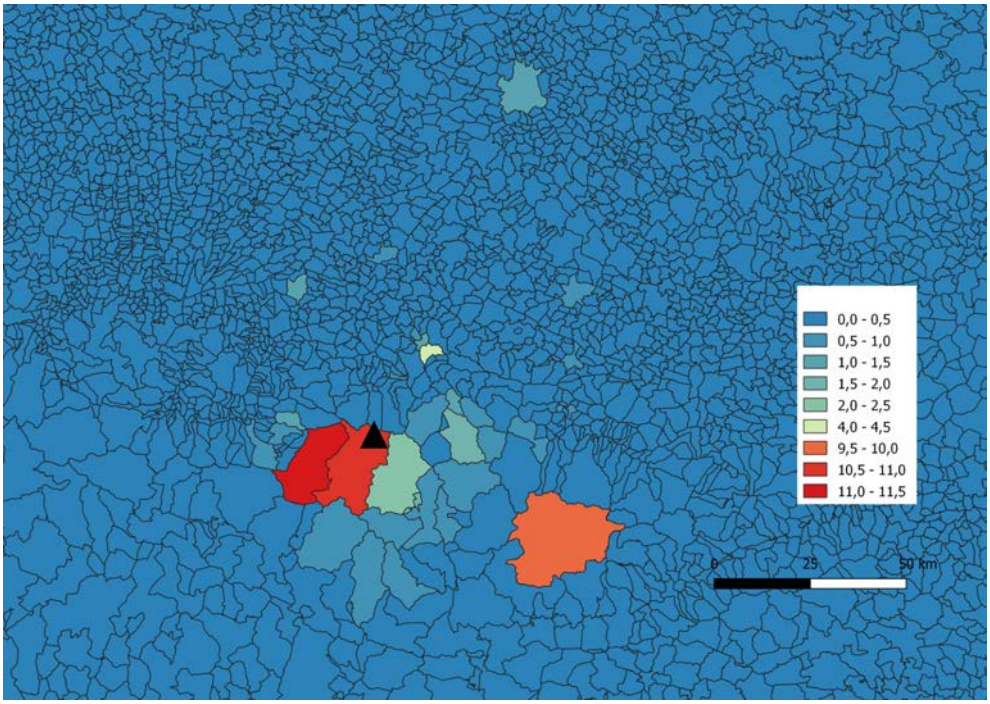

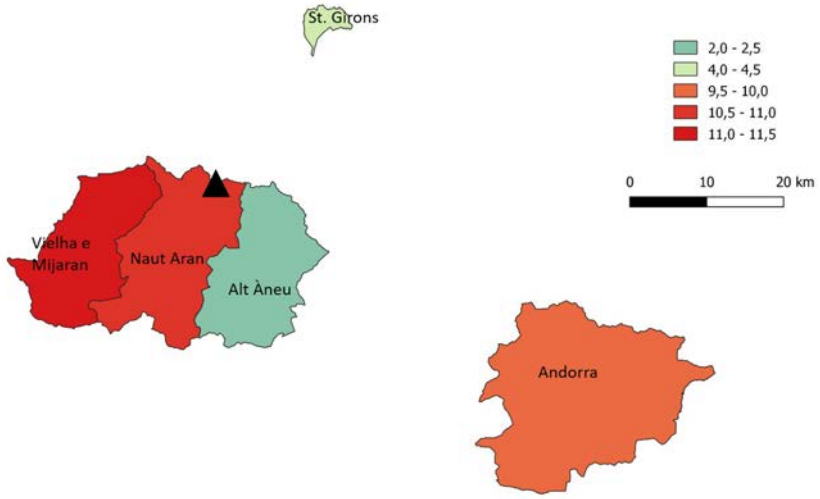

Figure 5.17: Percentage of artificial light emission by municipality received in the V band in Montgarri. Top: all the municipalities. Bottom: municipalities that contribute more than a 2%.

Source	Inventory (%radiance emitted-Techonology-ULOR)
Andorra	61-4LED-1, 16-MH-5, 13-HPS-5, 5-FLC-5, 3-3LED-1, 1-MV-5
General zone	43-HPS-10, 42-HPS-5, 15-4LED-1

Table 5.6: Characteristics of the light pollution sources included in the all-sky simulation over Montgarri. HPS: high pressure sodium. MH: metal halide. 4LED: LED 4000 K CCT. FLC: fluorescent. 3LED: LED 3000 K CCT. MV: mercury vapor.

the author in the 2019 campaign. The simulated map was created using Illumina v1.

The most obvious difference between both maps is the presence of the Milky Way. When the image was taken the Milky Way crossed the entire sky passing through the zenith. In simulated maps, as stated, we do not include the brightening effect of the Milky Way. Another big difference between measurements and simulations is the blocking effect of the surrounding orography. The DSLR image lacks information close to the horizon for most azimuths. In the simulated map there is no such problem.

Both maps agree on showing an almost pristine sky. Brightness values for elevations above 40º surpass 21.4 mag/arcsec^2. The darkest value in the SQC is 21.89 mag/arcsec^2 in NW at 70º in elevation due to Milky Way brightening of the zenith. Thus, it is one of the cases with darker values than the the expected natural value. In the simulated map the darkest direction is placed very close to the zenith with a value slightly below 21.7 mag/arcsec^2. The difference is within the order of magnitude expected.

They also agree in the most polluted directions that are between ESE and SE towards Andorra (20.4 and 20.6 mag/arcsec^2) and WSW towards Baqueira and Vielha (20.6 mag/arcsec^2 in both maps).

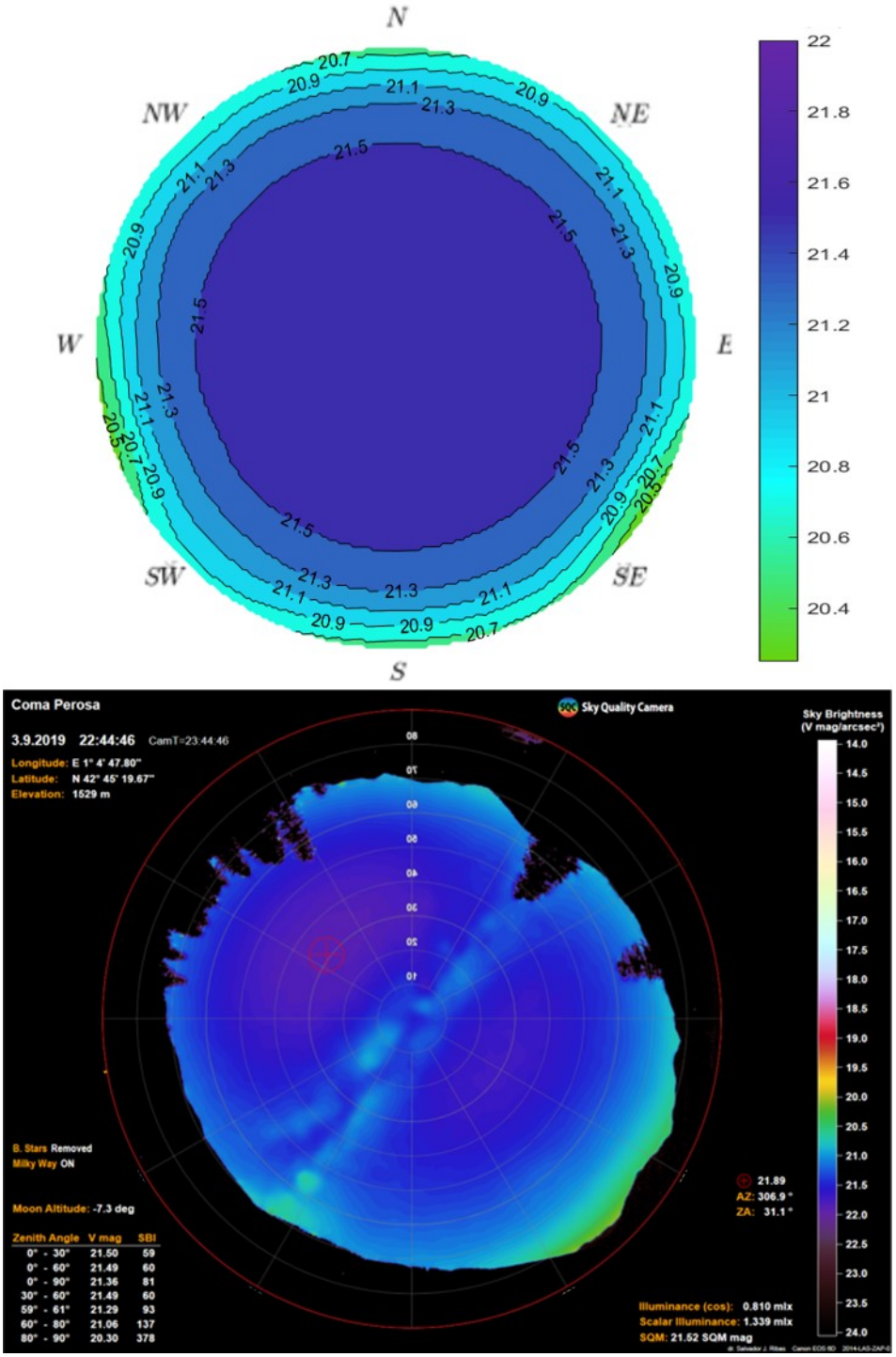

Figure 5.18: Montgarri all-sky brightness maps in the V band. Top: simulation. Bottom: SQC data.

5.3.3 Estany Llong

Estany Llong is a lake inside the National Park of Aigüestortes i Estany de Sant Maurici, the only National Park in Catalonia. It is a very low populated area with no big towns around. The National Park is placed in the western Pyrenees of Catalonia, a few kilometers west to the Alt Pirineu Natural Park.

The location studied is placed in the south border of the lake at 25 km south from the Montgarri location. The area is devoid from artificial light sources within a radius of 10 km. With its 2000 m of altitude, it is the highest location studied within Catalonia.

Contribution map

The municipality of Vielha e Mijaran (5k inhabitants) is clearly the biggest source of artificial brightness over Estany Llong with a contribution of 20.2%. It practically doubles the contribution of the second larger contributor that is Naut Aran (2k inhabitants), 10.6%. La Vall de Boí (1k inhabitants) is the third in the ranking due to the close proximity, 9.3%. Andorra (75k inhabitants) is also a significant source of artificial brightness, 6.4%, although it is placed more than 40 km away.

The three remaining municipalities that surpass the 2% threshold are not specially bright sources: La Torre de Cabdella (800 inhabitants) 4.6%, Sort (2k inhabitants) 3.3% and El Pont de Suert (2k inhabitants) 3.1%.

All-sky brightness map

As it happened in Montgarri's case, there is a lack of detailed information from the two biggest sources of artificial radiance: Vielha e Mijaran and Naut Aran. They have been defined using the general inventory. On the other hand, we did have detailed information of Sort and La Vall de Boí. Andorra, as in the previous case, has been defined by an estimated inventory, as it is quite different from the general inventory defined for the rest of the towns. See table 5.7 for detailed information.

The ASTMON data available for this location was not compared to the simulated all-sky brightness maps because the data was taken with abnormally high atmospheric absorption. This phenomena darkens sky brightness values. For instance, in relatively low elevation angles (30º), where light pollution normally increases the brightness of the sky, ASTMON data is way darker than the theoretical maximum at zenith in every filter: in B it surpasses 23.0, in V 22.0 and in R 21.6

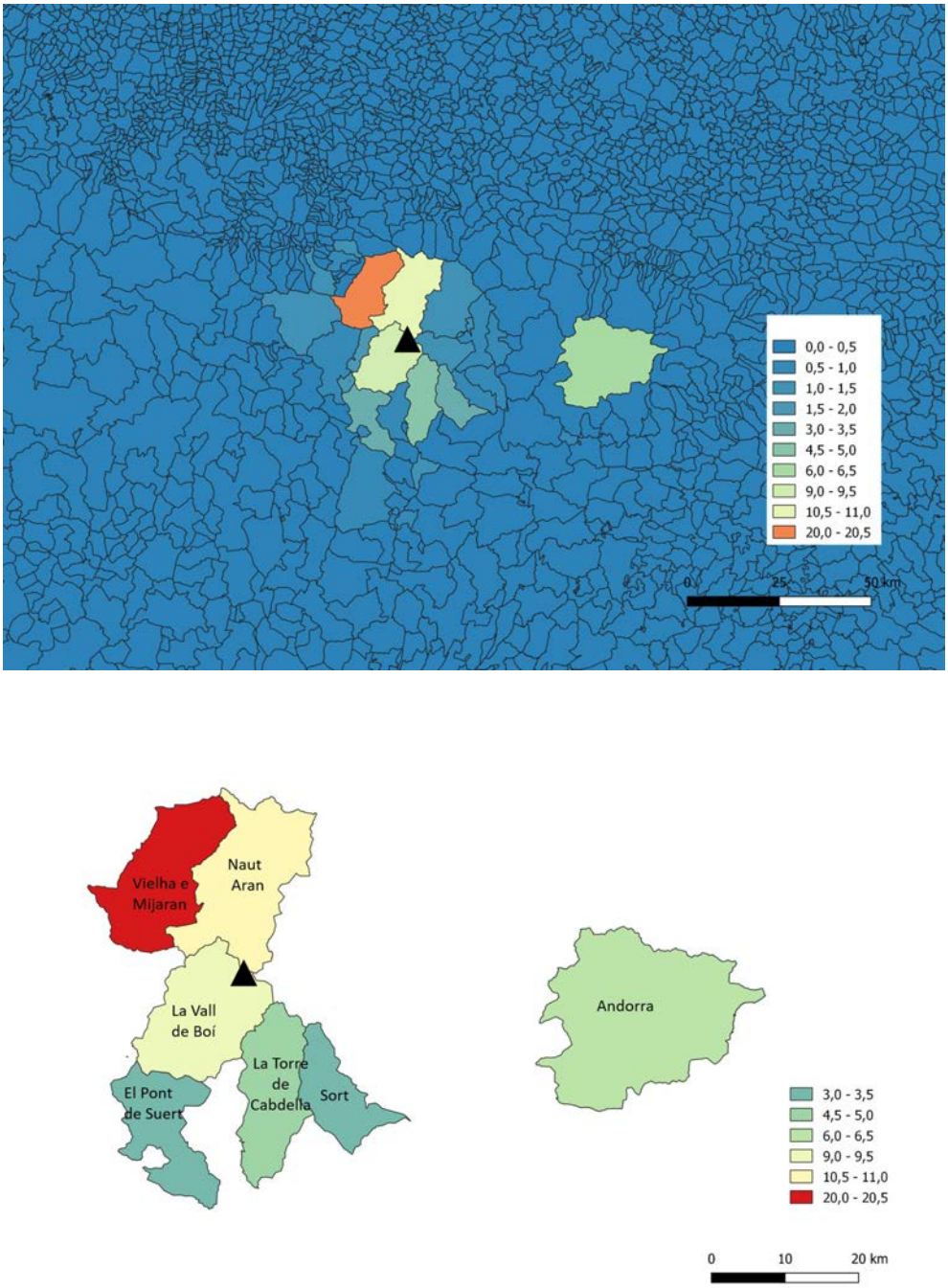

Figure 5.19: Percentage of artificial light emission by municipality received in the V band in Estany Llong. Top: all the municipalities. Bottom: municipalities that contribute more than a 2%.

Source	Inventory (%radiance emitted-Techonology-ULOR)
Andorra	61-4LED-1, 16-MH-5, 13-HPS-5, 5-FLC-5, 3-3LED-1, 1-MV-5
Sort	43-L-10, 42-L-5, 15-4LED-1
Vall de Boí	26-MV-10, 21-L-5, 21-L-10, 17-4LED-1, 15-FLC-10
General zone	43-HPS-10, 42-HPS-5, 15-4LED-1

Table 5.7: Characteristics of the light pollution sources included in the all-sky simulation over Estany Llong. HPS: high pressure sodium. MH: metal halide. 4LED: LED 4000 K CCT. FLC: fluorescent. 3LED: LED 3000 K CCT. MV: mercury vapor. L: low pressure sodium.

mag/arcsec^2. In the zenith direction, the Milky Way brightnes the sky making it even harder to compare the ASTMON values and the simulated values in this direction.

Simulated maps show that it is a very dark location, with values similar to what was obtained for the OAdM. Over 30^o in elevation: 22.5 in B filter, 21.4 in V filter and 20.6 mag/arcsec^2 in R filter. The most polluted direction are to the W towards Andorra, to the NW towards Vielha and to SW towards La Vall de Boí.

In the B filter, due to the large distance to the sources, artificial brightness is almost negligible in most of the sky. The darkest value is 22.6 mag/arcsec^2 in the zenith. The brightest direction is close to the horizon towards the SW, 22.2 mag/arcsec^2.

In the V filter, the darkest direction coincides with the zenith with a value of 21.6 mag/arcsec^2. There are three principal regions that have a value of 20.5 mag/arcsec^2: NW towards Vielha e Mijaran, E towards Andorra and SW towards La Vall de Boí and El Pont de Suert.

In the R filter, the darkest value is 20.6 mag/arcsec^2 in the zenith. In this filter the NW and E directions are brighter (19.8 mag/arcsec^2) than in the SW (20.0 mag/arcsec^2).

As a conclusion, the sky over Estany Llong is practically unpolluted over 30^o in elevation. The sources of artificial radiance are located at a great distance, which reduces the brightening of the sky of the B filter with respect the other bands.

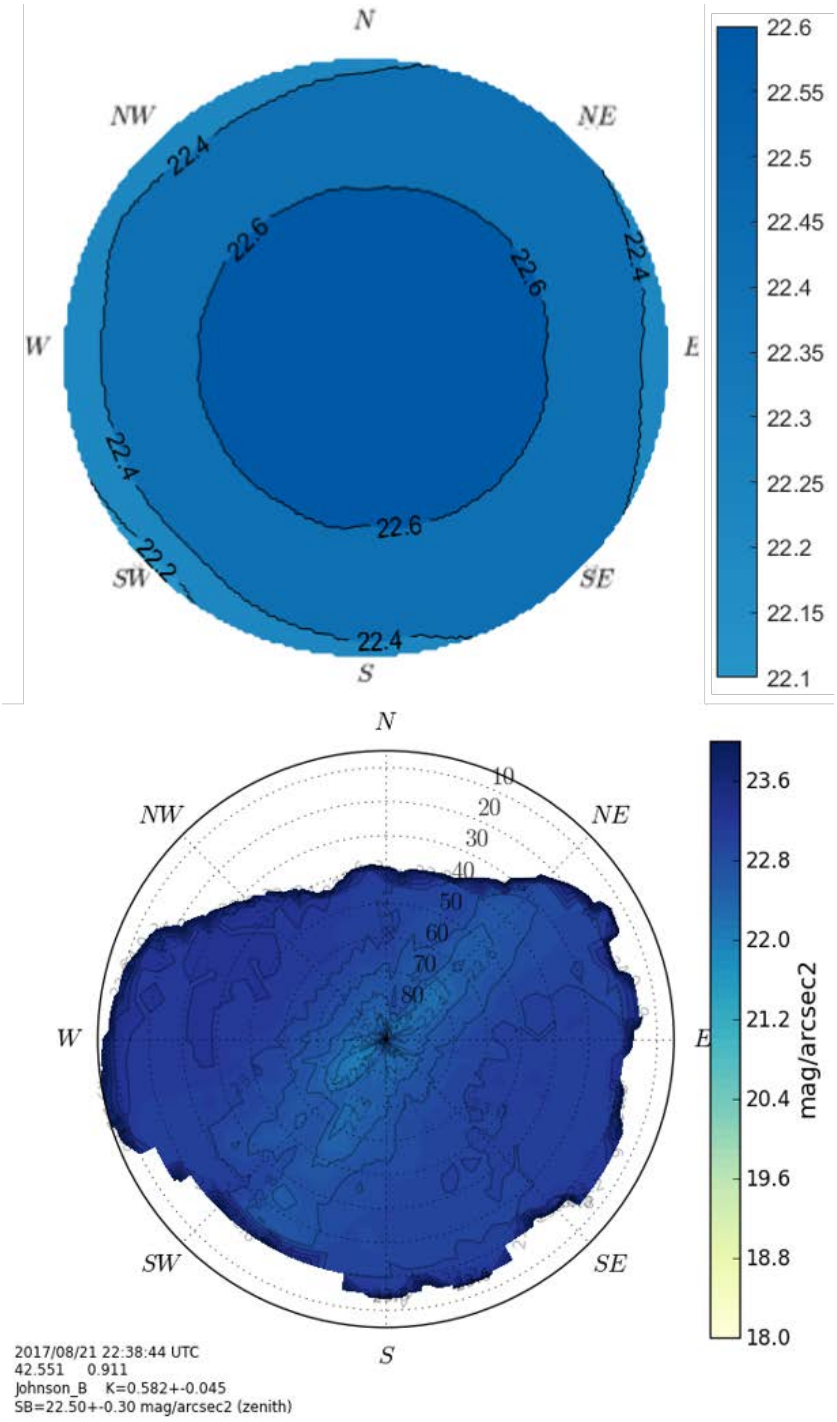

Figure 5.20: Estany Llong all-sky brightness maps in the B band. Top: simulation. Bottom: ASTMON data.

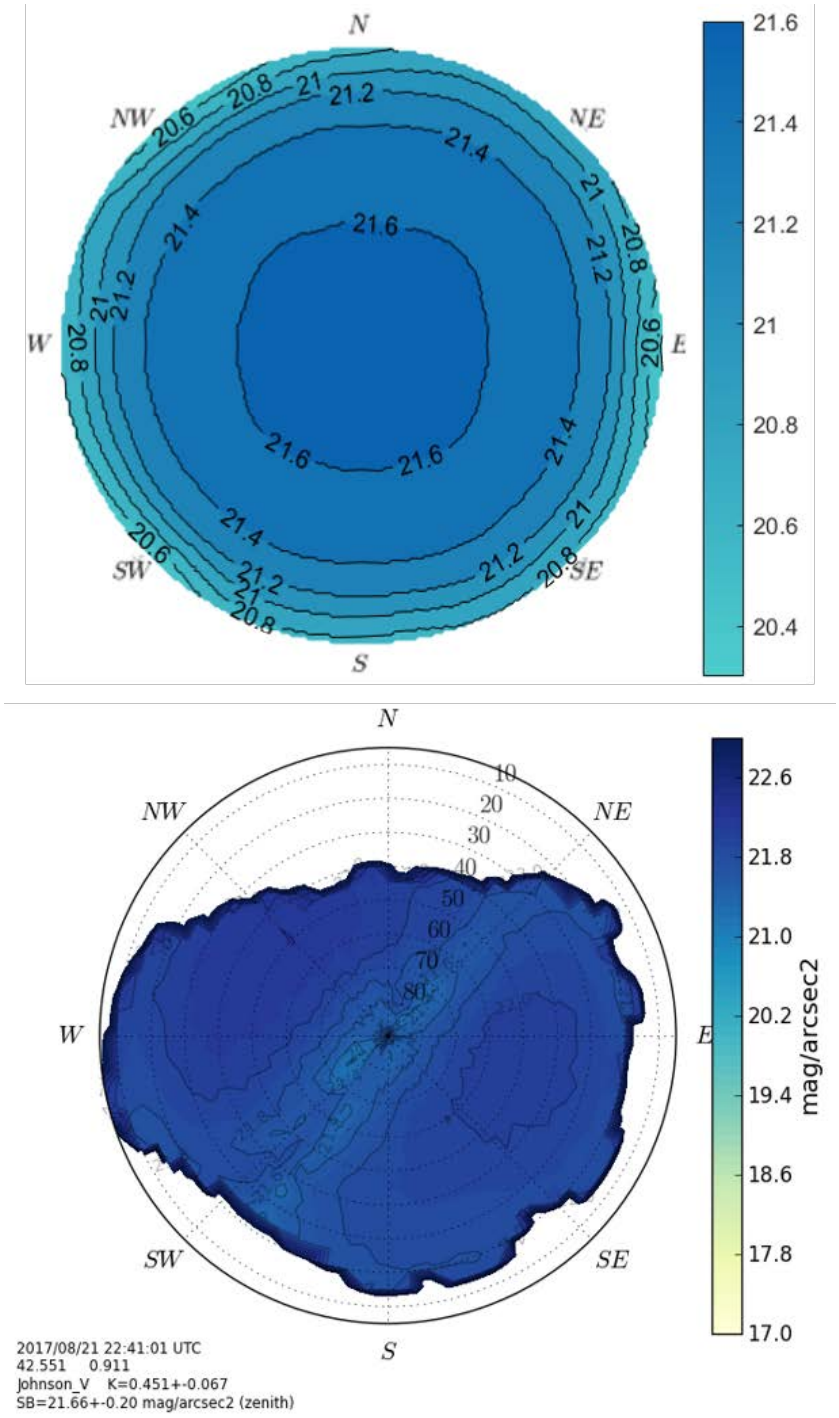

Figure 5.21: Estany Llong all-sky brightness maps in the V band. Top: simulation. Bottom: ASTMON data.

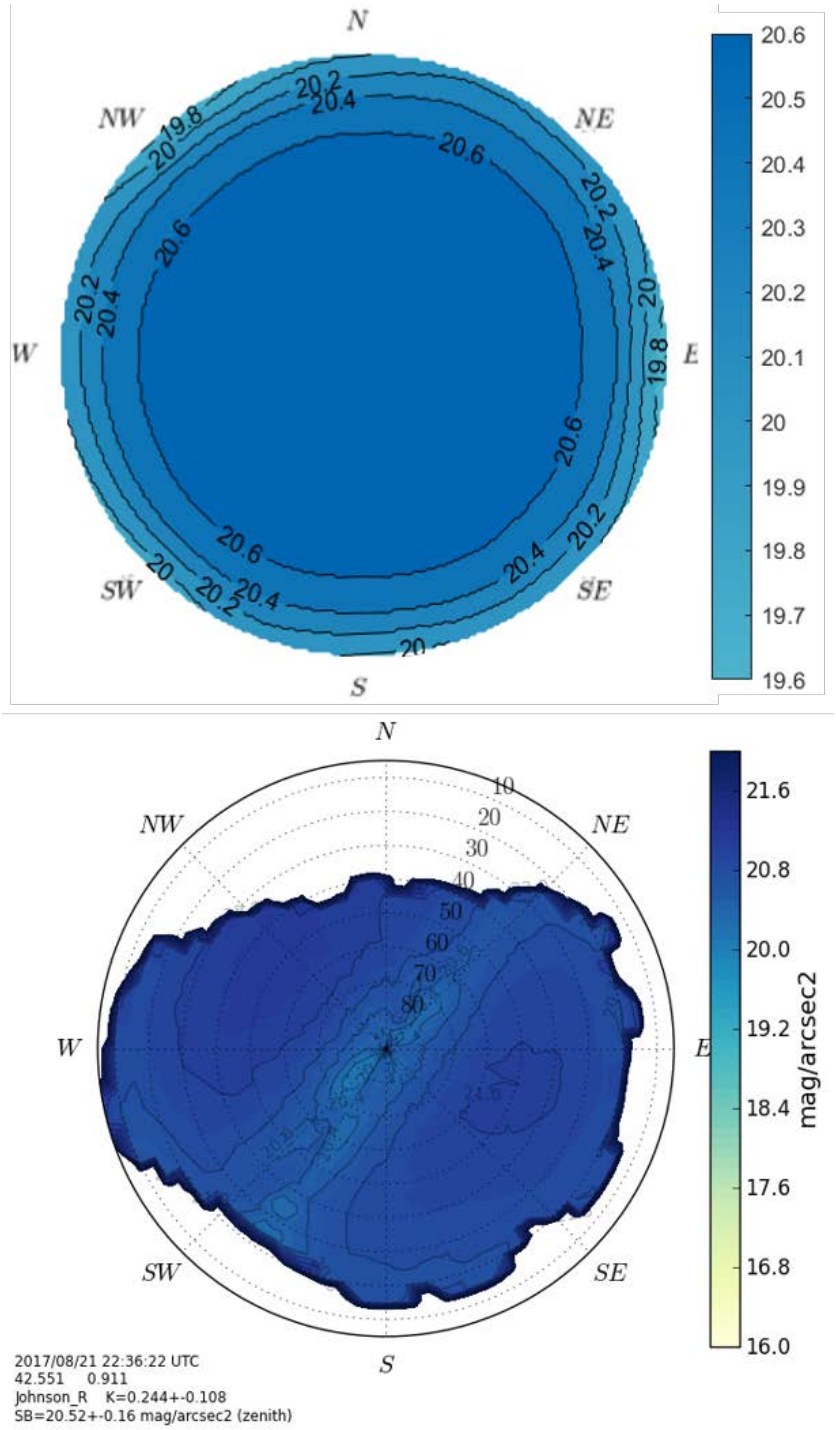

Figure 5.22: Estany Llong all-sky brightness maps in the R band. Top: simulation. Bottom: ASTMON data.

5.3.4 Pic de l'Orri

Pic de l'Orri is a peak, as it name indicates, of an altitude of almost 1500 m. It is placed within the border of the Alt Pirineu Natural Park as Montgarri's case but in the opposite side of the Park. Pic de l'Orri is 40 km SSE from Montgarri's location and 30 km SE from Estany Llong location.

In a radius of 15 km there are several small towns and some mid-size towns. On the top of the peak there is a telecommunication station.

Contribution map

The principal source of artificial brightness in this location is the country of Andorra (75k inhabitants), that accounts for almost a third, 32.3%, of the total received. It is practically three times as polluting as the second largest source of artificial brightness, Sort (2k inhabitants) that accounts for 11.1%, a mountain town close to the peak. The third greatest source is La Seu d'Urgell municipality (12k inhabitants) with 5.9%. Although the municipality is small, the city within is quite bright.

The other three regions that surpass the 2% threshold are just over the limit: Montferrer i Castellbó (1k inhabitants) 2.1%, La Torre de Cabdella (750 inhabitants) 2.1% and La Pobla de Segur (3k inhabitants) 2.0%. They are relatively close areas with no noticeable bright sources.

All-sky brightness map

In addition to the already explained light system estimation of Andorra, we have a detailed inventory of the second biggest source of artificial radiance, Sort. We also defined independently La Vall de Boí as we already had the inventory from the Estany Llong case. The rest of the artificial radiance sources in a radius of 50 km were defined with the general inventory (see table 5.8).

In this case there are no ASTMON data available. Moreover, the DSLR images that were taken during the 2019 campaign are of no use because the telecommunication center that is placed in the peak had the lights turned on. Luckily, Canal-Domingo (Parc Astroòmic Montsec) took DSLR pictures during 2020 in the same place when lights were shut down. We used them to compare to the simulated maps (Illumina v1). However, the set of images were taken with presence of clouds near the horizon at azimuth SSE to NE. High clouds over distant sources increase the artificial radiance scattered towards the observer (Ribas et al. 2016;

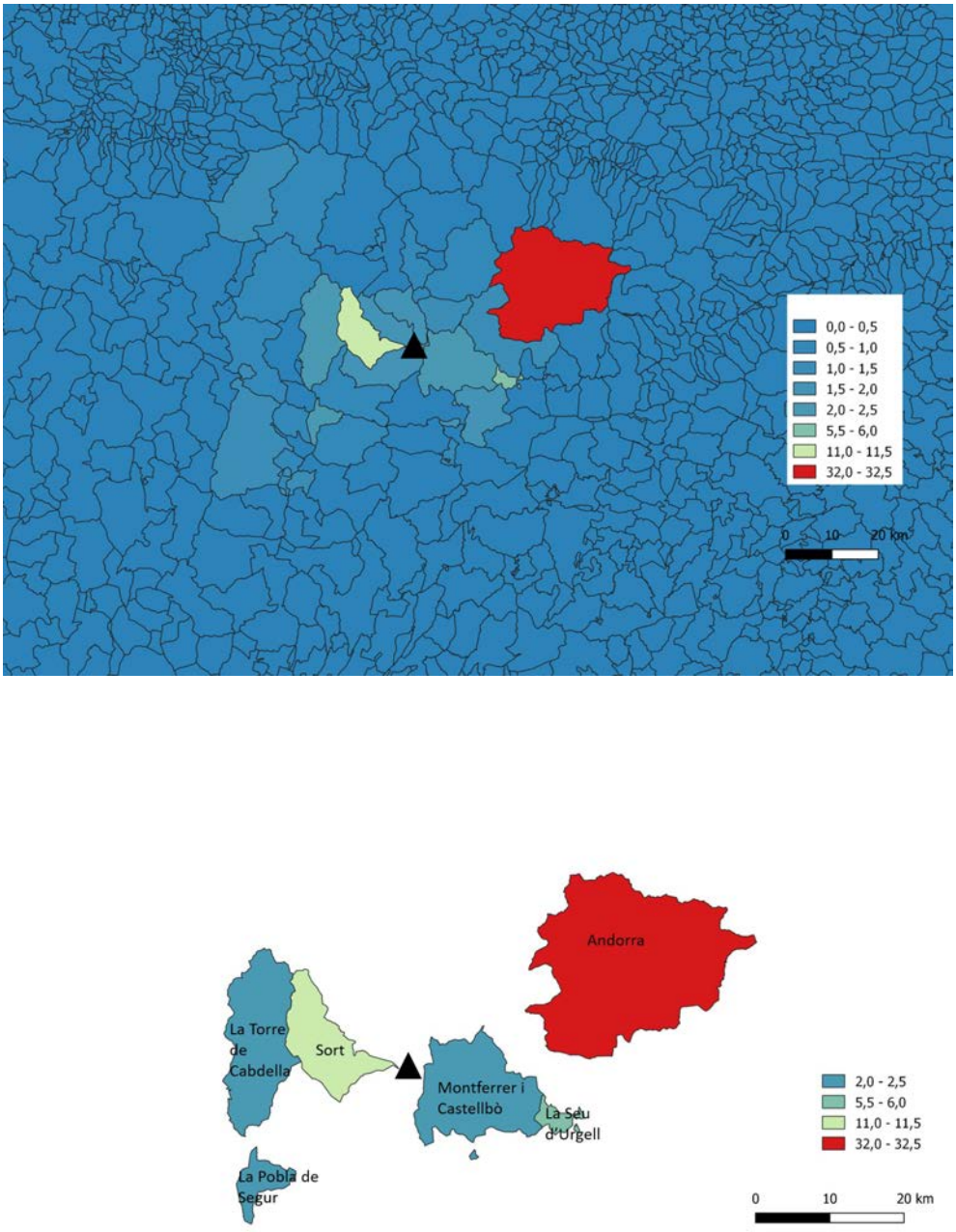

Figure 5.23: Percentage of artificial light emission by municipality received in the V band in Pic de l'Orri. Top: all the municipalities. Bottom: municipalities that contribute more than a 2%.

Source	Inventory (%radiance emitted-Techonology-ULOR)
Andorra	61-4LED-1, 16-MH-5, 13-HPS-5, 5-FLC-5, 3-3LED-1, 1-MV-5
Sort	43-L-10, 42-L-5, 15-4LED-1
Vall de Boí	26-MV-10, 21-L-5, 21-L-10, 17-4LED-1, 15-FLC-10
General zone	43-HPS-10, 42-HPS-5, 15-4LED-1

Table 5.8: Characteristics of the light pollution sources included in the all-sky simulation over Pic de l'Orri. HPS: high pressure sodium. MH: metal halide. 4LED: LED 4000 K CCT. FLC: fluorescent. 3LED: LED 3000 K CCT. MV: mercury vapor. L: low pressure sodium.

Jechow et al. 2017). In this case, it happens with Andorra, 20 km away towards NE, and Barcelona, 150 km away towards SE. The effect of the clouds is observable in the processed image (see figure 5.24): to the NE there is an elongated secondary dome at elevation between 10º and 15º over the expected dome of artificial radiance produced by Andorra; to the SE there is a huge dome of artificial radiance that would not have been distinguishable if not for high clouds over Barcelona.

Ignoring the effect of the clouds the biggest difference between the SQC map and the simulated map is the presence of the Milky Way. In the SQC map it is clearly visible crossing the sky near the zenith from WSW to ENE.

Both maps agree on that the sky over Pic de l'Orri is almost pristine. The darkest value of the SQC map almost reaches 21.8 mag/arcsec^2 whereas in the simulated map it reaches 21.6 mag/arcsec^2, in both cases very close to zenith.

Due to clouds the most polluted values are not comparable. In the simulated map is 20.4 mag/arcsec^2 NE near the horizon. The SQC map show a value of around 19.0 mag/arcsec^2 in this direction and even brighter (18.8 mag/arcsec^2) SE towards Barcelona.

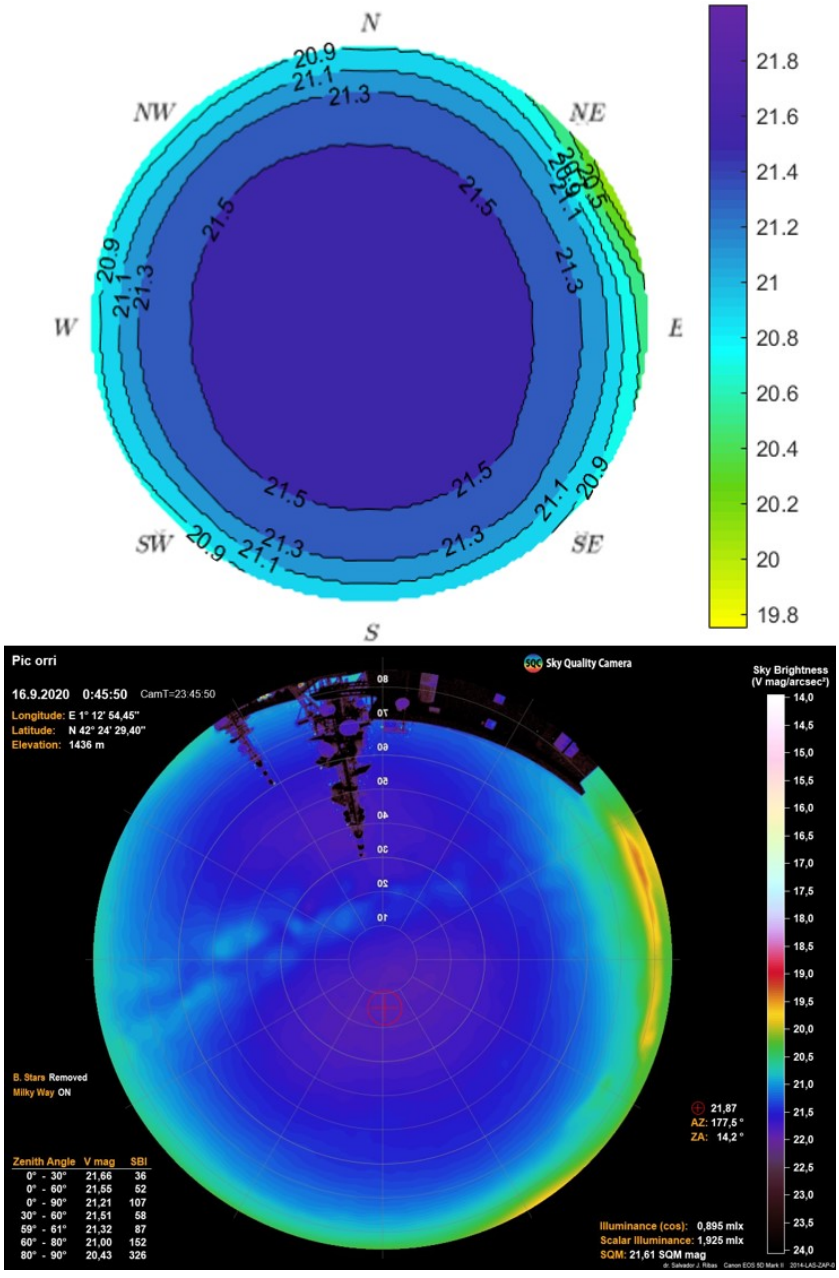

Figure 5.24: Pic de l'Orri all-sky brightness maps in the V band. Top: simulation. Bottom: SQC data from DSLR images taken by Canal-Domingo.

5.3.5 Montsant

The location of Montsant corresponds to a country house, Mas de l'Estrem, within Montsant Natural Park in Tarragona's province.

The 2018 SQM campaign covered this area (see section 3.2.2). The values of the closest SQM measurements to this location were over 21.0 mag/arcsec^2.

Tarragona metropolitan area is located 35-50 km towards ESE, and the power plants of Ascó and Vandellós are at 20 km SW and S respectively.

Contribution map

Tarragona metropolitan area (500k inhabitants) is the main contributor, 42%, to light pollution over Montsant (see figure 5.25). Mainly due to the cities of Reus (100k inhabitants), 7.3%, and Tarragona (132k inhabitants), 6.9%.

The city of Lleida (140k inhabitants) is of special interest. Although the city is located at the same distance (or even closer) than in the OAdM case, the percentage contribution is much smaller here: in the OAdM case is 6.4% and in Montsant is 3.2%. That indicates that the level of light pollution in Montsant is greater than in the OAdM. The relative contribution of Lleida is smaller because the artificial brightness received by the rest of sources is larger (mostly due to Tarragona metropolitan area).

In Montsant case there are two nuclear plants relatively close to the location studied. The plant of Ascó is located at 20 km SW and the one from Vandellós at almost 30 km south. The differences in their contribution is quite relevant (6.8% and 2.5% respectively). It may be partially explained by the distance difference, but it is very probable that the lighting system in Vandellós is better in terms of light pollution than the one in Ascó.

All-sky brightness map

In this case, the attempts to obtain a detailed public inventory of the city of Tarragona (or any of its surrounding municipalities) was in vain. We used the general inventory with the exception of Lleida, which was already defined for the OAdM case (see table 5.9).

ASTMON maps lack information for low elevation angles from WSW to ENE due to obstacles. ASTMON measurements were taken with presence of the Milky

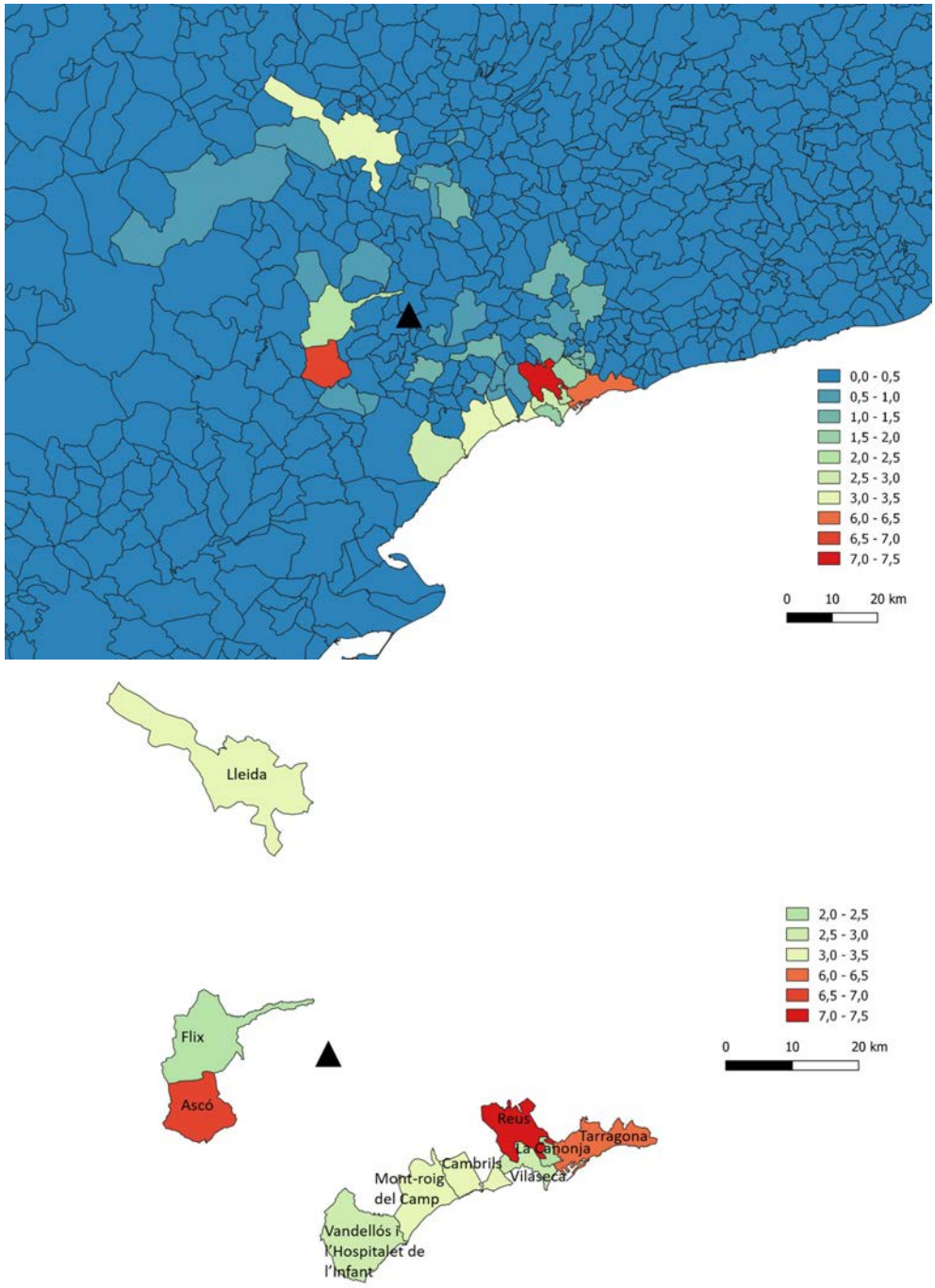

Figure 5.25: Percentage of artificial light emission by municipality received in the V band in Montsant. Top: all the municipalities. Bottom: municipalities that contribute more than a 2%.

Source	Inventory (%radiance emitted-Techonology-ULOR)
Lleida	67-HPS-0, 14-4LED-0, 12-MH-0, 7-HPS-10
General zone	43-HPS-10, 42-HPS-5, 15-4LED-1

Table 5.9: Characteristics of the light pollution sources included in the all-sky simulation over Montsant. HPS: high pressure sodium. MH: metal halide. 4LED: LED 4000 K CCT.

Way crossing the sky from SW to NE passing close to zenith.

Simulated maps (Illumina v1) are very similar to ASTMON maps in every filter. All the maps agree that it is a dark sky but far from pristine. The dominant source of light pollution is to the SE towards the metropolitan area of Tarragona in every map. Simulated maps show, for every band, a secondary dome of skyglow in low elevation angles in azimuth WSW towards the nuclear plant of Ascó. As stated, ASTMON measurement lacks information in this direction and therefore the radiance coming from the plant cannot be compared.

As a general comment, in the B filter the simulated map is slightly darker than ASTMON and in the V filter the opposite happens. The pattern agrees well with the effects of working only with public lighting spectrum and not taking into account the characteristics of the private lighting spectrum (normally richer in blue light) that has been mentioned in the introduction of this section.

In the B filter, ASTMON darkest value is found away from zenith due to the presence of the MW (22.4 mag/arcsec^2) whereas in the simulated map coincides with the zenith (22.5 mag/arcsec^2). In a night with the Milky Way away from zenith probably both values will be even closer. The most polluted direction is, in both maps, ESE close to the horizon: 20.6 and 21.1 mag/arcsec^2 for ASTMON and Illumina v1 respectively. As stated, this difference is probably due to an underestimation of the blue light content of the inventories of Tarragona metropolitan area.

In the V filter, the darkest direction are the same than for the B filters. Their values are 21.3 and 21.0 mag/arcsec^2 for ASTMON and Illumina v1 respectively. The most polluted direction is also at at ESE, with values of 18.8 and 18.4 mag/arcsec^2 for ASTMON and Illumina v1 respectively. The difference is also probably due to a overestimation of the light with spectrum emission within the borders of the V filter in detriment of emission in the blue region.

In the R filter, Illumina is brighter than ASTMON. This result was expected

because the model does not include molecular absorption which is no negligible in this filter. The darkest values are 20.6 and 20.3 mag/arcsec^2 for ASTMON and Illumina v1 respectively. The most polluted values are (ESE direction) 17.8 and 17.4 mag/arcsec^2 for ASTMON and Illumina v1 respectively.

As a conclusion, Montsant has a dark sky but not pristine. We observed a shift in the spectrum between measurements and simulated maps that is most probably due to private light with a emission richer in blue than public lighting systems.

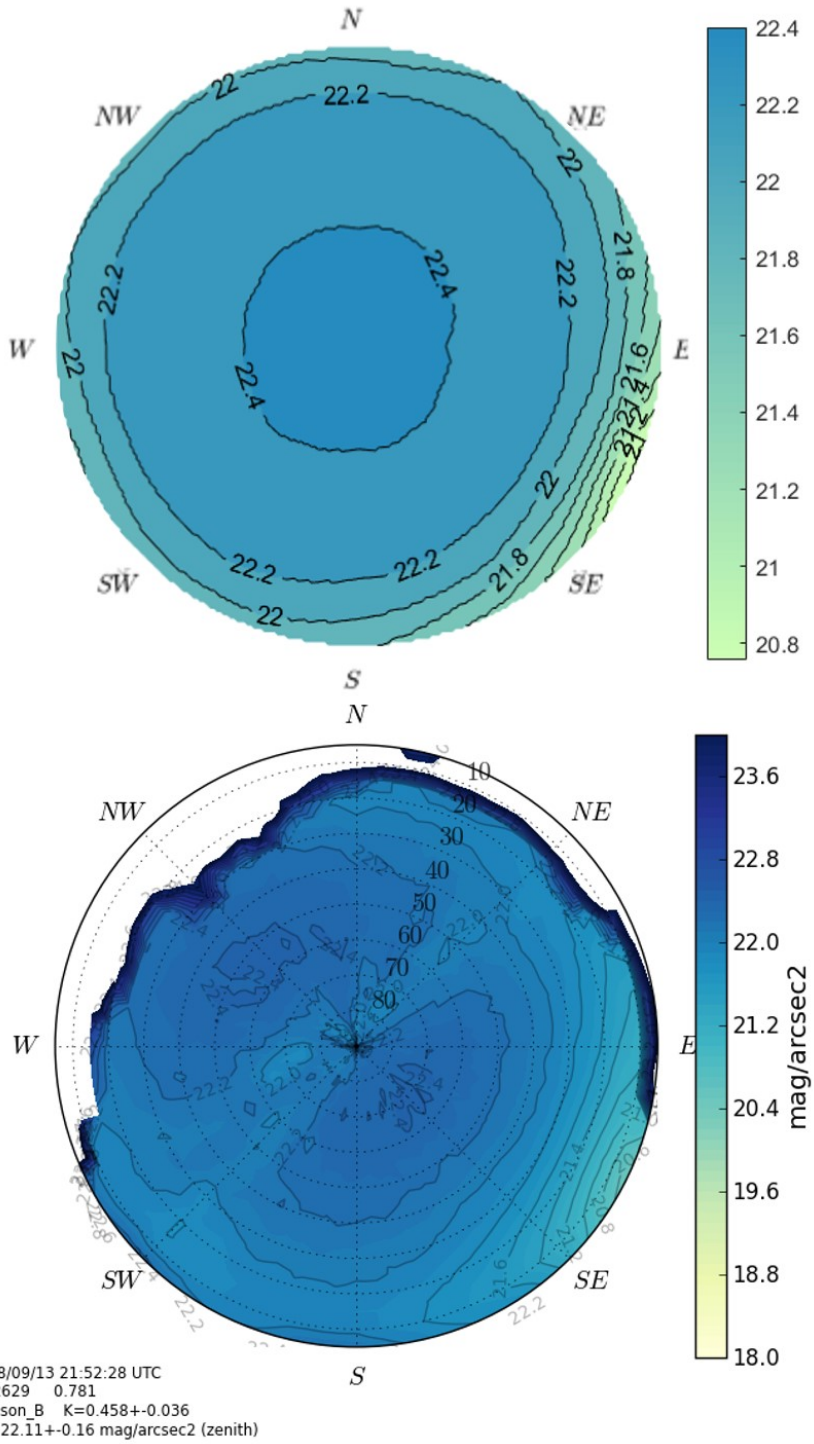

Figure 5.26: Montsant all-sky brightness maps in the B band. Top: simulation. Bottom: ASTMON data.

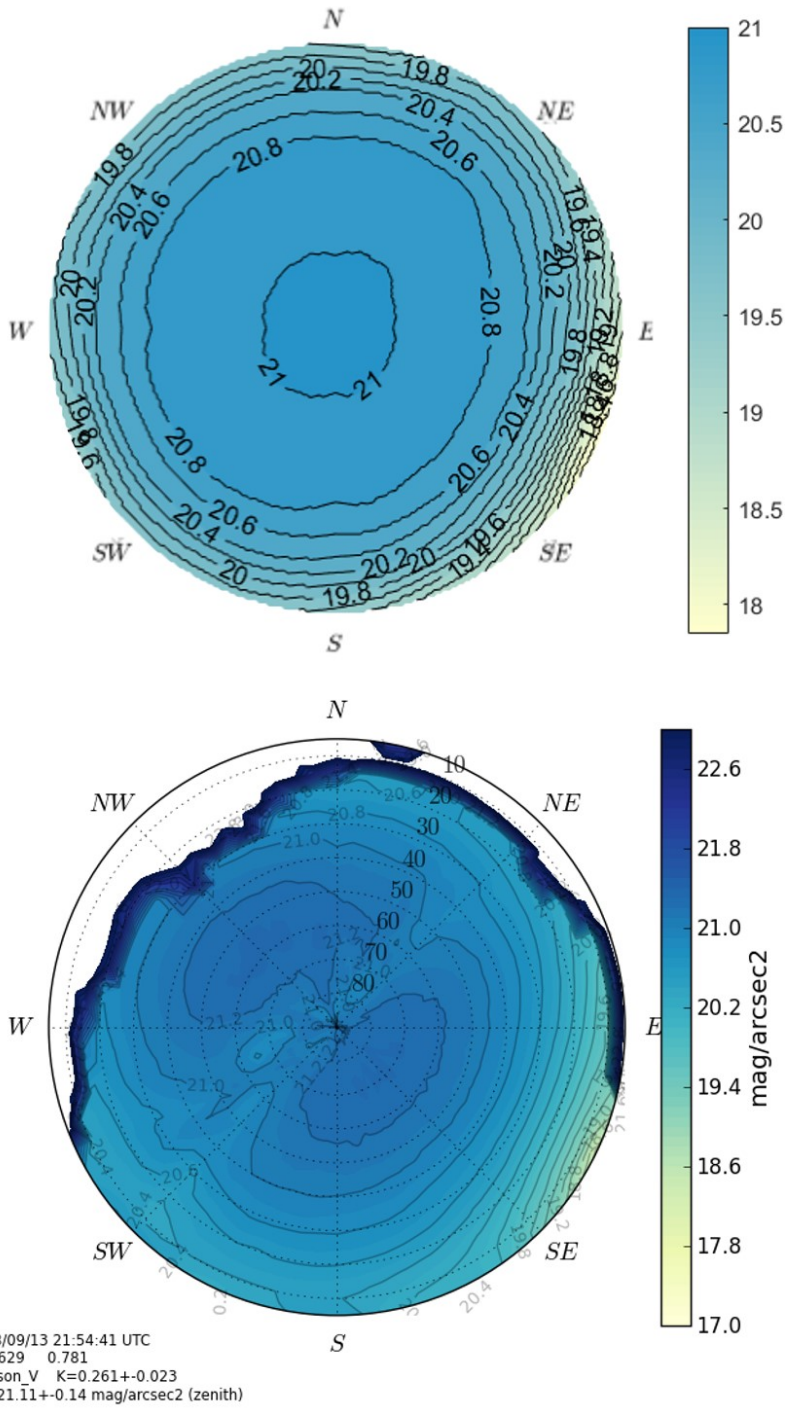

Figure 5.27: Montsant all-sky brightness maps in the V band. Top: simulation. Bottom: ASTMON data.

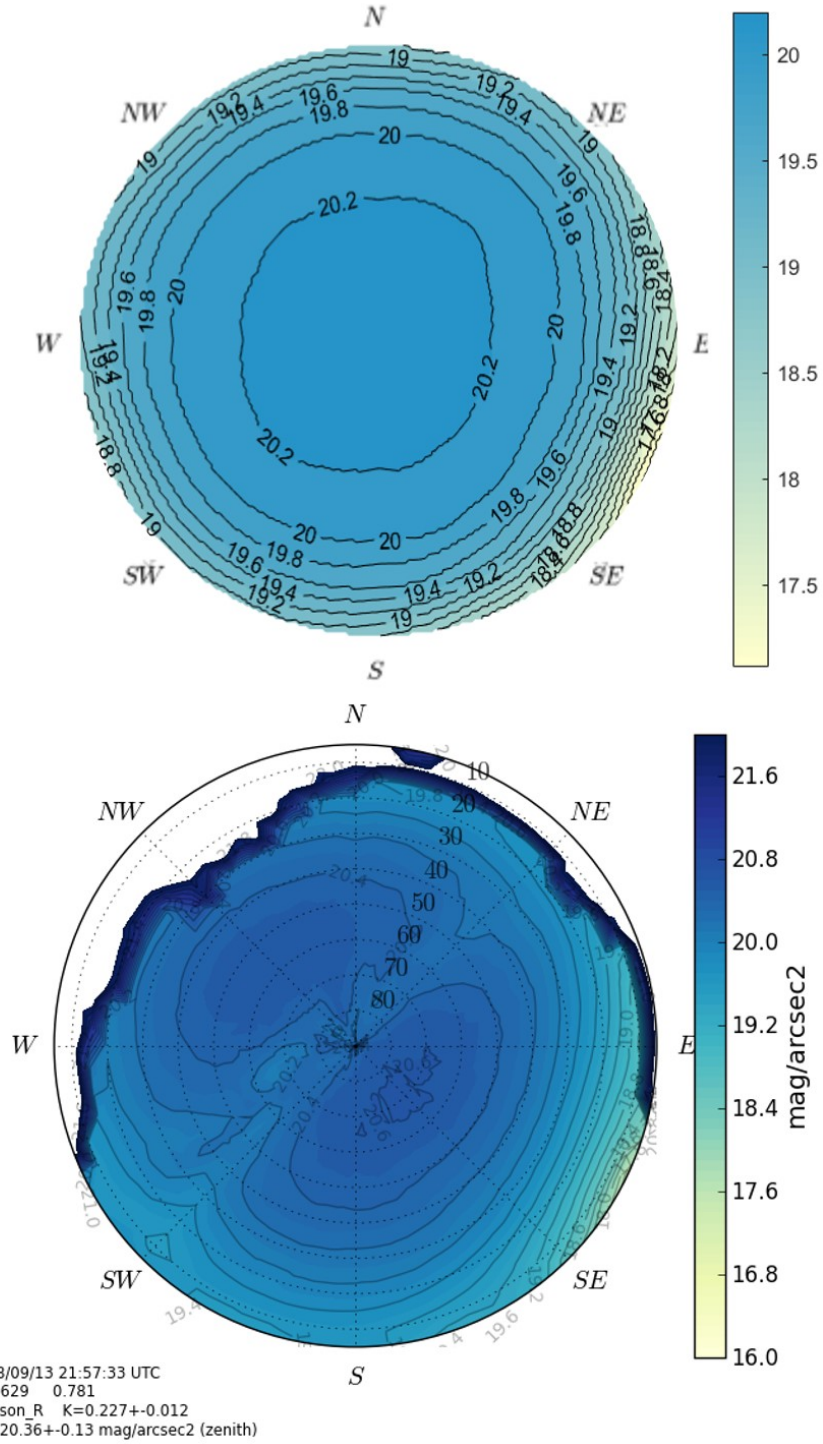

Figure 5.28: Montsant all-sky brightness maps in the R band. Top: simulation. Bottom: ASTMON data.

5.3.6 Centre Astronòmic de Prades

Centre Astronòmic de Prades is an astronomy outreach facility. It is located close to the small town of Prades (600 inhabitants) in Tarragona's province. The surrounding area is similar to Montsant, as it is located at a few kilometers north-east from that location. It is a low density population area but quite close, 20 km, to Tarragona metropolitan area. This area was also assessed with SQM dynamic measurements during the 2018 campaign (see section 3.2.2). The reference location for the all-sky measurements and simulations has an altitude of 1000 m.

Prades was chosen as a case of study for comparing the two versions of Illumina. The main reason is that it is the first case studied that has a big city closer than 30 km. As explained in section 4.2.6, the biggest difference in the results found between the two models of Illumina happens with close sources.

Contribution map

Tarragona metropolitan area dominates the contribution map due to its size, 500k inhabitants, and close proximity, 15 km to the nearest extreme to 30 km to the furthest. Almost 60% of all the artificial radiance received in Prades comes from this source. Breaking down the metropolitan area, the municipalities of Reus (9.7%) and Tarragona (9.4%) are by far the two greatest sources of artificial brightness over Prades astronomic center.

The unique contributors above 2% outside Tarragona metropolitan area are the cities of Valls (24k inhabitants), 3.4%, and Montblanc (7k inhabitants), 3.4%, located between 20 and 25 km to the west.

Lleida (140k inhabitants) works once again as a ruler since Prades and Montsant are approximately at the same distance with respect to the city. Its relative contribution is higher in Montsant (3,2%) than in Prades (1.5%). Thus, the total artificial brightness received in the location close to Prades is larger than in Montsant. This is mostly due to the closer proximity to Tarragona metropolitan area.

The municipality located at 40 km south-west that has a slightly greater contribution (1%) than its neighbours is Ascó (1.5k inhabitants). As explained in the previous case, the source of light is a nuclear plant that resides within the borders of the municipality.

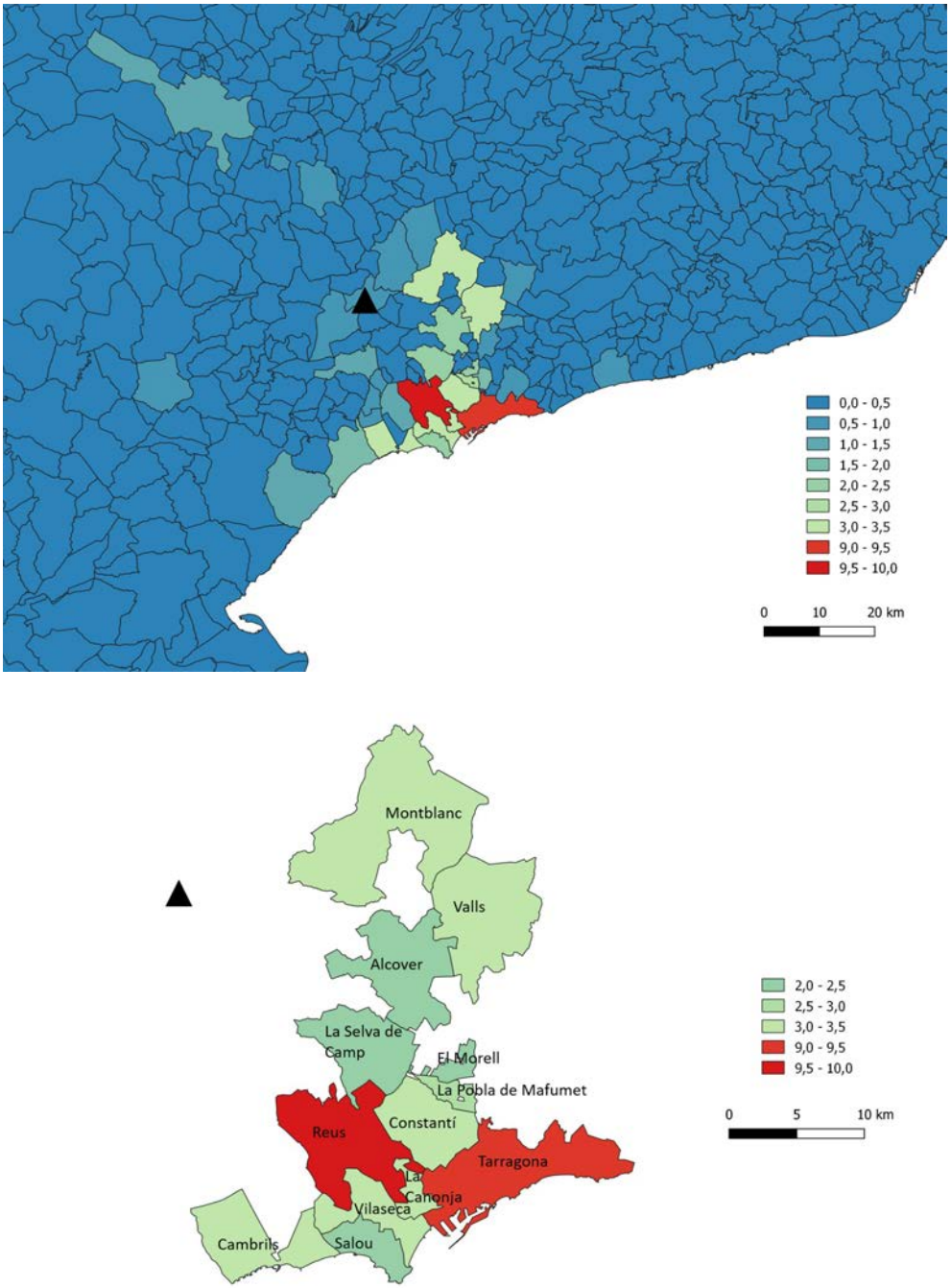

Figure 5.29: Percentage of artificial light emission by municipality received in the V band in Prades. Top: all the municipalities. Bottom: municipalities that contribute more than a 2%.

All-sky brightness map: Illumina v1 vs Illumina v2

The all-sky brightness maps of Prades are of special interest because we simulated the sky brightness using Illumina v1 and Illumina v2. The artificial radiance sources used in both simulation are the same and are defined in table 5.10.

As explained in the previous case, we did not have access to any kind of information regarding the public inventory of the city of Tarragona (or any of its surrounding municipalities). The general inventory was used instead. We also defined independently Lleida despite not being over 2% because we already obtained its inventory in the OAdM case.

Source	Inventory (%radiance emitted-Techonology-ULOR)
Lleida	67-HPS-0, 14-4LED-0, 12-MH-0, 7-HPS-10
General zone	43-HPS-10, 42-HPS-5, 15-4LED-1

Table 5.10: Characteristics of the light pollution sources included in the all-sky simulation over Prades. HPS: high pressure sodium. MH: metal halide. 4LED: LED 4000 K CCT.

We created all-sky brightness maps using Illumina v1 and Illumina v2 for the three bands and compared the results to ASTMON data (see figures 5.30, 5.31 and 5.32) and to DSLR images procesed with SQC (see figure 5.33).

ASTMON data was taken around 21h local time. At that hour private lighting is normally still a non negligible percentage of the light produced by a city. Thus, the radiance emitted by the sources is greater then than at 02h local time when the VIIRS information used for the simulated maps is taken. Private lighting has a dominant emission in the V band but it is typically richer in blue content than public light. The images processed with SQC were taken after 23h local time, hence the private lighting is expected to be reduced. Measurements agree on showing a sky far from pristine. It is darker than in suburban areas but it is quite brighter than the locations studied closer to the Pyrenees.

At first glance measured and simulated maps show the same brightness pattern: there is a dominant radiance direction from east to south that points directly to Tarragona metropolitan area and the sky darkens close to the zenith. The other two distinguishable polluted directions are to the north-west pointing to Lleida and to the east towards Montblanc and Valls.

The main difference is the presence of the Milky Way. ASTMON data was

obtained with the Milky Way crossing the sky from south-west to north-east passing slightly north from the zenith. SQC data also was taken with the Milky Way crossing the sky close to the zenith but from south-east to north-west. Its effect can be observed in the disruption of the typical pattern of concentric isolines around the darkest value (normally close to zenith).

To analyze in detail the differences between the two models and the measurements, we compared three key directions. First, zenith because it is a reference for the quality of the sky and normally the darkest. Second, SE close to the horizon because it is the brightest direction and because brightness produced comes from a big close source that is the main difference between Illumina v1 and Illumina v2. Third, NW close to the horizon pointing to Lleida because it appears as a small brightness dome in most of the maps, moreover Lleida is a middle-size city at 50 km and both models should provide similar results.

In the B filter, both simulated maps are significantly darker than the ASTMON map in practically any direction (see table 5.11). This effect is expected due to the difference in private lighting between 21h (when measurements were taken) and 02h (when VIIRS satellite gets radiance information). Close to the horizon the difference increases due to the direct light coming from Tarragona metropolitan area that is measured but not estimated in the simulations. Close to zenith the effect of the Milky Way also contributes in having brighter measured values.

Between the models the biggest difference is towards Tarragona (SE horizon) as expected. In the NW horizon direction both models provide the same values. Thus, the hypothesis that sources farther than 30 km are assessed similarly by both versions is confirmed so far. The value in the zenith is practically the same in both models, there is a difference 0.1 mag/arcsec^2.

Direction	ASTMON	Illumina v1	Illumina v2
Zenith	21.8	22.3	22.4
SE horizon	19.7	20.4	20.9
NW horizon	21.0	21.8	21.8

Table 5.11: B band (mag/arcsec^2)

In the V filter, the results from Illumina v1 and Illumina v2 are compared to SQC in addition to ASTMON (see table 5.12).

Regarding the zenith value, it was expected a similar trend than in the B filter: that the models provided darker values than measurements as they used information

from later on and there is no brightening effect of the Milky Way. Illumina v2 behaves as expected. However, Illumina v1 provides the brightest zenith value of all the maps. This unexpected behaviour of Illumina v1 is explained by the overestimation of radiance coming from close sources.

The overestimation hypothesis is confirmed in the SE horizon direction, as Illumina v1 provides by far the brightest value too. Illumina v2 and ASTMON show very similar values and the SQC is moderately brighter.

In the NW horizon direction where the light sources are further away, all maps show very similar values.

Direction	ASTMON	Illumina v1	Illumina v2	SQC
Zenith	20.9	20.8	21.2	20.96
SE horizon	18.5	17.5	18.4	18.10
NW horizon	19.6	19.4	19.6	19.49

Table 5.12: V band (mag/arcsec^2)

In the R filter, the behavior observed in the other bands is confirmed. The Illumina v1 overestimation of radiance coming from close sources brightens the sky up to the zenith (ASTMON and Illumina v1 provide the same value despite the Milky Way and difference in time). This effect is amplified in directions pointing towards close sources: SE horizon direction.

In the zenith direction Illumina v2 is darker than ASTMON because of the difference in time and the absence of the brightening effect of the Milky Way. In the NW horizon direction the three maps show similar values.

Direction	ASTMON	Illumina v1	Illumina v2
Zenith	20.0	20.0	20.4
SE horizon	17.7	17.0	17.9
NW horizon	18.8	18.7	18.9

Table 5.13: R band (mag/arcsec^2)

Prades case confirms that Illumina v2 and Illumina v1 agree well in cases with distant dominant sources. However, Illumina v2 is more accurate in cases with big sources of artificial radiance close to the location studied. Although the complexity of both models and the simulated scenario makes it difficult to get definitive results, our analysis shows that v1 overestimate the radiance coming from close sources.

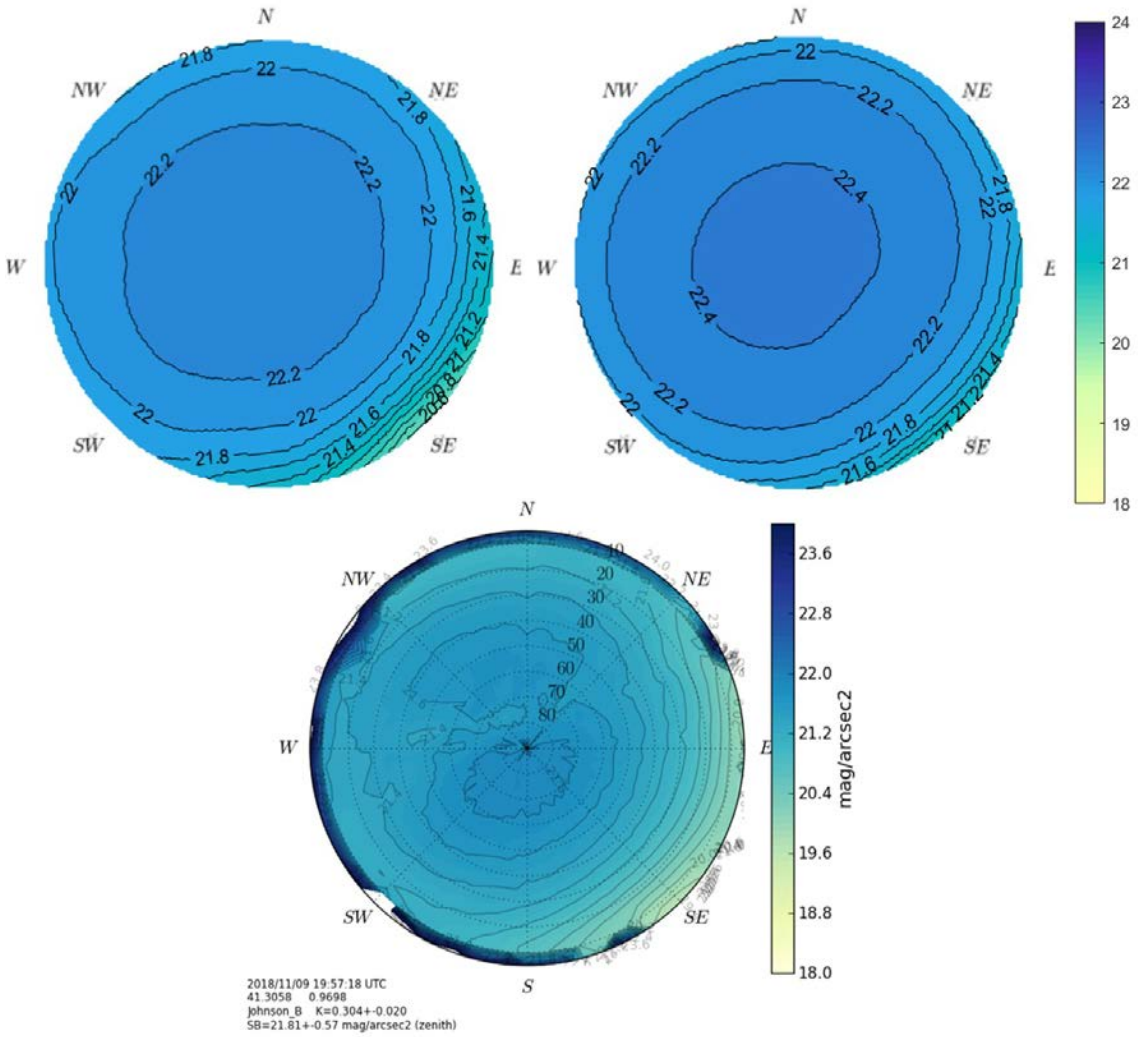

Figure 5.30: Prades all-sky brightness maps in the B band. Top left: Illumina v1. Top right: Illlumina v2. Bottom: ASTMON data.

The new version of the model is an improvement with respect the previous one. From this case forward we used solely Illumina v2 as it ensures reliable results even with big sources nearby.

The locations studied until Prades had no big sources closer than 25 km. Hence, the results obtained with Illumina v1 are valid and similar to measurements as shown in previous sections.

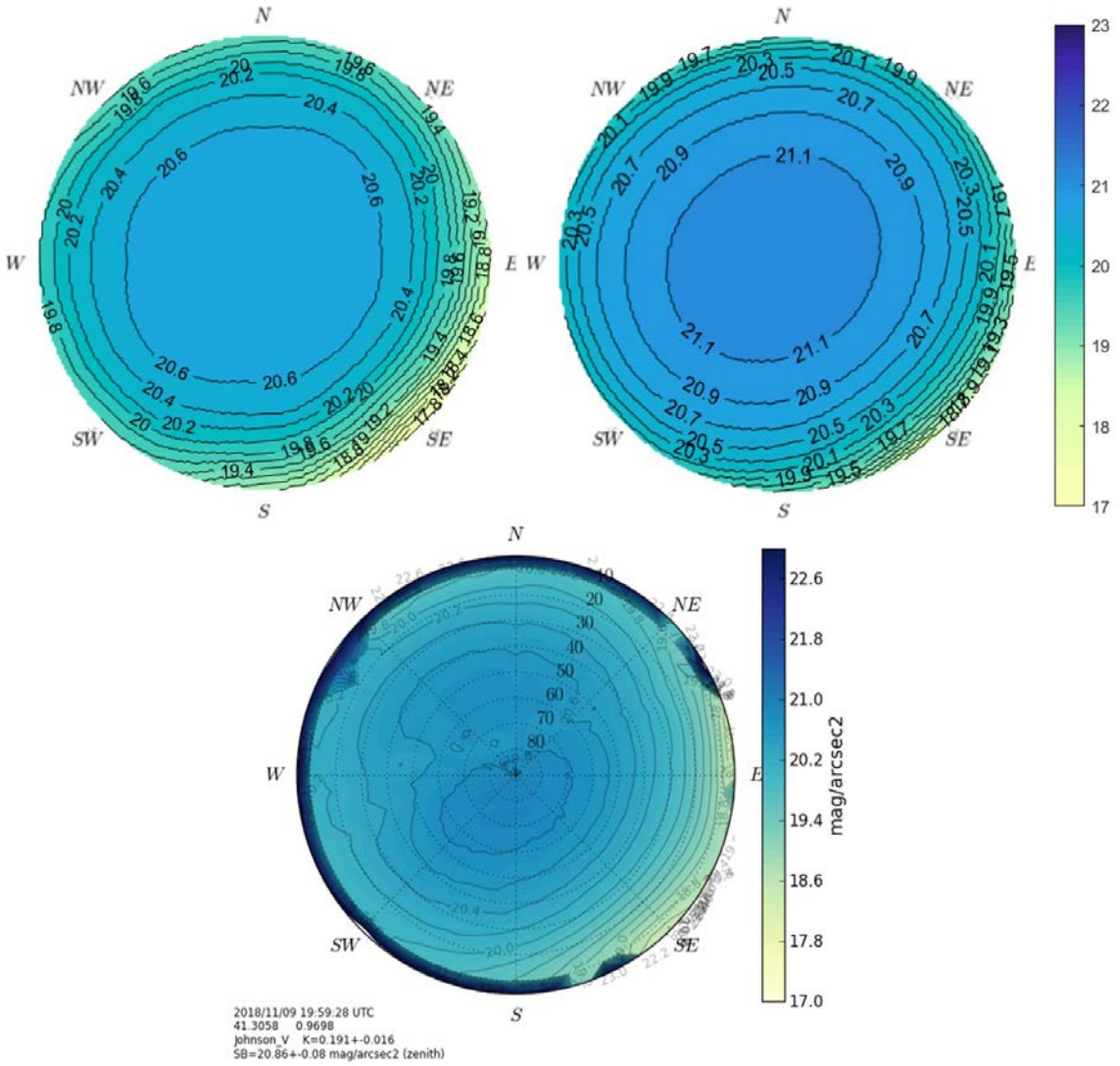

Figure 5.31: Prades all-sky brightness maps in the V band. Top left: Illumina v1. Top right: Illlumina v2. Bottom: ASTMON data.

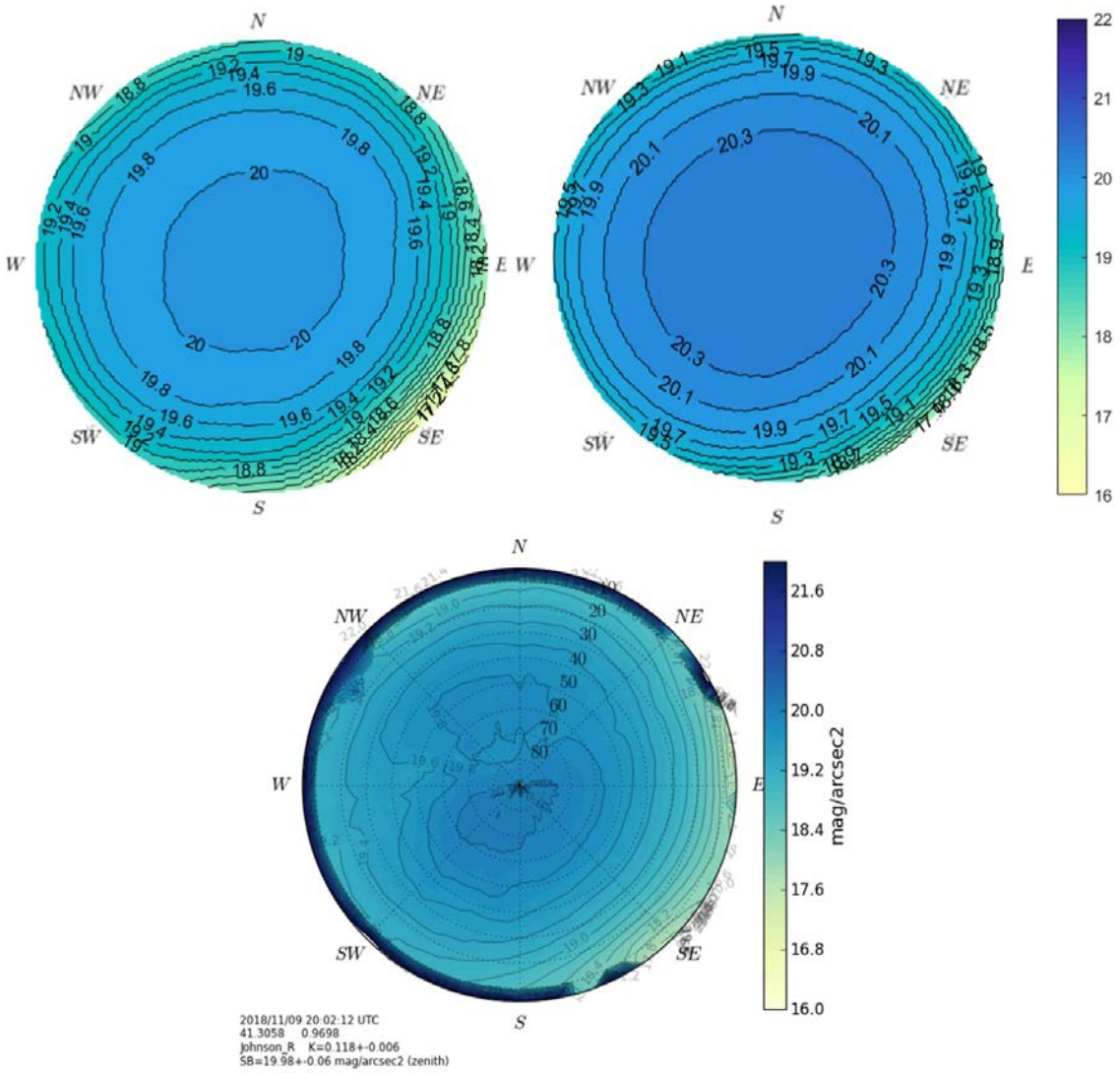

Figure 5.32: Prades all-sky brightness maps in the R band. Top left: Illumina v1. Top right: Illlumina v2. Bottom: ASTMON data.

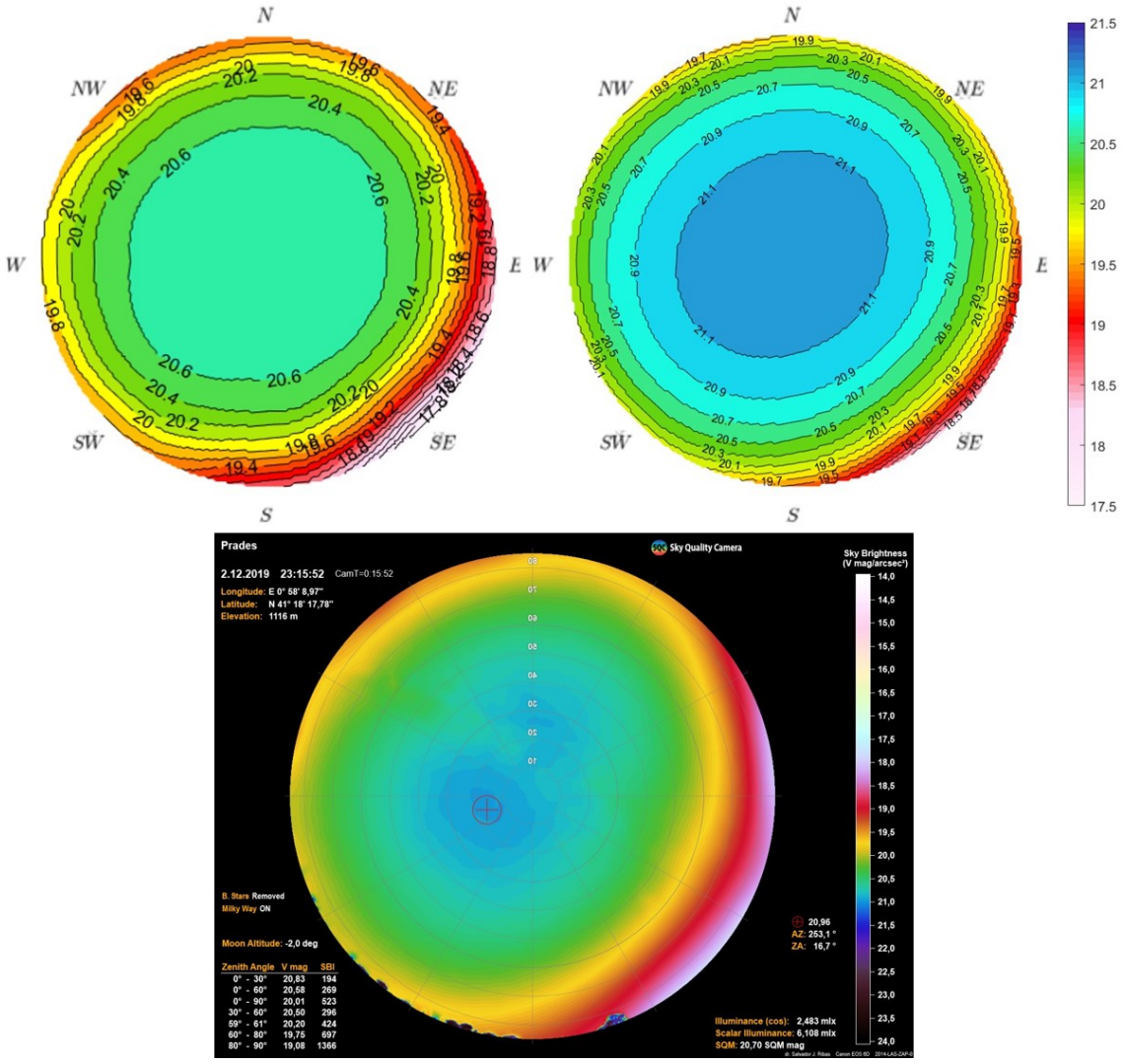

Figure 5.33: Prades all-sky brightness maps in the V band. Top left: Illumina v1. Top right: Illumina v2. Bottom: SQC data.

5.3.7 Pic du Midi de Bigorre

The Pic du Midi lies within the Parc National des Pyrenées located in the central region of the Pyrenees mountain range in the south of France. The location studied is inside the Pic du Midi astronomic observatory at an altitude of almost 2900 m. It is one of the three key locations of the Pyrenees la Nuit project.

It is a low population area. The nearest towns are La Mongie, 5 km SE, that is a winter sports center; Campan, 6 km NW; and Bagnères de Bigorre, 8 km N, within the same municipality than the observatory. There are middle-sized cities farther away and no big cities in a radius of at least 100 km.

Contribution map

The vast majority of artificial radiance received in the Pic du Midi comes from sources within a radius of 30 km (see figure 5.34). There are only four municipalities that surpass the 2% threshold: Lourdes (14k inhabitants) 9.8%, Bagnères de Bigorre (8k inhabitants) 8.4%, Tarbes (41k inhabitants) 6.9%, and Lannemezan (6k inhabitants) 3.0%.

There is a small metropolitan area around Tarbes. There are a few municipalities with a contribution between 0.5 and 1.5%.

The city of Toulouse, 500k inhabitants, 130 km NE, shows a negligible contribution in figure 5.34. That result is against the general opinion from astronomers from the observatory. It is important to recall that we are computing the contribution to the total artificial brightness received for the sky as a whole. Toulouse is clearly distinguishable in the measurements we took (see figure 5.35) but only in a very concentrated region of the sky. Moreover, our measurements were taken with presence of clouds over the city that enhanced the amount of artificial radiance received in the Pic du Midi. In the contribution map we are assuming cloudless situation for all the geographic domain.

All-sky brightness map

We did not receive any detailed information from the lighting systems of the towns around the Pic du Midi. We defined a general zone (radius 50 km around the location) with the same characteristics than in the other cases. We derived an estimated inventory of lights for the city of Pau from the information gathered in place by a member of the PLN project (F. Jáuregui).

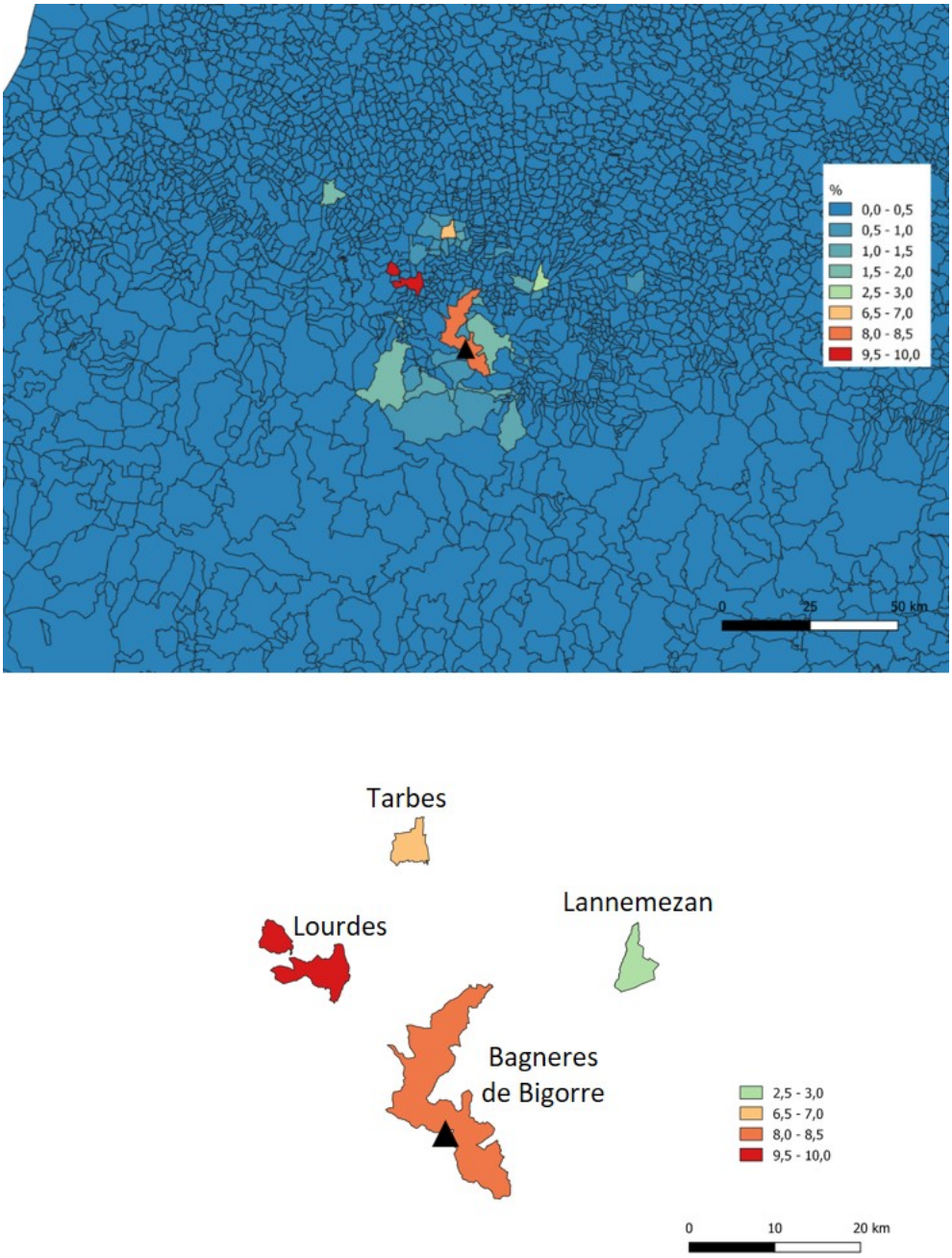

Figure 5.34: Percentage of artificial light emission by municipality received in the V band in the Pic du Midi. Top: all the municipalities. Bottom: municipalities that contribute more than a 2%.

The city of Toulouse was included even though figure 5.34 showed little contribution because it was clearly visible in the DSLR images we took from the Pic du Midi. The inventory of the city was derived using a method than implies pictures taken by the International Space Station (see section 5.4 for detailed information).

Source	Inventory (%radiance emitted-Techonology-ULOR)
Toulouse	54-HPS-5, 18-4LED-5, 17-3LED-5, 5-MH-5, 4-FLC-5, 1-MV-5
Pau	35-HPS-10, 35-HPS-5, 30-4LED-1
General zone	43-HPS-10, 42-HPS-5, 15-4LED-1

Table 5.14: Characteristics of the light pollution sources included in the all-sky simulation over Pic du Midi. HPS: high pressure sodium. MH: metal halide. 4LED: LED 4000 K CCT. FLC: fluorescent. 3LED: LED 3000 K CCT. MV: mercury vapor.

We present here only one of the three set of DSLR images that were taken (see section 3.4). The simulated map was created using Illumina v2. When this location was studied the newest version of the model was already available and validated.

The SQC map shows the effects of the Milky Way that crosses the sky E to W slightly north from the zenith.

The darkest value of the SQC map is 21.63 mag/arcsec^2 placed slightly south from the zenith. In the simulated map is practically the same value, 21.6 mag/arcsec^2, and it coincides with the zenith direction.

Close to the horizon SQC data is slightly brighter than Illumina v2 data. The images were taken with heavy snow coverage around the location which increases the sky brightness values close to the horizon.

Measured and simulated maps agree on showing two main polluted directions: NNW and NE. In both directions brightness values are 19.5 mag/arcsec^2 in the SQC processed image and 20.2 mag/arcsec^2 in the simulated map. In the NNW direction both maps show a quite wide skyglow. The artificial radiance from Tarbes, Lourdes, Pau and Bagnères de Bigorre add up in that direction being unable to divide the effect of each source. The NE direction points towards Lannemezan and Toulouse. We run a case to verify the effect of the city of Toulouse and found that the sky brightness in this direction without Toulouse would be around 20.6 mag/arcsec^2 (simulated value), thus the city increases the sky brightness in this direction in almost 0.4 mag/arcsec^2.

The huge difference (0.7mag/arcsec^2) between SQC and Illumina in the sky brightness values of the two most polluted directions could be related to the

brightening effect of clouds and direct light. We cannot discard that snow coverage is also contributing to this effect.

The presence of clouds is confirmed by the shape of the skyglow dome in these directions: it is wider than expected and bigger in 10º than closer to the horizon (see section 3.4 for the DSLR images with information of directions between 0º and 5º where the effect of clouds is easier to identify). That shape indicates presence of clouds over the sources that increase the scattered radiance towards the observer.

The least polluted azimuth in the horizon level is towards south, 20.9 mag/arcsec^2 in both maps.

As a conclusion, the sky over Pic du Midi is very dark. The horizon is polluted in very restricted azimuths but over 35º in elevation the sky is almost pristine.

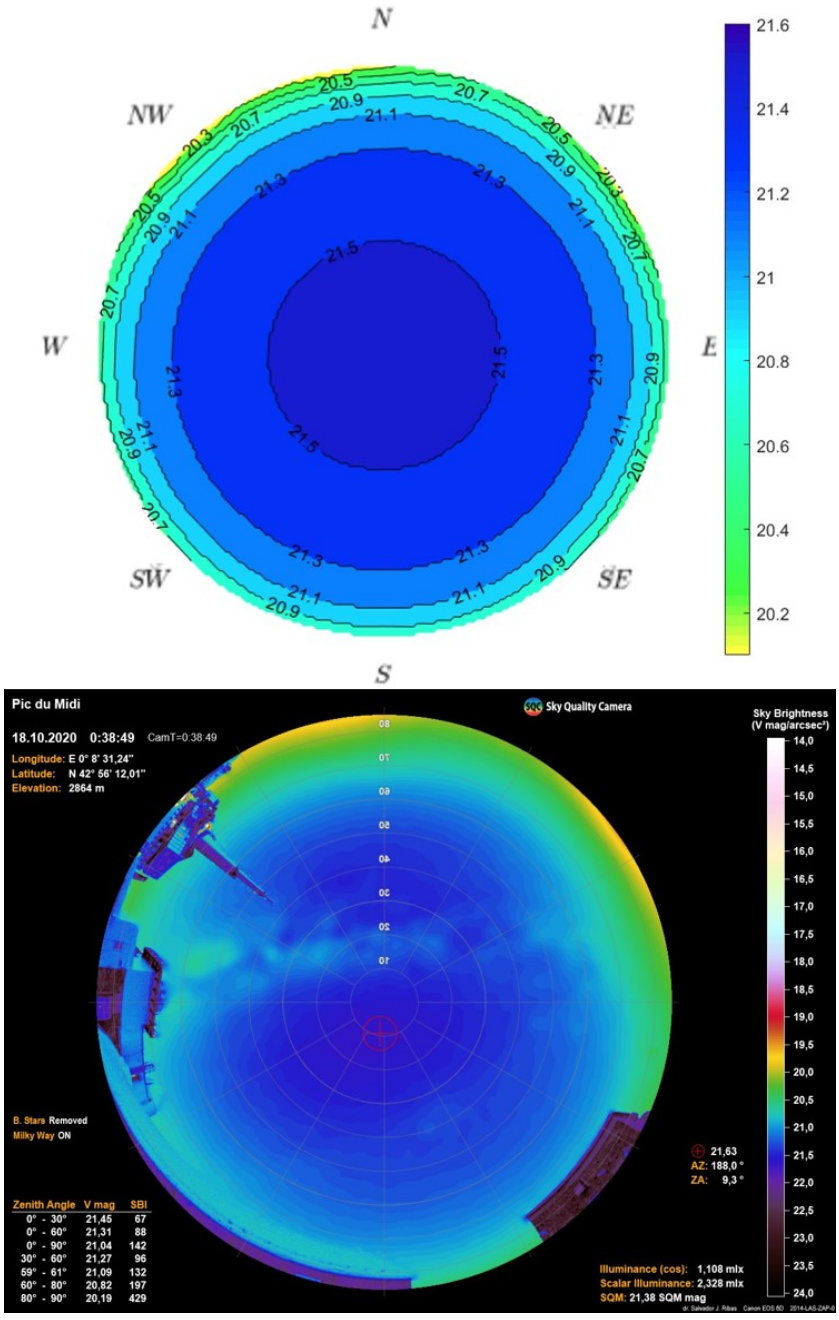

Figure 5.35: Pic du Midi all-sky brightness maps in the V band. Top: simulation. Bottom: SQC data.

5.3.8 Valle del Roncal (Larra-Belagua)

El Valle del Roncal is a valley within the Pyrenees of the region of Navarra. The mountain range that surrounds the valley is known as Larra-Belagua. It is one of the three key locations of the Pyrenees la Nuit project.

The point designated for the measurements and simulations was very close to Belagua refugee at 1428 m. However, after checking the spot we realized it was not a good choice because most of the horizon was blocked by the surrounding mountains. The all-sky measurements and simulation reference location was moved 6 km NW from the original spot to the top of the peak at 1773 m.

It is a very low population area. The closest town is Izaba (500 inhabitants) at 11 km to the SW. There are a few small towns (1000 inhabitants) in a 20 km radius. There are no mid-sized towns closer than 30 km.

Contribution map

Most of the artificial radiance received in Larra-Belagua comes from sources between 20 km and 50 km.

There are five municipalities over the 2% threshold: Olorons Sainte Marie (11k inhabitants) 9.2%, Pau (78k inhabitants) 6.1%, and Lons (13k inhabitants) 2.1% to the NE; Arette (1k inhabitants) 3.5%, is in the NE but most of the artificial radiance within this municipality comes from the ski resort Pierre Saint Martin located at the south border of the municipality, east north east from the location studied; and finally Jaca (13k inhabitants) 2.8%, to the SE. The only distant source that stand out from the rest is the city of Pamplona (1.7%) located at 65 km SW with 200k inhabitants.

All-sky brightness map

In the simulation of Valle del Roncal we included every light source within 50 km as well as several distant big sources (Toulouse, Tarbes, Pamplona, Irun and Donosti) because measurements showed brightness domes pointing to them. Moreover, in the previous case (Pic du Midi) we already evaluated a similar case: Toulouse was clearly brightening the sky close to the horizon but was not relevant in the contribution map of the whole sky.

The inventory of the general zone was defined as always. Pau, Pamplona, Jaca

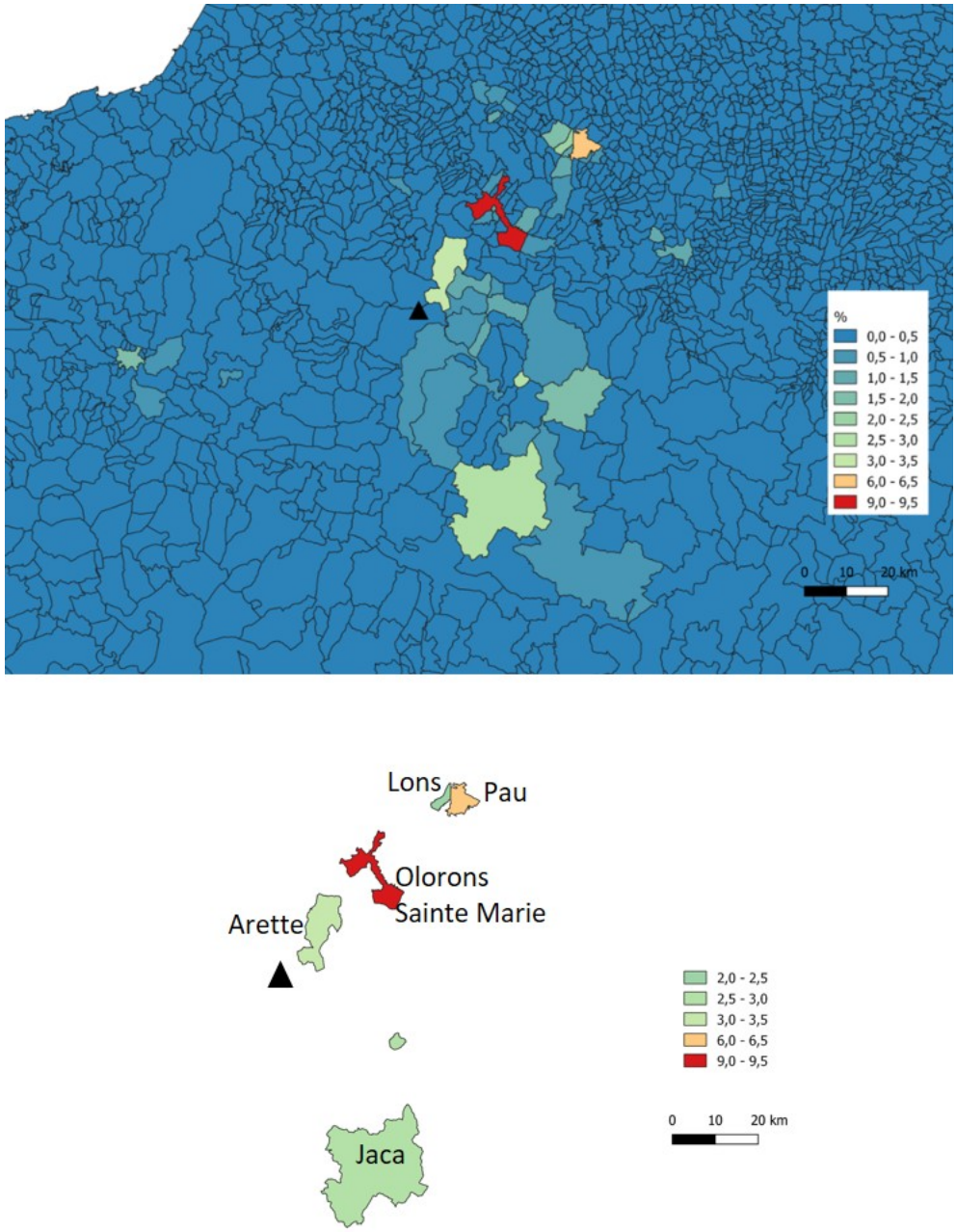

Figure 5.36: Percentage of artificial light emission by municipality received in the V band in Larra-Belagua. Top: all the municipalities. Bottom: municipalities that contribute more than a 2%.

and Isaba were estimated from the information gathered in place by a member of the PLN project (F. Jáuregui). Toulouse was estimated as explained in the Pic du Midi case. The rest of the distant sources were defined with the same inventory used for the general zone as there was no information available.

Source	Inventory (%radiance emitted-Techonology-ULOR)
Toulouse	54-HPS-5, 18-4LED-5, 17-3LED-5, 5-MH-5, 4-FLC-5, 1-MV-5
Pau	35-HPS-10, 35-HPS-5, 30-4LED-1
Pamplona	80-HPS-5, 20-3LED-1
Jaca	85-HPS-5 15-3LED-1
Isaba	70-HPS-5, 30-4LED-1
Tarbes	43-HPS-10, 42-HPS-5, 15-4LED-1
Irun and Donosti	43-HPS-10, 42-HPS-5, 15-4LED-1
General zone	43-HPS-10, 42-HPS-5, 15-4LED-1

Table 5.15: Characteristics of the light pollution sources included in the all-sky simulation over Larra-Belagua. HPS: high pressure sodium. MH: metal halide. 4LED: LED 4000 K CCT. FLC: fluorescent. 3LED: LED 3000 K CCT. MV: mercury vapor.

After eight months of patiently waiting due to the mobility restrictions imposed because of the global pandemic produced by SARS-CoV-2 and the lack of clear moonless night, a set of DSLR images from this site was taken in April 2021. At the moment of the measurements the Milky Way crossed the sky from south to north in low elevation angles to the west.

Both maps (see figure 5.37) show a very dark sky: values go darkest than 21.0 mag/arcsec^2 over 30^o in elevation in every azimuth. The darkest direction is very close to the zenith in both maps. Its value differ significantly between the two maps: 21.7 mag/arcsec^2 in the Illumina v2 map and 21.97 mag/arcsec^2 in the SQC map. As explained, we adopted a theoretical darkest value for a natural sky of 21.8 mag/arcsec^2. Measurements over that threshold are due to different atmospheric conditions than the ones assumed for simulations.

The most polluted direction is to the NE towards the line-up of Olorons Sainte Marie, Pau and Lons. The Illumina v2 map show a 20.0 mag/arcsec^2 and the SQC map 19.89 mag/arcsec^2. To the ENE there is a secondary dome mostly due to the skiing resort of Pierre Saint Martin, Tarbes contributes in a much lesser extent and Toulouse is almost negligible. The simulated value is 20.3 mag/arcsec^2 and the SQC value is 20.10 mag/arcsec^2. The SQC map shows a light pollution dome to the NW that coincides with the direction of Irun and Donosti, however it is not present in

the simulated map. It is possible that clouds in that direction were increasing the brightening effect of those sources. Towards WSW both maps show a brightness value around 20.5 mag/arcsec^2 that is produced by Pamplona. There is a litte brightness dome to the SW in the simulated map towards the towns of Valle del Roncal (mostly Isaba and Roncal) but it is hard to distinguish from the Milky Way in the SQC map.

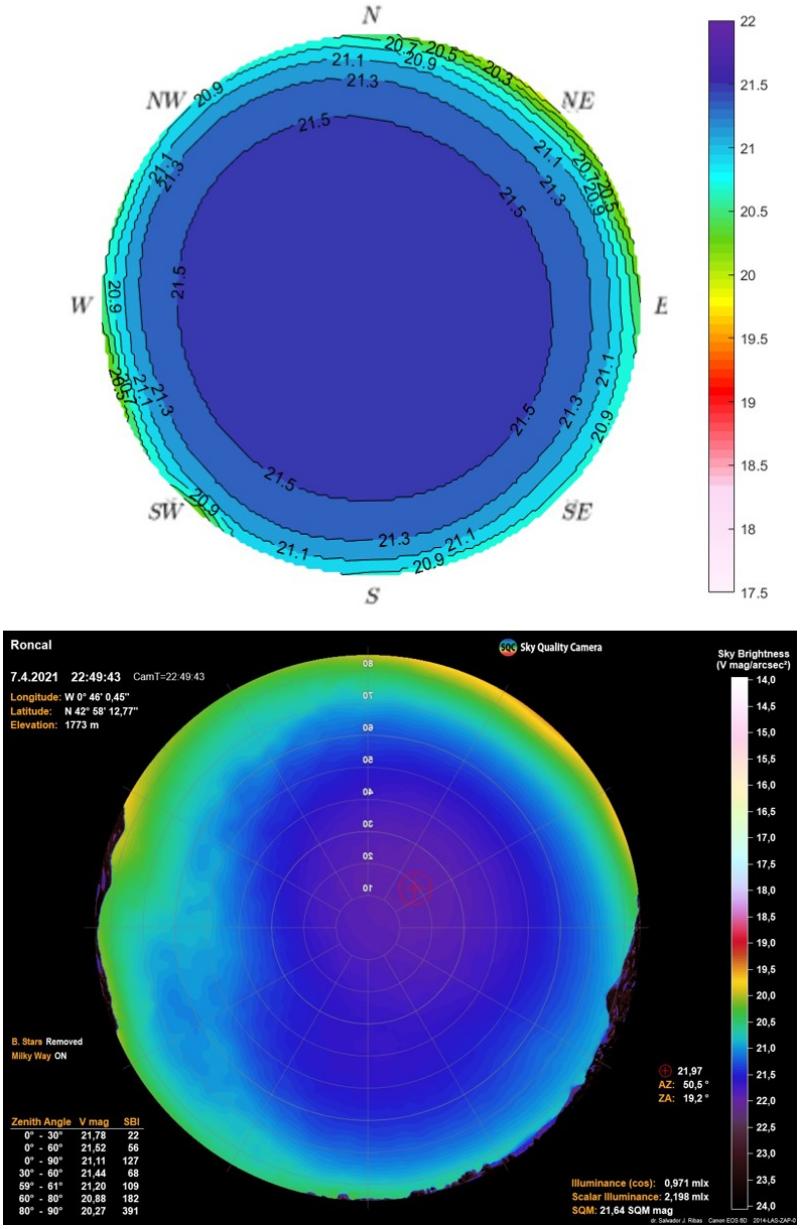

Figure 5.37: Valle del Roncal all-sky brightness maps in the V band. Top: simulation. Bottom: SQC data.

5.3.9 Summary

The eight cases were successfully assessed with contribution maps, ASTMON and/or SQC measurements and all-sky brightness simulations.

Contribution maps were confirmed as a useful tool to assess the light pollution situation of a location and to decide which sources to include in all-sky brightness simulations. However, they can be misleading with big and very distant towns (more than 100 km away). This kind of sources does not show a noticeable contribution to the whole sky but could affect significantly a reduced set of directions close to the horizon.

ASTMON data has been found to be very useful due to it includes information for the B, V and R bands of the Johnson-Cousins system. On the other hand, DSLR cameras are easier to carry and set up.

There are a few measurements that show darker values than the expected natural value, the theoretical darkest value for a non-polluted sky we used for the simulated map (see table 5.4). However, they were typically less than 0.1 mag/arcsec^2 over that threshold, and therefore the difference lays within the intrinsic uncertainty of the measurements.

Illumina v1 has been validated for cases with no big light sources nearby. This version of the model has been found to overestimate the radiance produced by big towns closer than 25 km from the observer position.

Illumina v2 is an improvement from the previous version as it is suited for any kind of situation. It has been tested in cases with big sources nearby and in cases with no sources around and the results agreed very well with measurements.

The biggest difference between all-sky simulated and measured map was the presence of the Milky Way. This effect could be solved by replacing our simple model of the natural sky to more complex models as the one presented by Masana et al. (2021).

Other issue to address is the atmospheric characterization. We have seen cases with very distant clouds that changed the brightness patterns significantly. We also presented measurements with abnormal atmospheric absorption that lead to unrealistic dark values. As when measuring it is close to impossible to ensure clear sky conditions hundreds of kilometers around the observer models should progress towards enabling different atmospheric characterization within the geographic domain.

A part from the Milky Way and the presence of clouds, the difference between measurements and simulations are of the order of magnitude of 0.1-0.2 mag/arcsec^2 for any direction and for all the cases studied.

As a conclusion, Illumina is a reliable tool to reproduce all-sky brightness measurements. It can be used for predicting the changes in the sky that would be produced by changes in the lighting scenario of the sources that are polluting the sky in a given location.

5.4 Catalonia zenith sky brightness maps

The work presented in this section is embedded in the "Catalonia simulated sky brightness map" project of the Departament de Territori i Sostenibilitat de la Generalitat de Catalunya. The long term goal of this project is to obtain sky brightness maps of Catalonia in a high spatial resolution (1x1 km), in several bands (B, V and R of the Johnson-Cousins system), that uses different brightness indicators (zenith brightness, most polluted value at 45^o in elevation, Artificial to natural light ratio, etc.) in several lighting systems scenarios (current configuration, change to LED of high CCT, change to LED of low CCT, etc.).

Here, we aim to make the first step towards achieving that long term goal by creating zenith sky brightness maps of Catalonia with a spatial resolution of 5x5 km (1310 locations) in the B and V bands of the Johnson system that simulates the current scenario.

5.4.1 Assessing the sky over large territories

To obtain an understandable and visual product that covers large territories is useful to assign a unique value to every location within the area we want to study. We have seen some indicators of this kind in the introduction of chapter 2, mainly zenith sky brightness (ZSB) and artificial to natural light ratio (ALR). In this regard, in chapter 3 the process for obtaining ZSB maps created with SQM measurements is explained in detail.

Our purpose is to define a methodology for assessing large areas using a light pollution model instead of measurements. In this sense, Falchi et al. (2016) created a simulated ZSB world atlas map based on VIIRS-DNB data and Garstang's model. The atlas gives information in the V band with a spatial resolution of approximately 1 km^2. In fact, the work was an update from Cinzano et al. (2000) and Cinzano

et al. (2001) that instead of VIIRS-DNB data, which was not available yet, used DMSP-OLS satellite data information. The final product of Cinzano et al. (2000) was a ZSB map of Europe in B and V bands, and in Cinzano et al. (2001) the map was expanded to a world atlas map but only for the V band. To reduce the computational time needed to create the atlas, several assumptions were made: same atmospheric conditions for every location, constant city emission function, constant spectrum of artificial lights and ignoring orographic screening effects. The atlas had a huge impact in the light pollution community and even beyond the scientific scope. It allowed to check pollution levels with ease and to compare pollution among countries and regions. It revealed that most of the world population lives under polluted skies.

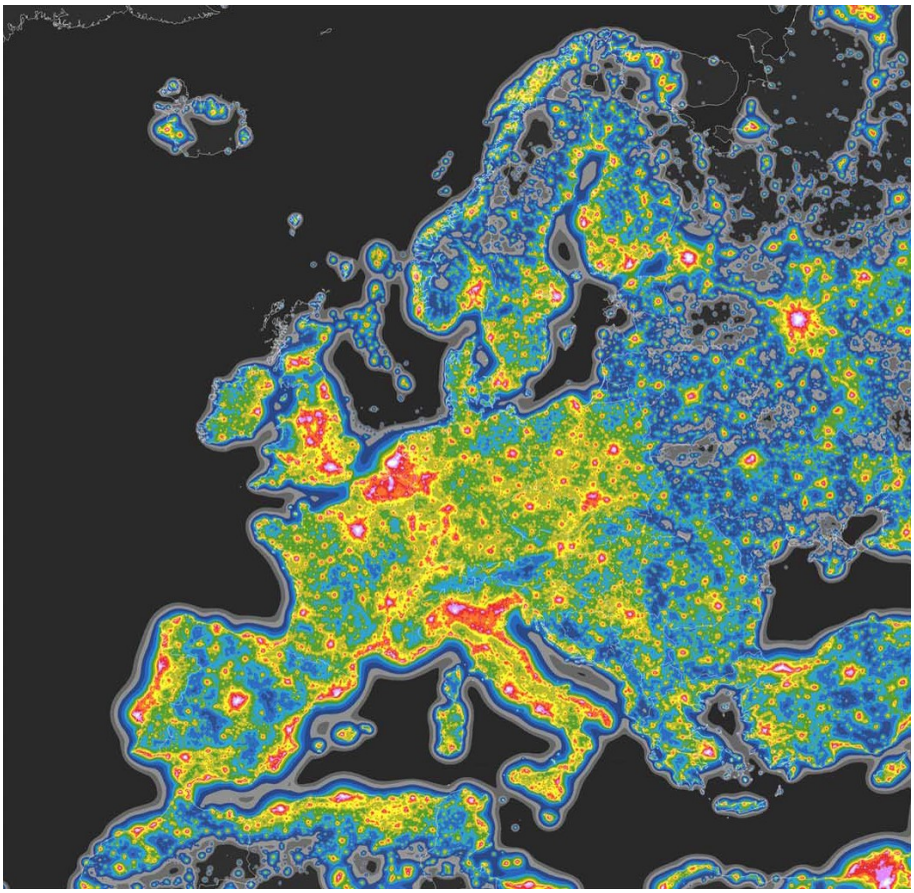

Figure 5.38: ZSB map of Europe by Falchi et al. (2016), in twofold increasing steps, as a ratio to the natural sky brightness (assumed to be 174 mcd/m2). The map shows the artificial sky brightness in V-band. Image from Falchi et al. (2016).

With the same goal, creating a zenith sky brightness world map, Sanchez de Miguel et al. (2020) proposed a new methodology that did not rely on any light

pollution model. It is based on the idea that the radiance received (from outside city borders) by the VIIRS-DNB (scattered upwards by the atmosphere) is symmetric to the received on the ground (scattered downwards by the atmosphere). This idea comes from two assumptions. First, that molecular scattering can be modeled as Rayleigh scattering that has back-forward and azimuthal symmetry. And second, that aerosol scattering can be modeled as Mie scattering. Although Mie scattering has a peak in the forward direction, when studying ZSB outside cities, most of the artificial light comes from low elevation LoS (horizontally directed light) that is scattered by the atmosphere close to zenith. Mie scattering azimuthal symmetry predicts that in this case similar amounts of light are scattered upwards and downwards.

An alternative strategy is using Illumina light pollution numerical model. Working with Illumina allows to use ZSB, ALR and practically any indicator, an improvement from previous methodologies. Illumina also takes into account variables ignored by the methods previously explained, such as orographic screening and heterogeneous city emission functions (spectral and optical properties). Additionally, with Illumina it is possible to study a wider spectrum that the V band. Any band within the working range of the model can be studied.

We decided to base our simulations on Illumina for this project because, unlike the methodologies used so far to assess large territories, it allows us to work with different brightness indicators, with changing lighting scenarios and with the B, V and R bands of the Johnson-Cousins system.

5.4.2 Catalonia zenith sky brightness map characteristics

As explained previously, we used Illumina v2 to create sky brightness maps of Catalonia with the following characteristics: they show zenith sky brightness, have a spatial resolution of 5x5 km (1310 locations), cover the B and V bands of the Johnson system and study the current lighting system.

We chose this configuration to maximize the computational resources that we have access to. The methodology is the same when working with other indicators or higher spatial resolution.

We used the same atmospheric characterization for all the locations deriving typical values from the two AERONET stations within the territory (Montsec and Barcelona): relative humidity 70%, clear sky, Angstrom coefficient of 1.0, and aerosol optical depth of 0.1 at 500 nm. The spectral definition of light sources has been made following the methodology introduced by Sánchez de Miguel et al. (2019) that

uses calibrated images taken from the International Space Station (ISS) to derive the spectrum of emitted light. The strategy followed is:

- Estimating the radiance ratios (defined as *colors* in astronomy) between three bands of the DSLR cameras (RGB) that the most used lighting technologies produces.
- Obtaining the ratios of the pixels from the images taken with DSLR cameras on board of the ISS.
- Comparing the ratios from the images to the most used lighting technologies and assigning a dominating technology to every pixel.
- Estimating the lighting system of a source by weighing by intensity all the pixels from the image that lie within the source.

In particular we used the image ISS052-E-31962 from the Earth Science and Remote Sensing Unit, NASA Johnson Space Center taken the 8th of April 2017 (see figure 5.39). Sánchez de Miguel helped us by processing the image and extracting the ratios (colors) of the pixels. The resulting inventories that were estimated using this method can be found in table 5.16.

Small cities and towns are difficult to estimate with this method because the signal to noise ratio is very small. For these cases, we used the general inventory that was already used in previous sections (General zone in table 5.16).

Comparing the information we had access to of public inventories to the estimated inventories of the same sources using the ISS image, we found that there are some that are very similar, such as Balaguer, Tremp and Sort. On the other hand, the city of Lleida has a public inventory dominated by HPS technology (see table 5.5) but using the method from Sánchez de Miguel et al. (2019) it is dominated by a LED 4000 K CCT instead. This phenomena can be explained for two reasons: first, the inventory information that we had access to could not be precise enough; second, the private lighting constitutes a big percentage of the light emitted by the city (the images taken from the ISS reveal spectrum information from public and private lighting). Detailed information from more big cities is needed to reach a conclusion, but if the second hypothesis is confirmed it would mean that private lighting has a non-negligible impact on the emission spectrum of a city and should be taken into account.

The methodology of Sánchez de Miguel et al. (2019) allows to define more accurate inventories. However, it is important to keep working with public inventories

Figure 5.39: Picture taken from the ISS centered in Catalonia. NASA Photo ID: ISS052-E-31962. Source: Earth Science and Remote Sensing Unit, NASA Johnson Space Center.

too. Having both will allow to estimate the percentage of public and private light that a city is emitting. This information is useful to estimate the real impact of changing the public lighting system.

Source	HPS	3LED	4LED	MH	MV	FLC
Lleida	23	5	51	14	1	6
Balaguer	76	14	7	2	0	1
Tremp	89	5	4	1	0	0
Vallès	53	13	19	6	2	7
Barcelona MA	61	15	12	4	1	5
Vilafranca del P.	57	14	16	6	1	7
Figueres	50	13	25	7	1	4
Girona	66	16	8	3	1	6
Igualada	72	13	10	3	0	2
Manresa	56	12	21	6	1	5
TGN petrochemical plant	35	9	14	9	6	27
Reus	59	14	18	5	1	4
Tarragona MA	31	7	37	12	2	10
Salou	47	11	9	7	4	21
Vic	69	17	9	3	0	2
Andorra	13	3	61	16	1	5
Barbastro	61	13	19	5	0	2
Binèfar	44	8	33	9	1	5
Fraga	47	13	21	7	2	9
Monzón	53	8	28	8	1	2
Perpignan	56	16	16	5	1	6
Toulouse	54	18	17	5	1	4
Vinarós	21	4	43	14	3	15
Peníscola	21	4	43	14	3	15
Benicarló	21	4	43	14	3	15
General zone	85	0	15	0	0	0

Table 5.16: Percentage of the radiance emitted by lighting technology of each source. Metholodogy from Sánchez de Miguel et al. (2019). HPS: high pressure sodium. MH: metal halide. 4LED: LED 4000 K CCT. FLC: fluorescent. 3LED: LED 3000 K CCT. MV: mercury vapor.

5.4.3 Results

The first step was validating the methodology by running a small test case. We simulated the ZSB of 19 points spread within Catalonia (see figure 5.40) and compared the simulated value to the measured reference value in each location. The locations were chosen with the aim to represent most of the territory. We also tried to select point with very different characteristics: some of them are close to the coastal line, others are in mountain regions, some are close to big cities, others are placed in very low population areas, etc.

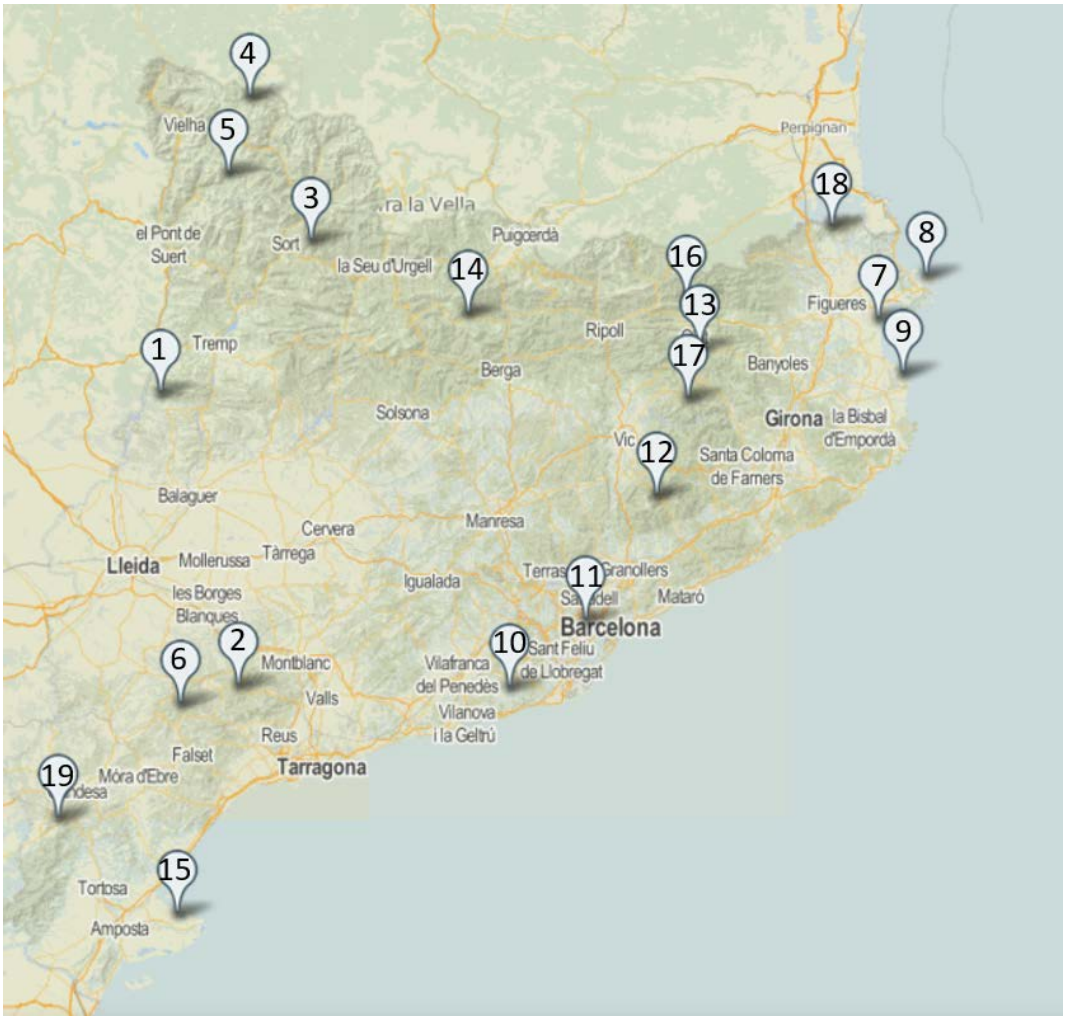

Figure 5.40: Test locations where the ZBM was estimated and compared against measurements.

The simulated ZSB values of the 19 points are shown in table 5.17 alongside with the available measured ZSB values. For the measurements we used SQM, SQC

and ASTMON data. The best option would be comparing results to ASTMON as it provides B and V band information, but only four locations had been measured with this device: OAdM, Prades, Montsant and Estany Llong/Aigüestortes. The best alternative to ASTMON is DSLR images processed by SQC. They provide ZSB in the V band but not in the B band. There are four locations measured with this method: OAdM, Prades, Orri and Montgarri. Detailed information of ASTMON data and DSLR images processed with SQC from these location was presented in section 5.3. Some of them were measured with the Milky Way close to zenith or abnormal absorption conditions, we acknowledged qualitatively the associated brightening effect when comparing to simulated values. The last option is using SQM values. It is not the best tool because SQM measures the brightness of the sky in a wider region of the sky (see section 2.2.1) and because the filter of the SQM is similar but not the same as the V band of the Johnson system (although it was designed to provide similar results). On the other hand, there are measurements with this device for every location that provides us with more points to use for validation.

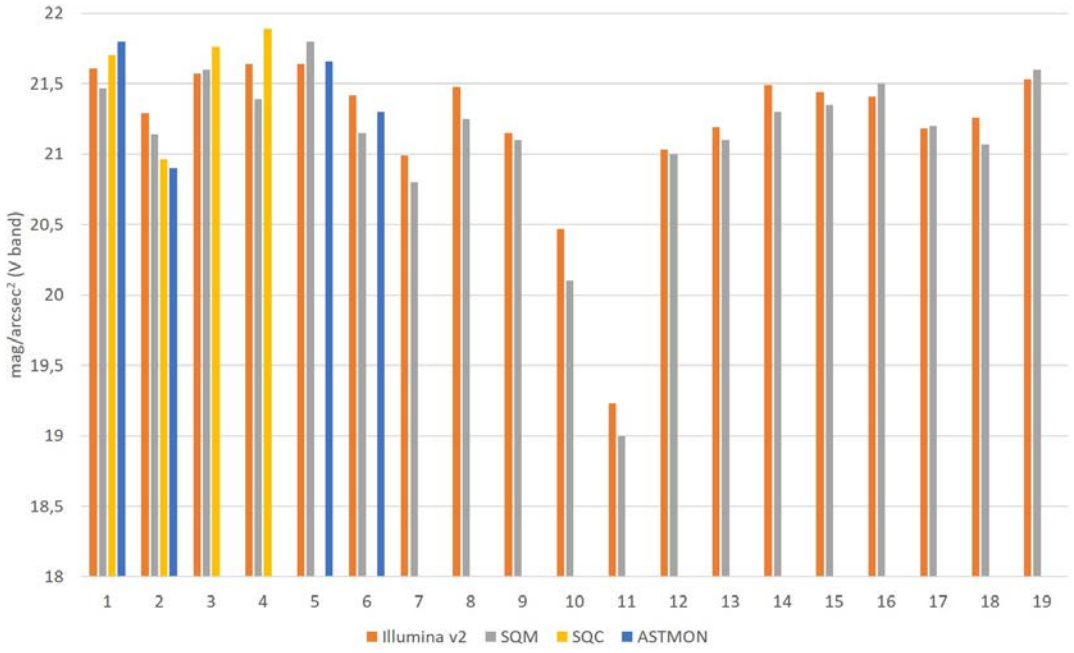

Figure 5.41: Zenith sky brightness values of the 19 test locations. Reference number according to table 5.17.

ZSB simulated values agree well with measurements (see table 5.17 and figure 5.41). The difference between the different measurements methods and the simulated values are typically within 0.2 mag/arcsec^2. As commented in section 2.2 the

	Location	Sim. in V Band	V ASTMON	V SQC	SQM	Sim. B	B ASTMON
1	OAdM	21.61	21.8	21.70	21.47	22.63	22.8
2	Prades	21.19	20.9	20.96	21.14	22.47	21.8
3	Orri	21.57	-	21.76	21.60	-	-
4	Montgarri	21.64	-	21.89	21.39	-	-
5	Aigüestortes	21.64	21.7	-	21.80	22.63	22.7
6	Montsant	21.42	21.3	-	21.15	22.54	22.5
7	Aiguamolls Empordà	20.99	-	-	20.80	-	-
8	Cap de Creus	21.48	-	-	21.25	-	-
9	Massís Montgrí	21.15	-	-	21.10	-	-
10	Garraf	20.47	-	-	20.10	-	-
11	Collserola	19.23	-	-	19.00	-	-
12	Montseny	21.03	-	-	21.00	-	-
13	Santa Pau	21.19	-	-	21.10	-	-
14	Saldes	21.49	-	-	21.30	-	-
15	Deltebre	21.44	-	-	21.35	-	-
16	Vall d'en Bac	21.41	-	-	21.50	-	-
17	Rupit	21.18	-	-	21.20	-	-
18	Requesens	21.26	-	-	21.07	-	-
19	Els Ports	21.53	-	-	21.60	-	-

Table 5.17: Comparison between measurements and simulated zenith brightness. Measurements values are shown alongside the instrumentation used: SQM, SQC or ASTMON.

intrinsic error of the measurements method is of the order of magnitude of 0.1 mag/arcsec^2.

There is no pattern in the sense of simulated values being systematically brighter or darker than measured, with the exception of the SQM that is typically brighter for the reasons commented above. In particular, the mean value of the difference between simulations and SQM (we used SQM because we have data for all the points) is +0.11 mag/arcsec^2 with and standard deviation of 0.14 mag/arcsec^2. Hence, the difference are within what it is expected due to different atmospheric conditions and intrinsic errors of the measurement devices.

Once the methodology and definition of sources were validated, we proceeded to create the ZSB maps of Catalonia in V and B bands.

B and V bands comparison

The results for the two bands are displayed in figure 5.42 with the same color scale with respect the natural sky brightness (i.e. 21.8 mag/arcsec^2 for the V band and 22.7 mag/arcsec^2 for the B band). We also present a map for the B band with a narrower step colorscale to better display the pattern of brightness in this band (see figure 5.43)

There are two main focus of light pollution in Catalonia in the two bands. The biggest one is Barcelona metropolitan area and the second one Tarragona metropolitan area. In the V band the two influence areas are almost fused together. The most polluted skies a part from the ones already mentioned are over Lleida and Girona, and in a lesser extent over Manresa. There are some isolated cells with bright values. It is possible that the location of the simulated ZSB coincides with a town or small city. As stated, the long term goal is to improve the resolution of the map to 1x1 km in the near future that will be of great help to have more accurate information of these situations. The maps also coincide in displaying a gradient of darkness from the coastal line towards the inland. The darkest areas are in Pyrenees of Lleida (NW) and towards the Els Ports de Beseit NP (SW).

Comparing both maps we derive that most of the main artificial light sources have an emission more dominant in the V band than in the B band. We created a comparison map (see figure 5.44) between the two bands with respect to the natural brightness level of each band using the color excess astronomic concept:

$$E_{B-V} = (B-V)_{total} - (B-V)_{natural} \tag{5.4}$$

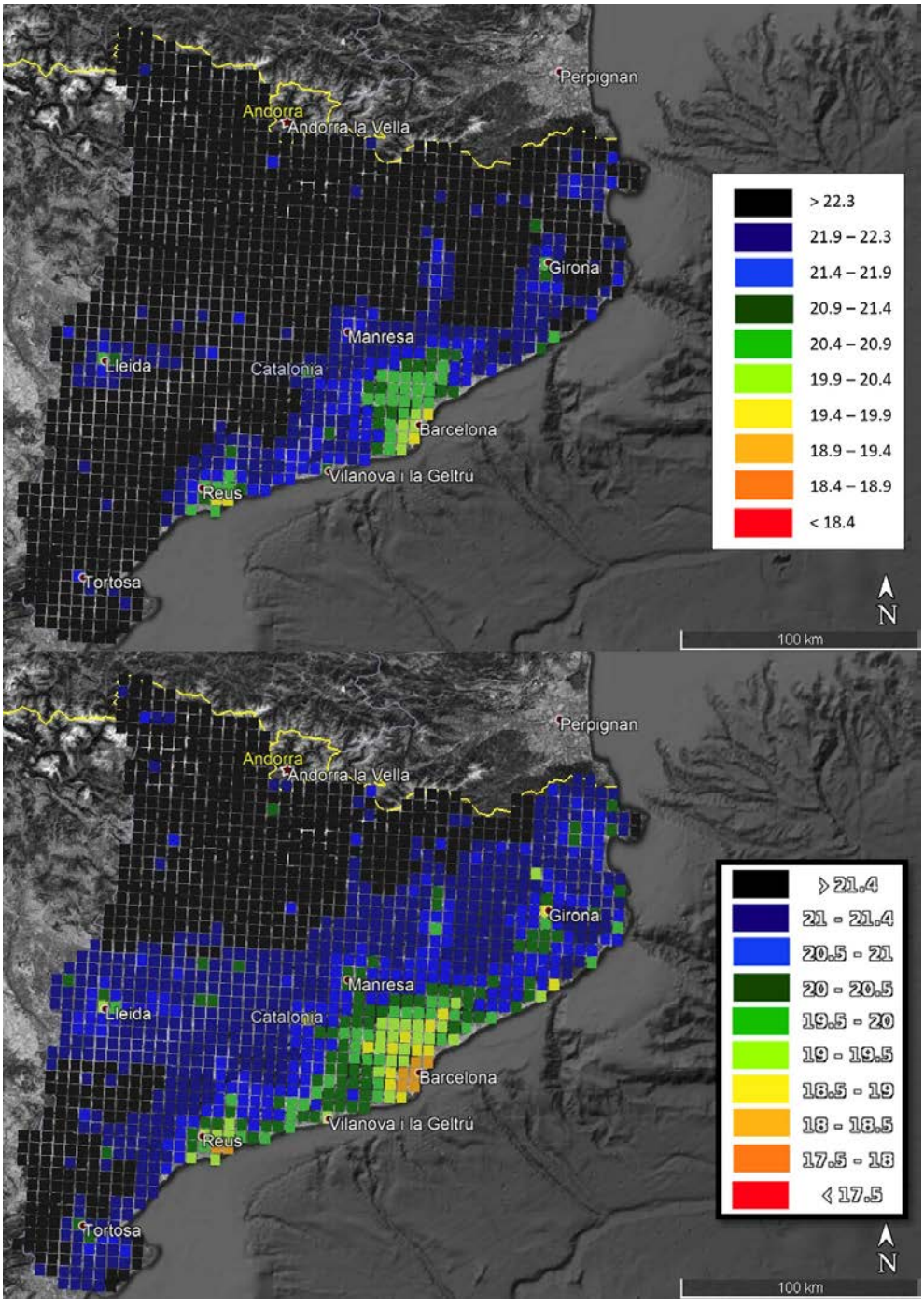

Figure 5.42: Zenith brightness map of Catalonia. Top: B band. Bottom: V band. Color scale in V is the same as used in the SQM maps. Color scale in B show the same brightening with respect to the natural value than the the used for the V band.

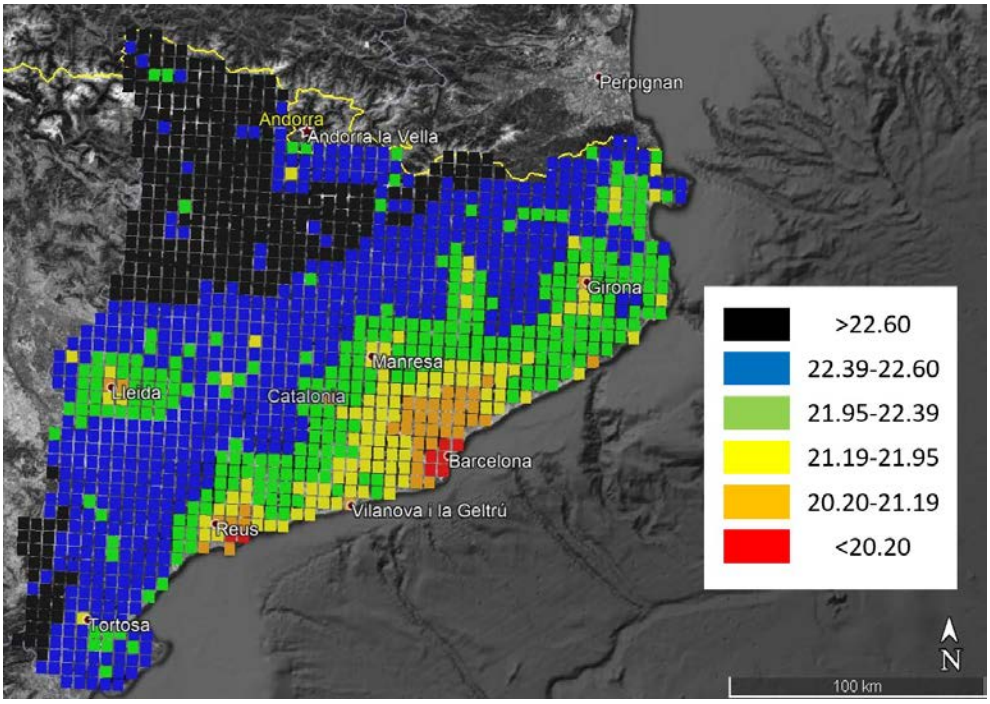

Figure 5.43: Illumina zenith brightness map of Catalonia in the B band. Narrower colorscale.

Positive values indicates a sky with more V band light proportion than the natural value. Negative values, a sky with more B band light proportion than the natural value.

There is not a single location where the brightening in the B band is greater than in the V band. The locations that have a more similar brightening in both bands are the less polluted ones (NW and SW). The locations that have a bigger different follow the same pattern, they are the most polluted ones in general. However, there are three cases that do not follow that pattern due to their lighting system is rich in blue light: Tarragona metropolitan area, Lleida and Andorra.

Simulated map compared to measurements

The results obtained for the ZSB map in the V band can be comparatively compared with the SQM assessment of the areas presented in section 3.2. In this sense, The color scale used for the V band in figure 5.42 is the same color scale that was used in the SQM maps.

The values obtained for the simulated ZSB map of Catalonia are slightly darker

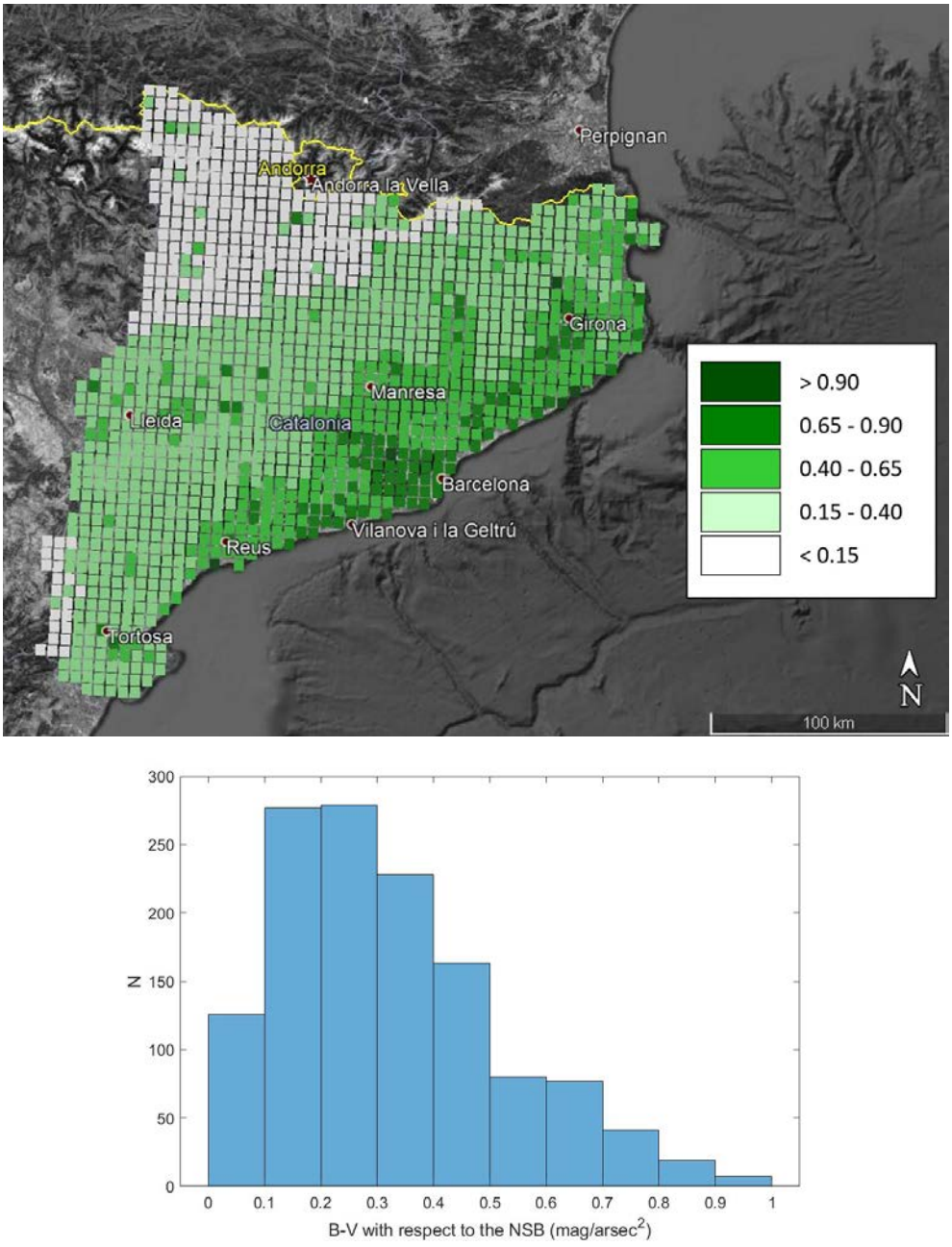

Figure 5.44: Comparison between V and B (B-V) bands sky brightening with respect the natural brightness. Top: Catalonia map. Bottom: histogram.

than the SQM values. Typically between 0.1 and 0.2 mag/arcsec^2. This was an expected result because of three main reasons. First, the area assessed with the SQM is a conic region of 20º FWHM whereas the ZSB value as it names indicates assess only the zenith direction. Sky brightness increases as directions get close to

the horizon so the SQM is in general brighter than the ZSB values for the same exact sky. Second, the conditions where the measurements were taken are not exactly the same as in the simulation. For instance, some nights the sky was measured with the Milky Way within the field of view of the SQM. Third, the spectrum sensitivity of the SQM includes the blue region, approximately from 380 nm to 650 nm, whereas the V band goes from approximately 470 nm to 740 nm. In areas with lighting system with emission around 400 nm (i.e. LED) the SQM would measure brighter values than what would be measured in the V band.

Taking those differences into account all the regions studied during the SQM campaings have been compared to the Illumina v2 ZSB map of Catalonia.

- Pyrenees region of the NE of Catalonia (see section 3.1 and 3.2.2). Both SQM and Illumina map show dark values but far from the darkest values of the country. The maps also agree that the darkest area in this region is in the north very close to the border with France.
- Montserrat region, around 10 km south from Manresa (see section 3.1). Both maps show a brightness gradient to the SW towards Barcelona and similar values all over the region.
- Montsant NP and Prades regions (see section 3.1). The maps coincide in showing a brightness gradient towards the SW where it stands Tarragona. The darkest region is on the opposite side, the NE.
- Delta de l'Ebre and Ports de Beseit NP region in the SW of Catalonia (see section 3.3). The extreme SW of Catalonia is one of the darkest regions of the country. The Delta de l'Ebre is dark but not pristine except for the maritime border of the delta. The coastal line close to Tarragona metropolitan area is quite polluted, it darkens as it moves south. South of Lleida both maps provide dark values and show a brightness gradient as cells get closer to Lleida.
- Pyrenees region of the NW of Catalonia (see section 3.3). SQM campaigns and the ZSB Illumina map agree on it is one of the darkest regions of the country. However, the SQM values are slightly brighter.
- Montsec area (see section 3.3). Both maps show a darkness pattern towards the north. They also show a similar dimension of the area of influence of Balaguer, Tremp and la Pobla de Segur.
- Coastal line of the NE (see section 3.4). In this region we crossed several towns that brightened the SQM readings taken within the towns due to direct light.

The Illumina map shows a similar patchy pattern due to the presence of those towns. They also agree that Cap de Creus is the darkest area of this region. However, as it happens in Delta de l'Ebre tue maritime line is darker in the Illumina map than in the SQM map. The Massís del Montgrí is the second darkest region in both maps.

- Montseny NP, 30 km NE from Barcelona (see section 3.4). The gradient of brightness towards the SW (Barcelona) in this region is big in both maps. The coastal line creates a secondary brightness gradient also observable in both maps. The darkest values are in the NE area.

As seen, the maps from the SQM campaigns coincide with the Illumina v2 map very well taking into account the differences explained before. The methodology is then validated and proven useful to study the country as a whole.

Illumina and Falchi's atlas comparison

We proceeded to compare the ZSB maps obtained with Illumina v2 to the one obtained by Falchi et al. (2016) for the V band (see figure 5.45).

Both maps assess a similar night sky (3 years a part) but the spatial sampling is not the same: 1x1 km in Falchi's map and 5x5 km in the map we created. A higher sampling creates a less patchy map with smoother transitions.

Both maps show an almost equal brightness pattern. A part from the general traits described in previous maps (metropolitan areas, dark values NW and SW, etc.), both map show light pollution trails from Barcelona towards secondary sources as Girona, Vic, Manresa and Igualada.

The darkest area is in the NW, both maps provide a sky birghtness between 21.54 and 21.66 mag/arcsec^2 with a reduced number of locations between 21.66 and 21.73 mag/arcsec^2. In the SW the sky is also very dark with values in both maps between 21.54 and 21.66 mag/arcsec^2.

The difference in spatial resolution hardens the comparison of brightness values of middle-size sources, as the nearest estimated location could be outside its borders. For the cases where the studied location is within its borders, such as Vielha, La Seu d'Urgell, Tremp, La Pobla de Segur, Tortosa, Valls, Banyoles and Solsona, both maps agree, but in general we see differences up to 0.4 mag/arcsec^2. Being darker in the Illumina map. For instance Manresa, Figueres, Roses, Mollerusa, Tàrrega, Flix and Amposta.

Barcelona is darker in the Illumina map, 18.2-18.4 mag/arcsec^2, than in Falchi's map, below 18.0 mag/arcsec^2. This difference is not seen in other big sources as Tarragona, Girona and Lleida, where the values of the locations closer to the center of the source show the same value in both maps.

The biggest difference between the two methods is the area of influence of big light pollution sources (middle-source too but in a lesser extent). One of the reasons why artificial radiance is widely spread in Falchi's map is because the blocking effect of the orography is not taken into account. For instance, Barcelona is surrounded in the north by Collserola mountain range. Tarragona metropolitan area too is surrounded in the NW by Prades Hills. In the Pyrenees this effect is even more relevant. That is why in the Illumina maps there are many more location with values over 21.66 mag/arcsec^2 in the NW and over 21.54 mag/arcsec^2 in the center area (reference thresholds from the colorscale used in Falchi's map). Another contributing factor to this difference could be the upward emission function definition. In Falchi's work the upward emission is dominated by a Lambertian (complemented with direct low angle emission). On the other hand, Illumina v2 uses specific information of the obstacle and luminaires characteristics to define and ad-hoc emission function for each source. Although it is beyond the scope of this thesis, it would be very interesting to see how both methodologies compare when using the same emission function.

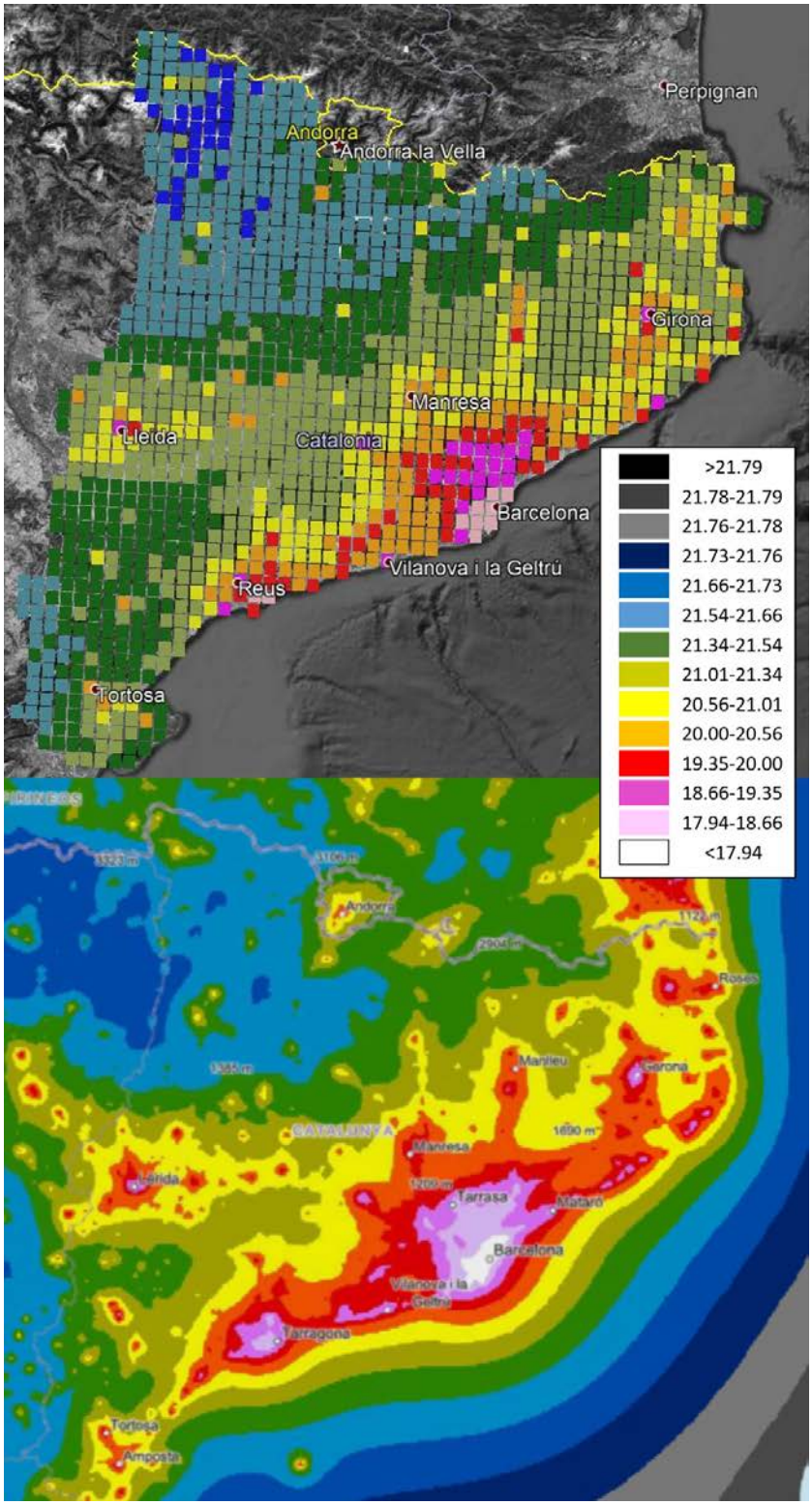

Figure 5.45: ZSB maps in V band of Catalonia. Top: Illumina v2 map. Bottom: Falchi et al. (2016).

Chapter 6

Conclusions

In this thesis we aimed to contribute to the progress towards a complete understanding of light pollution and to provide strategies to improve the sky brightness assessment.

We used two different strategies, measurements and modelling, to study the night sky over two main areas that overlap partially, Catalonia and the Pyrenees mountain range. Nevertheless, the methodologies described can be applied to any region.

The conclusions of the thesis are divided in different blocks: measurements, modelling and night sky characterization of Catalonia. We added at the end a future work section summarizing the lines of work that this thesis has led to.

6.1 Measurements

The methodology used for assessing the night sky over vast areas are SQM dynamic measurements. It allows to cover vast areas in relatively short time. In total, we covered more than 3500 km during 26 nights distributed in four annual campaigns. In long and stable nights we achieved to cover around 300 km. It has also an easy setup and requires small training to be able to gather data properly. Contrarily, processing properly the data is not trivial. We tried to ease and homogenize the process for obtaining reliable zenith sky brightness maps by creating the M2M software, which has been found to be very useful. However, the hand of an expert is still required when the routes covered present dense vegetation or other altering elements.

As a conclusion, the SQM dynamic measurements are a valid methodology for assessing vast areas as long as they are processed by experienced teams. The resulting zenith brightness maps have demonstrated to be an easy to read product for both experts and non-experts in light pollution. The use of surface cells smooths the inherent variability of individual measurements. On the other hand, the dimension of the cells should be small enough to recognize the paths that have been followed and to reveal the differences present within each region.

One of the major concerns is the temporary nature of the maps. Changing atmospheric conditions can alter rapidly the measured brightness levels. Some tracks that have been covered more than once in different nights, or even in the same night with several hours of difference, presented zenith values that differ 0.2 mag/arcsec^2 (in extreme cases the difference reached 0.3 mag/arcsec^2). Measuring the same area twice (or even more times) is not a practical solution to mitigate the problem, because clear sky moonless nights are not common and this approach would reduce significantly the capacity to cover vast areas.

In parallel, we assessed the whole sky over specific location using a different methodology: calibrated DSLR images processed with SQC software to obtain all-sky brightness images in the V band. The resulting all-sky maps are useful to point out the most polluted directions and as a consequence the most probable sources of light pollution. They also distinguish natural sources as the Milky Way and bright stars.

The directions close to the horizon are typically the most polluted and the most useful for obtaining information about the artificial radiance sources that are affecting the sky. It is also important to look for completely clear skies as clouds, even very distant, have been found to affect largely the sky brightness pattern.

We tried to use ASTMON to obtain information of the whole sky in multiple bands (B, V and R of the Johnson-Cousins system). However, the ASTMON instrumentation available was malfunctioning and it was not possible to obtain any data. We used pre-existent ASTMON measurements as a validation tool for simulation products. They were in good agreement with SQC data.

6.2 Light pollution models

Light pollution models have been validated as a helpful tool for assessing the night sky brightness and to understand light pollution at a physics level.

In particular we worked with the Illumina light pollution numerical model due to its completeness regarding the variables it takes into account. We used it with three different purposes: for deriving a sky brightness-distance relation in order to create contribution maps; for creating all-sky brightness maps; and for zenith sky brightness maps of large areas. During the course of this work the second version of Illumina model was released. We confirmed that Illumina v2 and Illumina v1 agree well in cases with distant dominant sources, but Illumina v2 is more accurate in cases with big sources of artificial radiance close to the location studied since Illumina v1 overestimate its polluting effect. Hence, in future works the new version of Illumina should be used.

When working on deriving a sky brightness-distance relation we studied the behaviour of the light with respect to the distance in several wavelengths. We found out that, assuming low levels of aerosol content, most of the radiance received at shorter distances comes from bluer sources. But as the distance increases most of the blue light is dissipated by scattering to other directions rarely reaching the receiver. In those cases, redder light, that is the least scattered, is the main contributor to the total radiance received. The phenomena is explained because the radiance received is produced by molecular Rayleigh scattering since the aerosol content is very small in our region of study.

Eight different locations were studied wuth contribution maps derived using the sky brightness-distance relation. The methodology was confirmed as a useful tool to sort the light pollution sources that are affecting the sky over a particular location. They have been found also useful for deciding which sources to include in all-sky brightness simulations. However, as the contribution maps we used study the sky as a whole, they can be misleading with big and very distant towns (more than 100 km away). This kind of sources does not show a noticeable contribution to the whole sky but could affect significantly a reduced set of directions close to the horizon.

The comparison between measured and simulated all-sky maps revealed that the biggest difference between them was the presence of the Milky Way. This effect could be solved by replacing the simple model of the natural sky we used for a more complex model as the one presented by Masana et al. (2021). A part from the Milky Way and cases with significant variation in the atmospheric condition, the difference between measurements and simulations are of the order of magnitude of 0.1-0.2 mag/arcsec^2 for any direction and for all the cases studied. As a conclusion, Illumina is a reliable tool to reproduce all-sky brightness measurements. It can be used for predicting the changes in the sky that would be produced by changes in the lighting systems.

Regarding lighting systems inventories, we had access to public inventories and the estimated inventories of the same sources using information from DSLR images taken from the ISS. Private lighting has a non-negligible impact on the spectral distribution of the radiance emitted by a city and should be taken into account.

Additionally, we created the first zenith sky brightness of a large area using Illumina light pollution model. It consited in a zenith sky brightness map of Catalonia in the B and V bands using a sampling resolution of 5 km. The results show similar values than the ones obtained during the SQM campaigns taking into account the differences between the SQM spectrum response and V band, and also the different sky region size they assess. The methodology for creating simulated zenith sky brightness maps with Illumina was then validated and proven useful to study the country as a whole.

The simulated zenith sky brightness map was compared to the reference data in this field, the light pollution atlas map of Falchi et al. (2016). Both maps show an almost equal brightness pattern. The biggest difference between the two methods is the area of influence of big light pollution sources. The differences are explained by the different methodologies used, in particular the accounting for orography and the emission function.

6.3 Night sky of Catalonia general remarks

From our measurements as well as our simulations, we observed that Catalonia has a complex pattern of light pollution. It is due to the heterogeneity of the country regarding population distribution and the orography of the territory.

All of our results agrree on the same general description of Catalonia regarding sky brightness:

- Barcelona and Tarragona metropolitan areas are by far the greatest and second greatest artificial light sources of Catalonia. Zenith sky brightness in a radius of tens of kilometers are heavily influenced by them.
- In a lesser extent, the rest of the coastal line is also a source of light pollution. There is a general pattern of darkening as we move away from the coast. The exception is Delta de l'Ebre that is a protected area and barely populated.
- The most polluted skies a part from the ones already mentioned are over Lleida and Girona, and in a lesser extent over Manresa.

- The Pyrenees area, as a general description, is a dark region due to its remoteness and low population, but the quality of the night varies with the longitude. In the east, Girona, Figueres and the coastal line brighten the sky, one only finds really dark values in a few valleys close to the border with France. In the center, Andorra dominates the sky brightness. And in the west, although light pollution models show that it is the darkest region of the Pyrenees and of Catalonia, the tracks measured were not as pristine as expected. We found skiing resorts polluting the sky. Light pollution models indicates that inaccessible areas are almost unaffected by light pollution.

- The two darkest regions we measured were Montsec mountain range and its surroundings, and Ports de Beseit NP. Both regions were already covered in previous campaigns with similar dark results.

Studying the simulated zenith sky brightness maps obtained with Illumina for the B and V band of the Johnson-Cousins system we found out that most of the main artificial light sources have an emission more dominant in the V band than in the B band.

6.4 Future work

The following items summarize the future work that would help improving our understanding of light pollution. They are based on the methodologies described in this work.

In the measurements line of action:

- Extend the photometric measurements to other spectral bands. It will allow to study the changes of the lighting systems. Studying the sky in a unique band could be misleading.

- Finding alternatives to terrestrial vehicles for assessing vast areas as they only cover the roads they can access to. Unmanned aerial vehicles as drones could be a realistic option.

- Including hygrometers to measure humidity levels and defining a maximum threshold of relative humidity beyond which measurements are not be reliable.

In the light pollution models line of action:

- Progressing towards enabling different atmospheric characterization within the geographic domain of a model.
- Combining light pollution models with natural sky brightness models.
- Improving the spatial resolution of zenith sky brightness maps. It is expected that a sampling of 1kmx1km solves the abrupt changes in brightness levels that are observed in the 5kmx5km sampling maps.
- Combining data from the methodology of Sánchez de Miguel et al. (2019) and from public inventories to estimate the percentage of public and private light that a city is emitting. This information is useful to estimate the real impact of changing the public lighting system.
- Using the presented simulation products for predicting the changes in the sky that would be produced by changes in the lighting systems. They can be used for deciding the best lighting system to implement.
- Creating contribution maps that estimate the contribution of a source in any region of the sky.

Chapter 7

Appendix

7.1 Artificial sources emission spectrum

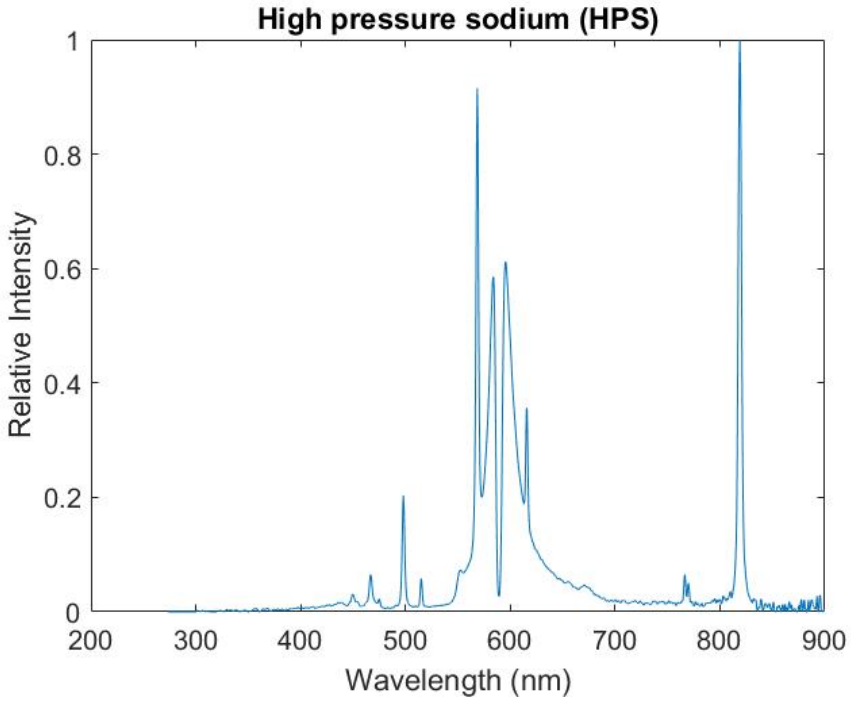

Figure 7.1: Light emission spectrum of high pressure sodium lamps.

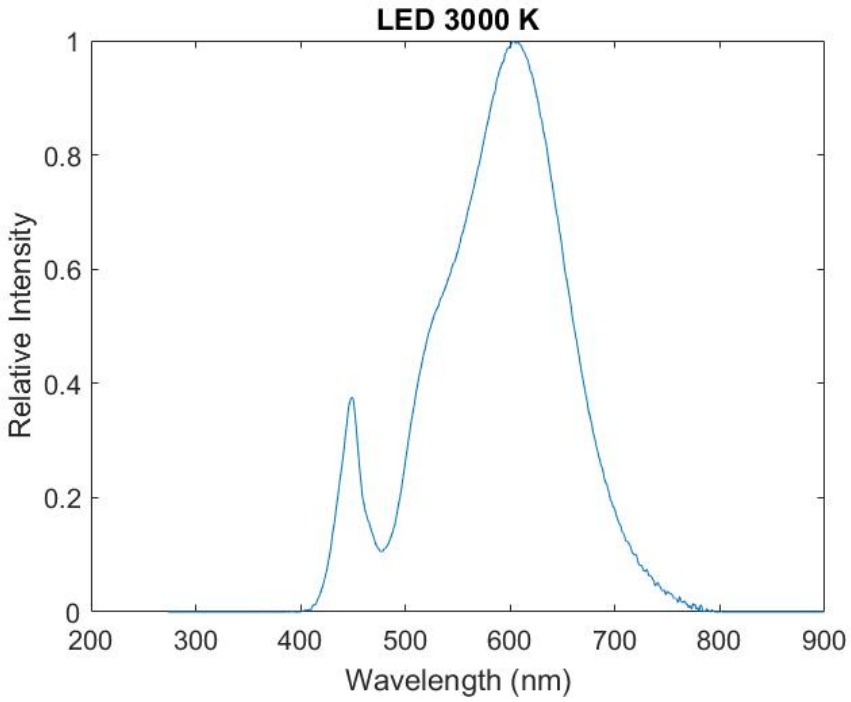

Figure 7.2: Light emission spectrum of LED of 3000 K CCT lamps.

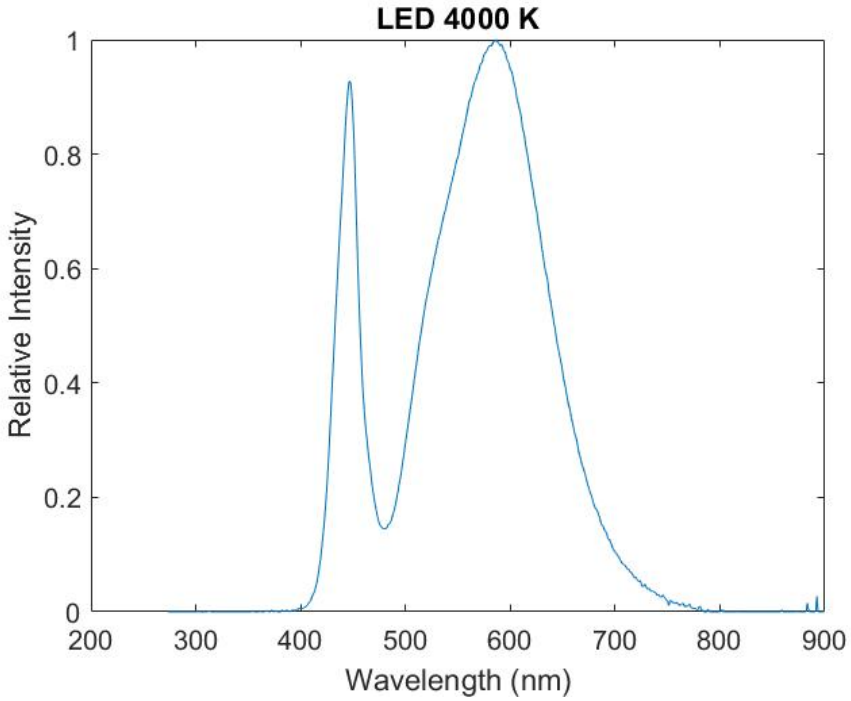

Figure 7.3: Light emission spectrum of LED of 4000 K CCT lamps.

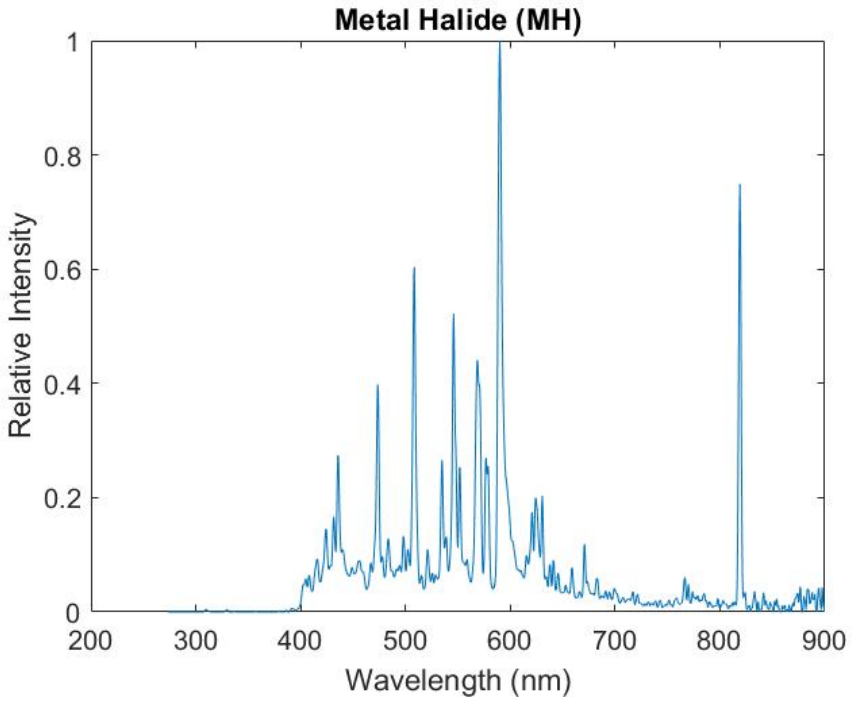

Figure 7.4: Light emission spectrum of metal halide lamps.

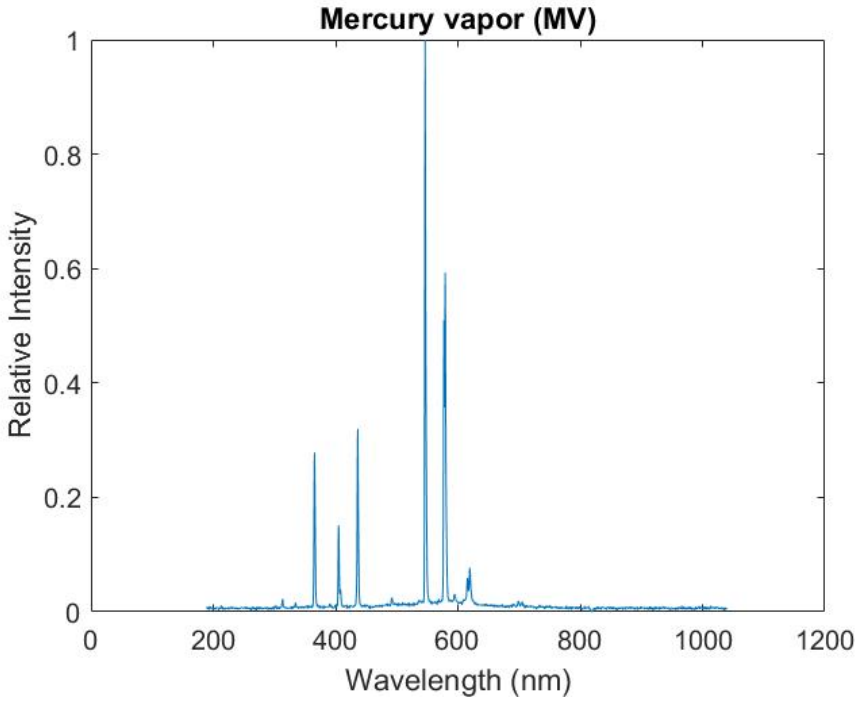

Figure 7.5: Light emission spectrum of mercury vapor lamps.

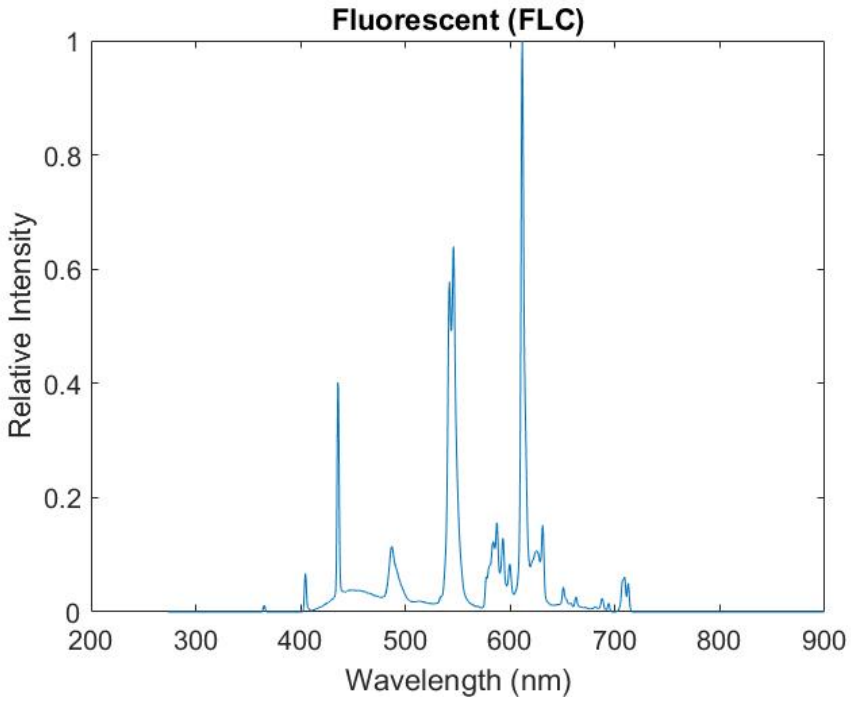

Figure 7.6: Light emission spectrum of fluorescent lamps.

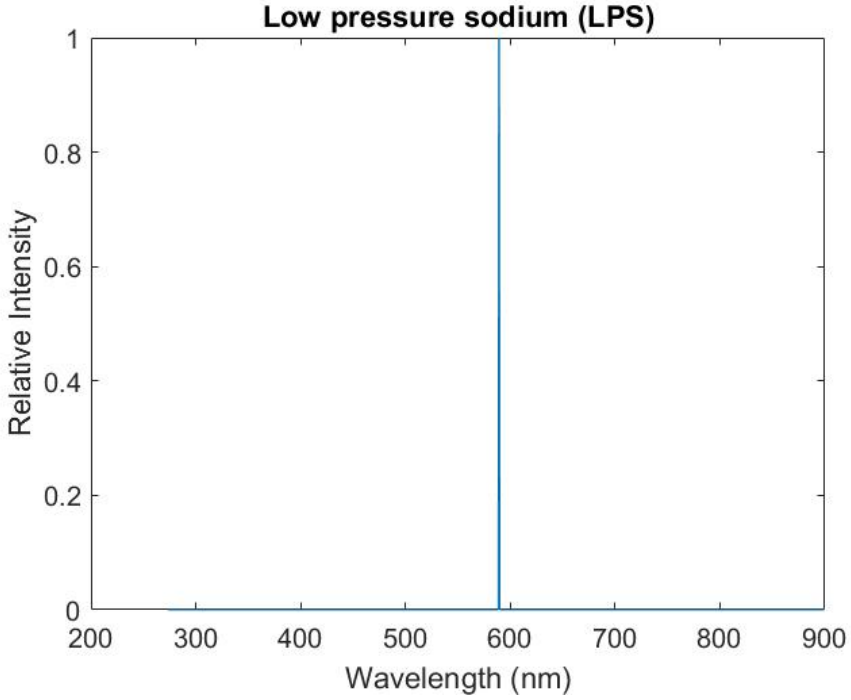

Figure 7.7: Light emission spectrum of low pressure sodium lamps.

References

Aceituno, J., Sánchez, S., Aceituno, F., et al. 2011, Publications of the Astronomical Society of the Pacific, 123, 1076

Aubé, M. 2007, in Proceedings of Starlight 2007 conference, La Palma, Spain

Aubé, M., Franchomme-Fossé, L., Robert-Staehler, P., & Houle, V. 2005, in Atmospheric and Environmental Remote Sensing Data Processing and Utilization: Numerical Atmospheric Prediction and Environmental Monitoring, Vol. 5890, International Society for Optics and Photonics, 589012

Aubé, M., & Kocifaj, M. 2012, Monthly Notices of the Royal Astronomy Society, 422(1), 819

Aubé, M., & Roby, J. 2014, Journal of Quantitative Spectroscopy and Radiative Transfer, 139, 52

Aubé, M., Roby, J., & Kocifaj, M. 2013, Plos One, 8(7)

Aubé, M., Simoneau, A., Muñoz-Tuñón, C., Díaz-Castro, J., & Serra-Ricart, M. 2020, arXiv e-prints

Aubé, M., Simoneau, A., Wainscoat, R., & Nelson, L. 2018, Monthly Notices of the Royal Astronomical Society, 478, 1776

Bará, S., & Lima, R. 2018, International Journal of Sustainable Lighting, 20(2), 51

Bará, S., Lima, R. C., & Zamorano, J. 2019a, Sustainability, 11, 3070

Bará, S., Marco, E., Ribas, S., et al. 2020, Preprint

Bará, S., Rigueiro, I., & Lima, R. C. 2019b, Journal of Quantitative Spectroscopy and Radiative Transfer, 239, 106644

Bará, S., Tapia, C., & Zamorano, J. 2019c, Sensors, 19(6), 1336

Berry, R. L. 1976, Journal of the Royal Astronomical Society of Canada, 70, 97

Bertiau, F., de Graeve, E., & Treanor, P. J. 1973, Vatican Observatory Publications, 1, 159

Bertolo, A., Binotto, R., Ortolani, S., & Sapienza, S. 2019, Journal of Imaging, 5, 56

Bird, R. E. 1984, Solar Energy, 32, 461

Braak, J. C., de Haan, J. F., Van der Mee, C. V. M., & Hovenier, J. W. 2001, J. Quant. Spectrosc. Radiat. Transfer, 69, 585

Buil, C. 2015, http://www.astrosurf.com/buil/us/iris/iris.htm

CIE. 1951, Proceedings of the Commission Internationale de l'Éclairage, Vol. 1, Sec 4; Vol 3, p. 37, Bureau Central de la CIE, Paris

—. 1990, Commission Internationale de l'Éclairage 1988 2˙ Spectral Luminous Efficiency Function for Photopic Vision

Cinzano, P., & Falchi, F. 2020, Journal of Quantitative Spectroscopy and Radiative Transfer, 253, 107059

Cinzano, P., Falchi, F., CD, E., & Baugh, K. 2000, Mon. Not. R. Astron. Soc, 318, 641–657

Cinzano, P., Falchi, F., & Elvidge, C. 2001, Mon. Not. R. Astron. Soc., 328, 689–707

Cousins, A. 1976, Monthly Notes of the Astronomical Society of South Africa, 35, 70

Deco, F. 2017, Revista Luminotecnia, 139

den Outer, P., Lolkema, D., Haaima, M., et al. 2011, Sensors, 11, 9603

—. 2015, Sensors, 15, 9466

Duriscoe, D. M. 2016, Journal of Quantitative Spectroscopy and Radiative Transfer, 181, 33

Falchi, F., Cinzano, P., Duriscoe, D., et al. 2016, Sciences Advances, 2

Galadí-Enríquez, D. 2018, Journal of Quantitative Spectroscopy and Radiative Transfer, 206, 399

Garcia-Saenz, A., Sánchez de Miguel, A., Espinosa, A., et al. 2018, Environ Health Perspect., 126(4)

Garstang, R. H. 1986, Publications of the Astronomical Society of the Pacific, 98, 364

Gocova, A. 2013, Alternative Journal, 39

Grubisic, M., van Grunsven, R., Manfrin, A., Monaghan, M., & Hölker, F. 2018, Environmental Pollution, 240, 630–638

Gueymard, C. 2001, Solar Energy, 71(5), 325

Hanel, A., Posch, T., Ribas, S. J., et al. 2018, Journal of Quantitative Spectroscopy and Radiative Transfer

Holben, B. N., Eck, T. F., Slutsker, I., et al. 1998, Remote sensing of environment, 66, 1

ImageJ. 2015, http://imagej.nih.gov/ij/

Jechow, A., Kollath, Z., Ribas, S. J., et al. 2017, Scientific reports, 7(1)

Jechow, A., Ribas, S. J., Domingo, R. C., et al. 2018, Journal of Quantitative Spectroscopy and Radiative Transfer, 229, 212

Johnson, H., & Morgan, W. 1953, The Astrophysical Journal, 117, 313

—. 1955, Ann. Astrophys, 18, 292

Kneizys, F., Abreu, L., Anderson, G., et al. 1996

Kneizys, F. X., Shettle, E. P., Gallery, W. O.and Chetwynd, J. H., et al. 1980, Tech. Rep. AFGLTR800067, Bedford, MA: U.5. Air Force Geophysics Laboratory

Kocifaj, M. 2007, Applied optics, 46, 3013

—. 2017, Optica, 4(2), 255

—. 2018, Journal of Quantitative Spectroscopy and Radiative Transfer, 206, 260

Kolláth, Z. 2010, Journal of Physics: Conference Series, 218, 012001

Kolláth, Z. 2010, Journal of Physics: Conference Series, 218

Kyba, C. C., Ruhtz, T., Fischer, J., & Holker, F. 2011, Plos one, 6(3), e17307

Kyba, C. C. M., Kuester, T., Sánchez de Miguel, A., et al. 2017, Science Advances, 3, doi:10.1126/sciadv.1701528

Liao, L. B., Weiss, S., Mills, S., & Hauss, B. 2013, Journal of Geophysical Research: Atmospheres, 118, 12,705

Linares, H., Masana, E., Ribas, S., et al. 2020, Journal of Quantitative Spectroscopy and Radiative Transfer, 249

—. 2018, Journal of Quantitative Spectroscopy and Radiative Transfer, 217, 178

Masana, E., Carrasco, J. M., Bará, S., & Ribas, S. J. 2021, Monthly Notices of the Royal Astronomical Society, 501, 5443

Nievas, M., & Zamorano, J. 2013, Master thesis, Universidad Complutense de Madrid

—. 2014, Tech. rep. Universidad Complutense de Madrid

Normandin, M. 1974, Appendix D in Demande d'Octroi au conseil national de recherches du Canada pour l'installation d'un observatoire astronomique au Quebec

Pun, C. S. J., Chu Wing So, C. W., Leung, W. Y., & Wong, C. F. 2014, Journal of Quantitative Spectroscopy and Radiative Transfer, 139, 90

Ribas, S., Cuc'o, M., & Vilajoliu, J. 2013, Centre d'Observaci'o de l'Univers

Ribas, S., Torra, J., Figueras, F., Paricio, S., & Canal-Domingo, R. 2016, International Journal of Sustainable Lighting, 35, 32

Ribas, S. J. 2016, PhD thesis

Riegel, K. W. 1973, Science, 179, 1285

Rosa Infantes, D. 2011, Fourth International Symposium for Dark Sky Parks, Montsec, Spain.

Sánchez de Miguel, A., Kyba, C. C. M., Aubé, M., et al. 2019, Remote Sensing of Environment, 224, 92

Sanchez de Miguel, A., Kyba, C. C. M., Zamorano, J., Gallego, J., & Gaston, K. J. 2020, Scientific reports, 10

Sanders, D., Frago, E., Kehoe, R., Patterson, C., & Gaston, K. 2020, Nat Ecol Evol, doi:https://doi.org/10.1038/s41559-020-01322-x

Saphiro, R. 1982, Tech. Rep.. Systems and Applied Sciences Corp Vienna VA

Tilve, V., Ling, J., Bará, S., et al. 2015, Highlights of Spanish Astrophysics VIII, 1, 874–874

Torra, J., Fernández, D., Asiain, R., et al. 2000, Tech. rep., Universitat de Barcelona

Treanor, P. J. 1973, The Observatory, 93, 117

Walker, A. 1987, NOAO newsletter, 10, 16

Walker, M. F. 1970, Publications of the Astronomical Society of the Pacific, 82, 672

—. 1973, Publications of the Astronomical Society of the Pacific, 85, 508

—. 1977, Publications of the Astronomical Society of the Pacific, 89, 405

Zamorano, J., Sánchez de Miguel, A., Nievas, M., & Tapia, C. 2014, Tech. rep., Universidad Complutense de Madrid

Zamorano, J., García, C., González, R., et al. 2016, International Journal of Sustainable Lighting, 35, 49